Engineering Enhanced Performance in Plant Diacylglycerol Acyltransferase and Long-Chain Acyl-CoA Synthetase

by

Yang Xu

A thesis submitted in partial fulfillment of the requirements for the degree of

Doctor of Philosophy

in

Plant Science

Department of Agricultural, Food and Nutritional Science
University of Alberta

Abstract

Triacylglycerol (TAG) is the major storage lipid in higher plants and has great nutritional and industrial value. Plant storage lipid biosynthesis involves different subcellular compartments and a complex network of enzymes and proteins. Among them, endoplasmic reticulum (ER)-bound diacylglycerol acyltransferase (DGAT) catalyzes the last and committed step in the acyl-CoA-dependent biosynthesis of TAG. Another key enzyme known as long-chain acyl-CoA synthetase (LACS) catalyzes the ATP-dependent formation of acyl-coenzyme As (CoAs) using free fatty acids. The LACS-catalyzed reaction provides an acyl donor to all the acyl-CoA-dependent acyltransferases including DGAT. Both DGAT and LACS are regarded as important targets for manipulating seed oil production. The overall goals of this thesis were to improve the enzyme performance of DGAT and LACS via protein engineering, and to explore their potential roles in TAG biosynthesis and the enhancement of the process.

Numerous *Brassica napus* DGAT1 (BnaDGAT1) variants generated through directed evolution were shown to increase TAG content in yeast. In the first study, the possible roles of the ninth and tenth predicted transmembrane domain (TMD) in affecting BnaDGAT1 performance were revealed by mapping the beneficial amino acid residue substitutions of BnaDGAT1 variants onto a predicted topology model. To further investigate how the amino acid residues would affect enzyme performance, several BnaDGAT1 variants with amino acid residue substitutions residing in predicted TMD9 were characterized. These BnaDGAT1 variants increased yeast TAG content for different reasons including increased enzyme activity, increased polypeptide accumulation and/or possible reduced substrate inhibition. BnaDGAT1 variant L441P was found to display possible weak substrate inhibition and high catalytic efficiency. The beneficial amino acid residue substitutions of BnaDGAT1 variants were then transferred to

Camelina sativa DGAT1 (CsDGAT1) and the resulting variant CsDGAT1 enzymes also possessed improved enzyme performance in yeast. Similarly to the equivalent BnDGAT1 variant L441P, possible reduced substrate inhibition was observed for CsDGAT1 variant L460P. Furthermore, the mutagenized libraries of *BnaDGAT1* were screened again using linoleic acid and α-linolenic acid (ALA), respectively, and one variant containing seven amino acid residue substitutions exhibited altered preference towards linoleoyl-CoA and α-linolenoyl-CoA.

In the second study, error-prone PCR was used to modify the enzyme performance of LACS9 from *Arabidopsis thaliana* (AtLACS9). Two AtLACS9 variants containing multiple amino acid residue substitutions were identified with improved enzyme activity. Site-directed mutagenesis suggested that increased enzyme activities of the two variants were mainly attributable to the single amino acid reside substitutions of C207F and D238E, respectively. C207 was found as a moderately conserved site among LACS9 from plant eudicots, whereas the unconserved site D238 was predicted under positive selection. Another two AtLACS9 variants, E520D and E630D, were identified to have increased preference toward linoleic acid.

Seed oil from flax (*Linum usitatissimum*) is enriched in ALA, but the biochemical processes underlying ALA enrichment in flax are not fully elucidated. In the third study, a potential process involving the catalytic action of LACS and DGAT was proposed for channeling ALA into TAG. Flax LACS (LuLACS8A) exhibited enhanced specificity for ALA. Flax DGAT2 (LuDGAT2-3) was also found to display approximately 20-times increased preference towards α-linolenoyl-CoA over oleoyl-CoA. Incorporation of ALA into TAG via substrate channeling between LuLACS8A and LuDGAT2-3-catalyzed reactions was supported by both *in vitro* and *in vivo* (in yeast) experiments.

Finally, membrane yeast two-hybrid assays revealed several interactions among enzymes involved in acyl-editing and TAG assembly in flax. Among these protein-protein interactions, the identification of a physical interaction between flax lysophosphatidylcholine acyltransferase 2 (LuLPCAT2) and LuDGAT1-1 supports previous evidence for biochemical coupling of the LPCAT-catalyzed reverse reaction to form acyl-CoA from phosphatidylcholine to the DGAT1-catalyzed forward reaction.

In summary, the findings in this thesis provide insight into the amino acid residues underlying plant DGAT1 and LACS9 function and will benefit the development of innovative strategies to manipulate oil production in oleaginous plants and microorganisms.

Preface

This thesis is based on the research presented in the following papers. My contribution to each paper is summarized. In general, I was responsible for most of the work including experimental design, data collection and analysis, and manuscript preparation. My supervisor, Dr. Randall Weselake, provided overall guidance in the research including experimental design and valuable suggestions/discussions. Dr. Weselake, and my co-supervisor Dr. Jocelyn Ozga, were involved in editing of the manuscripts and thesis.

Chapter three is based on the following three manuscripts (listed in the order of appearance in the text):

1. Chen G, Xu Y, Siloto RMP, Caldo KMP, Vanhercke T, Tahchy AE, Niesner N, Chen Y, Mietkiewska E, and Weselake RJ. (2017) High Performance Variants of Plant Diacylglycerol Acyltransferase 1 Generated by Directed Evolution Provide Insights into Structure-Function. Plant J doi: 10.1111/tpj.13652

Only the figures/results that I developed for this manuscript were included in the thesis.

2. Xu Y, Chen G, Greer MS, Caldo KMP, Ramakrishnan G, Shah S, Wu L, Lemieux MJ, Ozga J, and Weselake RJ. (2017) Multiple Mechanisms Contribute to Increased Neutral Lipid Accumulation in Yeast Producing Recombinant Variants of Plant Diacylglycerol Acyltransferase 1. J Biol Chem, doi: 10.1074/jbc.M117.811489

I designed the research, performed all experiments, analyzed the data and prepared the initial draft of the manuscript. Dr. Ramakrishnan isolated the cDNA of *CsDGAT1B* and designed

CsDGAT1B variants. All co-authors contributed to interpretation of the data and further editing of the manuscript.

3. Xu Y, Chen G, Ozga J, and Weselake RJ. Screening of *BnaDGAT1* Mutagenized Libraries Using Linoleic Acid and α-linolenic Acid. Manuscript in preparation.

I designed the research, performed all experiments, analyzed the data and prepared the initial draft of the manuscript. All co-authors contributed to interpretation of the data and revision of the manuscript.

Chapter four is based on the paper: Xu Y, Holic R, Chen G, Ozga J and Weselake RJ. Engineering Improved Variants of Arabidopsis Long-Chain Acyl-CoA Synthetase 9. Manuscript in preparation.

I designed the research, performed all experiments, analyzed the data and prepared the initial draft of the manuscript. Dr. Holic constructed yeast mutant strains *BYfaa1,4Δ* and *BYQMfaa1,4Δ*. All co-authors contributed to interpretation of the data and revision of the manuscript.

Chapter five is based on the following paper: Xu Y, Holic R, Li D, Pan X, Mietkiewska E, Chen G, Ozga J and Weselake RJ. (2017) Possible Role of Long-Chain Acyl-CoA Synthetase and Diacylglycerol Acyltransferase in Channeling α-linolenic Acid into Flax Seed Triacylglycerol. Manuscript ready for submission.

I designed the research, performed most of the experiments, analyzed the data and drafted the manuscript. Dr. Roman Holic constructed yeast mutant strains *BYfaa1,4Δ* and *BYQMfaa1,4Δ*.

Darren Li helped with the isolation of *LuLACS8A* and *LuLACS9A* cDNAs from flax. All co-authors contributed to interpretation of the data and revision of the manuscript.

Chapter Six is based on the following paper: Xu Y, Ozga J, and Weselake RJ. Membrane Yeast Two-Hybrid Assays Reveal Several Interactions between Storage Lipid Biosynthetic Enzymes from Flax. Manuscript in preparation.

I designed the research, performed the experiments, analyzed the data and drafted the manuscript. All co-authors contributed to interpretation of the data and revision of the manuscript.

Acknowledgements

This doctoral thesis would never have been possible without the inspiration, support and help of a number of people. First and foremost, I sincerely thank my supervisor, Dr. Randall Weselake, for offering me this great opportunity to pursue my doctoral degree in his lab and for introducing me into the world of plant lipids. I will always be grateful to his inspiration, guidance, support and encouragement throughout my studies. I am also very grateful to my co-supervisor, Dr. Jocelyn Ozga, for her generous support and valuable suggestions regarding my research. I also heartily thank my supervisory committee members, Drs. Janice Cooke and Habibur Rahman, for their inspiration and valuable advice and suggestions not only on my research but how to be a better plant scientist. I acknowledge Dr. Linda Hall for serving as the Chair of my candidacy exam, and Drs. Jianping Wu and Enrico Scarpella for serving as the arm-length examiners of my candidacy exam. I want to thank Dr. Mirko Betti for serving as the Chair of my defense, and Dr. Stephen Strelkov for serving as the arm-length thesis defense examiner. I am also truly grateful to Dr. Edgar Cahoon for agreeing to serve as the external examiner of my thesis defense.

I thank all the lab members of the Weselake group for their help. A big thank you goes to Dr. Guanqun (Gavin) Chen for his guidance at the beginning of my research and for his tireless support through the entire process. I own him immense gratitude for his constant encouragement and support of my research and incredible advice about my future and career. I also thank Dr. Roman Holic, a former visiting scholar from Slovak Academy of Sciences, for teaching me how to establish randomly mutagenized libraries and several techniques in yeast work. I especially thank Kristian Caldo, another PhD student in the lab, for valuable discussions and suggestions when I encountered problems during my experiments. I also thank Dr. Elzbieta Mietkiewska for

sharing her experience in molecular cloning and lipid analysis, to Dr. Xue Pan for giving me suggestions on the construction of yeast co-expression vectors, to Dr. Michael Greer for his advice about enzyme assays, and to Drs. Saleh Shah and Stacy Singer for answering my questions about plant transformation. I also thank our previous program/lab managers Chris Kazala, Robin Miles, Annie Wong and Champa Wijekoon for their hard and efficient work. I also acknowledge the financial support of my PhD program provided by China Scholarship Council and the Alberta Innovates Graduate Student Top-up Award. I addition, I thank Dr. Sten Stymne of the Swedish University of Agricultural Science for providing us with *Saccharomyces cerevisiae* H1246.

Lastly, I thank my friends: Lingbo Cheng, Shuai Zhi, Xiaohong Sun, Yuan Fang and Tingting Ju for their company and support, and my dearest parents Huaiqi Xu and Lihua Wang for their everlasting love and support.

Table of Contents

List of Tables

List of Figures

List of Abbreviations

ΔF	change in fluorescence
3PGA	3-phosphoglycerate
ACAT	acyl-CoA:cholesterol acyltransferase
ACCase	acetyl-CoA carboxylase
ACP	acyl carrier protein
ALA	α-linolenic acid
ANOVA	analysis of variance
ATP	adenosine triphosphate
cDNA	complementary DNA
CoA	coenzyme A
CPT	choline phosphotransferase
DAG	diacylglycerol
DGAT	acyl-CoA:diacylglycerol acyltransferase
ER	endoplasmic reticulum
FA	fatty acid
FACS	fatty acyl-CoA synthetase
FAD	fatty acid desaturase
FAE	fatty acid elongase
FAS	fatty acid synthase
FAT	acyl-ACP thioesterase
FAX	fatty acid export
G3P	*sn*-glycerol-3-phosphate

GC/MS	gas chromatography coupled mass spectrometry
GPAT	acyl-CoA:*sn*-glycerol-3-phosphate acyltransferase
GPC	glycerophosphocholine
GPCAT	acyl-CoA:glycerophosphocholine acyltransferase
Hexose P	hexose phosphate
hmACCase	homomeric acetyl-CoA carboxylase
htACCase	heteromeric acetyl-CoA carboxylase
LA	linoleic acid
LACS	long-chain acyl-CoA synthetase
LPA	lysophosphatidic acid
LPAAT	acyl-CoA:lysophosphatidic acid acyltransferase
LPC	lysophosphatidylcoline
LPCAT	acyl-CoA:lysophosphatidylcholine acyltransferase
LPCT	lysophosphatidylcholine transacylase
LRT	likelihood ratio test
MCAT	malonyl-CoA:ACP acyltransferase
ME	malic enzyme
MYTH	membrane yeast two-hybrid
NAD(P)+	oxidized nicotinamide adenine dinucleotide (phosphate)
NAD(P)H	reduced nicotinamide adenine dinucleotide (phosphate)
OA	oleic acid
OD	optical density
PA	phosphatidic acid

PAP	phosphatidic acid phosphatase
PC	phosphatidylcholine
PDAT	phospholipid:diacyglycerol acyltransferase
PDCT	phosphatidylcholine:diacylglycerol cholinephosphotransferase
PDH	pyruvate dehydrogenase
PEP	phosphoenolpyruvate
PLA_2	phospholipase A_2
PLC	phospholipase C
PLD	phospholipase D
PPP	pentose phosphate pathway
PTMD	predicted transmembrane domain
Pyr	pyruvate
qPCR	quantitative RT-PCR
Ru5P	ribulose-5-phosphate
RuBisCO	ribulose-1,5-bisphosphate carboxylase/oxygenase
RuBP	ribulose-1,5-bisphosphate
SAD	stearoyl-ACP desaturase
SD	synthetic drop-out
sn	stereospecific numbering
TAG	triacylglycerol
TLC	thin-layer chromatography
TMD	transmembrane domain
Triose P	triose phosphate

WS	wax ester synthase
WT	wild type
X-Gal	5-bromo-4-chloro-3-indolyl-β-D-galactopyranoside

Chapter 1 – Introduction

Vegetable oil, as the major energy storage compound in oilseeds, is an important plant product with great nutritional and industrial value. The major constituent of vegetable oil is triacylglycerol (TAG), which accounts for 90 to 98% of the oil (Srivastava and Prasad, 2000). TAG consists of three fatty acids esterified to a glycerol backbone and much of its value derives from its variable fatty acid composition. Since the worldwide demand for vegetable oil increased consistently over the past 50 years and is expected to continue increasing, manipulating plant oil production to enhance seed oil content and modify fatty acid composition can contribute to this demand.

In oilseed crops, fatty acid and TAG biosynthesis occur during seed development. Fatty acids synthesized in the plastid are transported to the outside of the plastid where they are activated to acyl-CoAs via the catalytic action of ATP-dependent long-chain acyl-CoA synthetase (LACS; EC 6.2.1.3) for use as acyl-donors in TAG assembly (Chapman and Ohlrogge, 2012; Snyder et al., 2009). In addition, LACS is proposed to contribute to the trafficking of modified fatty acids from phosphatidylcholine (PC) to TAG together with phospholipase A_2 (Lands, 1960; Bayon et al., 2015). Modified fatty acid released from PC could potentially be activated by LACS for used as an acyl donor in TAG assembly. LACSs with distinct substrate preferences have been identified in various plants and diatoms, suggesting a possible role for LACS in channeling modified fatty acids (Aznar-Moreno et al., 2014; He et al., 2007; Ichihara et al., 2003; Tonon et al., 2005).

TAG assembly occurs in the endoplasmic reticulum (ER) and includes three sequential acyl-CoA-dependent acylations of a glycerol backbone (Chapman and Ohlrogge, 2012). The final and committed step in acyl-CoA-dependent TAG biosynthesis is catalyzed by diacylglycerol acyltransferase (DGAT; EC 2.3.1.20), which, in some species, may represent a bottleneck in the flow of carbon into seed oil formation (Weselake et al., 1991; Liu et al., 2012; Harwood et al., 2013). At least two forms of membrane-bound DGAT (DGAT1 and DGAT2) have been identified in eukaryotes, which essentially share no sequence homology and are proposed to have distinct roles in TAG biosynthesis (Lung and Weselake, 2006). DGAT1s have been found to contribute primarily to TAG accumulation, whereas DGAT2s appear to be more involved in the formation of TAG containing unusual fatty acids (Burgal et al., 2008; Li et al., 2010a).

Given the importance of LACS and DGAT in TAG biosynthesis, further improving the performance of these two enzymes via directed evolution and/or site-directed mutagenesis could represent a valuable approach to increase oil accumulation or modify the fatty acid composition of oil. Indeed, both enzymes are regarded as attractive targets for boosting oil content in various organisms (Guo et al., 2014; Tan et al., 2014; Tonon et al., 2005; Pulsifer et al., 2012; Weselake et al., 2008; Taylor et al., 2009; Lardizabal et al., 2008; Roesler et al., 2016; Zheng et al., 2008; Misra et al., 2013). Mutagenesis approaches to modifying LACS or DGAT could also potentially shed light on the structure/function relationships in these families of enzymes.

The overall objectives of this thesis project were to engineer plant DGAT and LACS with enhanced performance, and explore the potential roles of these enzymes in

channeling PC-modified fatty acids into TAG using a combination of molecular biology and biochemistry approaches. My research was based on the following hypotheses.

1. Recombinant variants of *Brassica napus* DGAT1 (BnaDGAT1) with increased performance and modified substrate specificity can be generated through directed evolution. The amino acid residue substitutions in performance-enhanced BnaDGAT1 variants can affect enzyme activity, polypeptide accumulation, and regulatory properties of the enzyme when BnaDGAT1 variants are recombinantly produced in *Saccharomyces cerevisiae*. In addition, the information on the relationship between amino acid residue substitutions and enzyme performance in BnaDGAT1 variants can be used to guide the modification of a DGAT1 from another species.

2. Recombinant variants of *Arabidopsis thaliana* LACS9 (AtLACS9) with increased activity and modified substrate specificity can be generated through random mutagenesis. The amino acid residue substitutions in performance-enhanced AtLACS9 variants can affect enzyme activity and/or polypeptide accumulation when AtLACS9 variants are recombinantly produced in *S. cerevisiae*.

3. Flax (*Linum usitatissimum*) contains LACS and DGAT2 with preference towards *α*-linolenic acid (ALA; 18:3$\Delta^{9cis,12cis,15cis}$)-containing substrates. ALA selective LACS and DGAT2 can contribute to the ALA enrichment in TAG.

4. Enzymes of storage lipid biosynthesis in flax interact to facilitate possible channeling of ALA into TAG.

Numerous BnaDGAT1 variants resulting in increased TAG content in yeast were generated by directed evolution and these variants were found to boost yeast TAG content

via different mechanisms. The beneficial amino acid residue substitutions in BnaDGAT1 variants led to enhanced enzyme performance could be transferred to *Camelina sativa* DGAT1 through modification of equivalent amino acid residues. Error-prone PCR was used to modify the performance of AtLACS9 and several variants with increased enzyme activity or altered substrate specificity were generated. ALA-selective LACS and DGAT2 were identified from flax, and their contribution to ALA enrichment in TAG was evaluated *in vitro* and *in vivo* (in yeast). Potential protein-protein interactions between enzymes involved in acyl-editing and TAG assembly in flax were revealed by membrane yeast two-hybrid assays.

Chapter 2 – Literature Review

2.1. Oleaginous crops

Storage oils of vegetable origin are of major importance for the agricultural industry. Besides the great nutritional value of plant oils, there is a strong interest in using these oils as renewable feedstock for the chemical industry (Biermann et al., 2011). The demands for plant oils for edible and industrial applications increased consistently over the past 50 years and are expected to continue to rise due to the growing population and the increasing reliance on vegetable oil-derived chemicals, such as biodiesel (Chen et al., 2015; Lu et al., 2011). In addition, the finite availability of the arable lands will further limit the supply of plant oils, regardless of their renewable nature (Lu et al., 2011).

The global production of plant oil is dominated by four crops, including oil palm (*Elaeis guineensis*), soybean (*Glycine max*), oilseed rape (*Brassica napus*), and sunflower (*Helianthus annuus*), which account for 29, 23, 13 and 7%, respectively, of the world production (210.8 million tonnes) in 2014/2015 (United States Department of Agriculture, 2016; Food and Agriculture Organization of the United Nations, 2016). The remaining global oil production is mainly contributed by minor plant oils (palm kernel, peanut, cotton, coconut, olive, corn, sesame, linseed, and castor) and animal fats (tallow, lard, butter, and fish oil). The primary consumption of these oils and fats are for food purposes with the remaining being used in the oleochemical industry and for animal feed. Besides castor (*Ricinus communis*) and flax (*Linum usitatissimum L.*) oils, which are used almost exclusively as oleochemical feedstock, most of the oils and fats are of both food/feed and industrial importance (i.e., multipurpose oils and fats). The oil and fat consumption from

food, industrial use, and feed was considered to be in the ratio of 80:14:6 in the 1980s, but with growing biodiesel production this has probably shifted to 74:20:6 (Gunstone, 2008). Palm and oilseed rape oils have contributed the most to the growing industrial use of oils during the past decade, mainly due to the development of the oleochemical industry in southeast Asia and the biodiesel industry in Europe, respectively (List, 2015; Gunstone, 2009).

The growing demands for food-based oleochemicals, however, are exacerbating a conflict between food and fuel. One possible solution for meeting the increasing demands is to introduce novel oil crops for industrial applications. Alternative oil crops including *Jatropha curcas*, *B. carinata*, *Crambe abyssinica*, and Camelina (*Camelina sativa*) have received much attention for their potential roles in industry. Much of the interest in *J. curcas*, a perennial plant from the *Euphorbiaceae* family, is due to its ability to grow on non-arable land, which would not compete with food-producing crops (King et al., 2009). Some *Brassicaceae* species, including *B. carinata* and *C. abyssinica*, contain high erucic acid ($22{:}1\Delta^{13cis}$) levels and are considered as attractive candidates for green chemistry (or sustainable chemistry) (Zanetti et al., 2009; Li et al., 2012b). *C. sativa*, another member of the *Brassicaceae* family, possesses important agronomic traits (including low water and fertilizer requirements, high cold and pathogen resistance, and comparable yield to other oilseed crops) and is amenable to genetic manipulation, rendering this crop an ideal platform for the production of industrial oil (Bansal and Durrett, 2015; Feussner, 2015).

Another more important approach to meet global vegetable oil demands is to manipulate plant oil production through metabolic engineering. There are two main

challenges that lie ahead: firstly, to increase productivity and oil yield of crops and, secondly, to manipulate vegetable oils with fatty acids of greater nutritional and industrial value. To address these challenges, recent advances in our understanding of storage lipid metabolism are discussed in the following sections. After this, the two key enzymes investigated in this thesis project are discussed in more detail.

2.2. Oil biosynthesis

Triacylglycerol (TAG) is the major energy storage compound in the seeds of oleaginous plants and the major component of plant oils. TAG consists of a glycerol backbone with three fatty acid chains esterified at the three positions on the glycerol backbone. The general structure of TAG and stereospecific numbering of the fatty acyl chains are depicted in Figure 2.1. Exceptions for TAG as the major energy storage lipid are only found in a few plant species, including wax esters of jojoba (*Simmondsia chinensis*), TAG estolides of species from *Lesquerella*, and acetyl-TAG of *Euonymus alatus* (Durrett et al., 2010; Taylor and Smith, 2011). In developing oilseeds, TAG biosynthesis can be thought of consisting of three steps: *de novo* fatty acids biosynthesis in the plastid, exporting fatty acids from the plastid into the cytosol, and assembly of fatty acids into TAG in the endoplasmic reticulum (ER).

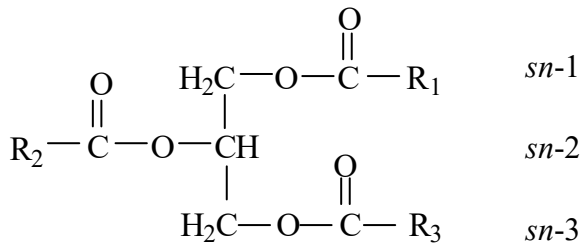

Figure 2.1. The general structure of triacylglycerol (TAG). TAG consists of three fatty acids esterified to three stereospecific positions on the glycerol backbone, where R_1, R_2 or R_3 is equivalent to fatty acyl chain minus one carbon. If the fatty acid esterified to the secondary hydroxyl group of the glycerol backbone is shown to the left of the second carbon in a Fisher Projection, the second carbon is numbered stereospecific numbering (*sn*)-2, and the carbon atom above and below the second carbon are numbered *sn*-1 and *sn*-3, respectively (IUPAC-IUB Commission on Biochemical Nomenclature, 1967).

2.2.1. Fatty acid biosynthesis

Unlike the cytosolic localization in other eukaryotes, plant fatty acid biosynthesis occurs in the plastid (chloroplast in green tissues and proplastid in non-green tissues) and uses acetyl-CoA as the building block. A general scheme outlining fatty acid biosynthesis is depicted in Figure 2.2. The process of plant fatty acid biosynthesis has been the subject of numerous reviews (Ohlrogge and Jaworski, 2003; Chapman and Ohlrogge, 2012; Harwood, 2005). Thus, the description of fatty acid biosynthesis in this literature review is mainly summarized based on these review articles. Where appropriate, additional references to more recent advances in the area, are included.

2.2.1.1. Carbon source and energy supply for fatty acid biosynthesis

Sucrose, the major form of assimilated carbon derived from photosynthesis, provides the ultimate source of carbon for fatty acid biosynthesis. The hexose phosphates from the cleavage of sucrose can be metabolized through glycolysis or the pentose phosphate pathway in the cytosol or plastid to generate pyruvate. Pyruvate then provides the direct precursor for acetyl-CoA production via the reaction catalyzed by a plastidial pyruvate dehydrogenase (PDH). Moreover, in seeds such as *B. napus* that are green during development, the action of ribulose-1,5-bisphosphate carboxylase/oxygenase (Rubisco) contributes to the fixation of CO_2 released from decarboxylation reactions such as the one catalyzed by PDH, which ultimately increases the carbon use efficiency (Schwender et al., 2004). It has also been suggested that plastidial pyruvate can be synthesized via

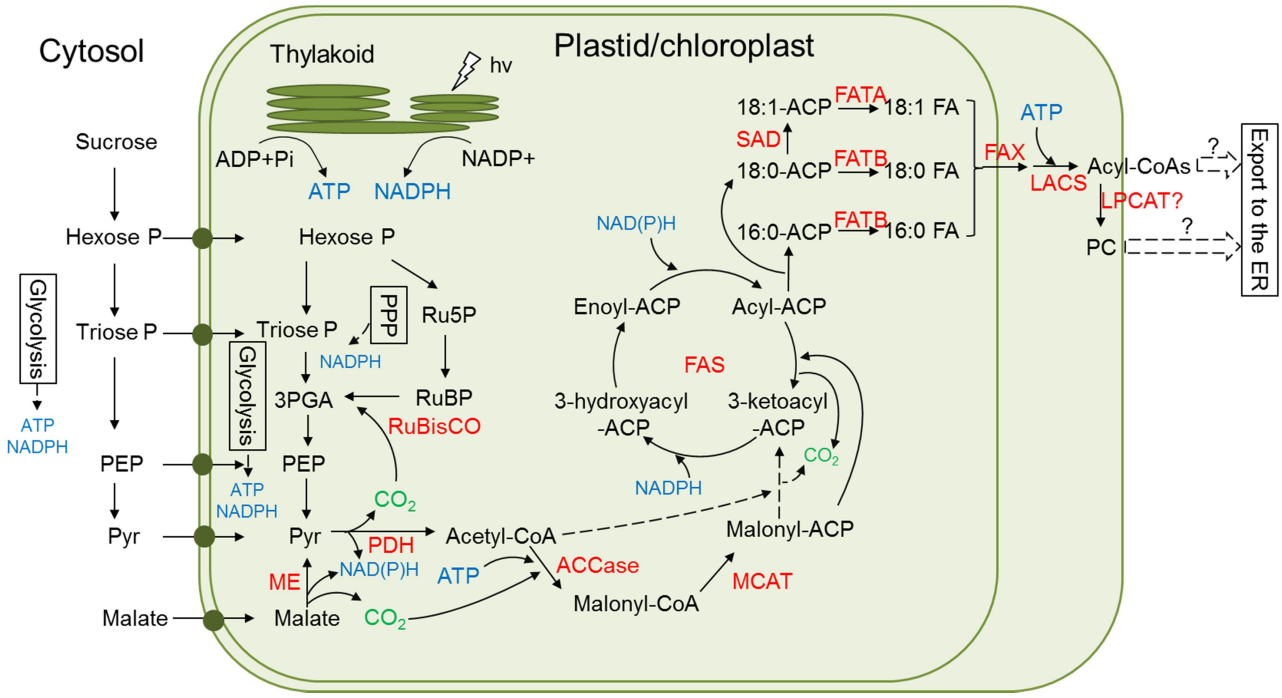

Figure 2.2. Schematic representation of fatty acid biosynthesis in plants. ACP, acyl carrier protein; ACCase, acetyl-CoA carboxylase; ATP, adenosine triphosphate; CoA, coenzyme A; ER, endoplasmic reticulum; FA, fatty acid; FAS, fatty acid synthase; FAT, acyl-ACP thioesterase; FAX, fatty acid export; Hexose P, hexose phosphate; LACS, long-chain acyl-CoA synthetase; LPCAT, lysophosphatidylcholine acyltransferase; MCAT, malonyl-CoA:ACP acyltransferase; ME, malic enzyme; NAD(P)H, reduced nicotinamide adenine dinucleotide (phosphate); NAD(P)+, oxidized nicotinamide adenine dinucleotide (phosphate); PC, phosphatidylcholine; PDH, pyruvate dehydrogenase; PEP, phosphoenolpyruvate; PPP, pentose phosphate pathway; Pyr, pyruvate; Ru5P, ribulose-5-phosphate; RuBP, ribulose-1,5-bisphosphate; RuBisCO, ribulose-1,5-bisphosphate carboxylase/oxygenase; SAD, stearoyl-ACP desaturase; Triose P, triose phosphate; 3PGA, 3-phosphoglycerate. This figure was developed based on information from reviews and articles on plant lipid biosynthesis (Ohlrogge and Jaworski, 2003; Chapman and Ohlrogge, 2012; Harwood, 2005; Li et al., 2015; Shearer et al., 2004; Baud and Lepiniec, 2010).

decarboxylation of imported malate by malic enzyme (ME) (Shearer et al., 2004). The relative contribution to fatty acid biosynthesis of these pathways appears to vary among different species (Baud and Lepiniec, 2010).

Fatty acid synthesis requires a large input of energy, including adenosine triphosphate (ATP) and reducing power provided by reduced nicotinamide adenine dinucleotide phosphate (NADPH) and reduced nicotinamide adenine dinucleotide (NADH) (Baud and Lepiniec, 2010; Chapman and Ohlrogge, 2012). ATP and reductant can be either taken up from the cytosol or generated inside the plastid. The glycolysis and pentose phosphate pathway in the cytosol or plastid and the citric acid cycle in the mitochondria provide potential sources of ATP and reductant for fatty acid biosynthesis. Another potential source of reductant is generated by NADP-dependent ME, which catalyzes the conversion of malate to pyruvate. In green seeds, light reactions of photosynthesis also provide ATP and NADPH for fatty acid biosynthesis in the plastid.

2.2.1.2. Formation of fatty acids from acetyl-CoA

The first committed step in *de novo* fatty acid biosynthesis is catalyzed by acetyl-CoA carboxylase (ACCase), which utilizes acetyl-CoA and bicarbonate to form malonyl-CoA. Two distinct forms of ACCase, heteromeric ACCase (htACCase) and homomeric ACCase (hmACCase), have been identified in nature (Sasaki and Nagano, 2004). HtACCase is a multi-enzyme complex consisting of four separate subunits: biotin carboxylase, biotin carboxylase carrier protein, and α- and β-carboxyltransferase, whereas hmACCase is composed of a single large multifunctional polypeptide with the above four

subunit domains. Most plants have both forms of ACCases, with htACCase in the plastid and hmACCase in the cytosol. Exceptions are found in the grass family, which only possesses the homomeric form in both the plastid and cytosol. One application of this detailed knowledge about ACCase is to selectively control grass weeds using the herbicides like aryloxyphenoxypropionates and cyclohexanedione, which specifically target the hmACCase in the plastid (Chen et al., 2015).

Malonyl-CoA produced by ACCase cannot be directly used by the fatty acid synthase (FAS) complex in the plant. It has to be converted into malonyl-acyl carrier protein (ACP) by the catalytic action of malonyl-CoA:ACP acyltransferase before entering the subsequent fatty acid biosynthesis pathway. The FAS complex utilizes acetyl-CoA as the starting unit and malonyl-ACP as the two-carbon unit donor to the growing fatty acid chain. There are four sequential reactions involved in each two-carbon elongation cycle: condensation catalyzed by β-ketoacyl-ACP synthase (KAS), first reduction catalyzed by β-ketoacyl-ACP reductase, dehydration catalyzed by β-hydroxyacyl-ACP dehydrase, and second reduction catalyzed by enoyl-ACP reductase. In plants, three isoforms of the KAS condensing enzymes have been identified. To produce an 18-carbon fatty acid, the three KASs are required to cooperate together with KASIII catalyzing the initial condensation of acetyl-CoA and malonyl-ACP (4:0 ACP), KASI catalyzing the subsequent condensations up to 16:0 ACP, and KASII catalyzing the final condensation (16:0 ACP to 18:0 ACP). 18:0-ACP can further be desaturated to 18:1 (18:1Δ^{9cis})-ACP by a soluble Δ9-acyl-ACP desaturase (SAD). The resulting 16-carbon or 18-carbon ACPs are then hydrolyzed via the catalytic action of acyl-ACP thioesterases (FATA or FATB) to release free fatty acids.

2.2.2. Exporting fatty acids from the plastid into the cytosol

In order to be used for phosphotidylcholine (PC) and TAG biosynthesis in the ER, the released fatty acids are required to be exported from the chloroplast by crossing both inner and outer envelopes of the plastid (Figure 2.2). The recently characterized fatty acid export (FAX) 1 appears to be involved in the transfer of free fatty acids across the inner envelope (Li et al., 2015). The fatty acids are then presumed to be converted to acyl-CoAs by long-chain acyl-CoA synthetase (LACS; EC 6.2.1.3) in the outer plastidial envelope (Schnurr et al., 2002) and exported to the ER through the cytosol, probably facilitated by acyl-CoA binding proteins (Xiao and Chye, 2011). Alternatively, the resulting acyl-CoA might be incorporated into PC via the catalytic action of lysophosphatidylcholine acyltransferase (LPCAT) at the plastidial envelope and then exported to the ER using PC as a carrier (Chapman and Ohlrogge, 2012). The presence of LPCAT activity associated with the outer plastidial envelope (Andersson et al., 2004; Mongrand et al., 2000) and the radiolabeling studies (Bates et al., 2007, 2009) support the latter hypothesis. It has also been proposed that lipid trafficking might proceed through direct membrane contact between the plastid and the ER (Andersson et al., 2007; Hanson and Sattarzadeh, 2011).

2.2.3. Triacylglycerol assembly

TAG assembly occurs in the ER and uses glycerol 3-phosphate (G3P), derived from glycolysis, and acyl-CoA as the primary substrates. In plants producing oils enriched in polyunsaturated fatty acids (PUFAs) or unusual fatty acids (e.g., ricinoleic acid [12-OH 18:1Δ^{9cis}]), the process of TAG formation occurs through a complex interplay with

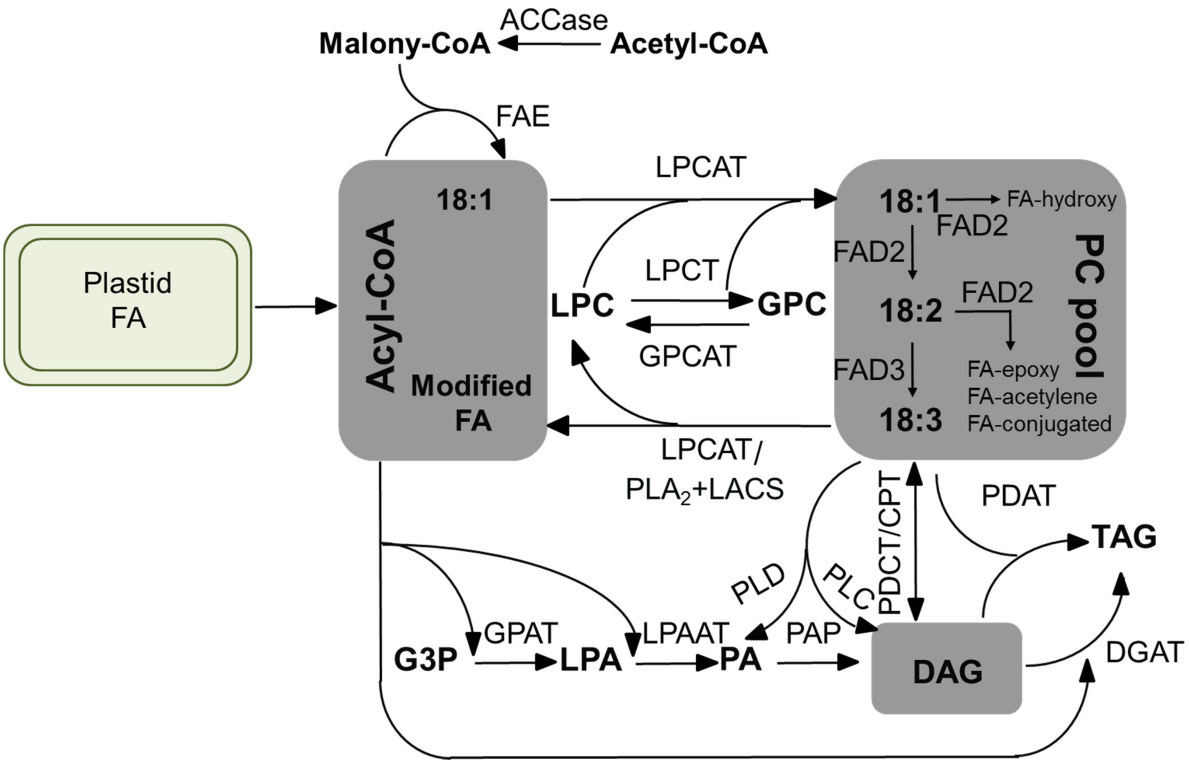

Figure 2.3. Schematic representation of triacylglycerol (TAG) biosynthesis and acyl-editing in plants. ACCase, acetyl-CoA carboxylase; CoA, coenzyme A; CPT, choline phosphotransferase; DAG, diacylglycerol; DGAT, diacylglycerol acyltransferase; FA, fatty acid; FAD, fatty acid desaturase; FAE, fatty acid elongase; GPAT, *sn*-glycerol-3-phosphate acyltransferase; GPC, glycerophosphocholine; GPCAT, glycerophosphocholine acyltransferase; G3P, *sn*-glycerol-3-phosphate; LACS, long-chain acyl-CoA synthetase; LPA, lysophosphatidic acid; LPAAT, acyl-CoA:lysophosphatidic acid acyltransferase; LPC, lysophosphatidylcoline; LPCAT, lysophosphatidylcholine acyltransferase; LPCT, lysophosphatidylcholine transacylase; PA, phosphatidic acid; PAP, phosphatidic acid phosphatase; PC, phosphatidylcholine; PDAT, phospholipid:diacyglycerol acyltransferase; PDCT, phosphatidylcholine: diacylglycerol cholinephosphotransferase; PLA_2, phospholipase A_2; PLC, phospholipase C; PLD, phospholipase D; TAG, triacylglycerol. This figure was developed based on recent reviews and articles on plant lipid biosynthesis (Chen et al., 2015; Chapman and Ohlrogge, 2012; Bates et al., 2013, 2012).

membrane metabolism. Multiple interconnected pathways have been proposed for TAG assembly and, particularly, the relative contribution of these pathways may be different among species (Figure 2.3). The following information on TAG assembly is mainly based on a few recent reviews and articles (Chen et al., 2015; Chapman and Ohlrogge, 2012; Bates et al., 2013, 2012).

2.2.3.1. The acyl-CoA-dependent Kennedy pathway

The Kennedy pathway involves the sequential acylation of the glycerol backbone of G3P at *sn*-1, 2, and 3 positions to yield TAG. Three acyl-CoA-dependent acyltransferases, including *sn*-glycerol-3-phosphate acyltransferase (GPAT), lysophosphatidic acid acyltransferase (LPAAT) and diacylglycerol acyltransferase (DGAT; EC 2.3.1.20) participate in this process (Snyder et al., 2009). GPAT catalyzes the first acylation of G3P with acyl-CoA to yield lysophosphatidic acid (LPA). Ten *GPAT* genes have been found in *Arabidopsis thaliana* (hereafter Arabidopsis), and the particular GPAT involved in the Kennedy pathway was identified very recently (Singer et al., 2016; Shockey et al., 2016). Evidence based on *in vitro* enzyme assays and functional evaluation in transgenic Arabidopsis have suggested that GPAT9 is the GPAT enzyme responsible for TAG biosynthesis (Singer et al., 2016; Shockey et al., 2016). LPA is further acylated by LPAAT to produced phosphatidic acid (PA), which is then converted to *sn*-1,2-diacylglycerol (DAG) via the catalytic action of PA phosphatase (PAP). DGAT catalyzes the final acylation of DAG with acyl-CoA to form TAG, which is the committed step in TAG biosynthesis.

2.2.3.2. The acyl-CoA-independent pathway and acyl-editing

TAG can also be synthesized through the acyl-CoA-independent pathway with the action of phospholipid:diacyglycerol acyltransferase (PDAT). PDAT catalyzes the transfer of the acyl moiety at the *sn*-2 position of PC to DAG (Dahlqvist et al., 2000; Stahl et al., 2004). It is believed that PDAT contributes to the channeling of modified fatty acids from PC into TAG in some plants because of its distinct substrate specificities (Kim et al., 2011; van Erp et al., 2011; Pan et al., 2013).

Plants, such as flax and *C. sativa*, which produce relatively high levels of PUFAs in the seed oil, require acyl trafficking mechanisms to enrich the resulting seed oil in PUFA content (Pan et al., 2013, 2015; Wickramarathna et al., 2015). In addition, some plant species, such as castor, tung tree (*Vernicia fordii*), ironweed (*Vernonia galamensis*) and *Momordica charantia*, accumulate unusual fatty acids in the storage TAG that have important industrial applications. These latter species also required acyl trafficking mechanisms to accommodate unusual fatty acids. In most species, fatty acids exported from the plastid are mainly saturated (16:0 and 18:0) and monounsaturated (18:1) fatty acids. To produce PUFA-enriched or unusual fatty acids, the nascent fatty acids derived from the plastid have to undergo further modification such as elongation, desaturation, or hydroxylation in the ER at the acyl-CoA or PC level. ER-bounded fatty acid elongase (FAE) catalyzes the elongation of the acyl chain at acyl-CoA level (Ghanevati and Jaworski, 2001; Rossak et al., 2001). Other modifications of fatty acids, including desaturation, hydroxylation, epoxidation and conjugation, primarily occur at the level of PC (Vrinten et al., 2005; van Erp et al., 2011; van de Loo et al., 1995; Liu et al., 1998; Bafor et al., 1993;

Cahoon et al., 1999). Fatty acid desaturase (FAD) 2 and FAD3 catalyze the sequential introduction of double bonds at the ω-6 and ω-3 carbons of fatty acids, respectively (Browse et al., 1993; Vrinten et al., 2005). The hydroxylase from castor (van de Loo et al., 1995), the epoxygenase from *V. galamensis* (Cahoon and Kinney, 2005) and the conjugase from *Momordica charantia* (Cahoon et al., 1999), are related to or derived from FAD2. The FADs and FAD2-related enzymes are mainly responsible for the modification of the nascent fatty acids on the *sn*-2 position of PC.

Following their synthesis on PC, modified fatty acids have to be moved out of PC and eventually incorporated into TAG via different routes of acyl-editing (Bates, 2016; Chen et al., 2015). As indicated previously, modified fatty acids may be channeled from PC to TAG directly by the catalytic action of PDAT (Kim et al., 2011; van Erp et al., 2011; Pan et al., 2013). Other metabolic routes involve transfer of PC-modified fatty acids to the acyl-CoA pool or conversion into modified DAG.

As suggested in the Lands cycle (Lands, 1960) more than 50 years ago, fatty acids synthesized on PC can enter the acyl-CoA pool via the combined action of phospholipase A_2 (PLA_2) and LACS. The cycle is then completed by the subsequent acylation of the resulting lysophosphatidylcholine (LPC) and unmodified acyl-CoA to regenerate PC by the forward action of LPCAT. Recently, the Land's cycle has been shown to be operative during seed development in Arabidopsis (Wang et al., 2012a).

A different process to move modified fatty acids from the *sn*-2 position of PC into the acyl-CoA pool involves possible acyl-exchange catalyzed by the combined forward and

reverse reactions catalyzed by LPCAT (Stymne and Stobart, 1984; Lager et al., 2013). The reverse reaction catalyzed by LPCAT, however, is thermodynamically unfavourable. A possible way of shifting the LPCAT-catalyzed reaction in the direction of acyl-CoA would be to reduce the free concentration of acyl-CoA and/or increase the concentration of CoA. For example, low molecular mass acyl-CoA binding protein interacts with acyl-CoA and may thus contribute to encouraging the reverse reaction of LPCAT by reducing the free concentration of the thioester (Yurchenko et al., 2009, 2014). In addition, acyl-CoA-dependent acyltransferases which utilize acyl-CoA as acyl donors could potentially contribute to encouraging the reverse reaction catalyzed by LPCAT. Recently, Pan et al. (2015) provided *in vivo* and *in vitro* evidence to demonstrate that coupling of the LPCAT-catalyzed reverse reaction to the DGAT-catalyzed forward reaction resulted in channeling of PUFA from the *sn*-2 position of PC into TAG.

The above mechanisms of exchanging acyl groups mainly occur on the *sn*-2 position of PC. Even though the *sn*-2 position of PC is the primary site for acyl-editing, a lower amount of acyl-editing flux was observed to go through *sn*-1 position based on *in vivo* metabolic labeling studies (Bates et al., 2009, 2007). It raised the possibility that the exchange of the acyl groups might occur between the *sn*-1 and *sn*-2 positions of PC. This may involve the catalytic action of glycerophosphocholine acyltransferase (GPCAT) and lysophosphatidylcholine transacylase (LPCT) (Lager et al., 2015).

PC-modified fatty acids can also be incorporated into TAG in the form of DAG. *De novo* DAG can be converted into PC by the catalytic action of CDP-choline:*sn*-1,2-diacylgycerol cholinephosphotransferase (CPT) for further modification (Slack et al., 1983,

1985). Once the acyl chains on PC are modified, conversion back to DAG and/or PA can occur via the catalytic action of phospholipase C and/or D, respectively (Bates et al., 2013; Chapman and Ohlrogge, 2012). Phospholipase C catalyzes the removal of the phosphocholine headgroup of PC to produce DAG whereas phospholipase D catalyzes the removal of the choline group to produce PA (Chen et al., 2011a). Recently, Yang et al. (2017) demonstrated that over-expression of a cDNA encoding a phospholipase D led to increased seed oil accumulation in Camelina. Previously, the reverse action of CPT was thought to also contribute to product of PUFA-enriched DAG in developing flax seed (Slack et al., 1985). The CPT-catalyzed reaction, however, is thermodynamically unfavorable in the direction of DAG synthesis (Chen et al., 2015). An alternative route to channel modified acyl chains in the DAG pool involves the action of phosphatidylcholine: diacylglycerol cholinephosphotransferase (PDCT), which catalyzes the transfer of the phosphocholine headgroup of modified-PC to *de novo* DAG containing 18:1 produced in the Kennedy pathway (Lu et al., 2009; Wickramarathna et al., 2015). Modified DAG is now available for use as an acyl acceptor by DGAT or PDAT, and 18:1-enriched PC can now be modified.

To date, many enzymes with unique substrate specificity, including PDAT, PDCT, LPCAT, PLA_2, LACS, and DGAT, have been identified from plants containing unique fatty acids in the storage TAG (Pan et al., 2013, 2015; Wickramarathna et al., 2015; Kim et al., 2011; van Erp et al., 2011; Bayon et al., 2015; Tonon et al., 2005). These might cooperate together to drive the channeling of modified fatty acids into TAG. By displaying

similar substrate specificity, these enzymes could preferentially channel the acyl moieties from various substrate pools into TAG.

When examining the acyl donor specificity of an acyl-CoA-utilizing enzyme such as DGAT, a series of assays are conducted with different molecular species of acyl-CoA and then the resulting enzyme activities are ranked in terms of the effectiveness of the acyl donor (Weselake, 2005). In the case of acyl donor selectivity, experiments need to be conducted with mixtures of different molecular species of acyl-CoA. The results of selectivity studies may not necessarily reflect what was observed in the substrate specificity experiments. For example, when BnaDGAT1 isoform BnaC.DGAT1.a was assayed with 16:0-CoA or 18:1-CoA separately and then using an equimolar mixture, the apparent preference for 16:0-CoA was increased in the competitive scenario (Greer et al., 2014). In another recent study, Aznar-Moreno et al. (2015) individually assayed the activities of four recombinant isoforms of BnaDGAT1 and reported that 16:0-CoA was preferred to 18:1-CoA. When enzyme assays were conducted at a ratio of 3:1 of 18:1-CoA to 16:0-CoA, which represented the physiological situation, all four isoforms catalyzed the incorporation of 18:1 into TAG at amounts two- to five-fold higher than for 16:0. From the two above studies of acyltransferase selectivity, it is clear that the proportions of different molecular species of acyl-CoA in the reaction mixture can have a large influence on the degree of incorporation of a particular fatty acyl moiety into TAG. The situation becomes far more complex when one considers presenting the acyltransferase with a mixture of different molecular species of DAG. An earlier study on the DAG specificities of microsomal DGATs from various plant sources was conducted by Vogel and Browse (1996).

The substrate or product pools of TAG biosynthetic and associated acyl-editing enzymes might even be separated from the *de novo* synthesized substrate pools. It has been suggested that the PC-derived DAG pool, rather than the *de novo* DAG pool serves as the major source of DAG for TAG biosynthesis (Bates et al., 2009; Lu et al., 2009). Meanwhile, an independent acyl-CoA pool in the ER lumen to provide substrates for TAG biosynthesis has been proposed previously (Kim et al., 2013). Furthermore, it is also possible that some of these enzymes might be physically associated with each other in the membrane. The physical interaction or co-localization of certain enzymes appears to be an important criterion for channeling of specific substrates in TAG biosynthesis. Previously, animal DGAT2 has been reported to interact with monoacylglycerol acyltransferase (Jin et al., 2014), stearoyl-CoA desaturase (Man et al., 2006) or acyl-CoA synthetase (Xu et al., 2012). In terms of a plant system, tung tree DGAT2 may interact with GPAT (Gidda et al., 2011) and Arabidopsis LPCAT was shown to interact with DGAT1 (Shockey et al., 2016).

2.3. Role of diacylglycerol acyltransferases in triacylglycerol biosynthesis and their properties

2.3.1. Identification of diacylglycerol acyltransferases

Although the first report of DGAT activity from chicken liver appeared in 1956 (Weiss and Kennedy, 1956; Weiss et al., 1960), over four decades passed before the genes were cloned and characterized (Cases et al., 1998). Two major forms of membrane-bound DGAT proteins (designated DGAT1 and DGAT2) have been identified in a wide variety of eukaryotes (Lung and Weselake, 2006). In addition, peanut (*Arachis hypogaea*) cytosolic DGATs (Saha et al., 2006; Chi et al., 2014) and an Arabidopsis bi-functional wax ester

synthase (WS)/DGAT (Li et al., 2008) have also been reported. Bifunctional WS/DGAT was first identified from the bacterium *Acinetobacter calcoaceticus* (Kalscheuer and Steinbüchel, 2003). Somewhat later, *DGAT3* encoding soluble enzyme was identified in Arabidopsis (Hernández et al., 2012; Peng and Weselake, 2011). In addition, Rani et al. (2010) identified a soluble Arabidopsis protein termed Defective Cuticle Ridge which exhibited DGAT activity. In addition to these DGATs, chloropastic phytyl ester synthases in Arabidopsis were also found to have DGAT activity (Lippold et al., 2012).

In 1998, the first *DGAT* gene, a member of DGAT1 family, was cloned from mouse (*Mus musculus*) based on sequence homology to acyl-CoA:cholesterol acyltransferase (ACAT) 1 (Cases et al., 1998). Immediately after the isolation of mouse *DGAT1*, *DGAT1* was first identified in Arabidopsis (Routaboul et al., 1999; Hobbs et al., 1999; Zou et al., 1999; Bouvier-Navé et al., 2000) and tabacco (*Nicotiana tabacum*) (Bouvier-Navé et al., 2000). DGAT1 was then identified in many other species including olive (*Olea europaea*) (Giannoulia et al., 2000), *B. napus* (Nykiforuk et al., 2002; Greer et al., 2015), castor bean (He et al., 2004b), burning bush (*Euonymus alatus*) (Milcamps et al., 2005), tung (Shockey et al., 2006), soybean (Wang et al., 2006), garden nasturtium (*Tropaeolum majus*) (Xu et al., 2008a), *Echium pitardii* (Mañas-Fernández et al., 2009), flax (*Linum usitatissimum*) (Siloto et al., 2009b; Pan et al., 2013), sesame (*Sesamum indicum*) (Wang et al., 2014), and more recently *Cuphea avigera* var. *pulcherrima* (Iskandarov et al., 2017). The above list, however, is by no means comprehensive.

In 2001, the first DGAT2 was identified from the oleaginous fungus *Umbelopsis ramanniana* (formerly *Mortierella ramanniana*), which has essentially no amino acid

sequence similarity with DGAT1 and ACAT1 (Lardizabal et al., 2001). In the same study, DGAT2 homologs were also isolated from *Saccharomyces cerevisiae*, *Caenorhabditis elegans* and Arabidopsis, whereas only DGAT2s from the former two species, rather than Arabidopsis, encoded active enzymes. Shortly thereafter, *DGAT2*-related genes were identified from mouse and human (*Homo sapiens*) based on the DGAT2 sequence from *U. ramanniana* (Cases et al., 2001). Despite the early unsuccessful attempt to produce active recombinant Arabidopsis DGAT2 (AtDGAT2), functional recombinant plant DGAT2s were isolated and characterized from tung tree, castor and ironweed on the basis of the putative AtDGAT2 sequence (Li et al., 2010a; Shockey et al., 2006; Kroon et al., 2006).

2.3.2. Role of diacylglycerol acyltransferases in triacylglycerol biosynthesis

As the enzyme catalyzes the final and committed step in acyl-CoA-dependent TAG biosynthesis, DGAT is considered to play a critical role in determining the flux of carbon into seed TAG in some species (Harwood et al., 2013). For instance, the level of DGAT activity was observed to be coordinated with oil accumulation during seed development in oilseed crops such as canola-type *B. napus* and safflower (*Carthamus tinctorius*) (Weselake et al., 1993; Tzen et al., 1993). Further analysis of *DGAT1* expression in many oilseed crops revealed that this gene is highly expressed in developing embryos (Hobbs et al., 1999; Lu et al., 2003) and its expression level is correlated with the oil accumulation during seed development (Li et al., 2010b). A more direct piece of evidence of DGAT1 affecting oil accumulation comes from forward and reverse genetics approaches (Katavic et al., 1995; Zou et al., 1999; Zheng et al., 2008). DGAT1 inactivation has been shown to result in a dramatic decrease in seed oil levels in Arabidopsis mutant AS11 (Katavic et al., 1995;

Zou et al., 1999), whereas the activation of DGAT1 by a phenylalanine insertion in maize (*Zea mays*) DGAT1-2 at position 469 has been shown to be responsible for the increased embryo oil content in a high-oil maize line (Zheng et al., 2008).

Unlike the large contribution of DGAT1 to seed oil production in Arabidopsis and other oilseeds, DGAT2 appears to play a minor role in oil accumulation. Expression of *AtDGAT2* failed to complement the TAG biosynthesis in *S. cerevisiae* mutant H1246 which is devoid of oil synthesizing ability (Zhang et al., 2009). Arabidopsis *dgat2* mutants did not show any changes in TAG accumulation and *dgat1* and *dgat2* double mutants did not lead to an aggravated phenotype compared to the *dgat1* mutation alone (Zhang et al., 2009). Recently, the functionality of AtDGAT2 in TAG biosynthesis was demonstrated by transient expression of the encoding cDNA in *Nicotiana benthamiana* leaves (Zhou et al., 2013) and heterologous expression in yeast (*S. cerevisiae*) using a codon-optimized version of the cDNA (Aymé et al., 2014). Nevertheless, the physiological role of DGAT2 in Arabidopsis remains to be further characterized. Interestingly, characterization of DGAT2 from species accumulating unusual fatty acids revealed that DGAT2 is likely to be important for incorporating unusual fatty acids into storage oils. The unusual fatty acids include eleostearic acid (18:3 $\Delta^{9cis,11trans,13trans}$) from tung tree (Shockey et al., 2006), ricinoleic acid from castor (Kroon et al., 2006), and vernolic acid (*cis*-12-epoxy-octadeca-*cis*-9-enoic acid) from ironweed (Li et al., 2010a). It has been observed that *DGAT2* transcripts were more enhanced than *DGAT1* transcripts in developing seeds from tung (Shockey et al., 2006), castor (Kroon et al., 2006), ironweed (Li et al., 2010a) or flax (Pan et al., 2013) during embryo development, whereas the expression of *DGAT2* from

Arabidopsis and soybean was far below the levels observed for *DGAT1* expression (Li et al., 2010b). Further analysis revealed that DGAT1 and DGAT2 from tung tree localize to different regions of the ER and the isozymes differ in substrate preference, suggesting that TAG production by DGAT1 versus DGAT2 occurs in distinct ER subdomains (Shockey et al., 2006). Thus, it appears that DGAT1 and DGAT2 contribute differentially to TAG biosynthesis and their relative contributions vary among species.

In mammals and yeasts, DGAT2, more so than DGAT1, appears to be the dominant DGAT enzyme for TAG synthesis. *Dgat2* knockout mice (*Dgat2*$^{-/-}$) were lipopenic, had abnormal skin and died early (Stone et al., 2004), whereas *Dgat1* knockout mice (*Dgat1*$^{-/-}$) were viable and capable of TAG synthesis (Smith et al., 2000). While the *DGAT2* gene is almost ubiquitously present in all eukaryotes, *DGAT1* is absent in the genome of certain yeasts (*S. cereviseae* and *Candida albicans*) and *Basidiomycetes* fungi (*Laccaria bicolor*, *Schizophillum commune* and *Agaricus bisporus*) (Turchetto-Zolet et al., 2011). It has also been suggested that DGAT2 is likely the primary TAG-synthesizing enzyme in *S. cerevisiae* (Sandager et al., 2002) and *Yarrowia lipolytica*, even though *Y. lipolytica* also has a *DGAT1* gene (Zhang et al., 2012).

The physiological role of soluble DGAT3 remains largely to be explored. It has been suggested that AtDGAT3 might be involved in recycling of 18:2 and 18:3 fatty acids into TAG when TAG breakdown was blocked (Hernández et al., 2012) and Arabidopsis Defective Cuticle Ridge, another soluble DGAT, appears to be related to the biosynthesis of cutin rather than seed oil (Rani et al., 2010). Soluble forms of other TAG-biosynthetic enzymes, including GPAT, LPAAT, PAP and monoacylglycerol acyltransferase, have also

been reported (Tumaney et al., 2001; Ghosh et al., 2009; Ichihara et al., 1990; Han et al., 2006; Turnbull et al., 2001). It is still unclear whether these soluble TAG-biosynthetic enzymes utilize different substrate pools and have different physiological roles compared to the membrane-bound isoforms.

2.3.3. Structural features and regulation of diacylglycerol acyltransferases

DGAT1 and DGAT2 are integral membrane-bound proteins which contain multiple transmembrane domains (TMDs) (Liu et al., 2012). Currently, no three-dimensional structure is available for any DGAT or closely homologous proteins (Liu et al., 2012; Lopes et al., 2015). Identification of possible functional motifs in the amino acid sequence of DGATs and determination of their membrane topologies can, however, contribute to developing insights into their structure-function relationships.

DGAT1 belongs to the membrane-bound O-acyltransferases (MBOAT) superfamily, which is characterized by multiple TMDs. DGAT1 proteins are predicted to contain 8 to 10 TMDs (Liu et al., 2012). The alignment of 55 DGAT1 proteins from different species indicated that the predicted TMDs were in preserved positions and shared high sequence identity among most DGAT1s (Liu et al., 2012). A membrane topology model of DGAT1 from *B. napus* (BnaC.DGAT1.a, Genbank accession No.: JN224473) was predicted by Phobius program (Käll et al., 2007) and is used to illustrate the putative functional motifs of DGAT1 (Figure 2.4). The active sites of the MBOAT superfamily are proposed to be composed of the conserved residues histidine (position 428 in BnaC.DGAT1.a, putative active site 5) and asparagine (position 391 in BnaC.DGAT1.a, putative active site 4)

(Chang et al., 2011). It has been demonstrated that the conserved histidine residue was essential for mouse DGAT1 activity (McFie et al., 2010). It has also been suggested that a conserved histidine (H) and an aspartic acid (D) in the motif HXXXXD (putative active site 2) or HXXXD (putative active site 1) might constitute the active sites in DGAT1. The HXXXXD motif was found to be necessary for the function of GPAT (PlsB) and the bifunctional enzyme 2-acyl-glycerophosphoethanolamine acyltransferase/acyl-acyl carrier protein synthetase (Aas) of *Escherichia coli* (Heath and Rock, 1998). Substitutions of the conserve histidine of PlsB and Aas or the aspartic acid of PlsB led to decreased acyltransferase activity. A similar HHXXXDG active-site motif was also found to be conserved in DGATs from prokaryotes (Daniel et al., 2004). In addition, it has been proposed that the conserved arginine (R) and glutamic acid (E) in the consensus sequence N(S/A/G)R(L/V)(I/F/A)(I/L)EN(L/V) (putative active site 3) of DGATs might have similar function to the histidine and aspartic acid residues, respectively (Jako et al., 2001). The N-terminus is the most variable region of DGAT1. The only conserved pattern of the N-terminus is the arginine cluster, which might assist in ER localization of DGAT1. It has been suggested that the N-terminus of mouse DGAT1 might be involved in the formation of dimers (active form) and tetramers (inactive form) and thus regulate DGAT1 activity (McFie et al., 2010). Many dimeric or multimeric enzymes appear to be allosterically regulated. Indeed, in *B. napus* or mouse, acyl-CoA may be an allosteric effector of DGAT1 in addition to serving as an acyl donor through the interaction of the N-terminal region of the enzyme (Siloto et al., 2008; Weselake et al., 2006). It was proposed that the region just preceding the predicted TMD1 (putative acyl-CoA binding site 1), which is the most conserved region of the N-terminus, might be a putative acyl-CoA binding site (Jako et al.,

2001). Another proposed acyl-CoA binding site (putative acyl-CoA binding site 2) includes the motif FYXDWWN, which is largely conserved among DGAT1 and ACATs (Lopes et al., 2014, 2015). Lopes et al. (2014) used a synthetic peptide of the FYXDWWN motif to analyze its interaction with acyl-CoA substrate and observed that this region appears to bind the acyl chain of the substrate. In the same study, they also demonstrated the interaction of DAG with the putative DAG binding site HXXXXRHXXXP (Lopes et al., 2014). This motif is also present in protein kinase C and diacylglycerol kinase. In addition, an ER retrieval motif was found in the C-terminus.

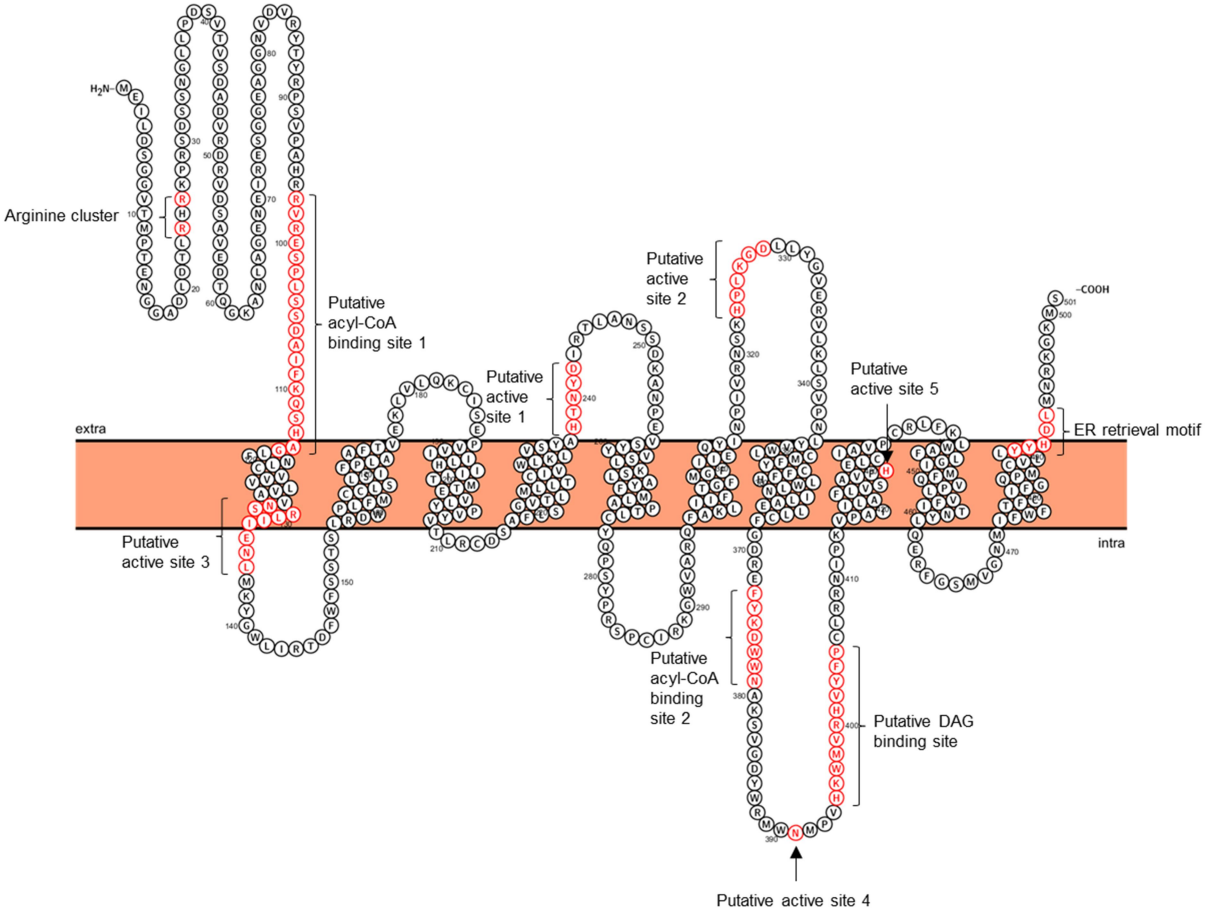

Figure 2.4. A predicted membrane topology model of DGAT1 from *Brassica napus* (BnaC.DGAT1.a, Genbank accession No.: JN224473). The predicted membrane protein topology was obtained using Protter (Omasits et al., 2014). The putative functional sites are represented by red amino acid residues. CoA, coenzyme A; DAG, diacylglycerol; ER, endoplasmic reticulum.

Distinct from DGAT1, DGAT2 is a member of the DGAT2/acyl-CoA:monoacylglycerol acyltransferase family, which also includes acyl-CoA:monoacylglycerol acyltransferases and wax synthases (McFie et al., 2010). DGAT2 proteins appear to possess fewer TMDs than DGAT1. To date, the membrane topology of DGAT2 from mouse and *S. cerevisiae* has been experimentally determined. Mouse DGAT2 was shown to contain two TMDs, where both N- and C-termini are oriented towards the cytosol (Stone et al., 2006). A limited topological analysis of tung tree DGAT2 also showed both the N- and C-termini on the cytosolic side of the ER (Shockey et al., 2006). DGAT2 from *S. cerevisiae* (ScDGAT2) has been shown to have four TMDs with both N- and C-termini residing in the cytosol (Liu et al., 2011). The membrane topology of ScDGAT2 proposed by Liu et al. (2011) and putative functional motifs are illustrated in Figure 2.5. The hydrophilic N-terminus appears to be unnecessary for maintenance of the DGAT activity. Deletion of the N-terminus of DGAT2 from *S. cerevisiae* (delete 1-33) or mouse (delete 1-55) has no effect on enzyme activity (Liu et al., 2011; Stone et al., 2009). It has been proposed that the FLXLXXXn (n=non polar amino acid) motif might be involved in neutral lipid binding in mouse DGAT2 (Stone et al., 2006). Substitution of the phenylalanine and the first leucine in mouse DGAT2 or corresponding amino acid residues in ScDGAT2 led to decreased DGAT activity (Liu et al., 2011; Stone et al., 2006). In mouse DGAT2, substitution of the second leucine residue completely abolished the DGAT activity (Stone et al., 2006). The conserved motif HPHG was proposed to represent part of the active site in mouse DGAT2 (Stone et al., 2006). Any mutagenesis in the corresponding residues in mouse DGAT2 and ScDGAT2 resulted in decreased or abolished enzyme activity, suggesting that this motif, especially the second histidine residue, is detrimental to

DGAT function (Liu et al., 2011; Stone et al., 2006). Some discrepancy has been observed, however, between the topology of mouse DGAT2 and ScDGAT2. For instance, the HPHG motif is exposed to the cytosol in mouse DGAT2 but embedded in the membrane in ScDGAT2. Similarly, LPAAT from *Thermotoga maritime* has also been suggested to position its active site inside the membrane (White et al., 2017). Furthermore, several conserved motifs, including motifs YFP, RXGFX(K/R)XAXXXGXX(L/V)VPXXXFG(E/Q) and GGXXE have been identified from DGAT2, which might be of functional importance (Liu et al., 2012). An ER retrieval motif was also found in the C-terminus of ScDGAT2 or mouse DGAT2 based on the sequence of the motif from tung tree DGAT2 (Shockey et al., 2006). Deletion of the ER retrieval motif in mouse DGAT2 had no effect on enzyme's ER localization (McFie et al., 2011).

The regulation of DGATs remains poorly understood. Available evidence indicates that DGATs can be regulated at the transcriptional level. In plants, abscisic acid insensitive 4 (ABI4) transcription factor was suggested to participate in transcriptional regulation of *DGAT1* during nitrogen deficiency (Yang et al., 2011). ABI4 was found to directly bind to the CE1-like element present in the *DGAT* promoter and thus up-regulated *DGAT* expression (Yang et al., 2011). In mammals, expression of *DGAT1* (<10-fold increase) and *DGAT2* (~200-fold increase) is up-regulated during adipogenesis, probably with the involvement of transcription factors such as CAAT/enhancer-binding protein beta or peroxisome proliferator-activated receptor gamma (Payne et al., 2007). Another transcription factor, X-box binding protein 1, was also found to regulate the expression of *DGAT2* in liver (Lee et al., 2014). The *DGAT* transcript abundance, however, was found

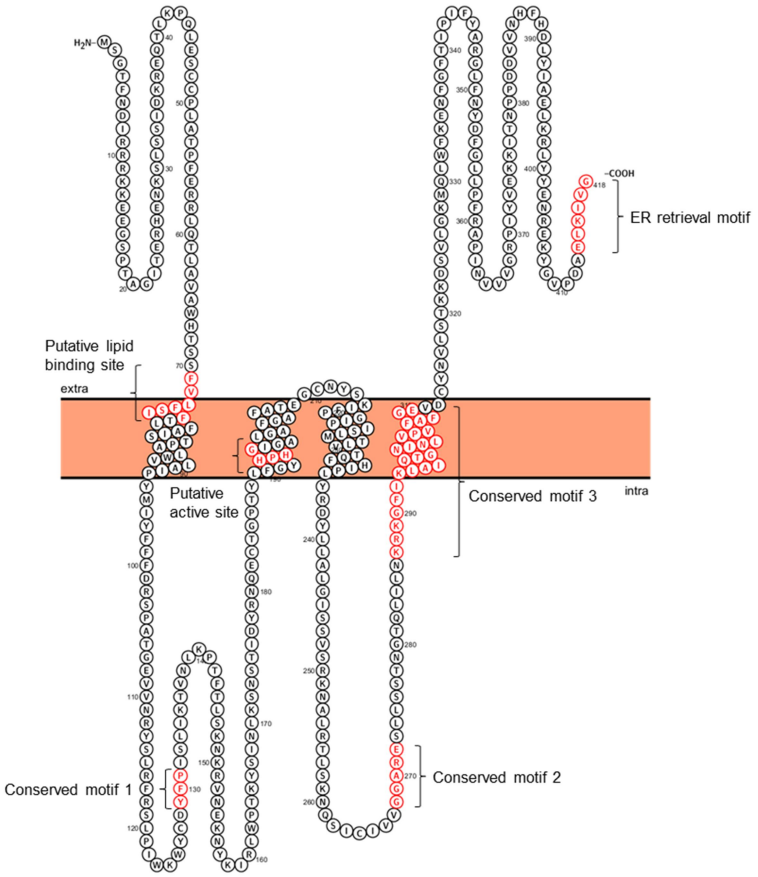

Figure 2.5. The proposed membrane topology model of DGAT2 from *Saccharomyces cerevisiae* (Genbank accession No.: NM_001183664). The membrane protein topology is adapted from Liu et al. (2011) and visualized using Protter (Omasits et al., 2014). The putative functional sites are represented red amino acid residues. ER, endoplasmic reticulum.

not to be correlated with cellular DGAT activity. For instance, *DGAT1* transcript levels and microsomal DGAT activity were not positively correlated in Arabidopsis or *B. napus* over-expressing a *DGAT1* (Jako et al., 2001; Taylor et al., 2009). A disparity between *DGAT1* expression and DGAT1 polypeptide accumulation has also been observed in developing castor seeds (He et al., 2004a) and a *B. napus DGAT1* antisense line (Lock et al., 2009). Similarly, over-expression of *DGAT1* in mouse adipocytes resulted in more than 20-fold increase in *DGAT1* mRNA, but only about 2-3-fold increase in DGAT activity (Yu et al., 2002). These results indicated that gene expression of *DGAT1* may also be regulated at the post-translational levels. DGAT1 was found to contain multiple putative phosphorylation sites (Yu et al., 2015). It has been suggested that DGAT activity in rat hepatocytes and adipose tissue can be controlled post-transcriptionally by modulating the enzyme phosphorylation state (Yen et al., 2008). Similarly, plant DGAT1 activity might also be regulated by phosphorylation. Substitution of the serine at position 197 in a putative sucrose non-fermenting-related protein kinase 1 target site in *Tropaeolum majus* DGAT1 resulted in increased DGAT activity (Xu et al., 2008a). In addition, protein ubiquitination might play a role in regulating DGAT2 stability (Brandt et al., 2016b; Choi et al., 2014).

2.3.4. Biotechnological application of diacylglycerol acyltransferases in oilseed engineering

As mentioned previously, there are two main challenges in manipulating plant oil production by oilseed biotechnology: to increase oil production and to produce oil with tailored fatty acid composition for specific applications. DGATs have been considered attractive candidates for engineering both aspects of plant oil production. Stimulating oil

accumulation in plants through the use of DGAT was first demonstrated in Arabidopsis (Jako et al., 2001) and then in oilseed crops such as canola-type *B. napus* (Taylor et al., 2009; Weselake et al., 2008), maize (Zheng et al., 2008; Oakes et al., 2011), soybean (Lardizabal et al., 2008; Roesler et al., 2016) and Camelina (Kim et al., 2016). In addition, over-expression of *DGAT* has been found to increase oil accumulation in microorganisms (Greer et al., 2015; Blazeck et al., 2014; De Bhowmick et al., 2015). DGAT can also be utilized in the production of oil with tailored fatty acid composition. Co-expression of a cDNA encoding an epoxygenase from *Stokesia laevis* with *DGAT1* or *DGAT2* from ironweed in soybean resulted in a 17.8% or 27.9% increase, respectively, in vernolic acid in the seed oil of the two transgenic lines (Li et al., 2010a, 2012a). As previously discussed, DGAT2 appears to play an important role in channeling unusual fatty acids into TAG; thus, it might represent a powerful tool in producing specialty oils. Co-expression of a cDNA encoding fatty acid hydroxylase with castor bean *DGAT2* in Arabidopsis elevated the hydroxy fatty acid content in the seed oil (Burgal et al., 2008). Similar results were observed when co-expressing *FATTY ACID HYDROXYLASE* with a cDNA encoding a ricinoleoyl selective *DGAT*2 from *Claviceps purpurea* (Mavraganis et al., 2010).

Besides over-expression of wild-type *DGAT*, a number of investigations have also been addressed in the manipulation of oil production using high performance *DGAT* variants. Due to the lack of detailed structural information for DGAT or any closely homologous proteins (Liu et al., 2012; Lopes et al., 2015), efforts to engineer DGAT enzyme performance have relied on natural selection (Zheng et al., 2008), sequence-based site-directed mutagenesis (Xu et al., 2008b) or directed evolution (Siloto et al., 2009a;

Roesler et al., 2016). A previous study in natural variation of maize oil revealed that a phenylalanine insertion in maize DGAT1-2 at position 469 was responsible for the increased enzyme activity and oil content (Zheng et al., 2008). Improved DGAT variants could potentially be generated by exploiting site-directed mutagenesis in putative enzyme regulation sites (Liu et al., 2012). Alteration of a serine residue in a putative protein kinase target site in *T. majus* DGAT1 was found to lead to enhanced enzyme activity and increased oil production in Arabidopsis (Xu et al., 2008b). The target sites for manipulating DGAT performance from natural variation and sequence-based prediction, however, are very limited and biased. In contrast, directed evolution provides a powerful approach for DGAT engineering in the absence of detailed structural information. Directed evolution has enabled the improvement in enzyme performance of DGAT1 from *B. napus* (Siloto et al., 2009a), *Corylus americana* and soybean (Roesler et al., 2016). Over-expression of performance-enhanced soybean *DGAT1* variants in soybean increased seed oil content by up 16% (relative increase) in field trials (Roesler et al., 2016).

2.4. Role of long-chain acyl-CoA synthetases in triacylglycerol biosynthesis and their properties

2.4.1. Identification of long-chain acyl-CoA synthetases

Fatty acids are required to be activated to acyl-CoAs before being utilized in various metabolic pathways, including the biosynthesis of PC, TAG, isoprenoids, sterols, cutin, suberin, jasmonate, and the oxidation of fatty acids. Activation of free fatty acids relies on the catalytic action of LACS. LACS activity was first reported in guinea pig liver by Kornberg and Pricer (1953), and later in other sources (Hongo et al., 1978; Watkins, 1997).

In the early 1990s, *LACS* genes from many species, including rat (*Rattus norvegicus*), human, *S. cerevisiae* and *E. coli* have been cloned (Black et al., 1992; Suzuki et al., 1990; Fujino and Yamamoto, 1992; Abe et al., 1992; Johnson et al., 1994b, 1994a; Duronio et al., 1992). The investigation of plant LACSs has lagged behind that of mammals, yeast and bacteria. In 2002, nine *LACS* genes (*AtLACS*s) encoding enzymes with distinct tissue distributions, subcellular locations, and biological functions were identified from Arabidopsis (Shockey et al., 2002). AtLACS6 and AtLACS7, which were shown to reside in the peroxisome, were suggested to be required for the activation of fatty acids for *β*-oxidation and successful seedling development (Fulda et al., 2002, 2004). In contrast, AtLACS1, AtLACS2 and AtLACS4 were found to localize in the ER and might be involved in the synthesis of surface lipids (Schnurr and Shockey, 2004; Lü et al., 2009; Weng et al., 2010; Jessen et al., 2011). AtLACS1 and AtLACS2 were demonstrated to have overlapping function in the biosynthesis of wax and cutin (Schnurr and Shockey, 2004; Lü et al., 2009). An Arabidopsis *lacs1 lacs2* double mutant had deficiencies in cuticular wax and cutin synthesis and thus displayed abnormal phenotypes such as organ fusion and susceptibility to drought stress (Weng et al., 2010). AtLACS1 and AtLACS4 were found to have a crucial role in the formation of pollen coat lipid in Arabidopsis (Jessen et al., 2011).

2.4.2. Role of long-chain acyl-CoA synthetases in triacylglycerol assembly

In addition to the essential functions of LACSs in plant development, it has also been suggested that LACS might be involved in TAG biosynthesis. As indicated earlier, fatty acid biosynthesis in plants primarily occurs in the plastid and the resulting fatty acids need to be exported outside of the plastid and activated to acyl-CoAs before utilized for

TAG assembly (Chapman and Ohlrogge, 2012). The presence of LACS activity in the plastidial envelope has been demonstrated since 1977 (Roughan and Slack, 1977), and then, further evidence suggested that LACS was specifically associated with the outer envelope (Andrews and Keegstra, 1983; Block et al., 1983). In Arabidopsis, AtLACS9 is the only plastid outer envelope-associated LACS and thus was considered as the most likely candidate for activating and exporting plastidially-derived fatty acids for TAG assembly (Zhao et al., 2010). Although the platidial LACS activity in the *lacs9* null mutant of Arabidopsis decreased by 90%, the mutant plant did not display any detectable phenotype, suggesting that additional LACS isoforms are involved in exporting plastidial fatty acids for TAG biosynthesis (Schnurr et al., 2002). Zhao et al. (2010) observed that a *lacs1 lacs9* double mutant resulted in a 11% decrease in fatty acid content, which indicated that ER-localized AtLACS1 might have overlapping function in TAG biosynthesis with AtLACS9 (Zhao et al., 2010). Recently, Jessen et al. (2015) found that AtLACS9 might contribute to lipid trafficking from the ER back to the plastid rather than exporting fatty acid outside of the plastid. In addition, LACS may also be involved in acyl-editing together with phospholipase A_2. As indicated previously, modified fatty acids can be released from the PC via the catalytic action of phospholipase A_2 and then enter the acyl-CoA pool for TAG assembly through the catalytic action of LACS (Lands, 1960; Bayon et al., 2015). It has been suggested that LACSs displayed distinct fatty acid specificities in different plants and diatoms producing oils enriched in unique fatty acids, revealing the possibility of the involvement of LACS in channeling modified fatty acids into TAG (Aznar-Moreno et al., 2014; He et al., 2007; Ichihara et al., 2003; Tonon et al., 2005).

2.4.3. Structural features of long-chain acyl-CoA synthetases

LACS activates fatty acids to acyl-CoAs in an ATP-dependent manner. This reaction involves a two-step reaction via a ping-pong mechanism, in which firstly an adenylyl from ATP is transferred to fatty acid forming an enzyme-bound acyl-adenylate intermediate and pyrophosphate; secondly, the acyl-adenylate intermediate is attacked by CoA yielding an acyl-CoA and AMP (Watkins, 1997). This reaction mechanism with the formation of adenylate intermediate is not exclusive to LACS but shared by a wide variety of enzymes from the adenylate-forming superfamily, to which LACS belongs (Gulick, 2009).

There are two highly conserved motifs present in the adenylate-forming enzymes, YTSGTTGXPKGV and GYGXTE, which comprise the ATP/AMP signature motif (Weimar et al., 2002). Mutations in these regions decrease or abolish the enzyme activity (Weimar et al., 2002). The crystal structure of *Mycobacterium tuberculosis* very-long-chain fatty acyl-CoA synthetase confirmed that the second motif (GYGXTE) is involved in the binding of the adenine group, whereas the first motif (YTSGTTGXPKGV) was shown to be partially disordered in the structure probably due to the absence of bound ATP (Andersson et al., 2012). All enzymes with acyl-CoA synthetase activity also contain another conserved motif, the fatty acyl-CoA synthetase (FACS) signature motif TGDxxxxxxxGxxxhx[DG]RxxxxhxxxxGxxhxxx[EK]hE (h = a hydrophobic residue), which was proposed for fatty acid binding (Watkins and Ellis, 2012). The three-dimensional structure of *Thermus thermophiles* LACS suggested that this motif may not be involved in fatty acid binding, as its fatty acid binding tunnel identified in the N-terminal

domain is formed by the residues located between the ATP/AMP signature motif and the FACS signature motif (Hisanaga et al., 2004). The crystal structure of *M. tuberculosis* very-long-chain fatty acyl-CoA synthetase, however, proposed a different fatty acid binding tunnel in the N-terminal domain, which extends from the ATP binding site to the protein surface (Watkins and Ellis, 2012). Mutation in the first conserved aspartic acid residue in the FACS signature motif of *M. tuberculosis* very-long-chain fatty acyl-CoA synthetase decreased its fatty acid binding affinity (as reflected by the K_m) by 4-fold (Khare et al., 2009), probably due to the influence of the internal surface of the fatty acid binding tunnel entrance at the ATP-binding site (Watkins and Ellis, 2012).

2.4.4. Biotechnological application of long-chain acyl-CoA synthetases in engineering of oleaginous organisms

Much attention has been focused on the application of LACS in engineering oleaginous microorganisms, such as *E. coli*, yeast and algae. As mentioned previously, LACS catalyzes the activation of free fatty acids to acyl-CoAs, which enables them to enter *β*-oxidation as well as further conversion into fatty acyl esters or reduction into derivatives like alcohols and alkanes. Due to the dual role of LACS in lipid metabolism, two main activities in modulating LACS activity with different purposes have been addressed: disrupting *LACS* to increase fatty acid production and over-expressing *LACS* to increase fatty ester, fatty alcohol, wax and TAG production.

In *E. coli*, enhanced fatty acid production was achieved by combining four genotypic changes, including deletion of *FadD* (*E. coli LACS*), overexpression of *ACCase*, and overexpression of both an endogenous thioesterase and a plant thioesterase (Lu et al.,

2008; Liu et al., 2010). In *S. cerevisiae*, the deletion of the *LACS* genes (*FAA1* and *FAA4*) enabled the yeast to secrete free fatty acids into the growth medium (Scharnewski et al., 2008). By disrupting *FAA1* and *FAA4*, the yeast was able to produce 81 mg fatty acid /L (Li et al., 2014), and the fatty acid production increased to 490 mg/L when the third *LACS* gene (*FAT1*) was disrupted together with *FAA1* and *FAA4* (Leber et al., 2015). Further combining the disruptions in *LACS* genes (*FAA1*, *FAA4* and *FAT1*) with disruptions in several genes in the *β*-oxidation pathway and overexpression of *DGAT2* (*DGA1*, belongs to *DGAT2*) and *TAG LIPASE* increased extracellular fatty acid production to 2.2 g/L (Leber et al., 2015). Secretion of fatty acids has also been observed in green algae *Chlamydomonas reinhardtii* when the *LACS* genes were disrupted (Jia et al., 2016).

Besides free fatty acids, compatible renewable fuels and chemicals such as fatty esters, fatty alcohols, waxes and TAG, are also of great value. Steen et al. (2010) reported the metabolic engineering of *E. coli* to produce renewable fuels and chemicals using combined approaches including over-expression of *LACS* (Steen et al., 2010). Over-expression of *LACS* cDNAs from diatoms (*Phaeodactylum tricornutum* or *Thalassiosira pseudonana*) and plants (Arabidopsis or *B. napus*) has been reported to facilitate fatty acids uptake and stimulate storage lipid deposition in yeast (Guo et al., 2014; Tan et al., 2014; Tonon et al., 2005; Pulsifer et al., 2012). In addition, Ford and Way (2015) used error prone PCR to modify FadD substrate specificity and generated several FadD variants with enhanced substrate specificity towards medium chain fatty acids, which provides potential candidates for the production of fuel-like compounds (alcohols and alkanes derived from medium chain fatty acids).

Chapter 3 – Different Factors Contribute to Increased Neutral Lipid Content in Yeast Producing Variants of *Brassica napus* Diacylglycerol Acyltransferase 1

3.1. Introduction

Canola-type *Brassica napus* is Canada's major oilseed crop. In 2016, canola seed production was about 18.4 million tonnes, contributing $26.7 billion in economic activity (Canola Council of Canada, 2017). A 1% absolute increase in canola seed oil content could potentially result in an additional $90 million/year for the seed oil extraction and processing industry in Canada (Canola Council of Canada, 2017). Triacylglycerol (TAG) is the predominant component of seed oil which is mainly used for food (Dyer et al., 2008). In addition, seed TAG is used in the production of biodiesel, cosmetics, surfactants, lubricants, and paints (Biermann et al., 2011). The development of strategies to increase seed oil content can benefit from a deeper understanding of TAG biosynthetic pathways.

During seed development, TAG is synthesized via acyl-CoA-dependent or acyl-CoA-independent pathways (Chapman and Ohlrogge, 2012). Diacylglycerol acyltransferase (DGAT, EC 2.3.1.20) catalyzes the acyl-CoA-dependent acylation of *sn*-1,2-diacylglycerol to produce TAG and CoA (Siloto et al., 2009a). Two forms of membrane-bound DGAT (DGAT1 and DGAT2), which essentially share no amino acid sequence homology, have been identified in eukaryotes (Lung and Weselake, 2006). In some oilseed species, the level of DGAT activity during seed development appears to have a substantial effect on the flow of carbon into seed TAG (Harwood et al., 2013). Over-expression of *DGAT1* during seed development leads to increased seed oil content in *B. napus* (Weselake et al., 2008; Taylor et al., 2009), soybean (*Glycine max*) (Lardizabal et al., 2008; Roesler et al., 2016), maize

(*Zea mays*) (Zheng et al., 2008) and Arabidopsis (*Arabidopsis thaliana*) (Misra et al., 2013). Further increase in seed oil content might be achieved by the introduction of DGAT modified through protein engineering.

DGAT, however, contains multiple transmembrane domains (TMDs), and to date, there is no three-dimensional structure available for any DGAT (Caldo et al., 2015; Liu et al., 2012). Directed evolution is a powerful approach to increase enzyme activity especially in the absence of a three-dimensional protein structure. In addition, directed evolution together with site directed mutagenesis has been useful in gaining insights into enzyme structure-function relationships (Cheng et al., 2015; Packer and Liu, 2015). Previously, we used directed evolution to successfully generate numerous *B. napus* DGAT1 (BnaDGAT1, Genbank accession No.: JN224473) variants resulting in increased TAG accumulation in *Saccharomyces cerevisiae* strain H1246 (*MATα are1-Δ::HIS3, are2-Δ::LEU2, dga1-Δ::KanMX4, lro1-Δ::TRP1 ADE2*) (Siloto et al., 2009a). Despite this, little is known about how the amino acid residue substitutions identified from directed evolution affect DGAT1 performance. A number of questions can be posed in this regard. Since no three-dimensional structures are available for any DGATs, would it bring about any interesting information if the amino acid residue substitution sites were mapped onto a predicted topological model? Is the observed increase in oil content attributable to the increased enzyme activity, increased polypeptide accumulation or both? Are the specific amino acid residue substitutions associated with the changes in the kinetic properties of the enzyme? Could the beneficial amino acid residue substitutions identified in BnaDGAT1 be used to guide the modification of another DGAT1? Moreover, these performance-enhanced

BnaDGAT1 variants were screened from the *BnaDGAT1* randomly mutagenized libraries using oleic acid as a selective agent. Since the import of fatty acids in yeast is coupled to their utilization by DGAT, could novel BnaDGAT1 variants with altered substrate specificity be identified if the mutagenized libraries were screened using other fatty acids? Indeed, lipotoxicity of *S. cerevisiae* H1246 cells in the selection medium containing medium chain fatty acids (octanoic and decanoic acids) could be rescued by expression of *Cuphea avigera* var. *pulcherrima DGAT1* which is supposed to prefer substrate containing medium chain fatty acids rather than the non-selective Arabidopsis *DGAT1* (Iskandarov et al., 2017).

To answer these questions, sequence-based analysis, extensive biochemical characterization and library screening were performed. The ninth predicted TMD (PTMD9) was found to have important effects on DGAT1 function. Three BnaDGAT1 variants (L441P, I447F and F449C) with amino acid residue substitutions in PTMD9 and one out-group variant, V125F, were chosen for characterization. These recombinant variants were characterized as having higher enzyme activity and/or exhibiting increased polypeptide accumulation in the yeast system. Possible reduced substrate inhibition also appeared to contribute to increased oil content in yeast. When the amino acid residue substitutions that led to increased enzyme performance were introduced into a recombinant *Camelina sativa* DGAT1 (CsDGAT1B, Genbank accession No.: XM_010417066), the performance of CsDGAT1B was improved. The *BnaDGAT1* mutagenized libraries were re-screened using polyunsaturated linoleic acid ($18{:}2^{\Delta 9cis,12cis}$) and α-linolenic acid ($18{:}3\Delta^{9cis,12cis,15cis}$) as

selective agents, respectively, and one variant with altered preference towards linoleoyl-CoA and α-linolenoyl- CoA was identified.

3.2. Results

3.2.1. Identification of high performance variants of BnaDGAT1

Developing insight into amino acid residues affecting BnaDGAT1 activity may be useful in probing structure-function in this enzyme. In our previous work, three libraries of BnaDGAT1 variants were created by error-prone PCR (Siloto et al., 2009a). The current study focused on 50 of the recombinant performance-enhanced BnaDGAT1 variants identified via directed evolution (Figure 3.1, Table S3.1). TAG content and fatty acid composition of the TAG of 50 *S. cerevisiae* H1246 strains hosting the BnaDGAT1 variants were further analyzed by GC/MS. All of the BnaDGAT1 variants resulted in higher TAG content when produced in yeast (Figure 3.1), but had almost no influence on the fatty acid compositions of the TAG produced (Table S3.2).

The cDNAs encoding the 50 BnaDGAT1 variants were sequenced to identify the positions of amino acid residue substitutions. A total of 104 amino acid residue substitutions at 81 sites were identified (Table S3.1). Analysis of 22 plant DGAT1s indicated that the majority of the 81 modification sites (67%) are conserved among different plant species (Table S3.3, Figure S3.1). In nature, positive selection (Darwinian selection) is a mode of natural selection by which new advantageous genetic variants sweep a population (Nielsen et al., 2007). As for a specific enzyme, positive selection can affect enzyme functional divergence (Yuan et al., 2017). Since the directed evolution approach

used in this study is an artificial selection mimicking the positive selection but toward a user-defined purpose (high activity in this case), it is interesting to identify positively selected sites in plant DGAT1 and compare them with the amino acid residue substitution sites identified in the current study. A total of 83 positively selected sites were identified and 21 of them, mainly in the less conserved N-terminus region, were included in the 81 BnaDGAT1 mutation sites (Figure S3.1). Therefore, these amino acid residue sites might play important roles in plant DGAT1s in general, in terms of molecular evolution.

Although the lack of a detailed three-dimensional structure makes it difficult to make a detailed structural interpretation of the effects of the various amino acid residue substitutions in the BnaDGAT1 variants, some interesting observations could be made by mapping the amino acid residue substitution sites onto a predicted topological model of BnaDGAT1 (Figure 3.2). It is known that different prediction algorithms vary in their prediction of membrane topology, particularly for membrane-bound O-acyltransferases (MBOAT) including DGATs (Matevossian and Resh, 2015). As shown in Table S3.4, BnaDGAT1 was predicted to possess 8 to 10 TMDs in four prediction programs. The amino acid residues in each PTMD slightly vary in different models, and the models predicted by TMHMM and SOSUI lack PTMDs 5 and 8 and PTMDs 5 and 6, respectively. The positions of most of the 81 amino acid residue substitutions in different PTMDs were similar in all four models, except the ones on PTMDs 5, 6, and 8, which have 1, 3, and 1 amino acid residue substitution sites, respectively. Here one model was chosen for further analysis (Figure 3.2). Although the amino acid residue substitution sites occurred throughout the BnaDGAT1 primary structure (Figure 3.2), topological analysis revealed

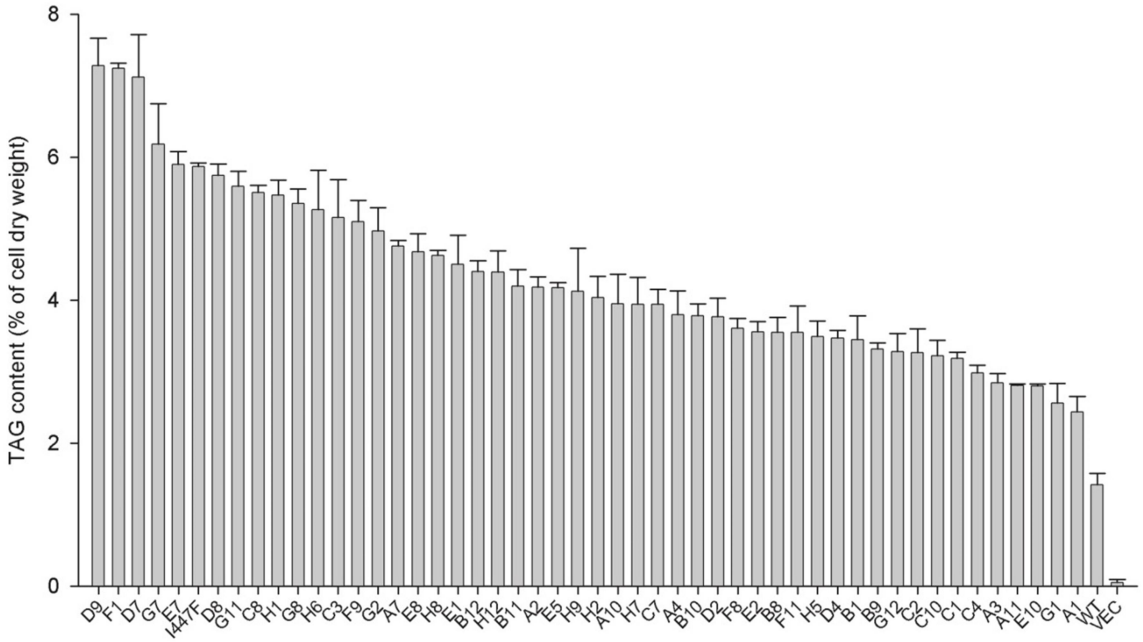

Figure 3.1. Triacylglycerol (TAG) content of yeast cells producing BnaDGAT1 variants. TAG contents (mean ± S.D.) of the yeast H1246 cells were analyzed by GC/MS. Vectors hosting mutagenized *BnaDGAT1s*, *LacZ* gene (negative control 1, VEC) and wild type (WT) *BnaDGAT1* (negative control 2, WT) were expressed in a quadruple mutant *Saccharomyces cerevisiae* strain H1246, which is devoid of TAG synthesis (Sandager *et al.*, 2002). Statistical analysis was performed using one-way ANOVA. TAG contents of all mutants were significantly higher than WT ($P < 0.01$).

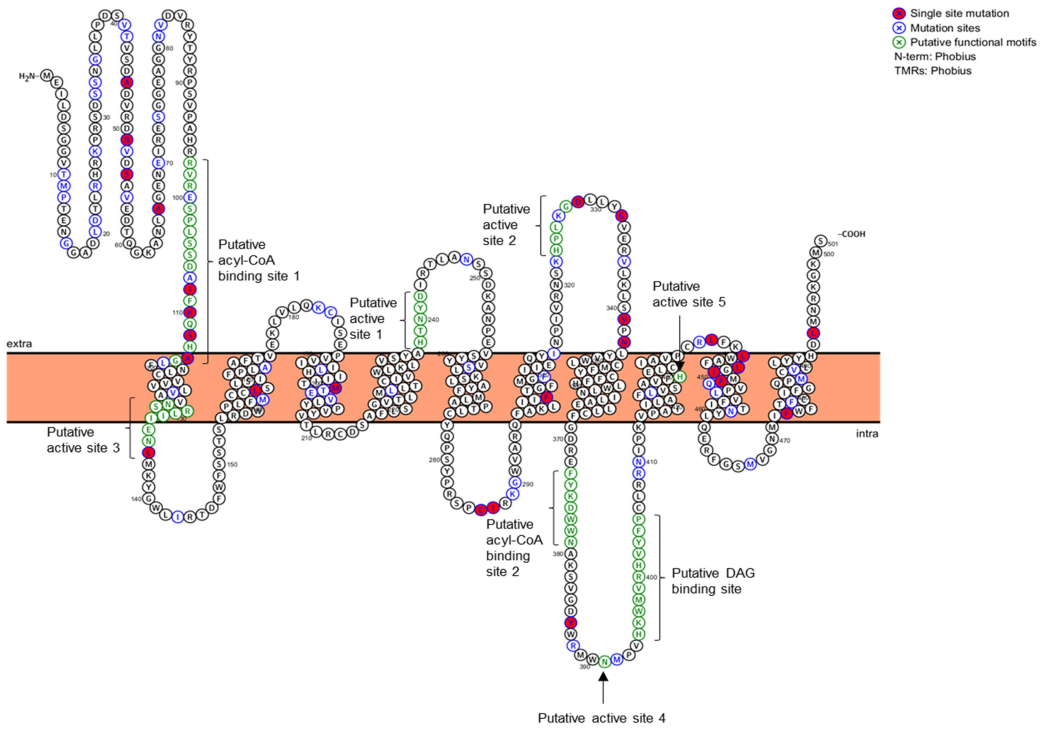

Figure 3.2. The positions of the identified amino acid residue sites on the predicted topology model of BnaDGAT1. The membrane topology of BnaDGAT1 was predicted by Protter (Omasits et al., 2014). The original amino acid sequence of BnaDGAT1 is represented by black circles. The putative functional sites are presented by green circles. The amino acid modifications selected by directed evolution are represented by blue circles. The single site modifications are represented by red-filled blue circles.

certain patterns. Among the 81 sites of amino acid residue substitution (Figure 3.2, blue circles), 24 sites (30%) were localized within the hydrophilic (residues 1 to 100) at the N-terminus, away from the first predicted TMD. Nine (residues 437 to 458) and five (residues 473 to 493) sites were identified within or close to the PTMD9 and 10 at the C-terminal, accounting for 38% and 23% of the amino acid residues of the TMDs, respectively.

3.2.2. BnaDGAT1 variants increased yeast neutral lipid content through increased activity and/or polypeptide accumulation

Previously, directed evolution of BnaDGAT1 generated numerous variants resulting in increased TAG accumulation in yeast strain H1246 (Siloto et al., 2009a, 2009b). To investigate the underlying mechanisms responsible for the increased neutral lipid content, several BnaDGAT1 variants were assessed for *in vitro* enzyme activity and protein production level. The relative levels of DGAT activity and protein accumulation varied among the variants (Figure S3.2A). When compared to the WT BnaDGAT1, the majority of the enzyme variants displayed higher activity, increased polypeptide accumulation, or higher activity combined with increased polypeptide accumulation (Figure S3.2A). Interestingly, some BnaDGAT1 variants resulted in decreased *in vitro* enzyme activity and/or decreased polypeptide accumulation even though the introduction of these variants resulted in increased TAG accumulation in yeast compared to WT BnaDGAT1 (Figure S3.2A). This might be explained by the dynamic changes in enzyme activity of BnaDGAT1 variants in yeast over their growth phase (Figure S3.2B). Based on these initial results (Figure S3.2), it was hypothesized that the increased TAG production (as reflected by increased neutral lipid production) in yeast is due to increased enzyme activity, increased

polypeptide accumulation or a combination of enzyme activation and increased polypeptide accumulation. To test this hypothesis, six BnaDGAT1 variants with widely distributed amino acid residue substitutions throughout the entire polypeptide were chosen from our previously established directed evolution library for characterization. Neutral lipid content in yeast cultures producing these variants was confirmed to be equal to or higher than yeast producing the recombinant WT enzyme by the Nile red assay (Figure 3.3A). Since the enzyme activities and protein accumulation of the BnaDGAT1 polypeptide varied during yeast growth, their production profiles were examined. The production of the variant enzymes followed a similar pattern after induction. The activity of the recombinant enzymes increased markedly during the log phase, and then decreased after reaching the stationary phase (Figure 3.3B). The highest activity of each variant occurred at the late log or early stationary phase. Significant increases in DGAT activity were observed for all variants relative to that of the WT enzyme except for K289N, which displayed relative activities over time similar to the WT enzyme (Figure 3.3C). The microsomes displaying the highest activity of each variant were analyzed for their corresponding recombinant protein accumulation (Figure 3.3D). When compared with recombinant WT BnaDGAT1, all recombinant BnaDGAT1 variants exhibited equal or higher band density with the exception of K289N. The enzyme activities were then normalized to the Western blot results and the normalized relative activity of each variant was similar to or higher than that of the WT enzyme (Figure 3.3E).

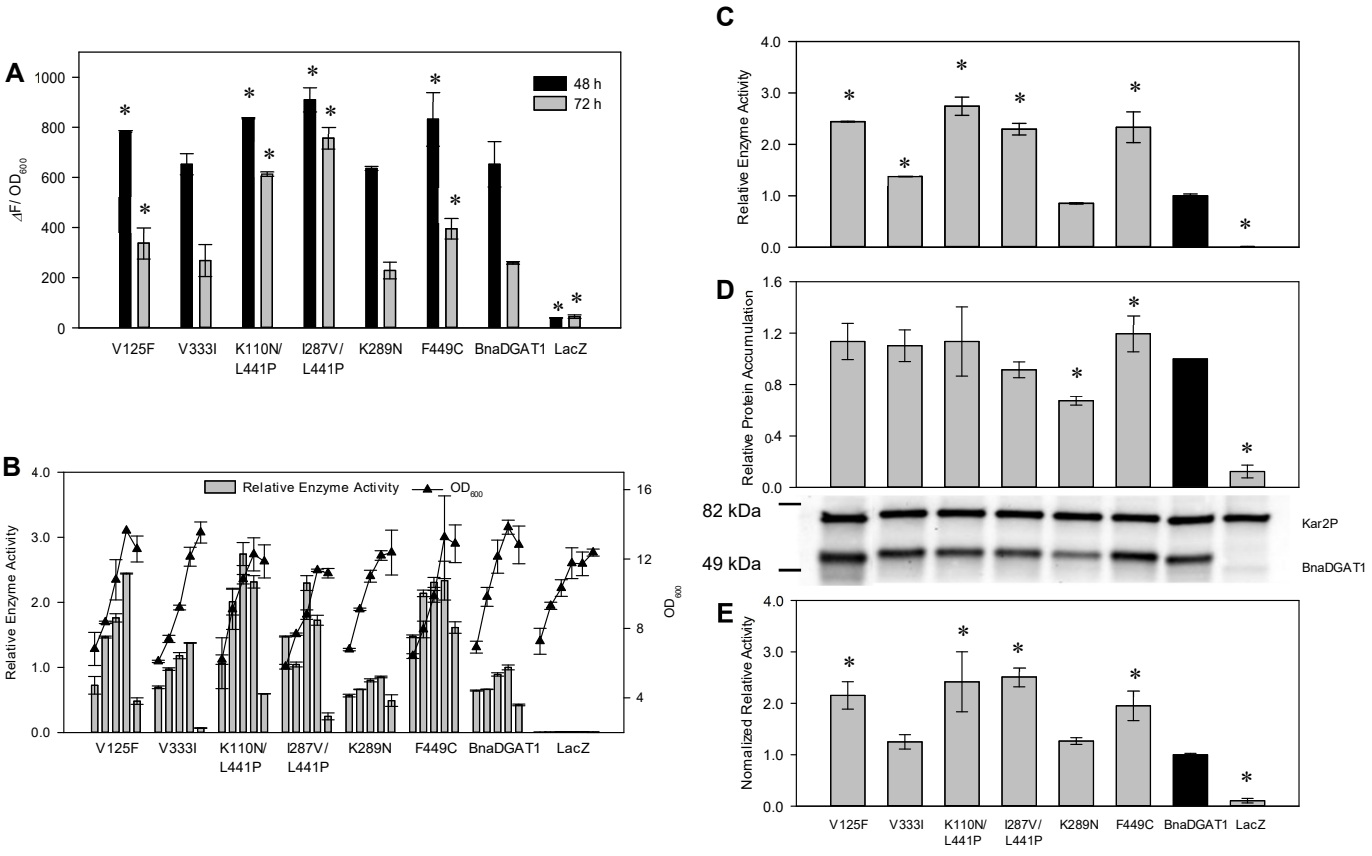

Figure 3.3. Characterization of BnaDGAT1 variants. A. Neutral lipid accumulation in yeasts transformed with different *BnaDGAT1* variants. Data are means ± range, n = 2 biological replicates. B. *In vitro* DGAT activities of different BnaDGAT1 variants. Microsomes from yeasts producing recombinant BnaDGAT1 variants were collected at different time points after induction and used for the DGAT assay. The highest microsomal activity of recombinant wild type (WT) BnaDGAT1 was set as 1.0. Growth curve was constructed by measuring OD_{600}. Data are means ± range, n = 2. C, Relative activities of BnaDGAT1 variants. The highest activity of each variant is shown, with recombinant WT BnaDGAT1 activity set as 1.0. Data are means ± range, n = 2. D, Relative protein

accumulation level of each variant. Ten μg of microsomal protein from the same batch of microsomes used to assess enzyme activity was used for Western blotting analysis. The relative polypeptide accumulation of recombinant WT BnaDGAT1 was set as 1.0. Data are means ± S.D, n = 3 to 4. E, The normalized relative activity of each enzyme variant was obtained by dividing the enzyme activity value by relative protein accumulation, with recombinant WT BnaDGAT1 activity set as 1.0. Data are means ± S.D, n = 2. The asterisks indicate significant differences in yeast neutral lipid accumulation (A), activity (C), protein accumulation (D), and normalized activity (E) of the yeast/microsomes containing recombinant BnaDGAT1 variants versus those of recombinant WT enzyme (ANOVA, LSD test) at $P < 0.05$ level.

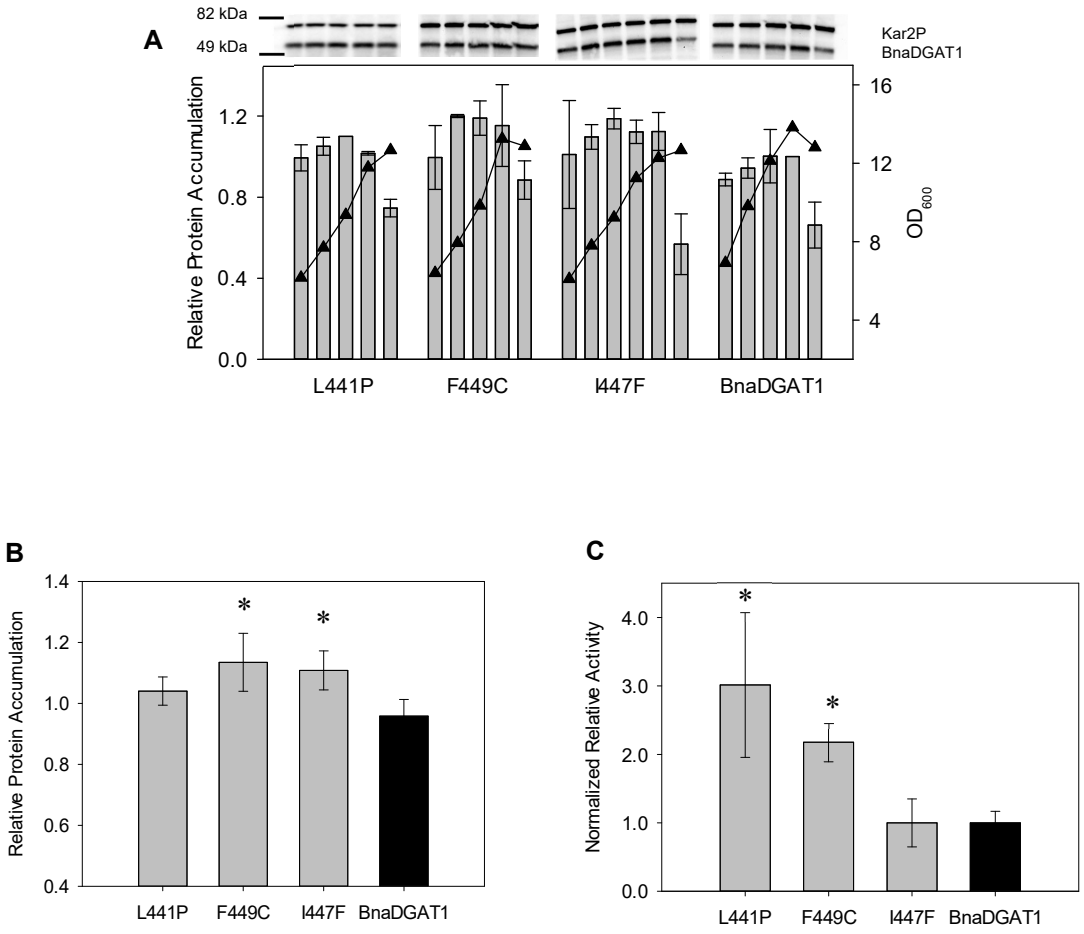

Figure 3.4. Impact of amino acid residue substitutions in the 9th predicted transmembrane domain of BnaDGAT1 on enzyme activity and accumulation in yeast. A, Production profile of (wild type) WT BnaDGAT1, variants L441P, I447F and F449C. Protein accumulation was determined by Western blotting analysis of microsomal protein of the same batch of cells harvested at different time points. The relative polypeptide accumulation of recombinant WT BnaDGAT1 from the microsomes with highest enzyme activity was set as 1.0. Growth curve was constructed by measuring OD_{600}. Data are means

± range, n = 2. B, Average protein accumulation of each variant. Data are means ± S.D. (n = 4 to 5) of variant protein accumulation in yeast microsomes at different time points. C, Normalized relative activity was calculated by dividing the activity value by the corresponding relative polypeptide accumulation, with the WT BnaDGAT1 normalized activity set as 1.0. Data are means ± S.D. (n = 4 to 5) of normalized activities for yeast microsomes at different time points. For B and C, the results for microsomes harvested at the last time point were not included. The asterisks indicate significant differences in protein accumulation (B), and normalized activity (C) of the microsomes containing recombinant BnaDGAT1 variants versus recombinant WT BnaDGAT1 (ANOVA, LSD test) at $P < 0.05$ level.

3.2.3. Impact of amino acid residue substitutions in the 9th predicted transmembrane domain on enzyme activity and accumulation in yeast

Directed evolution of BnaDGAT1 revealed that PTMD9 might contain important amino acid residue substitutions effecting on DGAT1 performance. In order to further investigate the effects of mutations in PTMD9 on enzyme activity and accumulation in yeast, three variants including L441P, I447F and F449C with amino acid residue substitutions in BnaDGAT1-PTMD9 were characterized in detail. Similar to previous results, variant L441P or I447F displayed increased enzyme activity relative to that of the WT enzyme (Figure S3.3). It is interesting to note that L441P, I447F or F449C had very different effects on enzyme activity (Figure 3.3B and S3.3) and accumulation (Figure 3.4A and 3.4B), even though all amino acid residue substitutions are located very closely in PTMD9 of BnaDGAT1. The normalized relative activity of L441P or F449C was significantly higher than that of WT BnaDGAT1. I447F, however, displayed similar normalized activity to WT enzyme (Figure 3.4C).

Altered polypeptide accumulation levels for the recombinant BnaDGAT1 variants in yeast H1246, however, might be attributable to variations in cDNA expression. DNA copy number and expression level of each *BnaDGAT1* variant were assessed by qPCR. All plasmids containing *BnaDGAT1* and its variants showed similar copy number (Figure S3.4A). Consistent with previous results (Chen et al., 2017), *BnaDGAT1* and its variants displayed high expression levels in the yeasts (Figure S3.4B) and no significant difference was observed for the selected *BnaDGAT1* variants compared to that of WT *DGAT1*.

3.2.4. Kinetic characterization of microsomal recombinant BnaDGAT1 variants

To kinetically characterize the effects of the single amino acid residue substitutions in BnaDGAT1-PTMD9, the activities of microsomal recombinant BnaDGAT1 variants (L441P, I447F, F449C and the out-group variant V125F) were examined over a range of oleoyl-CoA concentrations (Figure 3.5), which were below the critical micelle concentration of oleoyl-CoA (about 30 μM) (Faergeman and Knudsen, 1997). Variant V125F, I447F or F449C exhibited a similar enzyme activity dependence on increasing acyl donor concentration to microsomes containing the recombinant WT BnaDGAT1. DGAT1 activity increased markedly at low oleoyl-CoA concentration ranging from 0.1 to 5 μM and then the enzyme activity reduced gradually with further increases in oleoyl-CoA concentration. Variant L441P, however, displayed high activity at all oleoyl-CoA concentrations examined, suggesting that this enzyme variant may have a better tolerance for increased oleoyl-CoA concentration.

The initial reaction velocity data of BnaDGAT1 and its variants were fitted to the Michaelis-Menten or substrate inhibition equation, and the substrate inhibition kinetics was the preferred model for all these BnaDGAT1 variants (Figure 3.5A-E). The apparent kinetic parameters were calculated and are summarized in Table 3.1. Kinetic parameters are indicated as being 'apparent' because the enzyme, acyl acceptor (*sn*-1,2-diacylglycerol) and triacylglycerol product are all insoluble contributing to a potentially complex kinetic situation. Variant L441P displayed weak substrate inhibition for oleoyl-CoA, with K_i^{app} value increasing as much as 6.4-fold, compared with the WT BnaDGAT1 value of about 13.9 μM. There was also a slight increase (1.3-fold) in K_i^{app} value of variant F449C,

whereas no change in the K_i^{app} value for I447F or V125F was observed. Most microsomal recombinant BnaDGAT1 variants exhibited greater V_{max}^{app} values than the microsomal recombinant WT enzyme. After adjusting for protein abundance, the V_{max}, ^{app} values of the microsomal recombinant BnaDGAT1 variants ranged from about 1.2 to 2.4-fold greater than that of the WT BnaDGAT1 value of 6.09 nmol/min/mg microsomal protein. K_m^{app} values for the BnaDGAT1 variants were slightly higher than that of WT BnaDGAT1 with the exception of L441P. The catalytic efficiencies (V_{max}, ^{app} / K_m^{app}) of variant L441P and V125F were improved to 162% and 184%, respectively, over WT BnaDGAT1.

The N-terminal fragments of BnaA.DGAT1.b (GenBank ID: AF164434.1), another DGAT1 isoform from *B. napus*, and mouse DGAT1 (Siloto et al., 2008) were shown to bind acyl-CoA in a cooperative manner (Weselake et al., 2006). Recently, it has been reported that DGAT1s from *C. americana* and maize displayed sigmoidal kinetics in response to increasing acyl-CoA at lower concentration (Roesler et al., 2016). A closer look at the initial reaction velocities at lower oleoyl-CoA concentration (Figure 3.5 F-J) showed that microsomal recombinant WT BnaDGAT1 and its variants in fact exhibited sigmoidal kinetics.

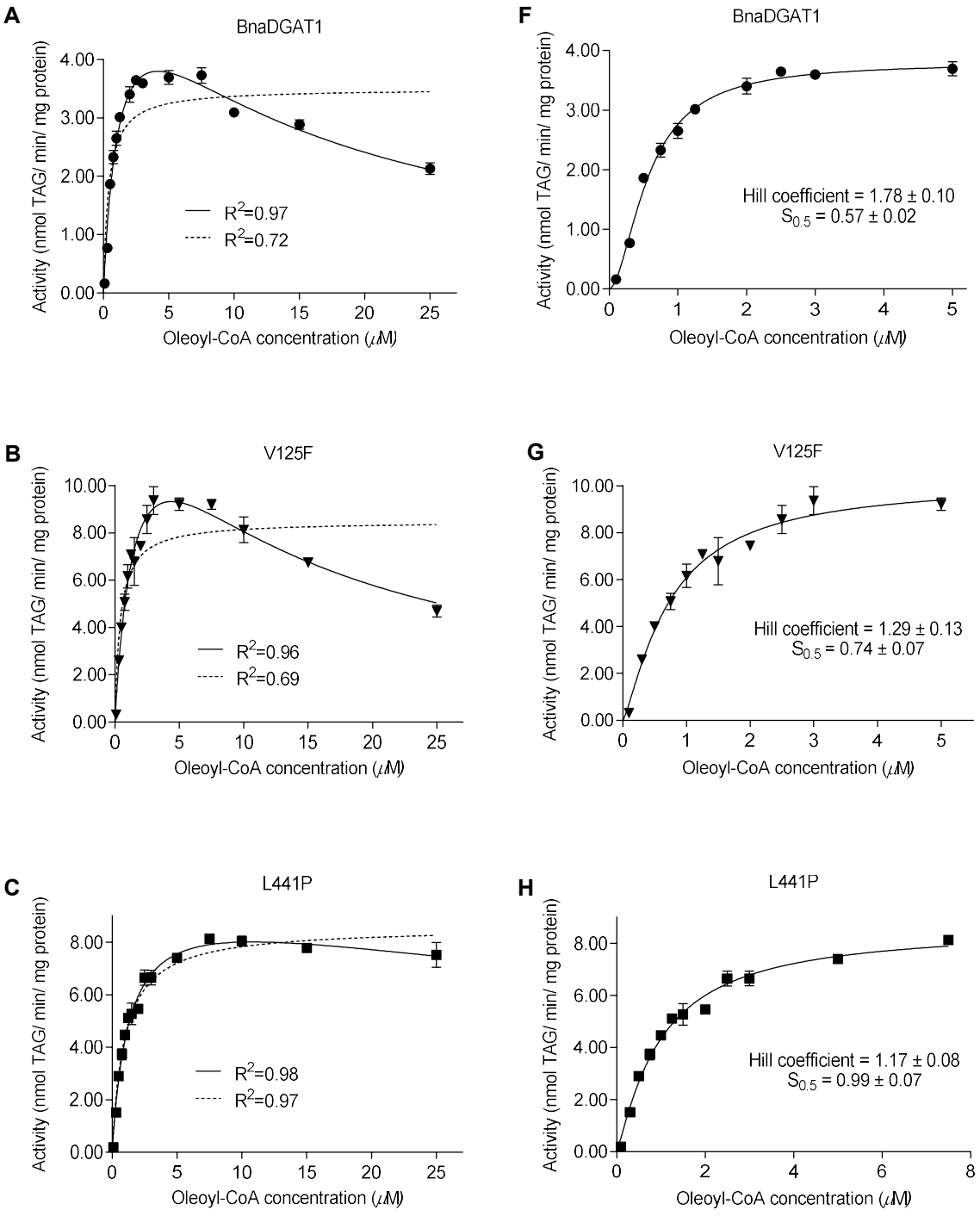
A
BnaDGAT1
Activity (nmol TAG/ min/ mg protein)
4.00
3.00
2.00
1.00
0.00
R2=0.97
R2=0.72
0
5
10
15
20
25
Oleoyl-CoA concentration (μM)
F
BnaDGAT1
Activity (nmol TAG/ min/ mg protein)
4.00
3.00
2.00
1.00
0.00
Hill coefficient = 1.78 ± 0.10
S0.5 = 0.57 ± 0.02
0
1
2
3
4
5
Oleoyl-CoA concentration (μM)
B
V125F
Activity (nmol TAG/ min/ mg protein)
10.00
8.00
6.00
4.00
2.00
0.00
R2=0.96
R2=0.69
0
5
10
15
20
25
Oleoyl-CoA concentration (μM)
G
V125F
Activity (nmol TAG/ min/ mg protein)
10.00
8.00
6.00
4.00
2.00
0.00
Hill coefficient = 1.29 ± 0.13
S0.5 = 0.74 ± 0.07
0
1
2
3
4
5
Oleoyl-CoA concentration (μM)
C
L441P
Activity (nmol TAG/ min/ mg protein)
8.00
6.00
4.00
2.00
0.00
R2=0.98
R2=0.97
0
5
10
15
20
25
Oleoyl-CoA concentration (μM)
H
L441P
Activity (nmol TAG/ min/ mg protein)
8.00
6.00
4.00
2.00
0.00
Hill coefficient = 1.17 ± 0.08
S0.5 = 0.99 ± 0.07
0
2
4
6
8
Oleoyl-CoA concentration (μM)

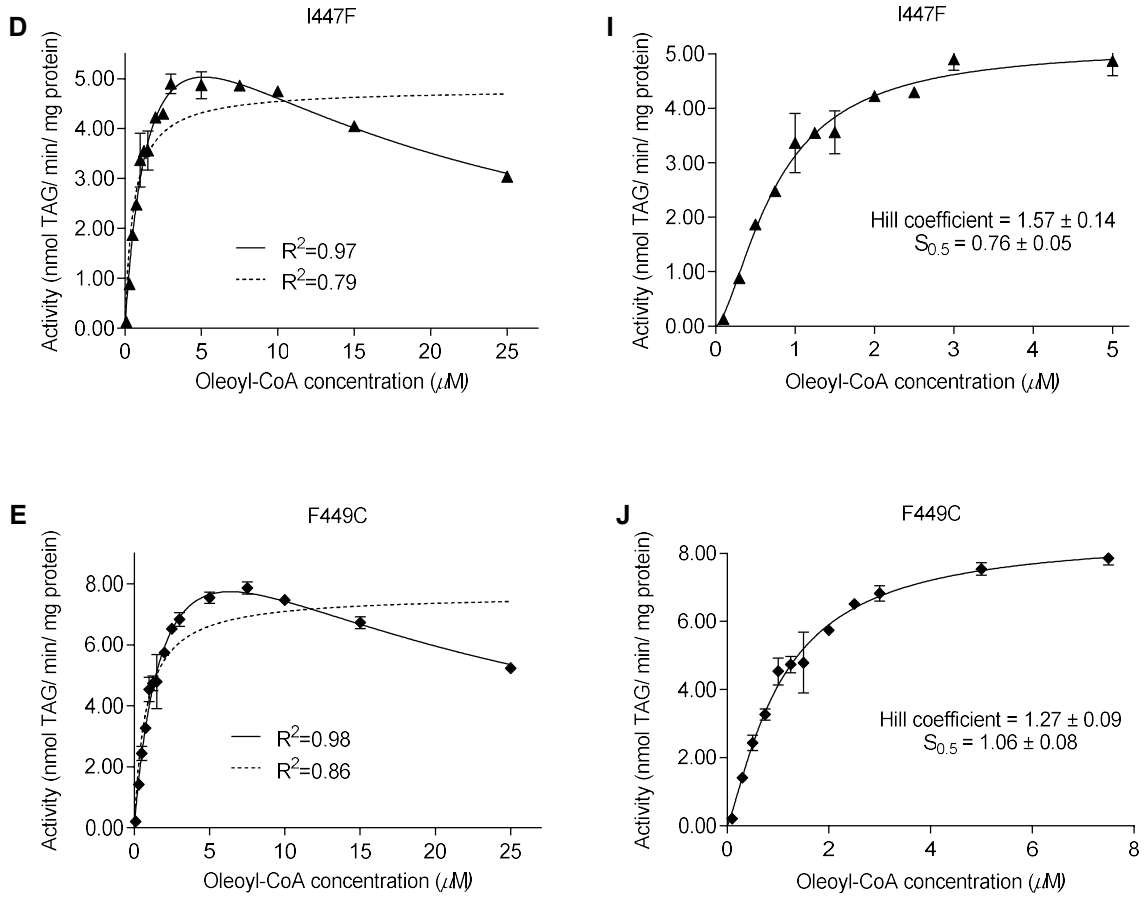

Figure 3.5. Microsomal DGAT activities of BnaDGAT1 variants at increasing oleoyl-CoA concentrations. A-E, DGAT activities of variants at oleoyl-CoA concentration from 0.1 to 25 μM. Data were fitted to a nonlinear regression using substrate inhibition (solid line) and Michaelis-Menten equation (dashed line). F-J, A closer look at BnaDGAT1 kinetics at lower oleoyl-CoA concentration from 0.1 to 5 μM for WT BnaDGAT1, V125F and I447F or from 0.1 to 7.5 μM for L441P and F449C. Data were fitted to a nonlinear regression using allosteric sigmoidal equation (solid line, R^2>0.96). Plots were generated with GraphPad Prism. Data points are means ± S.D, n = 3.

Table 3.1. Apparent kinetic parameters of BnaDGAT1 variants. Analysis was performed with GraphPad Prism software using the non-linear regression of the substrate inhibition model. Data shown are mean ± S.D, n = 3.

BnaDGAT1 variant	V_{max} ^{app} (nmol/min/mg)	K_m ^{app} (μM)	K_i ^{app} (μM)	DGAT protein abundance in microsomes (relative to BnaDGAT1)	$V_{max'}$ ^{app} adjusted for protein abundance (nmol/min/mg)	$V_{max'}$ ^{app} / K_m ^{app} (mL/min/mg)	$V_{max'}$ ^{app} / K_m ^{app} relative
BnaDGAT1	6.16 ± 0.32	1.30 ± 0.13	13.42 ± 1.61	1.00	6.16	4.74	1.00
V125F	16.67 ± 1.17	1.73 ± 0.22	11.15 ± 1.60	1.14	14.68	8.49	1.84
L441P	9.94 ± 0.32	1.31 ± 0.10	89.37 ± 18.85	1.02	9.78	7.47	1.62
I447F	8.49 ± 0.52	1.78 ± 0.20	15.00 ± 2.09	1.12	7.55	4.24	0.92
F449C	13.14 ± 0.71	2.23 ± 0.21	18.25 ± 2.33	1.15	11.39	5.11	1.11

3.2.5. Sequence alignment of the 9th predicted transmembrane domain of BnaDGAT1 among various DGAT1s

Given the fact that amino acid residue substitutions in BnaDGAT1-PTMD9 improved enzyme performance, it was hypothesized that PTMD9 would also be present in other DGAT1s. Amino acid sequence alignment of 43 DGAT1s suggested that PTMD9 of BnaDGAT1 is moderately conserved, with 59.6% sequence identity among all species and 79.2% sequence identity among DGAT1s from the plant kingdom (Figure 3.6). Different conservation levels were observed for the beneficial amino acid residue substitutions in BnaDGAT1-PTMD9, including L441P, I447F and F449C. According to the phylogenetic tree, BnaDGAT1-L441 and I447 are highly conserved among the DGAT1 from order

Rosids and land plants, respectively, whereas BnaDGAT1-F449 is more divergent. The high conservation of the beneficial amino acid residues in the predicted TMD9 suggested the possibility of modifying DGAT1 from other species by using the information obtained from BnaDGAT1.

3.2.6. Creation of high performance *Camelina sativa* DGAT1 variants

It was hypothesized that the amino acid residue substitutions resulting in the improved performance of BnaDGAT1 could be installed in DGAT1 enzymes for other oil crops. *C. sativa* is an emerging oil crop, which possesses important agronomic traits and is considered as an ideal platform for the production of oil feedstock for biofuels and industrial compounds (Bansal and Durrett, 2015). Three *C. sativa DGAT1* (*CsDGAT1A, B* and *C*) cDNAs were identified from developing *C. sativa* (cv. CAME) seeds (Kim et al., 2016). The deduced amino acid sequences of the three *CsDGAT1* cDNAs shared 98.5% sequence identity and around 85% sequence identity when compared with BnaDGAT1 (Figure S3.5). To determine whether the benefical amino acid residue substitutions in BnaDGAT1-PTMD9 also could improve a DGAT1 from another species, the corresponding substituitons of two conserved BnaDGAT1 variants (L441P and I447F) in BnaDGAT1-PTMD9 and one out-group variant V125F (in the first predicted TMD) were introduced into CsDGAT1B (I144F, L460P and I466F, Figure S3.5). As shown in Figure 3.7A, the three single CsDGAT1B variants (I144F, L460P and I466F) and a double mutant L460P/I466F were produced in yeast H1246 to determine the effects on neutral lipid content. The introduction of all four recombinant CsDGAT1B variants resulted in increased neutral lipid accumulation when compared to the effect of recombinant WT CsDGAT1B.

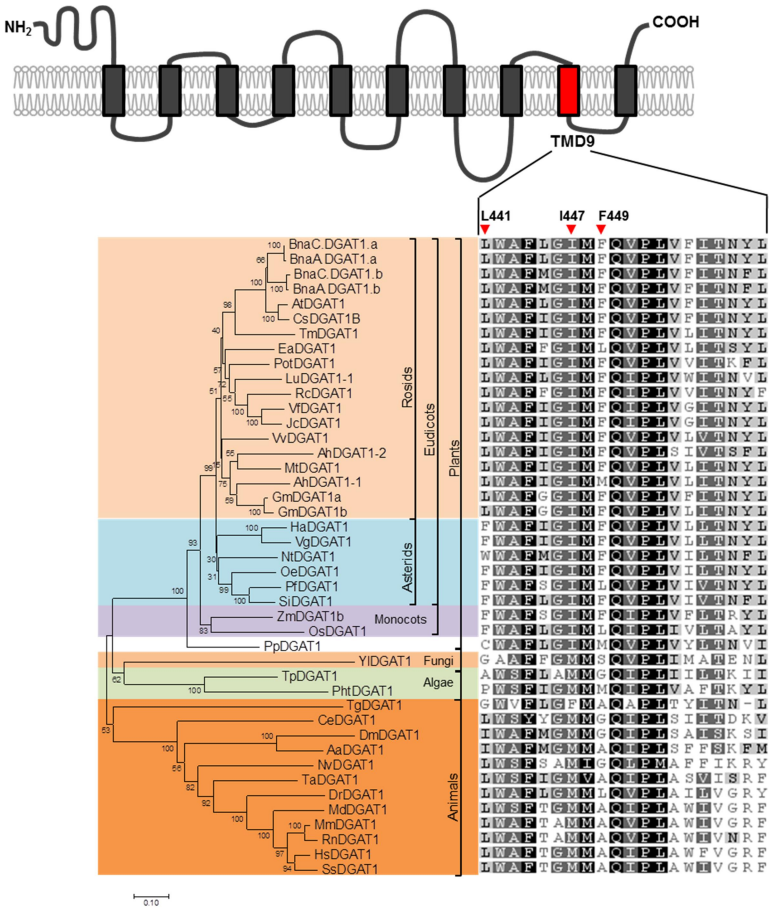

Figure 3.6. Amino acid sequence analysis of DGAT1 proteins from different species. Phylogenetic relationship among protein sequences of DGAT1 were constructed using the neighbour-joining method. Bootstrap values are shown at the tree nodes. The transmembrane domains (TMDs) of BnaDGAT1 were depicted based on the prediction by Phobius. Amino acid alignments of the 9th predicted TMD of each DGAT1 sequence are also indicated. The amino acid substitution sites of BnaDGAT1 variants are marked with red-filled triangle.

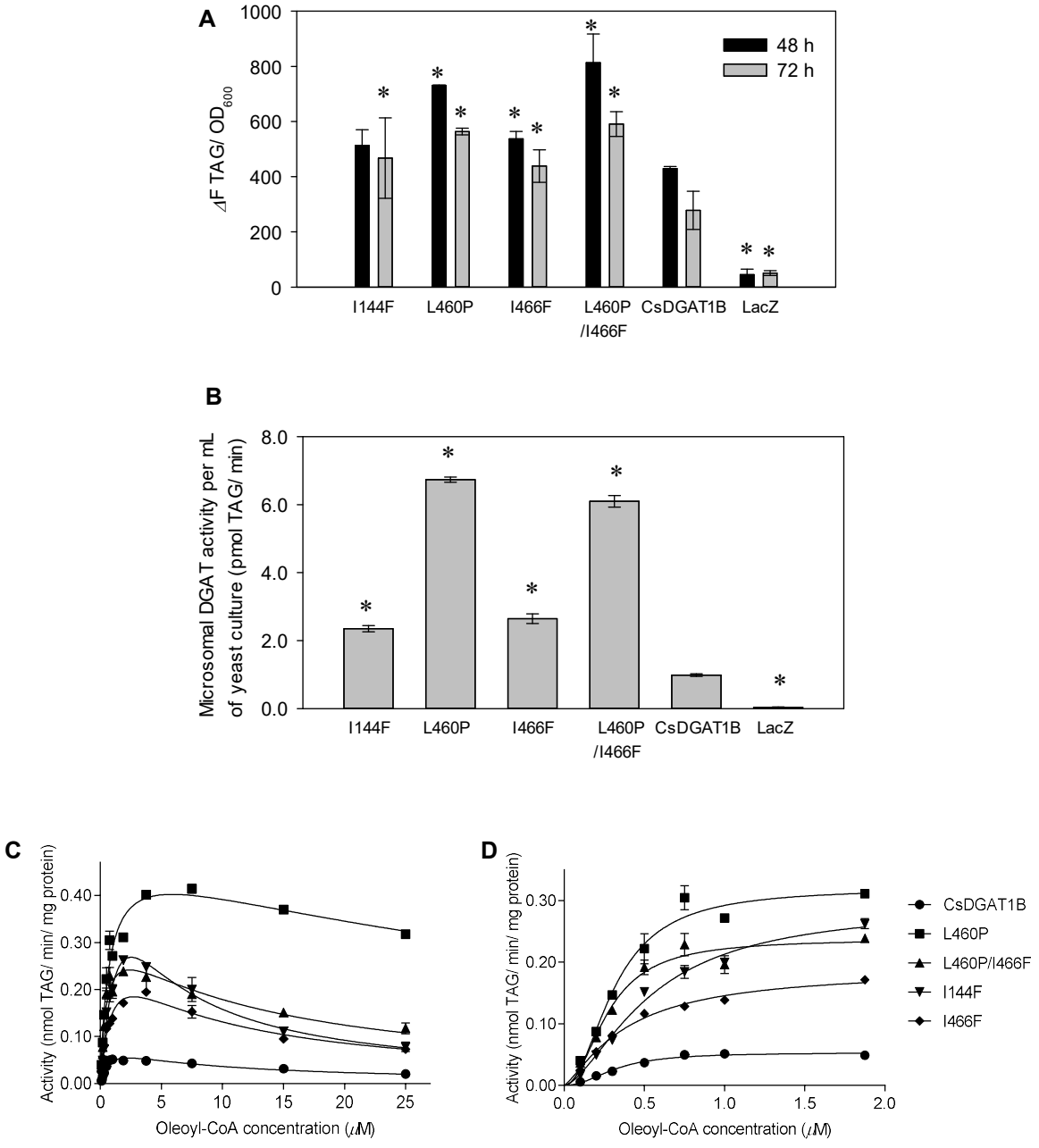

Figure 3.7. Characterization of CsDGAT1B variants. A. Neutral lipid accumulation in yeasts H1246 producing different recombinant CsDGAT1B variants. Data are means ± range, n = 2 to 3 biological replicates. B, Microsomal DGAT activities of recombinant

CsDGAT1B variants, with the recombinant wild type (WT) CsDGAT1B activity set as 1.0. Data are means ± range, n = 2. C, DGAT activities of variants at oleoyl-CoA concentrations ranging from 0.1 to 25 μM. Data are means ± S.D, n = 2 to 3. D, CsDGAT1B kinetics at oleoyl-CoA concentration from 0.1 to 1.85 μM. Data are means ± S.D, n = 2 to 3. Plots were generated with GraphPad Prism, and data were fitted to a nonlinear regression using substrate inhibition (C, R^2 between 0.91 and 0.97) or allosteric sigmoidal equation (D, R^2 between 0.96 and 0.99). The asterisks indicate significant differences in neutral lipid accumulation (A) of yeast producing recombinant CsDGAT1B variants or activity of the microsomes containing recombinant CsDGAT1B variants (B) versus the results from the recombinant WT CsDGAT1B (ANOVA, LSD test) at $P < 0.05$ level.

Table 3.2. Apparent kinetic parameters of CsDGAT1B variants. Analysis was performed with GraphPad Prism software using the non-linear regression of the substrate inhibition model. Data are means ± S.D, n = 2 to 3.

	V_{max}^{app} (nmol/min/mg)	K_m^{app} (μM)	K_i^{app} (μM)
CsDGAT1B	0.09 ± 0.01	0.76 ± 0.14	7.22 ± 1.45
I144F	0.74 ± 0.13	2.24 ± 0.53	2.88 ± 0.71
L460P	0.50 ± 0.03	0.71 ± 0.11	48.64 ± 13.39
I466F	0.32 ± 0.03	0.99 ± 0.15	7.51 ± 1.21
L460P/I466F	0.34 ± 0.03	0.50 ± 0.10	11.61 ± 2.60

Microsomal fractions containing recombinant CsDGAT1 variants were prepared from corresponding yeast cultures harvested with similar OD_{600} (about 7.5) at mid log phase and were used to determine enzyme activity. All of the variants exhibited higher DGAT activity than the WT enzyme, increasing as much as 6-fold for the most effective CsDGAT1B variants L460P and L460P/I466F (Figure 3.7B). Substrate inhibition kinetics were also observed for microsomal recombinant CsDGAT1B and the variants of CsDGAT1B (Figure 3.7C). The apparent kinetic parameters were calculated based on the substrate inhibition equation (Table 3.2). The kinetics of microsomal CsDGAT1B variants were similar to what was observed using yeast microsomes containing the corresponding recombinant BnaDGAT1 variants. All of the CsDGAT1B variants had greater V_{max}^{app} values (ranging from about 3.6 to 8.3-fold) than the V_{max}^{app} of 0.09 nmol/min/mg microsomal protein determined for the recombinant WT enzyme. V_{max}^{app} could not be adjusted by protein abundance as the V5 tag was not included in the CsDGAT1B variants. K_m^{app} values of the variants were slightly higher than that of WT CsDGAT1B, with the exception of L460P and L460P/I466F. CsDGAT1B variant L460P displayed weak substrate inhibition for oleoyl-CoA, with K_i^{app} value increasing as much as about 6.7-fold compared to the WT CsDGAT1B value of 7.22 μM. For the double mutant L460P/I466F, a 1.6-fold increase in K_i^{app} values was observed. However, I144F had a decreased K_i^{app} value (2.88 μM). A sigmoidal response of enzyme activity to increasing acyl donor concentration was also observed for microsomal recombinant WT CsDGAT1B and its variants at lower oleoyl-CoA concentrations (Figure 3.7D) with the Hill coefficient values ranged from 1.35 to 2.18. Similar to the BnaDGAT1 variants, there were no differences in

$S_{0.5}$ values based on kinetic data from microsomal recombinant WT CsDGAT1B and its variants.

3.2.7. A model which takes into consideration both sigmoidal and substrate inhibition kinetics

The observation of both sigmoidal and substrate inhibition kinetics for BnaDGAT1 and CsDGAT1B suggests that these DGAT1s are regulated by their substrates. Indeed, the classical sigmoidal (Equation 1) or substrate inhibition (Equation 2) model alone is not ideal for the prediction of the enzyme kinetics of the observed behaviours of BnaDGAT1 or CsDGAT1B. Thus, a new kinetic model (Dovala et al., 2016) which takes into account both substrate inhibition and sigmoidicity is shown in Equation 3.

$$v = \frac{V_{max} \times S^n}{S_{0.5}^n + S^n} \qquad \text{(Equation 1)}$$

Equation 1, where v represents the reaction velocity, S represents the substrate concentration, $S_{0.5}$ represents the substrate concentration resulting at 50% of V_{max}, and n represents the Hill coefficient.

$$v = \frac{V_{max} \times S}{K_m + S \times (1 + \frac{S}{K_i})} \qquad \text{(Equation 2)}$$

Equation 2, where v represents the reaction velocity, S represents the substrate concentration, K_m represents the substrate concentration resulting at 50% of V_{max}, and K_i represents the inhibition constant.

$$v = \frac{V_{max} \times S^n}{K_m^n + S^n \times (1 + \frac{S}{K_i})} \qquad \text{(Equation 3)}$$

Equation 3, where v represents the reaction velocity, S represents the substrate concentration, K_m represents the substrate concentration resulting at 50% of V_{max}, K_i represents the inhibition constant, and n represents the Hill coefficient.

This model predicts an initial lag in activity (sigmoidal) before reaching maximum activity, which is followed by a gradual reduction in activity due to the impact of substrate inhibition effect (Figure 3.8). This model resulted in a better fit for the kinetics of all DGAT1 variants (similar or slightly higher R^2 value, Table S3.5) when compared with the results obtained from the substrate inhibition model (Figure 3.5 and Figure 3.7).

3.2.8. Screening of *BnaDGAT1* mutagenized libraries using linoleic acid and *α*-linolenic acid

In order to identify novel variants with improved catalytic properties, especially with altered substrate preference, the *BnaDGAT1* mutagenized libraries were re-screened by the high-throughput screening system with a slight modification: oleic acid was replaced by linoleic acid or *α*-linolenic acid as the selective agent. Three variants were identified with increased yeast neutral lipid accumulation compared to that of WT BnaDGAT1 and their amino acid residue substitutions are shown in Table 3.3. To confirm the results, WT *BnaDGAT1* and its variants were re-cloned and transformed back into yeast strain H1246 for lipid analysis. Most of the variants were confirmed to contribute to higher oil content in H1246 yeast relative to that of WT BnaDGAT1 without affecting the fatty acid composition (Figure 3.9A and B). When linoleic acid or *α*-linolenic acid were exogenously supplemented (Figure 3.9 C and D), yeast cultures producing BnaDGAT1 variants accumulated higher amounts of TAG and corresponding linoleic acid or *α*-linolenic acid in TAG with no effects on TAG fatty acid composition (data not shown), compared to the yeast cultures producing WT BnaDGAT1.

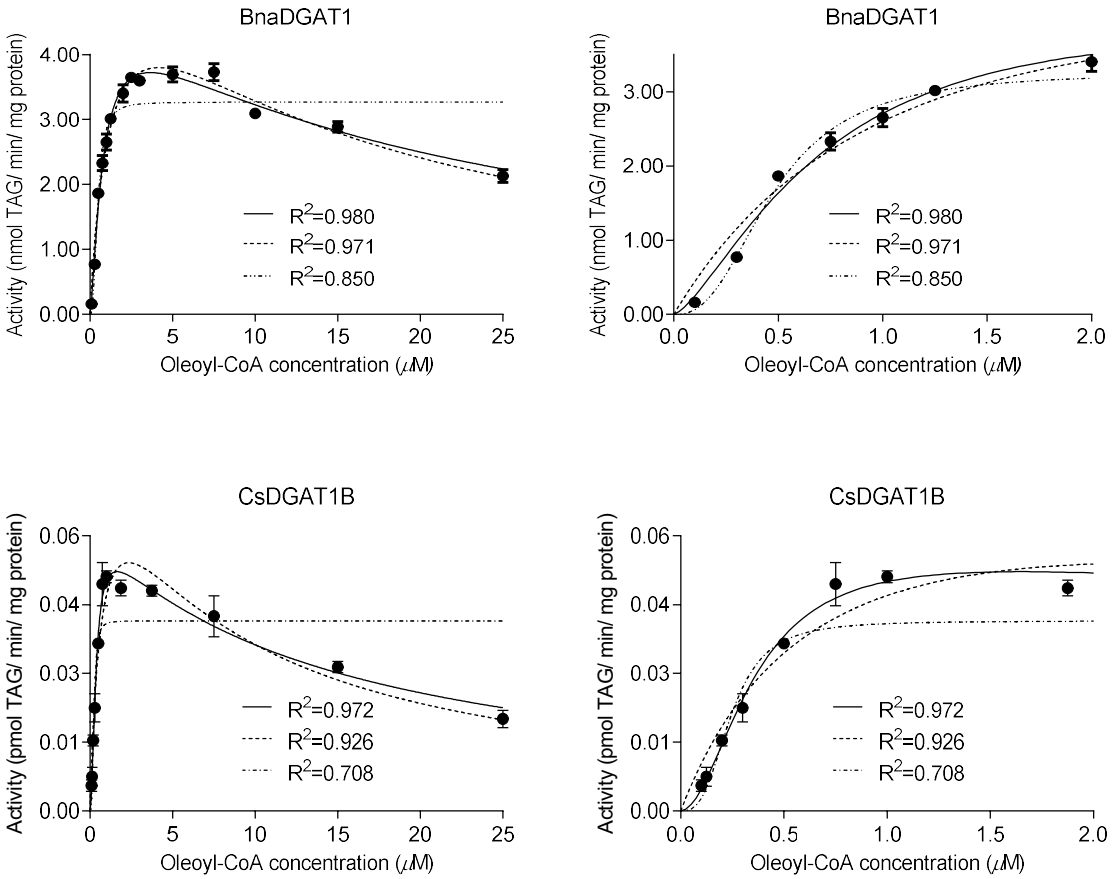

Figure 3.8. The kinetics of BnaDGAT1 and CsDGAT1B with increasing oleoyl-CoA concentration exhibit a better fit in a kinetic model which accounts for sigmoidicity and substrate inhibition. Plots were generated with GraphPad Prism, and data were fitted to a nonlinear regression using allosteric sigmoidal equation (Equation 1, dashed-dotted line), substrate inhibition (Equation 2, dashed line) or the proposed kinetic model (Equation 3, solid line).

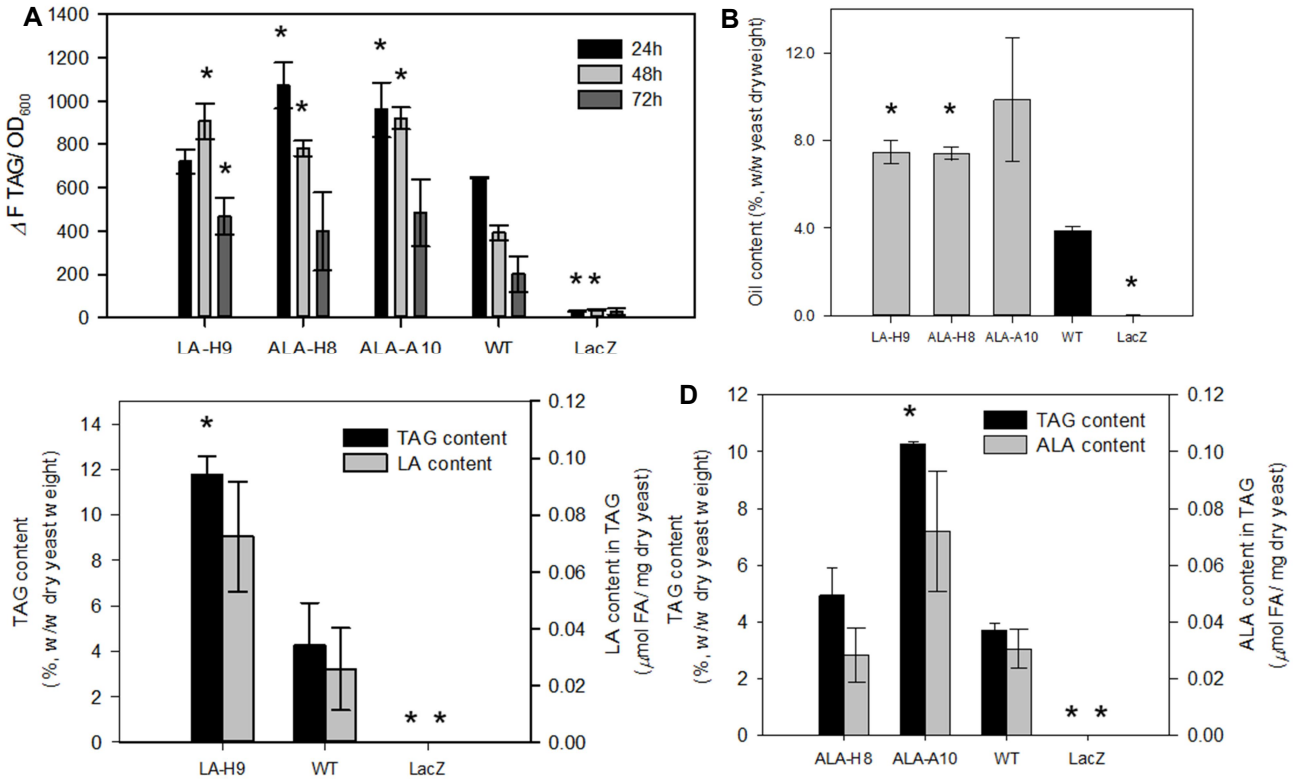

Figure 3.9. Expression of *BnaDGAT1* variants in yeast resulted in increased oil content. Neutral lipid accumulation (A) and TAG accumulation (B) in cultures expressing *BnaDGAT1* variants. TAG accumulation and amount of linoleic acid (LA) or α-linolenic acid (ALA) in TAG from the recombinant yeasts cultured in medium with 200 μM LA (C) or ALA (D). Data represent means ± range, n = 2 biological replicates. The asterisks indicate significant differences in neutral lipid content (A), TAG content (B, C and D), and fatty acid amount (C and D) from the cultures producing recombinant BnaDGAT1 variants versus recombinant wild type BnaDGAT1 (t-test) at $p < 0.05$ level.

To further evaluate the variant enzymes' performance, the microsomal activities of different BnaDGAT1 variants were analyzed *in vitro*. All of the variants exhibited higher DGAT activity than the WT enzyme (Figure 3.10A). BnaDGAT1 polypeptide accumulation was also monitored by Western blotting using the microsomal protein from the same batch of microsomes used to assess enzyme activity. As shown in Figure 3.10B, the recombinant BnaDGAT1 variants exhibited decreased band density compared with recombinant WT BnaDGAT1. Enzyme activities were then normalized by dividing the relative enzyme activity value by relative protein accumulation and the normalized relative activity of each variant was higher than that of the WT enzyme (Figure 3.10C). As suggested by the fatty acid feeding study, the recombinant BnaDGAT1 variants could efficiently utilize substrate containing linoleoyl or α-linolenoyl moieties (Figure 3.9C and D). To explore the substrate specificity of these BnaDGAT1 variants, their enzyme activities were accessed using linoleoyl-CoA and α-linolenoyl-CoA. All variants displayed higher activity towards linoleoyl-CoA and α-linolenoyl-CoA compared to the WT enzyme (Figure 3.10D). It is interesting to note that the ratio of enzyme activity towards linoleoyl-CoA versus α-linolenoyl-CoA was slightly changed for variant LA-H9 with a ratio of 1.05, whereas the ratio for the WT enzyme is about 0.65 (Figure 3.10E), indicating that variant LA-H9 might have altered preference towards linoleoyl-CoA and α-linolenoyl-CoA.

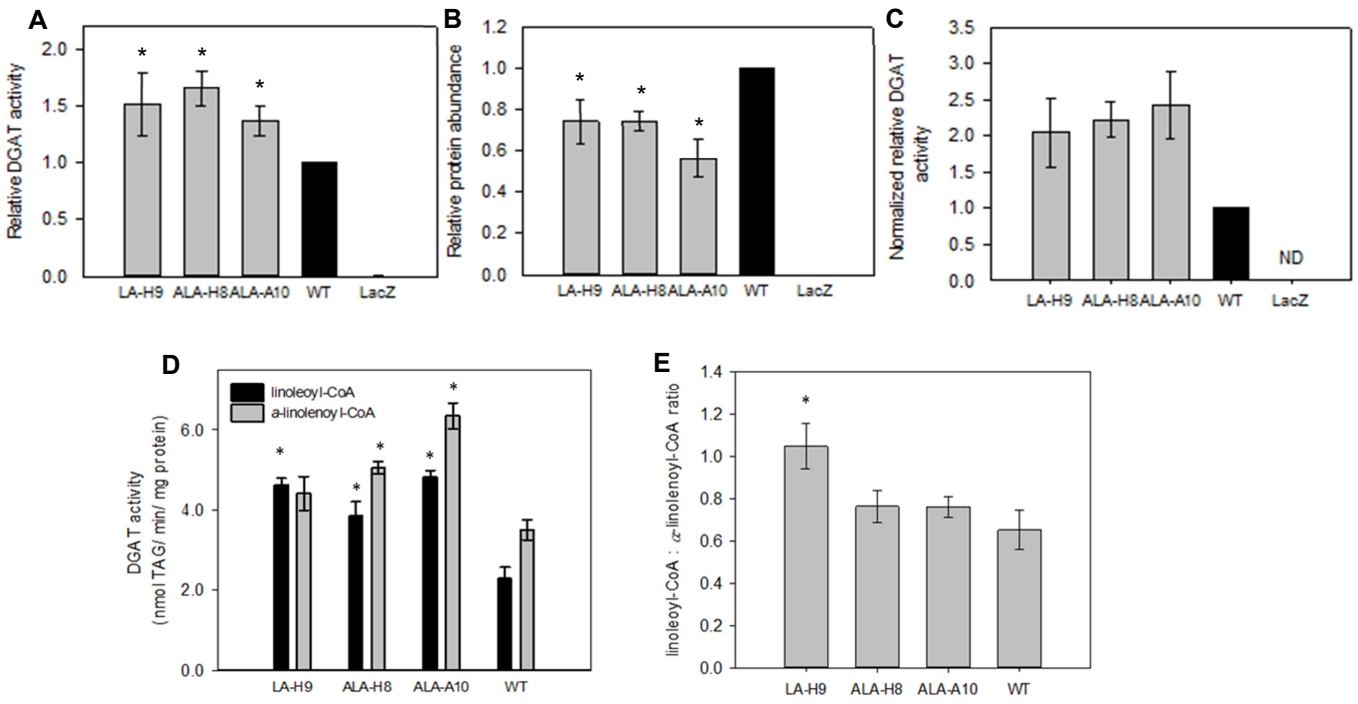

Figure 3.10. Enzyme activities and substrate specificities of microsomal recombinant BnaDGAT1 variants. A, Relative activities of BnaDGAT1 variants towards oleoyl-CoA. The wild type (WT) BnaDGAT1 activity was set as 1.0. B, Relative protein accumulation level of each variant. Protein accumulation was monitored by densitometry analysis using Image J software. The relative polypeptide accumulation of recombinant WT BnaDGAT1 was set as 1.0. C, The normalized relative activity of each enzyme variant was obtained by dividing the enzyme activity value by relative protein accumulation, with recombinant WT BnaDGAT1 activity set as 1.0. D, Enzyme activities of BnaDGAT1 variants towards linoleoyl-CoA and α-linolenoyl-CoA. E, Ratio of enzyme activities of BnaDGAT1 variants towards linoleoyl-CoA versus α-linolenoyl-CoA. For A, C, D, and E, data represent means ± S.D, n = 3. For B, data represent means ± S.D, n = 4. The asterisks indicate significant differences in activity (A and D), protein accumulation (B), and enzyme activity ratio of linoleoyl-CoA versus α-linolenoyl-CoA (E) of the microsomes containing recombinant BnaDGAT1 variants versus recombinant WT BnaDGAT1 (t-test) at $p < 0.05$ level.

Table 3.3. Screening of *BnaDGAT1* mutagenized libraries using linoleic acid or *α*-linolenic acid.

Variants	Fatty acid used to screen the libraries	Amino acid residue substitution
LA-H9	linoleic acid	D53V/L65S/V84E/L124F/K264R/L419I/F473L
ALA-H8	*α*-linolenic acid	G332S
ALA-A10		V292M/L441P

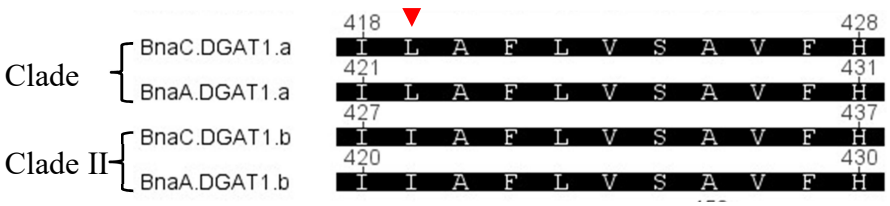

Figure 3.11. Sequence alignment of four DGAT1 proteins from *Brassica napus*. The mutation site is indicated by red-filled triangle.

3.3. Discussion

Amino acid residue substitutions in DGAT leading to enhanced activity have been reported in DGAT1s from maize (Zheng et al., 2008), *Tropaeolum majus* (Xu et al., 2008a), *Corylus americana* and soybean (Roesler et al., 2016). However, due to the absence of a three-dimensional structure of this enzyme, the exact mechanisms for the effect of the beneficial amino acid residue substitutions on DGAT function remain elusive. It has been suggested that the amino acid residues potentially affecting enzyme function may be far away from each other in the amino acid sequence (Roesler et al., 2016), but they may in fact move closely to each other to contribute to the active site after polypeptide folding.

By mapping the amino acid residue substitution sites onto a predicted topological model of BnaDGAT1, it was revealed that PTMD9 of BnaDGAT1 might contain key amino acid residues influencing the activity of the enzyme (Figure 3.2). Three BnaDGAT1 variants with amino acid residue substitutions in PTMD9 (L441P, I447F or F449C) and one out-group variant V125F were characterized in detail by analyzing their enzyme activities, production levels and enzyme kinetics. As shown in Figure 3.3, 3.4 and S3.3, BnaDGAT1 variants were found to boost neutral lipid production in the yeast transformants for different reasons. The amino acid residue substitutions affected BnaDGAT1 activity and/or polypeptide production. Variant L441P exhibited increased activity whereas variant I447F accumulated to higher levels than WT BnaDGAT1. In contrast, variant F449C exhibited both increased enzyme activity and polypeptide accumulation. These differences occurred despite the fact that amino acid residues 441, 447 and 449 were in close proximity in PTMD9. It should be noted that the increased enzyme activity for these variants during the

log phase was not tightly associated with changes in the level of polypeptide accumulation (Fig. 2). Since the DGAT assay was conducted using yeast 4 delta microsomal fractions, it is possible that the measured enzyme activity was affected by variations in the endogenous DAG content of the microsomes even though a relatively high amount of exogenous DAG was added to the reaction mixture.

The increased BnaDGAT1 polypeptide accumulation observed for variant I447F and F449C (Figure 3.3 and 3.4) may be related to enhanced protein synthesis and/or the increased cellular stability of the variant polypeptide. The expression of WT *BnaDGAT1* and its variants may also be controlled by transcriptional regulation. Even though expression and plasmid copy number of WT *BnaDGAT1* and that of its variants in yeast were at similar levels (Figure S3.4), we still cannot completely rule out the possibility of variations in cDNA expression affecting polypeptide accumulation levels, especially considering the *BnaDGAT1* variants were carried by a high copy plasmid and expressed under the control of the strong *Gal1* promoter. For BnaDGAT1 variants with increased activity (e.g., L441P), in addition to contributing to a more favourable conformation in support of catalysis, it is also possible that the increased enzyme activity may be related to an altered interaction with a hypothetical modulator. Indeed, certain protein partners and modulatory molecules have been shown to be required for DGAT function (Jin et al., 2014; Gidda et al., 2011; Xu et al., 2012; Man et al., 2006; Liu et al., 2012). It is also known that DGATs can be regulated at post-translational level via phosphorylation and/or ubiquitination (Brandt et al., 2016a; Xu et al., 2008a). Putative phosphorylation and ubiquitination sites in BnaDGAT1 were predicted by NetPhosK (Blom et al., 2004) and

UnPred (Radivojac et al., 2010), respectively, and among the selected variants only residue K110 is identified to be related to ubiquitination. No differences in protein accumulation were observed, however, between variant K110N/L441P and L441P (data not shown). It should also be noted that SDS-PAGE and subsequent western blotting of microsomal proteins, prepared from yeast cells harvested at different culture times, did not reveal additional polypeptide fragments lower in molecular mass than full length BnaDGAT1 (or the variants examined) suggesting that the enzyme was subject to little or no proteolysis. Nonetheless, it would be worthwhile to conduct a comprehensive study on the effects of amino acid residue substitutions on the protein stability of the BnaDGAT1 variants.

The enzyme kinetics of BnaDGAT1 were also affected by amino acid residue substitutions in PTMD9. When enzyme activity was determined at increasing acyl-CoA concentration, an eventual decrease in enzyme activity was observed for variant V125F, I447F, F449C, or WT BnaDGAT1 (Figure 3.5A, B, D, E). This might be explained by the effect of substrate inhibition. Previously, many acyl-CoA-dependent enzymes (Cao et al., 2003; Soupene et al., 2008, 2015; Bafor et al., 1990; Ruiz-López et al., 2010; Salas et al., 2014), including DGATs (Stöveken et al., 2005; Chung et al., 2006; Ganji et al., 2004), have been found to be inhibited at relatively high concentrations of acyl donor. It is interesting to note that L441P displayed high activity at all oleoyl-CoA concentrations examined (Figure 3.5C), suggesting that this enzyme variant may have a better tolerance of increasing oleoyl-CoA. An eventual decrease (to around 45% of the activity at 15 μM oleoyl-CoA) in enzyme activity, however, was observed for L441P with further increase in oleoyl-CoA concentration to 60 μM (data not shown). The formation of acyl-CoA micelles

(Little et al., 1994) and the inhibition of enzyme activity by detergent effect of acyl-CoA (Stöveken et al., 2005) might occur at such high concentration, together with substrate inhibition resulting in the final decrease in enzyme activity. In other examples, the removal of substrate inhibition led to a concomitant decrease in enzyme activity and/or increase in K_m value (Ziegler et al., 2009). Compared with WT BnaDGAT1, variant L441P displayed weak substrate inhibition accompanied by increased activity and similar K_m value (Table 3.1). Variant L441P may be particularly useful for increasing seed oil content when combined with a strategy for increasing the concentration of the acyl-CoA pool.

The beneficial amino acid residue substitutions in BnaDGAT1-PTMD9 are conserved among various species (L441 and I447, Figure 3.6), suggesting that the knowledge generated from BnaDGAT1 variants might be transferred to other DGAT1s. Introducing the equivalent amino acid residue substitutions into CsDGAT1B resulted in enhanced neutral lipid accumulation in yeast H1246 (Figure 3.7A), which may be explained by the increased performance of the CsDGAT1B variants relative to that of WT CsDGAT1B (Figure 3.7B). CsDGAT1B and its variants were found to exhibit substrate inhibition kinetics (Figure 3.7C) and more importantly, CsDGAT1B variant L460P (Table 3.2) also displayed the improved catalytic properties (decreased substrate inhibition and increased enzyme activity). Together, the similarity in enzyme activity effects and kinetics between BnaDGAT1 variants and the corresponding CsDGAT1B variants demonstrated that the beneficial amino acid residue substitutions in BnaDGAT1 could be transferred to a DGAT1 from another plant species.

Sigmoidal kinetics for BnaDGAT1, CsDGAT1B and their variants were observed at lower oleoyl-CoA concentrations (Figure 3.5F-J and Figure 3.7D). The observed sigmoidal kinetics is consistent with a recent investigation of the allosteric properties of WT BnaDGAT1 (Caldo et al., 2017). In addition, Roesler et al. (2016) reported the sigmoidal kinetics for DGAT1s from *C. americana* and maize when varying the oleoyl-CoA concentration (0.1-5 μM for *C. americana* DGAT1 and 1-10 μM for maize DGAT1). The investigators modified *C. americana* DGAT1 by DNA shuffling and identified nine kinetically improved *C. americana* DGAT1 variants with increased substrate affinity and/or cooperativity (Roesler et al., 2016). However, unlike Roesler et al. (2016), the current study did not identify any trends in $S_{0.5}$ or Hill coefficient values for the BnaDGAT1 (or CsDGAT1B) variants compared with WT BnaDGAT1 (or CsDGAT1B). This discrepancy might be explained by the difference in the degree of modification of the DGAT1 sequence. In our study, error-prone PCR was used to introduce mutations and by controlling the reaction conditions, the mean number of amino acid residue substitutions was estimated to be less than 3.8 in the resulting BnaDGAT1 variants (Siloto et al., 2009a). The BnaDGAT1 and CsDGAT1B variants examined only contained one or two amino acid residue substitutions. These very limited changes in amino acid sequence may not have resulted in large changes in enzyme conformation. In contrast, the *C. americana* DGAT1 variants generated by Roesler et al. (2016) contained 6 to 17 amino acid residue substitutions, probably resulting in more extensive effects on enzyme conformation and subsequent impacts on kinetic parameters. In addition, it would be useful to purify the most interesting BnaDGAT1 variants for additional kinetic studies under conditions where the variants are not potentially influenced by other proteins in the microsomes.

The combined substrate activation and inhibition kinetics observed for the WT plant DGAT1s and the variants might be explained by the presence of more than one acyl-CoA binding sites in the enzyme. Sigmoidal kinetics suggest that there is a cooperative effect when more than one substrate molecule bind to an allosteric enzyme (Cohen, 2014). In addition to the proposed acyl-CoA binding motif FYXDWWN in the hydrophobic segment (Lopes et al., 2014), the hydrophilic N-terminus domain has been shown to associate with acyl-CoA via an allosteric interaction (Caldo et al., 2017; Liu et al., 2012; Siloto et al., 2008; Weselake et al., 2006). Substrate inhibition could potentially arise when two substrate molecules bind to the enzyme to form a catalytically inactive ES2 complex by blocking second substrate binding (Dovala et al., 2016) or product release (Szegletes et al., 1999), or when the substrate binding leads to the formation of less thermodynamically favoured ES complex that turns over slowly (Liao et al., 2016; Efimov et al., 2012; Elamin et al., 2011). In this study, it is hypothesized that the substrate inhibition of plant DGAT1 is caused by the formation of ES2 complex. This assumption is supported by the decrease in substrate inhibition observed when replacing the bulky aliphatic Leu 441 in BnaDGAT1, or Leu 460 in CsDGAT1B with Pro (Figure 3.5 and 3.7), which might disturb the further binding of acyl-CoA to ES complex. It should be noted that the inhibition of DGAT activity observed at higher concentrations of acyl-CoA probably does not involve the allosteric acyl-CoA binding site in the hydrophilic N-terminal domain of BnaDGAT1 since a truncation of BnaDGAT1, devoid of the hydrophilic N-terminal domain, also displayed substrate inhibition (Caldo et al., 2017). Detailed structural information will be necessary to gain more insight into how the amino acid residue substitutions in BnaDGAT1 contribute to changes in the degree of substrate inhibition.

Despite that, the exact mechanisms of the newly identified BnaDGAT1 variants using LA or ALA remain unclear; some interesting observations were found when comparing them with the previous screening results. It turns out that the amino acid residue substitutions of these variants are novel (Table 3.3), but many of the mutation sites, including F473, G332 and L441, have been revealed before. It indicates that DGAT sequence may contain "hot spot" positions, which are crucial for enzyme performance. It would be interesting to see the combination effects of these "hot spot" mutations on DGAT. Consistent results in both *in vivo* and *in vitro* experiments suggested that the BnaDGAT1 variants resulted in an increase in yeast oil content (Figure 3.9) might be mainly caused by the increased enzyme activity (Figure 3.10 A, B, and C) rather than the modified substrate preference (Figure 3.10 D and E). Intriguingly, variant LA-H9 was observed to display an enhanced preference for linoleoyl-CoA (Figure 3.10 D and E). Variant LA-H9, however, contains multiple amino acid residue substitutions (D53V/L65S/V84E/L124F/K264R/L419I/F473L); thus it is hard to say whether the altered substrate preference is attributed to a single amino acid residue substitution or all of these amino acid substitutions might contribute together. It has been suggested previously that four *DGAT1* genes from *B. napus* diverged into two clades with different substrate preference, even though they share high amino acid pairwise identify (91.0%) (Greer et al., 2015, 2016). The clade II enzymes (BnaA.DGAT1.b and BnaC.DGAT1.b) displayed enhanced preference for linoleoyl-CoA (Greer et al., 2016). Based on the sequence alignment of the four BnaDGAT1s, almost all the amino acid residue substitution sites in variant LA-H9 are identical in enzymes from both clades, with the only exception of L419. L419 is present in the clade I enzymes, whereas the clade II enzymes have an I at that

position, which is exactly the same to the amino acid residue substitution (L419I) in variant LA-H9 (Figure 3.11). Moreover, position 419 is just after the putative acyl-CoA binding site and putative DAG binding site. Thus, it would be interesting to further analyze the substrate preference of the single mutant L419I in the future.

In conclusion, the results of this study suggested that the beneficial amino acid residue substitutions in BnaDGAT1-PTMD9 led to enhanced enzyme performance in yeast via different mechanisms. The increased TAG accumulation in yeast producing these variants was due to the variant enzymes with increased enzyme activity, increased protein accumulation and/or reduced substrate inhibition. It was also demonstrated that the beneficial amino acid residue substitutions in a DGAT1 from one species improved a DGAT1 from another species, which points out the possibility of systematically engineering of DGAT1 by taking the advantage of the amino acid residue substitution database generated based on the BnaDGAT1 variants. Selection for high performance variants of BnaDGAT1 using different fatty acids suggests that it is also possible to use directed evolution to produce enzyme variants with altered substrate specificity. The fact that a single amino acid residue substitution can lead to an improved DGAT1 suggests that non-transgenic approaches such as Targeting-Induced Local Lesions IN Genomes (TILLING) (Till et al., 2006) or clustered regularly interspaced short palindromic repeats (CRISPR) (Belhaj et al., 2013) may represent useful methods for improving DGAT action *in planta*. Indeed, genome editing has recently been used to introduce loss-of-function mutations into *DGAT1* and *PHOSPHOLIPID:DIACYLGLYCEROL ACYLTRANSFERASE*

genes in *C. sativa*, thereby leading to a reduction in seed TAG content (Aznar-Moreno and Durrett, 2017).

3.4. Experimental procedures

3.4.1. Construct preparation, yeast transformation and heterologous expression of *DGAT1* variants

BnaDGAT1 variants together with wild type (WT) *BnaDGAT1* were re-cloned into the pYES2.1/V5-His TOPO yeast expression vector (Invitrogen, Burlington, ON, Canada), under the control of the galactose-inducible *GAL1* promoter. The stop codon of each gene was eliminated from the sequences for in-frame fusion with a C-terminal V5 tag encoded on the pYES2.1/V5-His TOPO vector. The *CsDGAT1* variants were chemically synthesized by Invitrogen and inserted into the pYES2.1 vector.

After the integrity of all constructs was confirmed by sequencing, they were transformed into the quadruple mutant strain *S. cerevisiae* H1246 (kindly provided by Dr. Sten Stymne of the Swedish University of Agricultural Science) using an *S.c.* EasyComp Transformation Kit (Invitrogen). Yeast transformed with *pYES-LacZ* was used as a control. The recombinant yeast cells were first grown in liquid minimal medium (0.67% (w/v) yeast nitrogen base and 0.2 % (w/v) SC-Ura) with 2% (w/v) raffinose for 24 h. An aliquot of the yeast cell culture (at a starting optical density of 0.4 at 600 nm; OD_{600}) was used to inoculate minimal medium containing 2% (w/v) galactose and 1% (w/v) raffinose (referred as induction medium). Cultures for all experiments were grown at 30^{o}C with shaking at 220 rpm. In order to generate time-course production profiles for the various BnaDGAT1

variants, cells were harvested by centrifugation (at 3000 g for 5 min at 4°C) every 2 h starting at the OD_{600} of 5 until the stationary growth phase.

3.4.2. Rescreening of *BnaDGAT1* mutagenized libraries using linoleic acid or α-linolenic acid

The previously generated *BnaDGAT1* mutagenized libraries (Siloto et al., 2009a) were re-screened by a high-throughput screening system (Siloto et al., 2009a) with linoleic acid or α-linolenic acid. In brief, the yeast strain H1246 expressing randomly mutagenized *BnaDGAT1* genes was cultivated on solid minimal medium (0.67% (w/v) yeast nitrogen base and 0.2 % (w/v) SC-Ura) with 2% (w/v) galactose and 1% (w/v) raffinose supplemented with 1 mM linoleic acid or α-linolenic acid. Linoleic acid or α-linolenic acid was first dissolved in ethanol at 0.5 M, and then mixed with warm induction medium containing 0.1% (v/v) tyloxapol and 2% agar immediately before plating. After incubation at 30°C for 2-3 days, the positive colonies were transferred to induction medium with the presence of 200 μM linoleic acid or α-linolenic acid in the wells of 96-well microplates and cultivated at 30°C to the stationary phase. Fatty acids were dissolved in ethanol at 0.5 M first and then mixed with induction medium containing 0.1% (v/v) tyloxapol. For the feeding experiment, recombinant yeasts were induced in induction medium with supplementation of 200 μM linoleic acid or α-linolenic acid.

3.4.3. Analysis of lipid content in yeast

Yeast neutral lipid content was analyzed by Nile Red assay. The Nile Red fluorescence assay was conducted as described previously (Siloto et al., 2009b). Yeast

cultures were aliquoted (100 μL per well) into 96-well solid black plates (Corning Inc., Corning, NY, USA) and incubated with 5 μL of Nile Red solution (0.1 mg/mL in methanol) for 30 s at room temperature. The fluorescence was measured before and after the addition of Nile Red solution with excitation at 485 nm and emission at 538 nm using a Synergy H4 Hybrid reader (Biotek, Winooskit, VT, USA). The Nile Red values were calculated based on the change in fluorescence over OD_{600} ($\Delta F/OD_{600}$). TAG content and fatty acid composition of TAG extracted from yeast cells hosting various *BnaDGAT1* mutants were analyzed by GC/MS (Pan et al., 2013). Total yeast lipids were extracted from lyophilized yeast cells as described previously (Pan et al., 2013). The isolated lipids were resolved on the thin-layer chromatography (TLC) plates (0.25 mm Silica gel, DC-Fertigplatten, Macherey-Nagel, Germany) with the development solvent hexane/diethyl ether/acetic acid (80:20:1). TAG bands on the TLC plate were visualized by primulin staining and then were scraped and derivatized by incubation with 3N methanolic HCl for 1 h at 80°C. The fatty acid methyl esters were analyzed on an Agilent 6890N Gas Chromatograph (Agilent Technologies, Wilmington, DE, USA) with a 5975 inert XL Mass Selective Detector.

3.4.4. Preparation of microsomes

Microsomal fractions were isolated from recombinant yeast cells as described previously (Siloto et al., 2009b). In brief, the recombinant yeast cells were resuspended in 1 mL of lysis buffer (20 mM Tris-HCl pH 7.9, containing 10 mM $MgCl_2$, 1 mM EDTA, 5% (v/v) glycerol, 300 mM ammonium sulfate and 2 mM dithiothreitol), and homogenized in the presence of 0.5 mm glass beads by a bead beater (Biospec, Bartlesville, OK, USA). The

crude homogenate was centrifuged at 10 000 g for 30 min to sediment cell debris and glass beads. The supernatant was transferred into an ultracentrifuge tube and centrifuged at 105 000 g for 70 min to pellet the microsomes. The resulting microsomal fraction was resuspended in 3 mM imidazole buffer (pH 7.4) containing 125 mM sucrose. All procedures were conducted at 4^{o}C. The concentration of crude protein was quantified by the Bradford assay (Bio-Rad, Mississauga, ON, Canada) using BSA as a standard (Bradford, 1976).

3.4.5. *In vitro* DGAT1 activity assay

The DGAT assay was conducted according to the procedure described previously (Caldo et al., 2015). Briefly, the assay mixture (60 μL) contained 200 mM HEPES-NaOH (pH 7.4), 3.2 mM $MgCl_2$, 333 μM *sn*-1,2-diolein dispersed in 0.2% (v/v) Tween 20, 15 μM [1-^{14}C] oleoyl-CoA (55 μCi/μmol; PerkinElmer, Waltham, MA, USA), and 2 μg of microsomal protein. The reaction was initiated by adding microsomes containing recombinant DGAT1 variants and incubated at 30^{o}C for 4 min with shaking before quenching with 10 μL of 10% (w/v) SDS. The entire reaction mixture was spotted onto a TLC plate (0.25 mm Silica gel, DC-Fertigplatten) and the plate was developed with hexane/diethyl ether/acetic acid (80:20:1, v/v/v). The resolved lipids were visualized by phosphorimaging (Typhoon Trio Variable Mode Imager, GE Healthcare, Mississauga, ON, Canada) and corresponding TAG spots were scraped, and radioactivity was quantified by a LS 6500 multi-purpose scintillation counter (Beckman-Coulter, Mississauga, ON, Canada).

For kinetic studies of recombinant BnaDGAT1 variants, enzyme assays were allowed to proceed for 1 min using 0.2 μg of microsomal protein. Recombinant CsDGAT1B variants were assayed for 4 min and the quantity of microsomal protein used was as follows: for WT CsDGAT1B, 10 μg of microsomal protein; I144F and I466F, 2.5 μg of microsomal protein; L460P and L460P/I466F, 1 μg of microsomal protein. The concentration of [1-^{14}C] oleoyl-CoA was varied from 0.1 to 25 μM while *sn*-1,2-diolein were held constant at 333 μM. Kinetic parameters were calculated by fitting the data to the Michaelis-Menten, substrate inhibition or allosteric sigmoidal equation using the program GraphPad Prism (version 6.0; GraphPad Software, La Jolla, CA, USA).

For the substrate specificity assay, radiolabelled linoleoyl-CoA and linolenoyl-CoA were synthesized from [1-^{14}C] linoleic acid (58.2 mCi/mmol, PerkinElmer, Waltham, MA, USA) and [1-^{14}C] linolenic acid (51.7 mCi/mmol, PerkinElmer), respectively, according to the protocol described before (Taylor et al., 1990). Fifteen micromolar of each synthesized acyl-CoA was used in the assay.

3.4.6. Western blotting

Equivalent amounts of microsomal proteins (10 μg) from yeast strain H1246 producing recombinant BnaDGAT1 variants and LacZ were resolved using 8-16% gradient Mini-Protean TGX Precast Gels (Bio-Rad) and electrotransferred (overnight at 30 mA and 4^{o}C) onto polyvinylidene difluoride membrane (Amersham, GE Healthcare). The target C-terminal-tagged recombinant BnaDGAT1 variants were detected using anti-V5-HRP conjugated antibody (Invitrogen). To ensure equal protein loading, yeast constitutively

producing Kar2p protein was used as an internal standard. Kar2p polypeptide was detected using a rabbit polyclonal anti-Kar2p (Santa Cruz Biotechnology, Santa Cruz, CA, USA) as the primary antibody followed by HRP goat anti-rabbit IgG (H+L) secondary antibody (Invitrogen). Both HRP conjugated antibodies were detected by chemiluminescence (FluorChem SP, Alpha Innotech Corp., San Leandro, CA, USA) using an ECL Advance Western Blotting Detection Kit (Amersham). The band densities of BnaDGAT1 variants and internal standard were quantified with ImageJ software (Schneider et al., 2012). The relative DGAT polypeptide accumulation level was calculated based on the density of the DGAT band after normalizing to internal standard.

3.4.7. Amino acid sequence analysis

Multiple amino acid sequence alignments of 43 DGAT1 proteins from different species (Table S3.6) were conducted using ClustalW in MEGA 7 with default settings (Kumar et al., 2016). The alignment was used to construct a neighbour-joining tree using the same software with 1000 bootstrap repetitions. The topology organization of BnaDGAT1 was predicted using Phobius (Käll et al., 2007), TMpred (Hofmann and Stoffel, 1993), TMHMM (Krogh et al., 2001), and SOSUI (Hirokawa et al., 1998).

3.4.8. Statistical analysis

All experiments were repeated at least twice (n = the number of independent experiments). Data are shown as means ± standard deviation (S.D.) when $n \geq 3$, or mean ± range when n = 2, unless otherwise stated. Statistical analysis was performed using the SPSS statistical package (SPSS 16.0, Chicago, IL, USA). Significant differences between

groups were assessed using a one-way analysis of variance (ANOVA) with LSD test or a two-tailed Student's t-test assuming equal variances or not (depending on the Levene's test result) as indicated in the figure legends. Means were considered significantly different at $P < 0.05$.

3.5. Supplementary material

3.5.1. Supplementary methods

3.5.1.1. Quantitative RT-PCR

Quantitative RT-PCR (qPCR) was performed on a StepOnePlus Real-Time PCR System (Applied Biosystems, Foster, CA, USA) using the Platinum SYBR Green qPCR Master Mix (Invitrogen) as described previously (Chen et al., 2011b).

Plasmid copy number assay

Plasmid copy numbers were quantified according to Karim et al. (2013). Total DNA was extracted using glass bead beating followed by phenol-chloroform extraction (Lõoke et al., 2011). Plasmid copy number was calculated using the standard curve method. To quantify the copy number, a section of the *BnaDGAT1* gene (avoiding the mutated region) on the plasmid was targeted (with primers 5'-GGCCAATCCTGAAGTCTCCTACT-3' and 5'-TGGGAGCAAGCATGAAATACG-3') and compared to a genomic target in the single copy *ScALG9* gene (*Saccharomyces* Genome Database (SGD) ID: S000005163, with primers 5'-GCCGTTGCCATGTTGTTGTA-3' and 5'-GACCCAGTGGACAGATAGCG-3'). Standard curves were created using plasmid containing both *BnaDGAT1* and *ScALG9*

genes in the pYES2.1 vector. A serial dilution of this plasmid with concentration ranging from 5×10^2 to 5×10^7 copies per μL was used to create standard curves for both *BnaDGAT1* and *ScALG9*. Copy number here refers to the copy number per haploid genome rather than per cell considering there are two copies of genome per cell during certain phases of cell division.

Gene expression analysis

Gene expression of *BnaDGAT1* and its variants in yeast was analyzed as follows. Total RNA was isolated from yeast cells at the mid-log phase using the RNeasy kit according to the manufacturer's instruction (Qiagen, Toronto, ON, Canada). First-strand cDNA was synthesized in a 10-μL reaction mixture with 1 μg of total RNA using the SuperScript III first-strand cDNA synthesis kit (Invitrogen). The relative expression levels of the *BnaDGAT1* variants in yeast were calculated using the comparative Ct method ($2^{-\Delta\Delta Ct}$ method) (Livak and Schmittgen, 2001). The results are presented as fold differences in gene expression after normalizing to the yeast stably expressing *ScACT1* gene (SGD ID: S000001855). cDNA of variant V333I was used as a calibrator to normalize for plate-to-plate variation. The primers for *BnaDGAT1* and its variants were the same as the primers we used to quantify plasmid copy number. The primers for *ScACT1* cDNA were 5'-TCGTTCCAATTTACGCTGGTT-3' and 5'-CGGCCAAATCGATTCTCAA-3'.

3.5.1.2. Positive selection

Twenty-two DGAT1 sequences were collected (Table S3.3) from different plant species including *Arabidopsis thaliana*, *Arachis hypogaea L.*, *Brassica napus*, *Camelina*

sativa, *Glycine max*, *Helianthus annuus L.*, *Jatropha curcas*, *Linum usitatissimum*, *Nicotiana tabacum*, *Olea europae*, *Oryza sativa*, *Perilla frutescens*, *Ricinus communis*, *Sesamum indicum*, *Tropaeolum majus*, *Vernicia fordii* and *Zea mays.* Multiple sequence alignment of DGAT1 proteins was performed using ClustalW in MEGA 7 with the default parameters (Kumar et al., 2016). The coding sequences were then aligned according to their corresponding aligned protein sequences using PAL2NAL server (www.bork.embl. de/pal2nal/). A maximum likelihood phylogenetic tree was constructed with the PhyML webserver (http://www.atgc-montpellier.fr/phyml/, cited 29 Sept 2017) under the GTR+G+I model. Positively selected sites were predicted by the codon-based likelihood methods with site models in CodeML program in the PAML version 4 software (Yang, 2007). Three sets of models were used in the analysis: M0 (one ratio) vs. M3 (discrete); M1a (nearly neutral) vs. M2a (positive selection); and M7 (β) vs. M8 (β + ω) using the F3X4 codon frequency model. The likelihood ratio test was performed to compare the fit of two nested models. A Bayes empirical Bayes approach was used to identify the sites under positive selection (Yang et al., 2005). The alignment was visualized for editing and displayed with Jalview (Waterhouse et al., 2009).

Supplementary Table S3.1. Amino acid residue substitutions of the BnaDGAT1 variants.

DGAT variant	Amino acid residue substitutions	TAG content (% DW, mean ± S.D.)
D9	I287V / L441P	7.3 ± 0.4
F1	F302C	7.2 ± 0.1
D7	R51Q / L164F / Y386F	7.1 ± 0.6
G7	R29H/L136F / V341L	6.2 ± 0.6
E7	A114P / M199T / C286Y / G332A / L438H / L445V / F473L	5.9 ± 0.2
I447F	I447F	5.9 ± 0.1
D8	L224V / K322E / L422F	5.7 ± 0.2
G11	F473L	5.6 ± 0.2
C8	F473I	5.5 ± 0.1
H1	M11T / N410K / L441P	5.5 ± 0.2
G8	G290S / I314M	5.3 ± 0.2
H6	N343I	5.3 ± 0.6
C3	S32Y / V56I / E70K / S74F / L136I / N248Y / V486E	5.2 ± 0.5
F9	F449C	5.1 ± 0.3
G2	S112R / F302L	5.0 ± 0.3
A7	V125F	4.8 ± 0.1
E8	G16S / D21G / R437H / F473L	4.7 ± 0.3
H8	C286G / F302L / R388S	4.6 ± 0.1
E1	A66S / C184Y / D328E / L493*	4.5 ± 0.4
B12	V52D / F302I / F308L / Y386F	4.4 ± 0.2
H12	T42I / L193F / F473L	4.4 ± 0.3
B11	V125G / M161K / R409S / L441P/F477L	4.2 ± 0.2
A2	S33T / R51Q / L164F / Y386F	4.2 ± 0.1
E5	K27R / E70K / N81D / L116I / K326Q / N458D / M484I	4.2 ± 0.1
H9	P12S / F473I	4.1 ± 0.6
H2	K27E / G35R / A46P / I108T	4.0 ± 0.3
A10	M484L	3.9 ± 0.4
H7	L20H / L136F / V341L	3.9 ± 0.4
C7	L441P	3.9 ± 0.2
A4	V82E / E100D / V202I / V336M / Y386F / M467K	3.8 ± 0.3
B10	L441P	3.8 ± 0.2
D2	G332V	3.8 ± 0.3

F8	K289N	3.6 ± 0.1
E2	G35E / C286S / M484V	3.6 ± 0.1
B8	V41L / A114D / K183R / K322E	3.5 ± 0.2
F11	L224F	3.5 ± 0.4
H5	L136F / V341L	3.5 ± 0.2
D4	K110N / L441P	3.5 ± 0.1
B1	A172G / N248I / K326N / L441P	3.4 ± 0.3
B9	T10N / I143F / T200I / Y386F / M392K	3.3 ± 0.1
G12	E70V	3.3 ± 0.3
C2	R24S / L438H / L493*	3.3 ± 0.3
C10	A107T	3.2 ± 0.2
C1	S54T / F449L	3.2 ± 0.1
C4	E70G / L453M	3.0 ± 0.1
A3	I143V	2.8 ± 0.1
A11	L441V	2.8 ± 0.0
E10	V52I / E201V / S262T / Q450H	2.8 ± 0.0
G1	R51Q	2.6 ± 0.3
A1	K322E / L438I	2.4 ± 0.2
WT		1.4 ± 0.2
VEC		0.0 ± 0.0

* means a stop codon; sequencing of all 50 BnaDGAT1 variants was done by Dr. Siloto.

Supplementary Table S3.2. Fatty acid composition of triacylglycerol of yeast cells producing BnaDGAT1 variants.

DGAT1 variants	C16:0	C16:1	C18:0	C18:1
D9	15.6 ± 0.1	43.2 ± 1.4	8.6 ± 0.7	32.6 ± 0.6
F1	15.5 ± 0.2	37.0 ± 0.6	12.9 ± 0.4	34.6 ± 0.0
D7	15.0 ± 0.2	40.5 ± 0.4	9.4 ± 0.5	35.1 ± 0.2
G7	15.3 ± 0.3	39.3 ± 1.4	11.8 ± 0.6	33.6 ± 1.0
E7	15.2 ± 0.1	41.1 ± 0.5	9.5 ± 0.2	34.3 ± 0.3
I447F	15.6 ± 0.1	43.8 ± 3.0	8.7 ± 1.1	31.9 ± 2.0
D8	16.0 ± 1.0	44.6 ± 2.8	8.6 ± 1.1	30.8 ± 0.7
G11	15.1 ± 0.3	41.8 ± 1.3	9.2 ± 0.7	33.9 ± 0.4
C8	14.9 ± 0.2	39.0 ± 0.4	10.2 ± 0.2	35.9 ± 0.4
H1	15.5 ± 0.3	36.6 ± 0.3	9.9 ± 0.5	38.0 ± 1.0
G8	15.9 ± 0.2	39.1 ± 0.5	10.2 ± 0.1	34.7 ± 0.6
H6	15.0 ± 1.2	38.1 ± 2.9	11.8 ± 1.4	35.1 ± 2.8
C3	14.8 ± 0.4	38.2 ± 1.1	11.0 ± 0.6	35.9 ± 1.0
F9	16.6 ± 1.1	36.4 ± 3.0	12.2 ± 1.8	34.9 ± 1.2
G2	15.2 ± 0.6	34.3 ± 1.9	12.1 ± 0.1	38.4 ± 2.4
A7	14.6 ± 0.4	36.7 ± 2.8	12.2 ± 0.8	36.4 ± 2.4
E8	14.7 ± 0.3	35.5 ± 5.0	10.4 ± 1.2	39.5 ± 5.0
H8	15.8 ± 0.9	41.8 ± 1.5	11.3 ± 0.6	31.1 ± 1.8
E1	15.9 ± 0.6	40.8 ± 4.0	11.3 ± 1.7	32.0 ± 2.9
B12	17.0 ± 0.7	41.1 ± 2.2	10.2 ± 1.2	31.7 ± 0.3
H12	14.2 ± 0.1	43.8 ± 4.4	8.6 ± 1.5	33.4 ± 3.0
B11	15.0 ± 0.6	37.8 ± 0.4	11.8 ± 0.0	35.4 ± 0.2
A2	15.7 ± 0.8	43.7 ± 3.1	8.9 ± 1.2	31.7 ± 2.7
E5	15.6 ± 1.4	44.9 ± 4.6	9.1 ± 2.4	30.4 ± 0.9
H9	14.9 ± 0.2	48.9 ± 3.0	6.8 ± 0.5	29.9 ± 2.4
H2	15.5 ± 0.6	36.4 ± 0.1	12.1 ± 0.1	36.0 ± 0.7
A10	18.8 ± 0.5	42.5 ± 2.0	10.1 ± 1.2	28.6 ± 1.2
H7	15.0 ± 0.2	41.1 ± 0.7	11.5 ± 0.1	32.4 ± 0.8
C7	16.6 ± 3.2	46.3 ± 4.1	8.2 ± 1.9	28.9 ± 3.4
A4	16.6 ± 0.2	44.1 ± 5.3	8.8 ± 2.1	30.4 ± 3.2
B10	14.7 ± 0.3	37.9 ± 1.0	11.8 ± 0.2	35.8 ± 1.1
D2	15.4 ± 0.5	40.0 ± 3.0	10.9 ± 0.9	33.7 ± 2.6
F8	15.3 ± 0.5	41.2 ± 3.1	10.1 ± 1.2	33.3 ± 2.3
E2	14.2 ± 0.2	40.6 ± 0.3	9.9 ± 0.0	35.3 ± 0.5

B8	14.9 ± 0.4	41.0 ± 8.5	10.8 ± 4.0	33.4 ± 4.1
F11	19.4 ± 6.0	32.6 ± 4.1	12.5 ± 2.2	35.5 ± 6.2
H5	14.9 ± 0.2	39.6 ± 2.6	11.8 ± 1.1	33.8 ± 1.7
D4	15.0 ± 0.9	46.9 ± 3.2	7.9 ± 0.7	30.2 ± 3.4
B1	15.7 ± 2.0	38.7 ± 1.1	10.0 ± 1.9	35.7 ± 0.8
B9	13.3 ± 0.7	38.6 ± 2.3	11.4 ± 0.8	36.7 ± 2.2
G12	14.0 ± 1.3	40.7 ± 2.3	10.9 ± 0.8	34.4 ± 2.9
C2	18.2 ± 0.2	43.6 ± 1.7	9.7 ± 0.2	28.6 ± 1.7
C10	13.7 ± 0.0	40.8 ± 3.4	11.1 ± 1.1	34.4 ± 2.3
C1	14.3 ± 0.4	37.2 ± 1.0	11.4 ± 0.4	37.1 ± 0.9
C4	11.5 ± 0.2	32.2 ± 0.8	14.3 ± 0.2	42.0 ± 0.9
A3	15.3 ± 0.3	41.2 ± 4.9	10.1 ± 2.0	33.4 ± 3.3
A11	14.2 ± 0.6	34.8 ± 1.6	13.0 ± 0.6	37.9 ± 1.5
E10	13.3 ± 1.4	40.6 ± 2.6	11.0 ± 1.0	35.0 ± 2.9
G1	10.8 ± 1.2	40.0 ± 6.2	12.1 ± 1.6	37.0 ± 5.8
A1	11.9 ± 0.7	35.5 ± 2.8	13.2 ± 1.1	39.3 ± 2.4
WT	8.8 ± 2.1	36.7 ± 6.0	12.6 ± 2.2	41.9 ± 6.2
VEC	34.4 ± 11.5	25.5 ± 8.2	14.8 ± 3.9	25.4 ± 10.0

Fatty acids (mean ± S.D.) of the yeast H1246 cells were analyzed by GC/MS. Vectors hosting mutagenized *BnaDGAT1s*, *LacZ* gene (negative control 1, empty vector control [VEC]) and wild type *BnaDGAT1* (negative control 2, WT) were expressed in a quadruple mutant *Saccharomyces cerevisiae* strain H1246, which is devoid of triacylglycerol synthesis.

Supplementary Table S3.3. Twenty-two plant DGAT1s for sequence alignment.

Gene	GenBank accession number	Organism
AhDGAT1-1	KC736068	*Arachis hypogaea L.*
AhDGAT1-2	KC736069	*Arachis hypogaea L.*
AtDGAT1	NM_127503	*Arabidopsis thaliana*
BnaA.DGAT1.a	JN224474	*Brassica napus*
BnaA.DGAT1.b	JN224475	*Brassica napus*
BnaC.DGAT1.a	AF251794	*Brassica napus*
BnaC.DGAT1.b	JN224476	*Brassica napus*
CsDGAT1B	XM_010417066	*Camelina sativa*
GmDGAT1a	AY496439	*Glycine max*
GmDGAT1b	AB257590	*Glycine max*
HaDGAT1	HM015632	*Helianthus annuus L.*
JcDGAT1	DQ278448	*Jatropha curcas*
LuDGAT1	KC485337	*Linum usitatissimum L.*
NtDGAT1	AF129003	*Nicotiana tabacum*
OeDGAT1	AY445635	*Olea europae*
OsDGAT1	NM_001061404	*Oryza sativa*
PfDGAT1	AF298815	*Perilla frutescens*
RcDGAT1	XM_002514086	*Ricinus communis*
SiDGAT1	JF499689	*Sesamum indicum*
TmDGAT1	AY084052	*Tropaeolum majus*
VfDGAT1	DQ356680	*Vernicia fordii*
ZmDGAT1b	EU039830	*Zea mays*

Supplementary Table S3.4. Predicted transmembrane domains (TMDs) in BnaDGAT1.

	TMpred	TMHMM	SOSUI	Phobius
TMD1	112-133	114-133	112-134	114-133
TMD2	157-176	157-176	156-178	154-176
TMD3	189-210	188-210	186-208	188-208
TMD4	215-234	215-237	215-237	215-237
TMD5	261-280			257-276
TMD6	295-314	296-318		296-314
TMD7	347-366	344-366	351-373	344-368
TMD8	414-432		413-435	414-435
TMD9	441-457	438-456	440-462	441-460
TMD10	467-490	471-490	465-487	472-491

Supplementary Table S3.5. Apparent kinetic parameters of BnaDGAT1 and CsDGAT1B variants obtained from a kinetic model which accounts for sigmoidicity and substrate inhibition. Analysis was performed with GraphPad Prism software using the non-linear regression of the proposed kinetic model (Equation 3). Data are means ± S.D, n = 2 to 3. ND, Not determined.

	V_{max} ^{app} (nmol/min/mg)	K_m ^{app} (μM)	K_i ^{app} (μM)	Hill coefficient	DGAT protein abundance in microsomes (relative to BnaDGAT 1)	V_{max}, ^{app} adjusted for protein abundance (nmol/min/ mg)	V_{max}, ^{app} / K_m ^{app} (mL/min/ mg)	V_{max}, ^{app} / K_m ^{app} relative	R^2
BnaDGAT1 variants									
BnaDGAT1	4.77 ± 0.22	0.79 ± 0.06	22.34 ± 2.92	1.40 ± 0.11	1.00	4.77	6.04	1.00	0.98
V125F	18.95 ± 3.90	2.26 ± 0.96	9.20 ± 2.86	0.92 ± 0.11	1.14	16.69	7.39	1.32	0.96
L441P	9.13 ± 0.45	1.09 ± 0.11	138.80 ± 52.53	1.13 ± 0.08	1.02	8.98	8.24	1.47	0.98
I447F	6.93 ± 0.55	1.19 ± 0.17	22.02 ± 4.24	1.23 ± 0.11	1.12	6.17	5.18	0.93	0.97
F449C	12.84 ± 1.48	2.13 ± 0.48	19.01 ± 4.22	1.02 ± 0.08	1.15	11.13	5.23	0.93	0.98
CsDGAT1B variants									
CsDGAT1B	0.06 ± 0.00	0.37 ± 0.03	14.53 ± 1.84	1.89 ± 0.16	ND	ND	ND	ND	0.97
I144F	0.48 ± 0.08	1.04 ± 0.27	5.06 ± 1.28	1.27 ± 0.14	ND	ND	ND	ND	0.98
L460P	0.46 ± 0.04	0.59 ± 0.12	63.49 ± 26.44	1.14 ± 0.17	ND	ND	ND	ND	0.96
I466F	0.47 ± 0.16	2.34 ± 1.82	4.47 ± 1.98	0.80 ± 0.11	ND	ND	ND	ND	0.97
L460P/I466F	0.26 ± 0.01	0.31 ± 0.03	20.52 ± 4.00	1.81 ± 0.26	ND	ND	ND	ND	0.95

Supplementary Table S3.6. Forty-three DGAT1s from different species used for multiple sequence alignment.

Gene	GenBank accession number	Organism
AaDGAT1	XM_001658249	*Aedes aegypti*
AhDGAT1-1	KC736068	*Arachis hypogaea*
AhDGAT1-2	KC736069	*Arachis hypogaea*
AtDGAT1	NM_127503	*Arabidopsis thaliana*
BnaA.DGAT1.a	JN224474	*Brassica napus*
BnaA.DGAT1.b	JN224475	*Brassica napus*
BnaC.DGAT1.a	AF251794	*Brassica napus*
BnaC.DGAT1.b	JN224476	*Brassica napus*
CeDGAT1	NM_001269372	*Caenorhabditis elegans*
CsDGAT1B	XM_010417066	*Camelina sativa*
DmDGAT1	AF468649	*Drosophila melanogaster*
DrDGAT1	NM_199730	*Danio rerio*
EaDGAT1	AY751297	*Euonymus alatus*
GmDGAT1a	AY496439	*Glycine max*
GmDGAT1b	AB257590	*Glycine max*
HaDGAT1	HM015632	*Helianthus annuus*
HsDGAT1	NM_012079	*Homo sapiens*
JcDGAT1	DQ278448	*Jatropha curcas*
LuDGAT1-1	KC485337	*Linum usitatissimum*
MdDGAT1	XM_007488766	*Monodelphis domestica*
MmDGAT1	AF078752	*Mus musculus*
MtDGAT1	XM_003595183	*Medicago truncatula*
NtDGAT1	AF129003	*Nicotiana tabacum*
NvDGAT1	XM_001639301	*Nematostella vectensis*
OeDGAT1	AY445635	*Olea europae*
OsDGAT1	NM_001061404	*Oryza sativa*
PfDGAT1	AF298815	*Perilla frutescens*
PhtDGAT1	HQ589265	*Phaeodactylum tricornutum*

PotDGAT1	XM_006371934	*Populus trichocarpa*
PpDGAT1	XM_001770877	*Physcomitrella patens*
RcDGAT1	XM_002514086	*Ricinus communis*
RnDGAT1	AB062759	*Rattus norvegicus*
SiDGAT1	JF499689	*Sesamum indicum*
SsDGAT1	NM_214051	*Sus scrofa*
TaDGAT1	XM_002111989	*Trichoplax adhaerens*
TgDGAT1	AY327327	*Toxoplasma gondii*
TmDGAT1	AY084052	*Tropaeolum majus*
TpDGAT1	XM_002287179	*Thalassiosira pseudonana*
VfDGAT1	DQ356680	*Vernicia fordii*
VgDGAT1	EF653276	*Vernonia galamensis*
VvDGAT1	AM433916; CAN80418	*Vitis vinifera*
YlDGAT1	XM_502557	*Yarrowia lipolytica*
ZmDGAT1b	EU039830	*Zea mays*

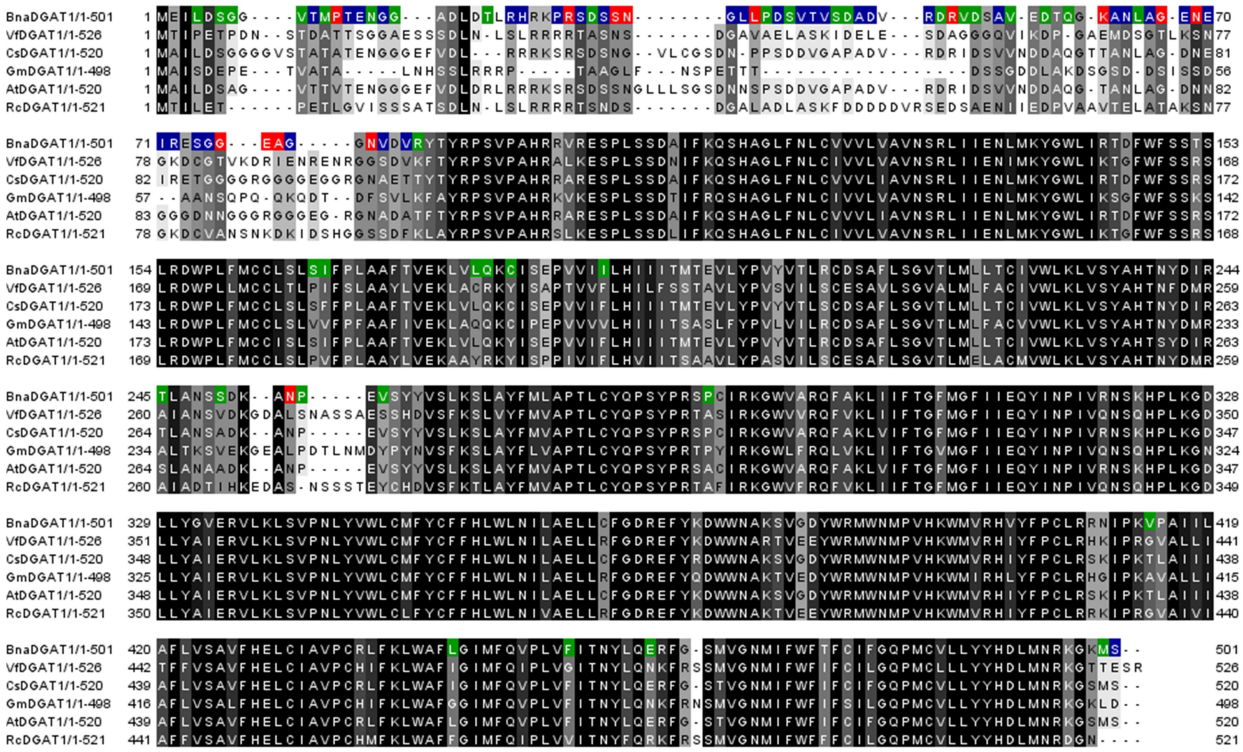

Supplementary Figure S3.1. Sequence alignment of DGAT1 from five typical plant species and location of positive selection sites. Conserved sites are shaded. Amino acid residue sites in green, blue or red background indicate positive selection sites with a Bayes Empirical Bayes posterior probability less than (<) 95%, higher than (≥) 95%, or higher than (≥) 99%, respectively.

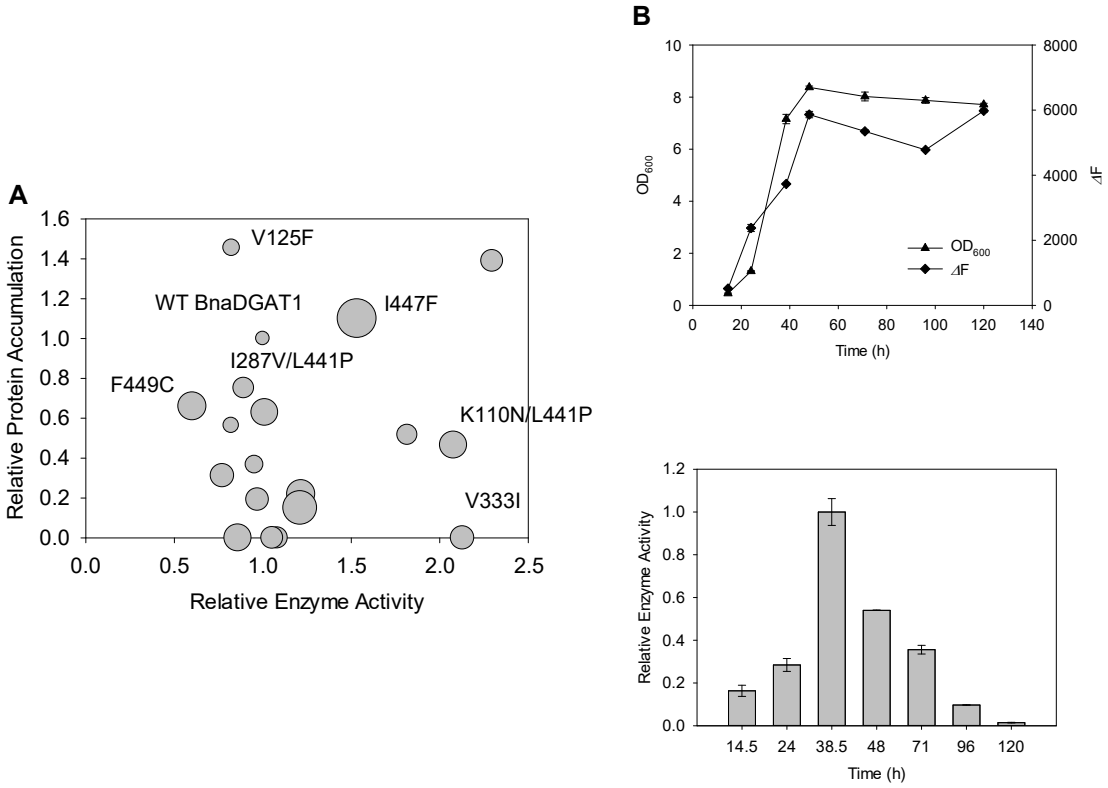

Supplementary Figure S3.2. Initial characterization of BnaDGAT1 variants. A. Analysis of enzyme activity and protein accumulation. Yeast strain H1246 producing recombinant variant enzymes were harvested during the log or stationary phase and then used to prepare microsomes for analysis of *in vitro* DGAT activity, and polypeptide quantification by Western blotting. Each circle represents one BnaDGAT1 variant. Neutral lipid content of yeast expressing corresponding variants was determined by the Nile Red assay and indicated by the size of circle. The relative activity and protein accumulation of wild type (WT) BnaDGAT1 were set as 1.0. B. Production profile of recombinant WT BnaDGAT1 in yeast H1246. Growth rate (optical density, OD_{600}), neutral lipid content (change in fluorescence, ΔF, in arbitrary units) and microsomal DGAT activities of yeast cultures producing BnaDGAT1 are shown. The highest microsomal activity (at 38.5 h) of recombinant WT BnaDGAT1 was set as 1.0. Data are means ± range, n = 2.

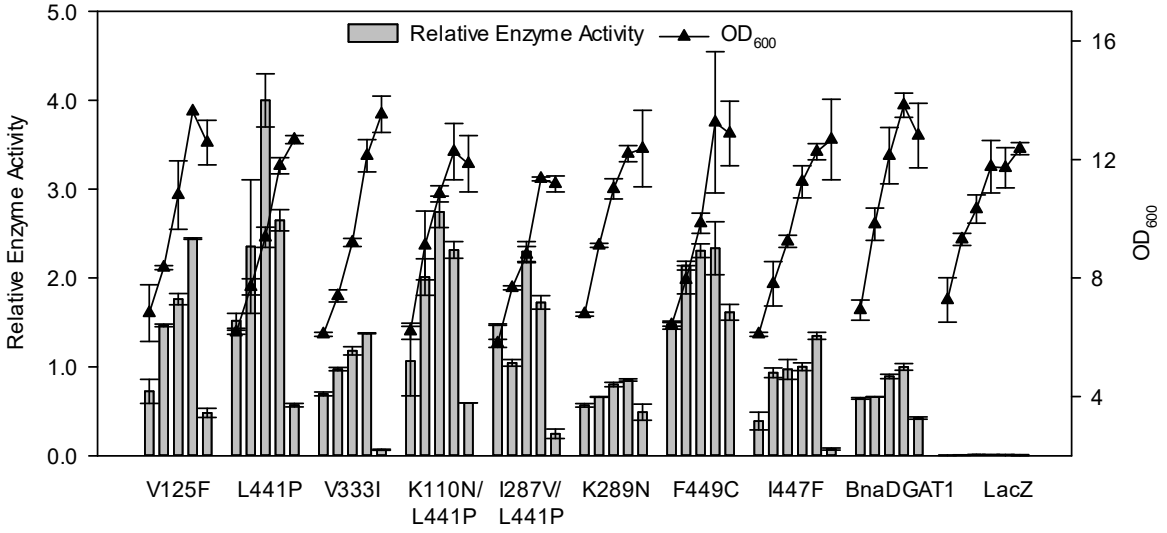

Supplementary Figure S3.3. *In vitro* DGAT activities of BnaDGAT1 variants L441P and I447F. Microsomes from yeasts producing recombinant BnaDGAT1 variants were collected at different time points after induction and used for the DGAT assay. The highest microsomal activity of recombinant wild type (WT) BnaDGAT1 was set as 1.0. Growth curve was constructed by measuring OD_{600}. Data are means ± range, n = 2.

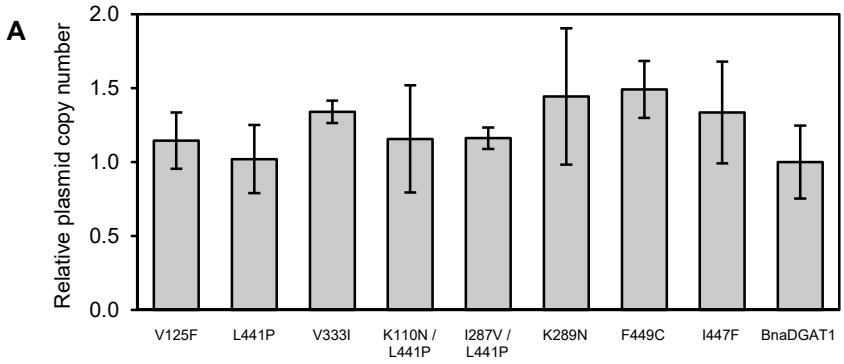

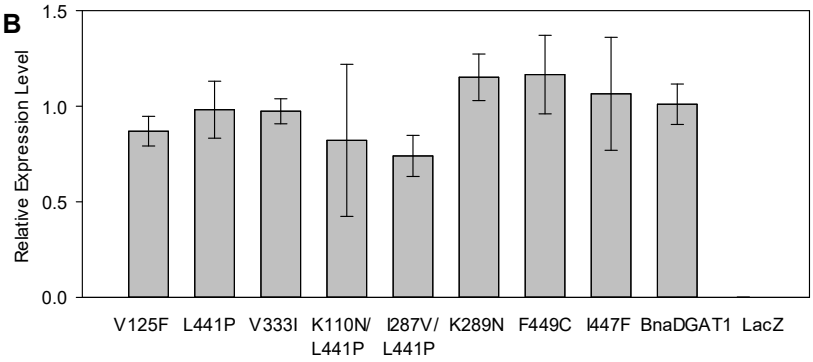

Supplementary Figure S3.4. Copy number (A) and gene expression level (B) of *BnaDGAT1* variants in yeast H1246. Data are means ± S.D, n = 3 biological replicates.

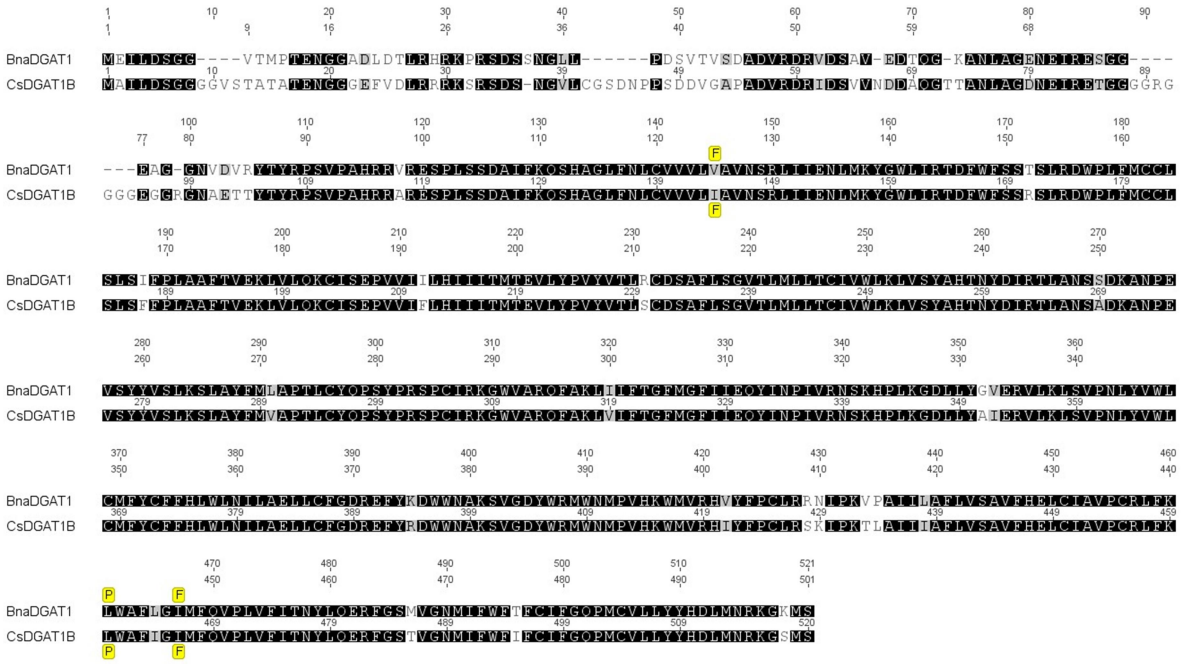

Supplementary Figure S3.5. Alignment of deduced amino acid sequences of DGAT1 cDNAs from *B. napus* and *C. sativa*. The highlighted amino acid residues indicate the amino acid residue substitutions of BnaDGAT1 variants and the corresponding CsDGAT1B variants.

Chapter 4 – Engineering Improved Variants of Arabidopsis Long-Chain Acyl-CoA Synthetase 9

4.1. Introduction

Long-chain acyl-CoA synthetase (LACS, EC 6.2.1.3) catalyzes the ATP-dependent thioesterification of free fatty acid with coenzyme A (CoA) to form acyl-CoA, which serves as a key metabolite for different lipid metabolic pathways. This reaction involves a two-step ping-pong reaction mechanism, in which firstly an adenylyl from ATP is transferred to fatty acid forming an enzyme-bound acyl-adenylate intermediate and PP_i, and secondly the acyl-adenylate intermediate is attacked by CoA yielding an acyl-CoA and AMP (Watkins, 1997).

In *Arabidopsis thaliana* (hereafter Arabidopsis), nine *LACS* genes with distinct expression patterns, subcellular localizations and functions have been identified (Shockey et al., 2002). While peroxisomal LACS6 and LACS7 appear to be required for fatty acid *β*-oxidation (Fulda et al., 2002, 2004), endoplasmic reticulum (ER) localized LACS1, LACS2 and LACS4 have been found to be involved in the synthesis of surface lipids (Schnurr and Shockey, 2004; Tang et al., 2007; Lü et al., 2009; Weng et al., 2010; Jessen et al., 2011). In addition to the essential functions in plant development, LACS is believed to be involved in TAG biosynthesis. *De novo* fatty acids are synthesized in the plastid and required to be activated to acyl-CoAs before utilized for TAG assembly in the ER (Chapman and Ohlrogge, 2012). The plastidial outer envelope-associated LACS9 was regarded as the most likely candidate for activating and exporting plastidially-derived fatty acids for TAG assembly (Zhao et al., 2010). Its function, however, is debatable as a recent study has

shown that LACS9 might contribute to lipid trafficking from the ER back to the plastid (Jessen et al., 2015).

Regardless of the puzzling role of LACS in the plant, the applications of LACS in engineering oleaginous microorganisms have been widely explored. Over-expressing *LACS* has been shown to increase fatty ester, fatty alcohol, wax and TAG production in *Escherichia coli* and yeast (*Saccharomyces cerevisiae*). Steen et al. (2010) reported the metabolically engineering of *E. coli* to produce renewable fuels and chemicals using combined approaches including over-expression of *LACS*. Over-expression of *LACS* from diatoms (*Phaeodactylum tricornutum* or *Thalassiosira pseudonana*) or higher plants (*Arabidopsis* or *B. napus*) has been reported to facilitate fatty acids uptake and stimulate oil deposition in yeast (Guo et al., 2014; Tan et al., 2014; Tonon et al., 2005; Pulsifer et al., 2012). In this regard, it would be worthwhile to further increase the enzyme activity of LACS.

In the current study, we used error-prone PCR to generate several AtLACS9 variants with improved enzyme activity or altered substrate specificity. The identified amino acid residue substitutions provide valuable information for the modification of LACS from other species.

4.2. Results

4.2.1. Enzyme activity and protein accumulation of recombinant AtLACS9 variants

Initially, we generated several AtLACS9 variants by error-prone PCR. To characterize their enzyme performance, the DNA sequences encoding these AtLACS9

variants were transformed into *S. cerevisiae* mutant *BYfaa1,4*Δ, which has both *FAA1* and *FAA4* genes knocked out and only retains less than 10% of LACS activity in yeast (Guo et al., 2014). Expression of these variants in the yeast mutant *BYfaa1,4*Δ, however, did not contribute to consistent change in neutral lipid accumulation relative to that of the wild type (WT) AtLACS9 (Figure 4.1A). To examine the production profiles of four AtLACS9 variants in yeast mutant *BYfaa1,*4Δ, the growth of the yeast cells producing various AtLACS9 variants was monitored by measuring the OD_{600} value of cells collected periodically from the log to the stationary growth phase. Microsomal fractions containing these variant enzymes were prepared from cells and used for the *in vitro* LACS assays. As shown in Figure 4.1B, the activity of the recombinant enzymes remained at a high level during the log phase, and then decreased after reaching the stationary phase. AtLACS9 variants displayed the highest activity at the early log phase while the highest activity of the WT enzyme occurred at the late log or early stationary phase. Increased LACS activity was observed for variants L12F/C207F/L656F and D238E/P659S, whereas variants E520D and E630D displayed overall lower activity than the WT AtLACS9.

The microsomes of each variant with the highest enzyme activity are presented (Figure 4.2A), and the corresponding protein accumulation levels were analyzed by Western blotting (Figure 4.2B). AtLACS9 variant enzymes displayed different polypeptide accumulation levels in yeast and the lowest protein abundance was observed for variant E630D, which probably led to the low microsomal enzyme activity. After normalizing the enzyme activity to the corresponding protein accumulation, all of the variants displayed higher or similar normalized relative activity compared to the WT enzyme (Figure 4.2C).

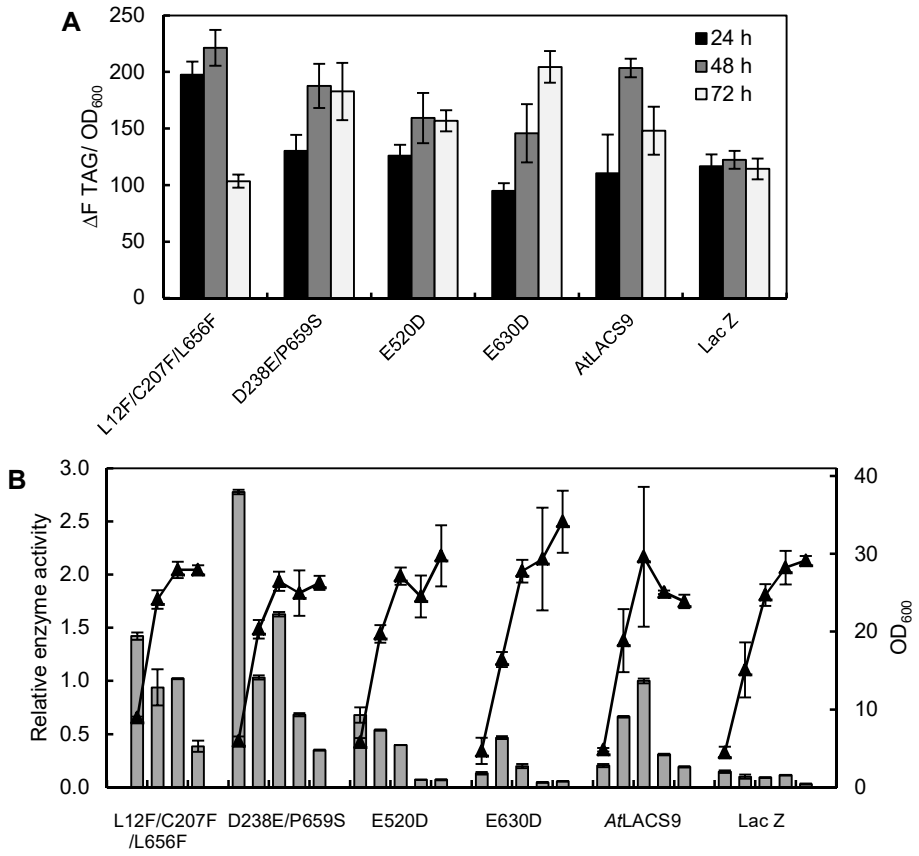

Figure 4.1. Characterization of AtLACS9 variants. A, Neutral lipid content of yeast producing AtLACS9 variants harvested from the log to the stationary growth phase. B, *In vitro* LACS activities of different AtLACS9 variants. Microsomal fractions from yeasts producing recombinant AtLACS9 variants were harvested at different time points after induction and used for the enzyme assay. The highest microsomal activity of recombinant wild type (WT) AtLACS9 was set as 1.0. The growth plot was constructed by measuring OD_{600}. Neutral lipid content in panel A was based on Nile red assay. Data are means ± S.D, n = 2.

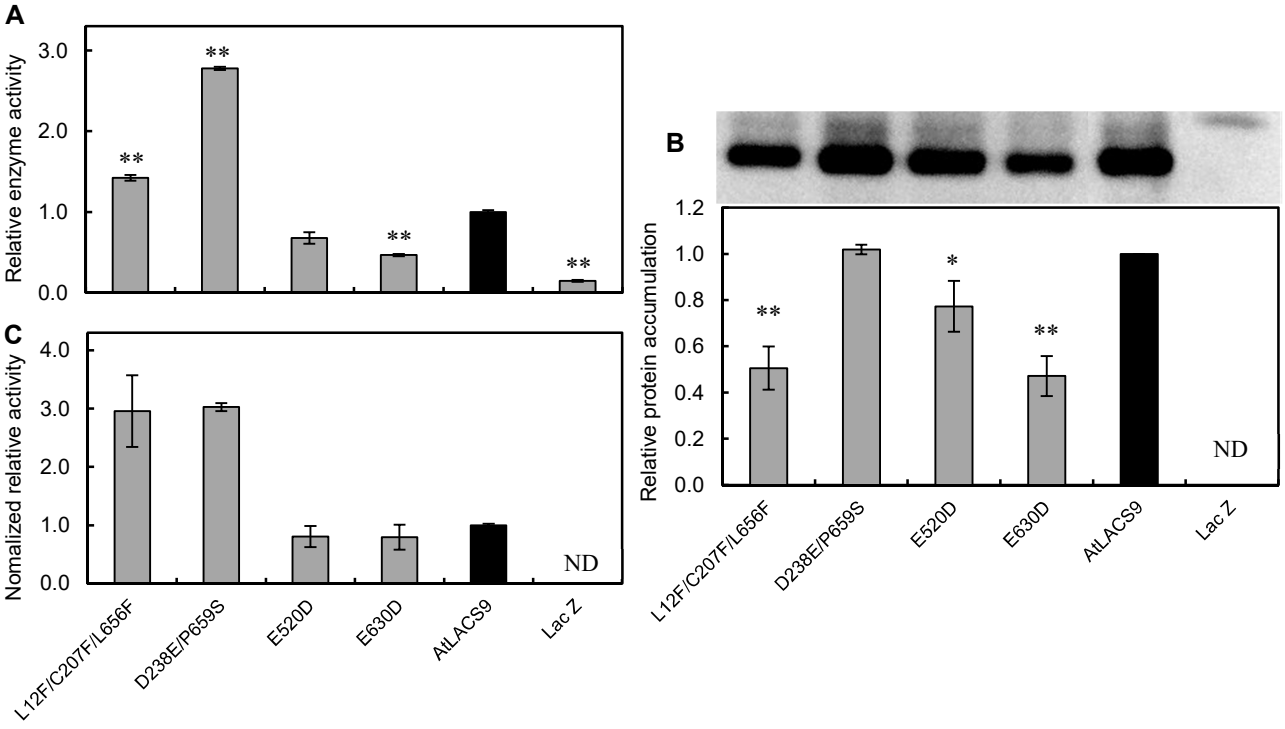

Figure 4.2. Microsomal enzyme activities and corresponding protein abundances of AtLACS9 variants. A, Relative enzyme activities of AtLACS9 variants. The highest activity of each variant is shown, with the wild type (WT) AtLACS9 activity set as 1.0. Data are means ± S.D, n = 2. B, Relative protein abundance. Five micrograms of microsomal protein from the same batch of microsomes used to assess enzyme activity were used for Western blotting analysis. The relative protein accumulation of recombinant WT AtLACS9 was set as 1.0. Data are means ± S.D, n = 3. C, The normalized relative activity of each enzyme variant was obtained by dividing the enzyme activity value by relative protein abundance, with recombinant WT AtLACS9 activity set as 1.0. Data are means ± S.D, n=2. The asterisks indicate significant differences in activity (A), and protein abundance (B) of the microsomes containing recombinant AtDGAT9 variants versus recombinant WT AtLACS9 (t-test, ** $P<0.01$, * $P<0.05$). ND, not determined.

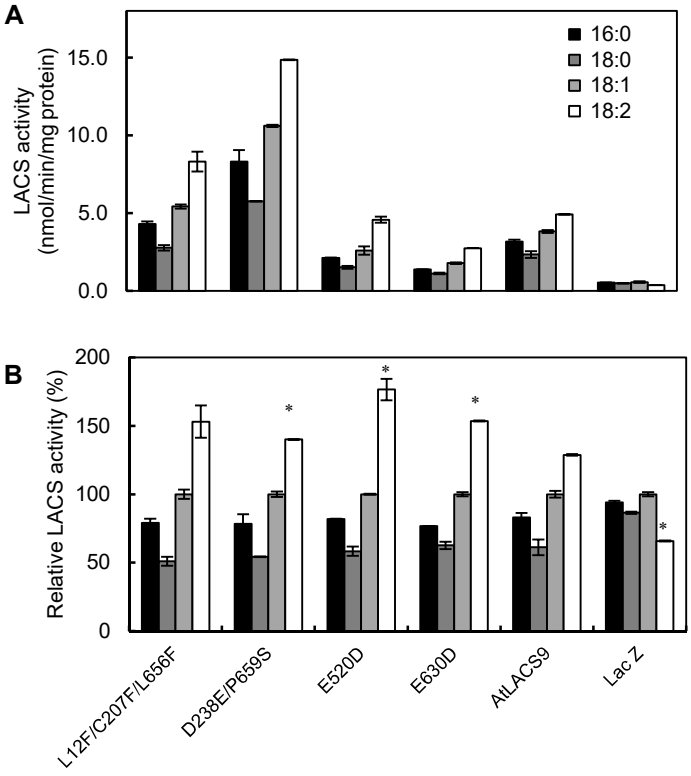

Figure 4.3. Substrate specificities of AtLACS9 variants. A, LACS activities of AtLACS9 variants towards different fatty acids. B, Enzyme activity data normalized to activity observed using oleic acid (18:1Δ^{9cis}) as substrate (i.e., oleic acid supported activity set at 100%). Microsomal preparations from the yeast mutant *BYfaa1,4*Δ producing AtLACS9 variants were used for analysis of enzyme assay. Data represent means ± S.D, n = 2. 16:0, palmitic acid; 18:0, stearic acid; 18:1, oleic acid; 18:2, linoleic acid (18:2$\Delta^{9cis, 12cis}$). The asterisks indicate significant differences in substrate specificity (B) of recombinant AtDGAT9 variants versus recombinant wild type (WT) AtLACS9 (t-test, $P < 0.05$).

The substrate specificity of each recombinant microsomal AtLACS9 variant was assessed using different radiolabeled fatty acids as substrates (Figure 4.3). AtLACS9 and its variants were able to utilize all assessed fatty acids, with oleic acid ($18{:}1\Delta^{9cis}$; hereafter 18:1) and linoleic acid ($18{:}2\Delta^{9cis,\,12cis}$; hereafter 18:2) as the most effective substrates. Consistent with previous analysis of enzyme activity (Figure 4.2A), variants L12F/C207F/L656F and D238E/P659S were more active towards all assessed fatty acids, whereas variants E520D and E630D were less active than the WT AtLACS9 (Figure 4.3A). When enzyme activity was normalized to the activity observed using oleic acid as a substrate, variants E520D and E630D displayed enhanced preference towards linoleic acid (Figure 4.3B).

4.2.2. Detailed characterization of selected single site mutants

Since the two AtLACS9 variants with increased LACS activity contained multiple amino acid residue substitutions, the effect of single amino acid residue substitutions on enzyme activity were separately determined. Five single site mutants were generated and transformed into yeast mutant *BYfaa1,4Δ* together with the original variants and *AtLACS9*. The microsomal fractions containing the recombinant enzymes were used for enzyme assays and Western blotting (Figure 4.4). When compared to the WT enzyme, increased microsomal enzyme activity and polypeptide accumulation were observed for variants L12F/C207F/L656F and D238E/P659S, as well as their single site mutants C207F, L656F, D238E and P659S (Figure 4.4A and B). Variant L12F, however, displayed comparable microsomal activity but decreased protein accumulation. The enzyme activity for each

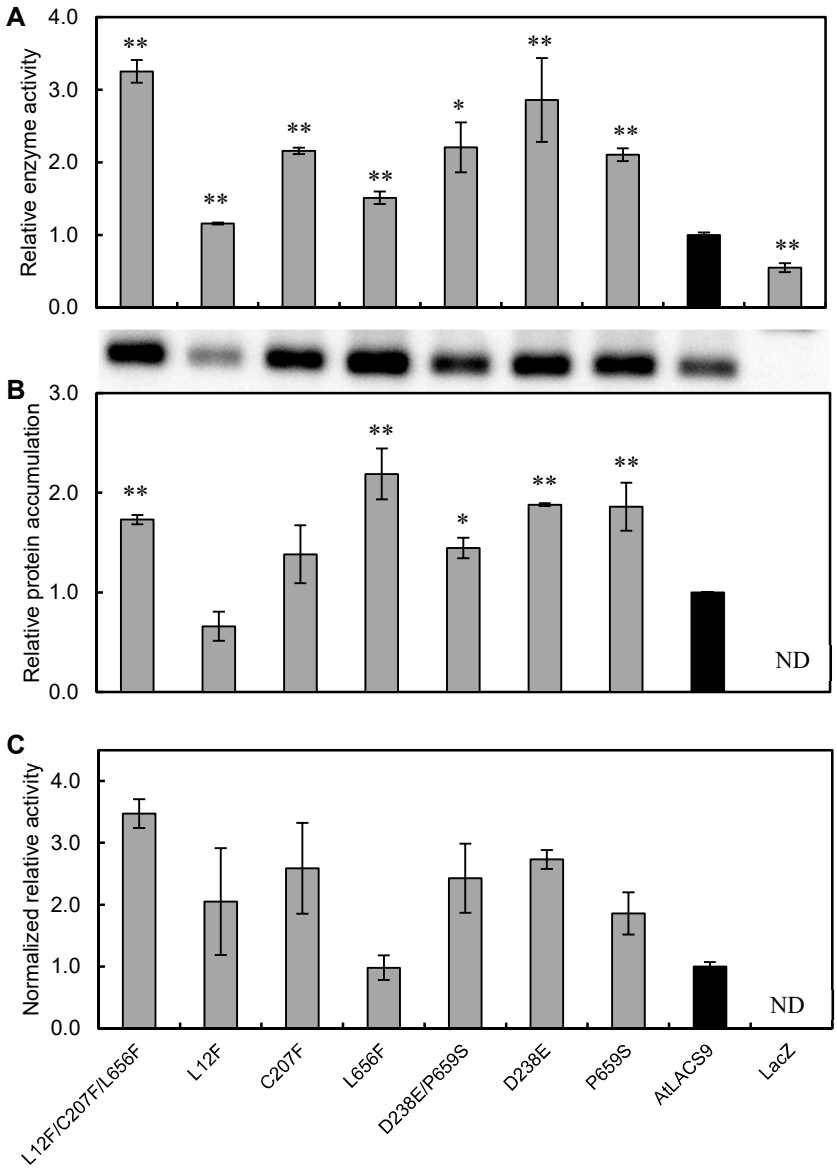

Figure 4.4. Enzyme activities and corresponding protein abundances of AtLACS9 single site mutants. A, Relative enzyme activities of single site mutants. The wild type (WT) AtLACS9 activity set as 1.0. Data are means ± S.D, n = 3. B, Relative protein abundance. Five μg of microsomal protein from the same batch of microsomes used to assess enzyme activity was used for Western blotting analysis. The relative abundance of

recombinant WT AtLACS9 was set as 1.0. Data are means ± S.D, n = 3. C, The normalized relative activity of each mutant was obtained by dividing the enzyme activity value by relative protein accumulation, with recombinant WT AtLACS9 activity set as 1.0. Data are means ± S.D, n=3. The asterisks indicate significant differences in activity (A), protein abundance (B), and normalized activity (C) of the microsomes containing recombinant AtDGAT9 variants versus recombinant WT AtLACS9 (t-test, ** P<0.01, * P < 0.05). ND, not determined.

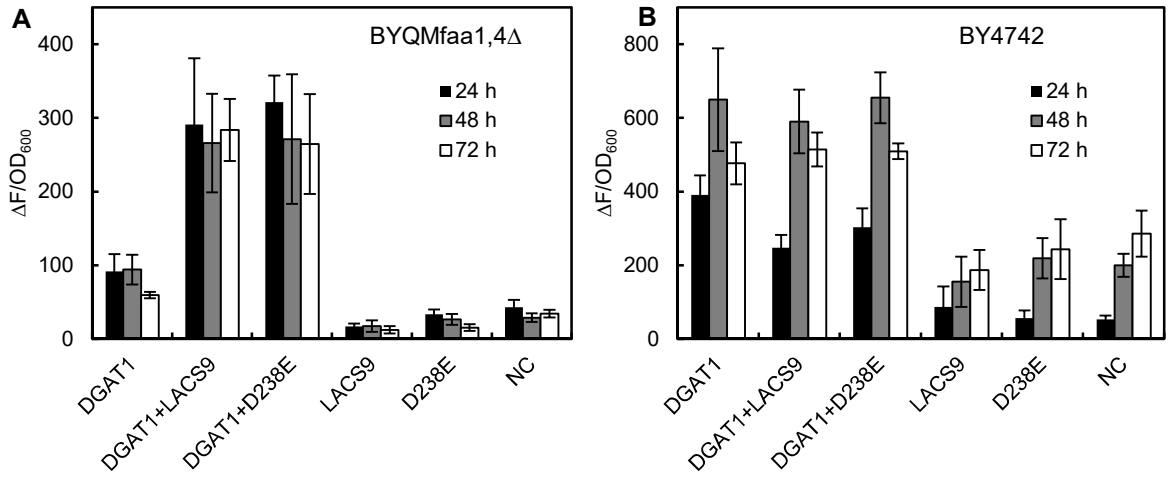

Figure 4.5. Neutral lipid accumulation in yeast mutant *BYQMfaa1,4*Δ (A) and wild type yeast BY4742 (B) expressing *AtLACS9* or variant *D238E* alone or combination with *BnaDGAT1*. Neutral lipid content of yeast was analyzed by Nile red assay. Data represent means ± S.D, n = 4-8 biological replicates.

variant was then normalized to the corresponding protein accumulation (Figure 4.4C). Single site mutants C207F and D238E were found to possess the highest normalized activity, which might contribute primarily to the increased enzyme activity of the original variants.

4.2.3. Co-expression of *AtLACS9* variant *D238E* and *DIACYLGLYCEROL ACYLTRANSFERASE* in yeast

Since two AtLACS9 variants were identified with improved enzyme activities, the ability of these variants to increase lipid content in yeast was examined. Over-expression of *AtLACS9* variants did not further increase lipid accumulation in the yeast mutant *BYfaa1,4*Δ (Figure 4.1A). It is possible that even though over-expression of *AtLACS9* variants in yeast enhances the acyl-CoA pool, the further conversion of acyl-CoA to TAG might be limited due to the lack of an efficient diacylglycerol acyltransferase (DGAT). In this regards, *Brassica napus DGAT1* (*BnaDGAT1*, encoding isoform BnaC.DGAT1.a (Greer et al., 2015)) was chosen to co-express with *AtLACS9* or its variant *D238E* in *S. cerevisiae* strain *BYQMfaa1,4*Δ and WT yeast BY4742, respectively, to test for TAG biosynthesis capacity. *S. cerevisiae* strain *BYQMfaa1,4*Δ is a yeast mutant devoid of TAG-synthesis capacity and with low LACS activity. Expressing *BnaDGAT1* or co-expressing *BnaDGAT1* and *AtLACS9* (or its variant) in *BYQMfaa1,4*Δ led to large accumulation of neutral lipid, whereas expression of empty vector p*NC, AtLACS9,* or its variant alone failed to complement yeast oil synthesis (Figure 4.5A). The co-expression groups resulted in yeast cells accumulating lipid at higher levels when compared to the yeast expressing *BnaDGAT1* alone, which is probably due to the enhancement in the acyl-CoA pool. No difference in

neutral lipid accumulation was observed between the yeasts co-expressing *BnaDGAT1* with *AtLACS9* variant *D238E* or with WT *AtLACS9*. Similarly, expression of *BnaDGAT1* in WT yeast BY4742 increased the yeast lipid content dramatically, whereas co-expressing *AtLACS9* (or its variant) with *BnaDGAT1* did not lead to further increase in neutral lipid accumulation (Figure 4.5B).

4.2.4. Multiple sequence alignment and positive selection prediction for LACS proteins

Several amino acid residue substitutions in AtLACS9 have been found to affect LACS activity (Figure 4.4). It would be interesting to explore their relationship with the putative functional motifs and other sites with functional importance in LACS protein. In this regard, sequence-based approaches, including multiple sequence alignment and positive selection prediction were performed for various LACS proteins (Table S4.2). Multiple sequence alignment is an effective approach to identify conserved functional motifs and subfamily specific positions. Some unconserved sites under positive selection may also have crucial role in the evolution of protein function (Yuan et al., 2017), since positive (Darwinian) selection was considered to drive the sweep and fixation of the advantageous mutations throughout a population (Biswas and Akey, 2006). To test whether some amino acid residue sites in the LACS sequence are under positive selection, site-specific non-synonymous (dN) to synonymous (dS) substitutions ratio (dN/dS or ω) test was conducted by using three sets of models (M0 versus M3, M1 versus M2, and M7 versus M8) from the PAML version 4 software (Yang, 2007). As the results shown in Table 4.1, the likelihood ratio test (LRT) of the comparison between the model pair of M1 (null

and neutral) versus M2 (selection) did not give a significant result to reject the null hypothesis of neutral selection. However, the comparison between the model pairs, M0 (null and neutral) versus M3 (selection), and M7 (null and neutral) versus M8 (selection) yielded the LRT statistics of 7909.3 and 783.0, respectively, suggesting that certain sites were indeed under selective pressures in LACS proteins. No positively selected sites were detected from the model M3 (ω2=0.89758), whereas in total 63 amino acid residues were identified as sites of positive selection from the model M8 (ω=1.22349) using Bayes empirical Bayes (BEB) analysis (Yang et al., 2005).

By mapping the detected positively selected sites and putative functional motifs (Black et al., 1997; Weimar et al., 2002; Hisanaga et al., 2004) onto the aligned sequences of AtLACS9 and other LACS proteins (Figure 4.6), it turns out that the positively selected sites were mainly located at the N- and C- termini of the enzymes, whereas no sites on the putative functional motifs were observed under positive selection. The amino acid residue substitutions in the identified AtLACS9 variants were also compared with the positively selected sites and putative functional motifs. Most of the amino acid residue substitutions are in the less conserved region with exception of E520 and D630. L12 and D238 are identified as positive selection sites, even though the posterior probabilities of both sites are only higher than 50%. According to the phylogenetic tree (Figure 4.7), AtLACS9-C207 is highly conserved among the LACS9 from plant eudicots, whereas AtLACS9-D238 is more divergent and the substitution of D238E is found to exist naturally in other LACSs.

Table 4.1. Parameter estimates and likelihood scores of LACS for sites models.

Model	Estimates of parameters	lnL	LRT pairs	df	2ΔlnL	p-value	Positively selected sites
M0: one ratio	ω= 0.19727	-63498.3	M0/M3	4	7909.3	<0.0001	none
M3: discrete	p0=0.82713, p1=0.15115, p2=0.02172, ω0=0.01143, ω1=0.18961, ω2=0.89758	-59543.7					
M1: nearly neutral	p0= 0.96980, p1=0.03020, ω0=0.06927, ω1=1.00000	-60172.6	M1/M2	2	0	1.00000	none
M2: positive selection	p0=0.96980, p1=0.02844, p2=0.00176, ω0=0.06927, ω1=1.00000, ω2=1.00000	-60172.6					
M7: β	p=0.08048, q=0.83695	-59838.9	M7/M8	2	783.0	<0.0001	30 sites (>50%)
M8: β + ω	p0=0.99029, p=0.14171, q=2.31642, p1=0.00971, ω=1.22349	-59447.4					15 sites (>95%) 18 sites (>99%)

Positive selection by site models was performed using CODEML program in PAML. The number of positively selected sites is also shown, with the Bayes empirical Bayes (BEB) posterior probability in blankets. df, degrees of freedom; LRT, likelihood ratio test; lnL, log likelihood scores; 2ΔlnL, twice the log-likelihood difference of the models compared.

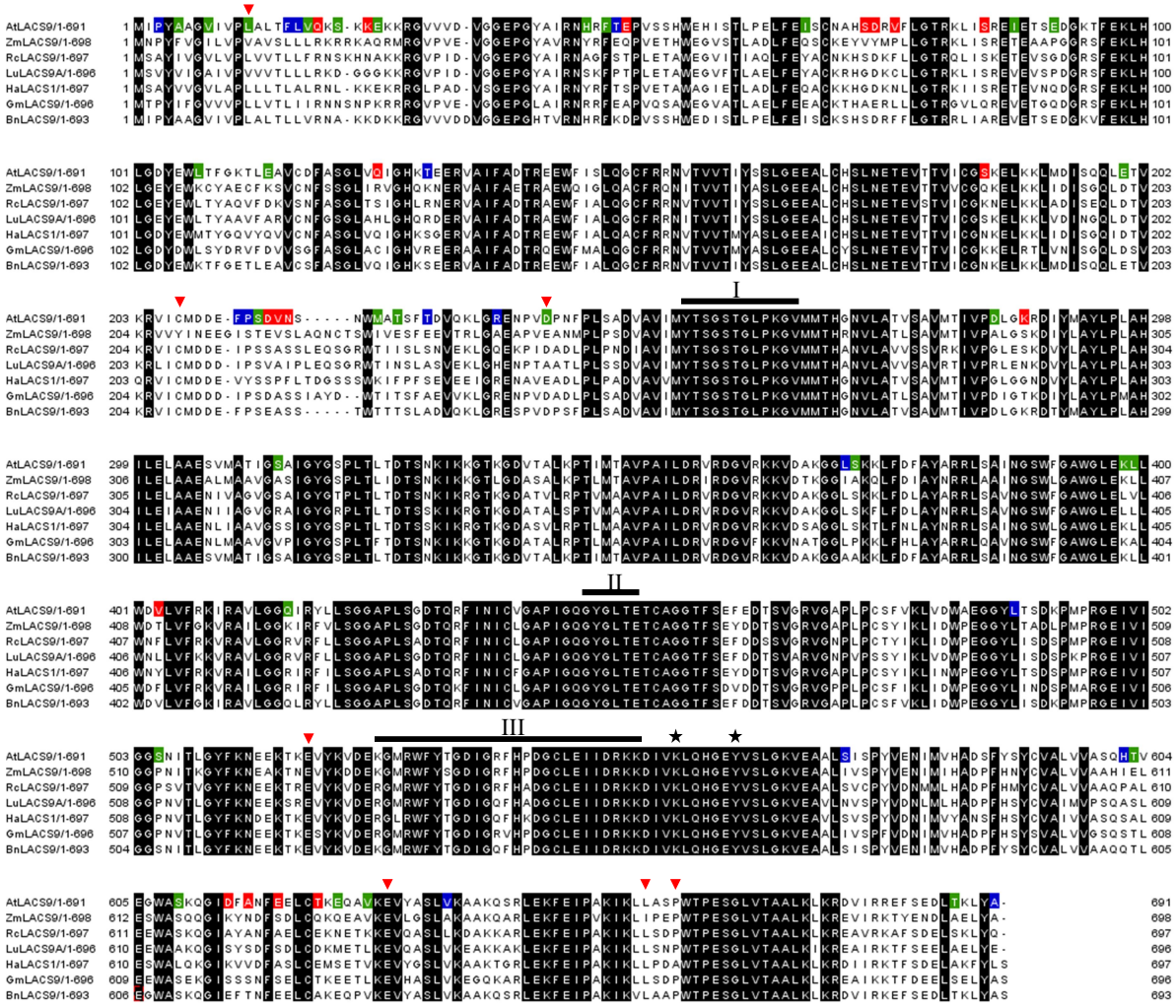

Figure 4.6. Sequence alignment of LACS9 proteins from seven typical plant species. Conserved sites are shaded. Positively selected sites with a Bayes Empirical Bayes posterior probability higher than (≥) 50%, higher than (≥) 95%, and higher than (≥) 99% are indicated by the amino acid sites in green, blue, and red background, respectively. The single mutation sites are indicated by red-filled triangle. The bar above the sequence corresponds to the ATP/AMP signature motifs (I & II) and the fatty acyl-CoA synthetase signature motif (III). The putative active sites are indicated by black-filled stars. The alignment was visualized and displayed using Jalview (Waterhouse et al., 2009).

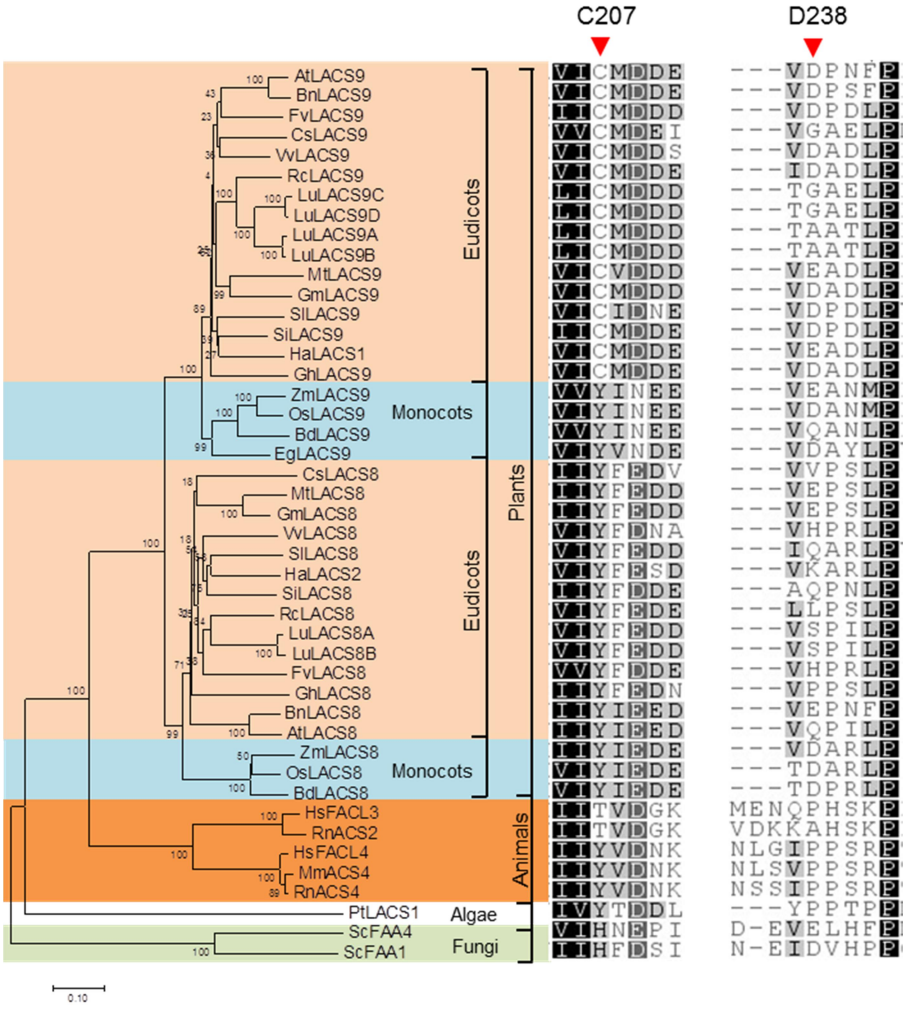

Figure 4.7. Amino acid sequence analysis of LACS proteins from different species. Phylogenetic relationship among protein sequences of LACS were constructed using the neighbour-joining method. Bootstrap values are shown at the tree nodes. The amino acid residue substitution sites of AtLACS9 variants are marked with red-filled triangles.

4.3. Discussion

The current study reports on the generation of performance enhanced variants of AtLACS9. The mutations were introduced in AtLACS9 by error-prone PCR and several variants were identified with increased microsomal activity and/or altered substrate specificity (Figure 4.1 and 4.3). Both enzyme activity and polypeptide accumulation level contributed to increased microsomal activity (Figure 4.2). The microsomal activity of each variant was then normalized to the corresponding polypeptide accumulation and compared. All the variants had increased or similar normalized activity compared to that of the WT enzyme (Figure 4.2). Since the two activity-improved variants (L12F/C207F/L656F and D238E/P659S) contained more than one amino acid residue substitution, single site mutants were generated using site-directed mutagenesis to further elucidate the contribution of each amino acid residue substitution. Single site mutants C207F and D238E were considered mainly responsible for the increased enzyme activity, although amino acid residue substitutions of L12F and P659S also led to increases in enzyme activity to some extent (Figure 4.4).

It has been suggested that both moderately conserved sites (e.g. subfamily specific positions) (Suplatov et al., 2012) and unconserved sites (particularly positively selected sites) (Yuan et al., 2017) may have a crucial role in affecting protein function. To interpret the effects of amino acid residue substitutions on AtLACS9 variants, the amino acid residue substitutions of each variant and the positively selected sites were mapped onto the multiply aligned sequences of LACS9 proteins (Figure 4.6). It is not surprising that none of the amino acid residue substitutions was found to reside in the putative functional motifs of

LACS. Indeed, it has been suggested that the substitutions which could affect enzyme function may be far away from the enzyme functional sites as observed for variants of soybean (*Glycine max*) DGAT1 (Roesler et al., 2016). The amino acid residue substitution of C207F led to increased enzyme activity was found at the moderately conserved site (C207, Figure 4.4 and 4.7). Two additional activity-improved variants (L12F and D238E) were found with amino acid residue substitutions at the predicted positively selected sites (Figure 4.4 and 4.6).

Amino acid residue substitution E520D causing altered substrate specificity is localized in vicinity of the fatty acyl-CoA synthetase signature motif (FACS motif), which has been proposed to be involved in fatty acid binding (Watkins and Ellis, 2012). Even though this motif was suggested to not be involved in fatty acid binding based on the structure of *Thermus thermophiles* LACS (Hisanaga et al., 2004), the crystal structure of *Mycobacterium tuberculosis* very-long-chain fatty acyl-CoA synthetase (MtVLACS) indicated a different fatty acid binding tunnel extending from the ATP binding site to the protein surface, which involved the FACS motif (Watkins and Ellis, 2012). Mutations in the FACS signature motif of MtVLACS resulted in up to a 4-fold decrease in fatty acid binding affinity (Khare et al., 2009), probably due to the influence of the internal surface of the fatty acid binding tunnel entrance at the ATP-binding site (Watkins and Ellis, 2012). The observed fatty acid specificity of microsomal AtLACS9 (Figure 4.3) was in general consistent with the previously reported substrate specificity of AtLACS9 (Shockey et al., 2002). The only difference is that Shockey et al. (2002) observed that AtLACS9 showed a slightly higher preference towards oleic acid over linoleic acid, whereas AtLACS9 was

observed to prefer linoleic acid slightly more than oleic acid in this study. This discrepancy may be a result of the different sources of recombinant AtLACS9 used in the assay. In our study, *AtLACS9* and its variants were expressed in yeast stain *BYfaa1,4*Δ, which contains less than 10% LACS enzymes in yeast background (Guo et al., 2014), and as a result, the control microsomes (LacZ) still displayed a low level of LACS activity (Figure 4.1 to 4.4). On the other hand, Shockey et al. (2002) used the *Escherichia coli* mutant strain K27 to produce recombinant AtLACS9, which provided a clean background for the LACS assay due to the complete loss of endogenous LACS activity in *E.coli* K27.

Over-expression of *LACS* has been shown to increase oil deposition in yeast (Guo et al., 2014; Tan et al., 2014; Tonon et al., 2005; Pulsifer et al., 2012). In the current study, however, attempts to increase yeast oil content by the introduction of activity-improved recombinant AtLACS9 variants or introduction of variant AtLACS9 with BnaDGAT1 were not successful (Figure 4.1 and 4.5). Even though co-expression of *BnaDGAT1* with *AtLACS9* or its variants resulted in higher oil content in yeast mutant *BYQMfaa1,4*Δ relative to yeast expressing *BnaDGAT1* alone, no difference in oil content was observed between the yeast cells producing BnaDGAT1 with AtLACS9, or its variant D238E (Figure 4.5A). The results in Figure 4.5A are also supported by the results from the co-expression of *BnaDGAT1* and *AtLACS9* in WT yeast BY4742 (Figure 4.5B). These observations may be associated with the limitations in the DGAT1-catalyzed reactions. Recombinant BnaDGAT1 was certainly effective in substantially boosting neutral lipid content in WT yeast (Figure 4.5B), which is in agreement with previous study (Greer et al., 2015). In addition, BnaDGAT1 is certainly capable of utilizing 16:0, 18:0 or 18:1-CoA (Greer et al.,

2016; Caldo et al., 2015), which are some of the major fatty acids found in *S. cerevisiae* lipids (Greer et al., 2015). Further insight may be gained through analysis of acyl-CoA and *sn*-1,2-diacylglycerol content of the yeast cells and the fatty acid composition of the lipid classes. In addition, it may be worthwhile repeating the experiment with addition of exogenous linoleic acid to the growth medium. This aspect would take advantage of the known preference of AtLACS9 and its variants for linoleic acid (Figure 4.3).

In conclusion, several AtLACS9 variants with enhanced performance were identified. Two variants with multiple amino acid residue substitutions displayed increased enzyme activity. Sequence analysis and site-directed mutagenesis revealed that amino acid residue substitution at the conserved site C207 and the positively selected site D238 were responsible for the increases in enzyme activity, respectively. In addition, AtLACS9 variants with amino acid residue substitutions of E520D and E630D, which displayed altered substrate specificity, were located in the vicinity of the putative fatty acid binding motif. Our findings provide valuable information for increasing LACS activity and altering substrate specificity of the enzyme.

4.4. Experimental procedures

4.4.1. Cloning, mutagenesis of *AtLACS9*, plasmid construction and yeast heterologous expression

The open reading frame of *AtLACS9* was amplified using a cDNA preparation from Arabidopsis developing seeds and was cloned into the pYES2.1 vector (Invitrogen, Burlington, ON, Canada). Site-directed mutagenesis within *AtLACS9* was conducted using

the QuikChange™ Site-Directed Mutagenesis Kit (Stratagene Cloning Systems, La Jolla, CA). The primers used for the construction of various mutants are listed in Table S4.1.

The co-expression vectors of *AtLACS9* (or *AtLACS9* variant *D238E*) and *BnaDGAT1* were constructed as described previously (Pan et al., 2015). In brief, the cDNA of *BnaDGAT1* was ligated into the multiple cloning sites of the pESC vector. The region from *CYC1* terminator to *ADH1* terminator of pESC construct (pESC-URA or *BnaDGAT1* in pESC) and the entire plasmid of pYES2 construct (pYES2, *AtLACS9* or *AtLACS9-D238E*) were amplified and yielded fragment 1 and 2, respectively. Fragment 1 was then cloned into fragment 2 using enzymatic assembly method (Gibson, 2011). Six different plasmids resulted from the different combinations of DNA fragments: 1) p*AtLACS9+BnaDGAT1* contains both *AtLACS9* and *BnaDGAT1* cDNAs; 2) p*AtLACS9-D238E+BnaDGAT1* contains both *AtLACS9-D238E* and *BnaDGAT1* cDNAs; 3) p*AtLACS9* contains only *AtLACS9*; 4) p*AtLACS9-D238E* contains only *AtLACS9-D238E;* 5) p*BnaDGAT1* contains only *BnaDGAT1*; 6) pNC is the control plasmid.

After the integrity of all constructs was verified by sequencing, the constructs were transformed into yeast using the *S.c.* EasyComp Transformation Kit (Invitrogen). The recombinant yeast cells were cultured in 2% (w/v) raffinose minimal medium (0.67% (w/v) yeast nitrogen base and 0.2 % (w/v) SC-Ura). After overnight growth, the yeast cultures were inoculated into minimal medium with 2% (w/v) galactose and 1% (w/v) raffinose to an optical density of 0.4 at 600 nm (OD_{600}). Yeast cultures were grown at 30^{o}C with shaking at 220 rpm.

S. cerevisiae strain *BYfaa1,4Δ* (*MATα his3Δ1 leu2Δ0 lys2Δ0 ura3Δ0, faa1 Δ::HIS3, faa4 Δ::LYS2*) was used for heterologous expression of *AtLACS9* and its variant. For the co-expression study, the co-expression constructs were transformed into *S. cerevisiae* strain *BYQMfaa1,4Δ* (*MATα, his3Δ1, leu2Δ0, lys2Δ0, ura3Δ0, dga1 Δ::kanMX, lro1 Δ::kanMX, are1 Δ::kanMX, are2 Δ ::kanMX, faa1 Δ::HIS3, faa4 Δ::LYS2)* and WT yeast BY4742 (*MATα, his3Δ1, leu2Δ0, lys2Δ0, ura3Δ0*). Construction of *BYQMfaa1,4Δ* was described by Sec et al. (2015). Construction of *BYfaa1,4Δ* was done by the same approach as the *BYQMfaa1,4Δ* (Sec et al., 2015).

4.4.2. Protein extraction and western blotting

Microsomal fractions were recovered from the recombinant yeast cells as described previously (Pan et al., 2013, Siloto et al., 2009). In brief, the recombinant yeast cells were collected at similar OD_{600} during the log growth phase and then resuspended in lysis buffer containing 20 mM Tris-HCl pH 7.9, 10 mM $MgCl_2$, 1 mM EDTA, 5% (v/v) glycerol, 300 mM ammonium sulfate and 2 mM dithiothreitol before homogenization using a bead beater (Biospec, Bartlesville, OK, USA). The crude homogenate was centrifuged for 30 min at 10 000 g, and the supernatant was further centrifuged at 105 000 g for 70 min to separate the microsomal fractions. The microsomal fractions were resuspended in 3 mM imidazole buffer (pH 7.4) containing 125 mM sucrose. All procedures were carried out at 4^{o}C. The protein content was determined by Bradford assay using BSA as a standard (Bradford, 1976).

For Western blotting, 5 μg of microsomal proteins were separated by 10% denaturing SDS-PAGE gel and electrotransferred (overnight at 30 mA and 4^{o}C) onto polyvinylidene difluoride membrane (Amersham, GE Healthcare, Mississauga, ON, Canada). The membrane was first blocked with 2% ECL prime blocking reagent (Amersham) and then was incubated with V5-HRP-conjugated antibody (Invitrogen). HRP conjugated antibody was detected using ECL Advance Western Blotting Detection Kit (Amersham) with a FluorChem SP imager (Alpha Innotech Corp., San Leandro, CA, USA).

4.4.3. *In vitro* LACS enzyme assays

The LACS assay was performed according to de Azevedo Souza et al. (2009) and Shockey et al. (2002), with slight modifications. In brief, the enzyme assay was carried out in a 60-μL reaction mixture containing 100 mM Bis-Tris-propane (pH 7.6), 10 mM $MgCl_2$, 5 mM ATP, 2.5 mM dithiothreitol, 1 mM CoA, 20 μM [1-^{14}C] oleic acid (56.3 mCi/mmol, PerkinElmer, Waltham, MA, USA) and 2 μg of microsomal protein. The reaction was initiated by adding microsomal protein and quenched with 10 μL of 10% (w/v) SDS after incubation at 30^{o}C for 5 min with shaking. The entire reaction mixture was extracted 4 times using 900 μL of 50% (v/v) isopropanol saturated hexane. An aliquot of the aqueous phase was analyzed for radioactivity by a LS 6500 multi-purpose scintillation counter (Beckman-Coulter, Mississauga, ON, Canada). For the substrate specificity assay, 20 μM [1-^{14}C] fatty acids, including palmitic acid (60 mCi/mmol, PerkinElmer), stearic acid (58.9 mCi/mmol, American Radiolabeled Chemicals, St. Louis, MO, USA), oleic acid, and linoleic acid (58.2 mCi/mmol, PerkinElmer) were used in the assay.

4.4.4. Sequence alignment and positive selection

Forty-five LACS sequences were collected from different species (Table S4.2). Multiple sequence alignment of LACS proteins were performed using ClustalW in MEGA 7 under the default setting (Kumar et al., 2016). A neighbour-joining with 1000 bootstrap repetitions tree was built using the same software. A web server PAL2NAL (http://www.bork.embl.de/pal2nal/, cited 29 Sept 2017) was then used to construct a multiple codon alignment based on the corresponding aligned amino acid sequences. The output alignment was imported into the jModelTest 2 program (Santorum et al., 2014) to determine the best-fitting evolutionary model. The general time reversible (GTR) model plus Gamma distribution plus invariant site model of molecular evolution (GTR + G + I) was determined as the best-fit substitution model based on the lowest value of the Akaike Information Criterion. A maximum likelihood phylogenetic tree was then constructed with the PhyML webserver (http://www.atgc-montpellier.fr/phyml/, cited 29 Sept 2017) (Guindon et al., 2005, 2010) according to the best-fit predictive model. The posterior probabilities of sites under positive selection were calculated using CodeML program in the PAML version 4 software (Yang, 2007) based on site-specific Bayes empirical Bayes probabilities (Yang et al., 2005). Three sets of models were carried out using the F3X4 codon frequency model, including M0 (one ratio) vs. M3 (discrete); M1 (nearly neutral) vs. M2 (positive selection); and M7 (β) vs. M8 (β + ω).The statistical significance of each pair of nested models was evaluated by the LRT.

4.4.5. Statistical analysis

Data are means ± standard deviation (S.D.) for the number of independent experiments as indicated. All statistical analyses were performed using the SPSS statistical package (SPSS 16.0, Chicago, IL, USA). Significant differences between two groups were determined using a two-tailed Student's t-test. The equality of variances was determined by the Levene's test. When the variances were equal, the unpaired Student's t-test assuming equal variances was performed. When the variances were unequal, the unpaired Student's t-test with Welch corrections assuming unequal variances was used.

4.5. Supplementary material

Supplementary Table S4.1. Primers used for site-directed mutagenesis. Mutation is indicated by underline, and primers are shown from 5' to 3'.

Mutation	Forward primer	Reverse primer
L12F	GCTGCTGGTGTTATTGTGCCATTTGCTTTGACGTTTC	GAAACGTCAAAGCAAATGGCACAATAACACCAGCA GC
C207F	GAAACTGTGAAACGTGTGATATTCATGGATGATGAA TTCCCAT	ATGGGAATTCATCATCCATGAATATCACACGTTTCAC AGTTTC
L656F	TGAGATACCAGCAAAGATCAAATTATTTGCATCTCC ATGGAC	GTCCATGGAGATGCAAATAATTTGATCTTTGCTGGTA TCTCA
P659S	ATCAAATTATTGGCATCTTCATGGACGCCAGAGTCA G	CTGACTCTGGCGTCCATGAAGATGCCAATAATTTGAT

Supplementary Table S4.2. Accession numbers of the *LACS* sequences from different species used for multiple alignment.

Gene	Accession number	Organism
AtLACS8	AF503758	*Arabidopsis thaliana*
AtLACS9	AF503759	*Arabidopsis thaliana*
BdLACS8	XM_003577057	*Brachypodium distachyon*
BdLACS9	XM_003577743	*Brachypodium distachyon*
BnLACS8	XM_013831345	*Brassica napus*
BnLACS9	NM_001316278	*Brassica napus*
CsLACS8	XM_004164005	*Cucumis sativus*
CsLACS9	XM_004161121	*Cucumis sativus*
EgLACS9	XM_010932582	*Elaeis guineensis Jacq.*
FvLACS8	XM_004303531	*Fragaria vesca*
FvLACS9	XM_004290818	*Fragaria vesca*
GhLACS8	XM_016889481	*Gossypium hirsutum*
GhLACS9	XM_016853003	*Gossypium hirsutum*
GmLACS8	XM_003556847	*Glycine max*
GmLACS9	XM_003542913	*Glycine max*
HaLACS1	HM490305	*Helianthus annuus*
HaLACS2	HM490306	*Helianthus annuus*
HsFACL3	NM_004457	*Homo sapiens*
HsFACL4	Y12777	*Homo sapiens*
LuLACS8A	Lus10016083	*Linum usitatissimum*
LuLACS8B	Lus10012307	*Linum usitatissimum*
LuLACS9A	Lus10042707	*Linum usitatissimum*
LuLACS9B	Lus10029669	*Linum usitatissimum*
LuLACS9C	Lus10025657	*Linum usitatissimum*
LuLACS9D	Lus10018178	*Linum usitatissimum*
MmACS4	AB033885	*Mus musculus*
MtLACS8	XM_003601477	*Medicago truncatula*
MtLACS9	XM_003601977	*Medicago truncatula*
OsLACS8	NM_001061712	*Oryza sativa*
OsLACS9	NM_001072788	*Oryza sativa*
PtLACS1	KF359938	*Phaeodactylum tricornutum*
RcLACS8	XM_002532166	*Ricinus communis*
RcLACS9	XM_015716012	*Ricinus communis*
RnACS2	D30666	*Rattus norvegicus*
RnACS4	NM_053623	*Rattus norvegicus*
ScFAA1	NM_001183737	*Saccharomyces cerevisiae*
ScFAA4	NM_001182754	*Saccharomyces cerevisiae*
SiLACS8	XM_011087111	*Sesamum indicum*

SiLACS9	XM_011071232	*Sesamum indicum*
SlLACS8	XM_004243540	*Solanum lycopersicum*
SlLACS9	XM_004250346	*Solanum lycopersicum*
VvLACS8	XM_002267381	*Vitis vinifera*
VvLACS9	XM_002285817	*Vitis vinifera*
ZmLACS8	NM_001158459	*Zea mays*
ZmLACS9	XM_008664290	*Zea mays*

Chapter 5 – Possible Role of Long-Chain Acyl-CoA Synthetase and Diacylglycerol Acyltransferase in Channeling α-linolenic Acid into Flax Seed Triacylglycerol

5.1. Introduction

Long-chain acyl-CoA synthetase (LACS, EC 6.2.1.3) catalyzes the ATP-dependent activation of free fatty acids to form acyl-CoAs. *De novo* synthesis of free fatty acids occurs in the plastid with activation to acyl-CoAs occurring on the outside of the plastid (Chapman and Ohlrogge, 2012). The resulting cytosolic acyl-CoA pool in turn serves as an acyl-donor in acyltransferase reactions catalyzing triacylglycerol (TAG) assembly (Snyder et al., 2009). In addition, LACS may be involved in catalyzing the activation of modified fatty acids released from the membrane lipid, phosphatidylcholine (PC), through the catalytic action of phospholipase A_2 (Lands, 1960; Bayon et al., 2015). In *Arabidopsis thaliana*, nine *LACS* genes have been found to participate in fatty acid and glycerolipid metabolism (Shockey et al., 2002) with distinct tissue distributions, subcellular locations, and biological functions. AtLACS6 and AtLACS7 are peroxisomal-localized proteins which are required for the activation of fatty acids for β-oxidation during seedling development (Fulda et al., 2004, 2002). In contrast, AtLACS1 and AtLACS2, localized in the endoplasmic reticulum (ER), are involved in both wax and cutin biosynthesis (Schnurr and Shockey, 2004; Tang et al., 2007; Lü et al., 2009; Weng et al., 2010). AtLACS4, another ER-bound LACS, has been found to functionally overlap with AtLACS1 in mediating the synthesis of lipid for pollen coat formation (Jessen et al., 2011).

The identification of specific LACS involved in TAG biosynthesis has remained elusive. AtLACS9 and AtLACS1 have been suggested to have overlapping function in

activating plastidially-derived fatty acids (Zhao et al., 2010), whereas a more recent study revealed that instead of being involved in exporting fatty acids from the plastid, AtLACS9, the most likely candidate for TAG biosynthesis, contributed to lipid trafficking from the ER to plastid together with AtLACS4 (Jessen et al., 2015). Specialized LACSs with unique substrate specificities have been identified in various plants (*Helianthus annuus*, *A.thaliana*, *Oryza sativa*, and *Ricinus communis*) and a diatom (*Thalassiosira pseudonana*) (Tonon et al., 2005; Aznar-Moreno et al., 2014; Shockey et al., 2002; Ichihara et al., 2003; He et al., 2007), suggesting the possible role of LACS in the fatty acid channeling process.

Flax (*Linum usitatissimum*) oil, which is enriched in α-linolenic acid (ALA; $18{:}3\Delta^{9cis,12cis,15cis}$), has numerous applications in industry and nutrition (Pan et al., 2013). In plants, polyunsaturated fatty acids (PUFAs), such as ALA, are synthesized on PC and then channeled into TAG in processes involving acyl-editing (Bates et al., 2012; Lager et al., 2015). PUFA-channeling in flax may involve the action of phospholipid:diacylglycerol acyltransferase (PDAT) (Pan et al., 2013), phosphatidylcholine:diacylglycerol cholinephosphotransferase (PDCT) (Wickramarathna et al., 2015), and/or the combined reactions catalyzed by lysophosphatidylcholine acyltransferase (LPCAT) and diacylglycerol acyltransferase (DGAT, EC 2.3.1.20) (Pan et al., 2015). Considering the high level of ALA accumulation in flax seed oil, it is possible that flax LACSs contribute to TAG biosynthesis through enhanced specificity for ALA.

The resulting α-linolenoyl-CoA from LACS action would be utilized as the substrate for the acyltransferases from the Kennedy pathway to form TAG. The Kennedy pathway leading to TAG involves the sequential acylation of *sn*-glycerol-3-phosphate via

the catalytic action of three different acyl-CoA-dependent acyltransferases, including *sn*-glycerol-3-phosphate acyltransferase, lysophosphatidic acid acyltransferase and DGAT (Snyder et al., 2009). The last and only committed step of the Kennedy pathway is catalyzed by DGAT, which might represent a bottleneck in TAG biosynthesis (Liu et al., 2012). At least two forms of microsomal DGAT, having very different amino acid sequences, have been designated DGAT1 and DGAT2. It has been suggested that DGAT1 contributes more generally to TAG biosynthesis, whereas DGAT2 seems to be more important in the formation of TAG containing unusual fatty acids such as ricinoleic and α-eleostearic acid from castor (*Ricinus communis*) and tung (*Vernicia fordii*), respectively (Burgal et al., 2008; Li et al., 2010a).

In this study, three putative *LACS* cDNAs (*LuLACS8A*, *9A*, *9C*) were cloned and characterized from flax. LuLACS8A was found to display increased substrate preference towards ALA. The resulting linolenoyl-CoA might be further utilized to form ALA-enriched TAG by LuDGAT2, which showed enhanced preference towards this substrate. To test this hypothesis, *LuLACS8A* and *LuDGAT2* were co-expressed in *Saccharomyces cerevisiae* mutant *BYQMfaa1,4Δ* and their combined performance for the channeling of ALA into TAG was evaluated both *in vitro* and *in vivo*. These results suggest that the LuLACS8A-catalyzed reaction may contribute to the enhanced accumulation of ALA in flax oil by the cooperation with LuDGAT2.

5.2. Results

5.2.1. Identification of *LACS* cDNAs and deduced amino acid sequences

Based on the results of a BLAST search of the flax genome database, six putative *LACS* genes (designated as *LuLACS8A*, *8B*, *9A*, *9B*, *9C*, *9D*) were identified. The corresponding cDNAs and their encoded proteins are presented in Table 5.1. Although the sequence similarity of all these encoded proteins is 59.2%, the protein sequences of each cDNA pair share very high identity (Table 5.2), with similarity from 96% (LuLACS8A and 8B) to 98% (LuLACS 9A and 9B; LuLACS 9C and 9D). Analysis of the synonymous substitution rates (*K*s, Table 5.2) observed within cDNA pairs indicated that divergence occurred approximately 6.8 million years ago, which is consistent with the recent genome duplication event (5-9 million years ago) in flax (Wang et al., 2012b).

Phylogenetic analysis of LuLACS sequences was performed together with other known or predicted LACS8 and LACS9 protein sequences from oil crops (Figure 5.1A). The LuLACS proteins were separated into two groups based on homology, with LuLACS8A and B grouping with AtLACS8, and LuLACS9A, B, C and D with AtLACS9. LuLACSs were more closely related to the LACSs from castor (*Ricinus communis*) which also belongs to the order *Malpighiales*. The AtLACS8-like group and AtLACS9-like group share 70.4% and 75.2% pairwise identity, respectively, whereas the pairwise identity for all selected LACS proteins is 67.9%. Protein sequence analysis revealed the presence of highly conserved ATP/AMP signature motifs and a fatty acyl-CoA synthetase signature motif (Black et al., 1997; Weimar et al., 2002), which may be essential for LACS function. One

major difference among deduced LACS protein sequences resides in the N terminal region, resulting in different protein lengths of the two LACS groups. The lengths of AtLACS8-like proteins were significantly longer than that of AtLACS9-like proteins, primarily due to the presence of N-terminal extensions (Figure 5.1B).

The membrane topologies of LACSs from flax and Arabidopsis were predicted by different topological prediction programs (Table S5.3). AtLACS8, LuLACS8A and LuLACS9C are likely to possess one transmembrane domain at their N-termini, which is similar to the common architecture of very-long-chain acyl-CoA synthetase (Obermeyer et al., 2007; Lewis et al., 2001). The predicted membrane topology of LuLACS8A (by Phobius (Käll et al., 2007)) was visualized by Protter (Omastis et al., 2014) and the result suggested that its N and C termini may orient toward the cytosolic and lumen sides, respectively (Figure S5.1). Signature motifs and putative active sites based on the structure of LACS from *Thermus thermophilus* are also indicated in the topology figure (Black et al., 1997; Weimar et al., 2002; Hisanaga et al., 2004). The predictions for AtLACS9 and LuLACS9A, on the other hand, are incompatible among different programs, even though AtLACS9 was reported to localize to the outer envelope of the chloroplast (Schnurr et al., 2002).

Table 5.1 Overview of putative *LACS* cDNAs identified in flax.

Genes	cDNA length (bp)	Protein length	Molecular mass (KDa)	Isoelectric point
LuLACS8A	2199	732	79.667	6.19
LuLACS8B	2193	730	79.499	5.94
LuLACS9A	2091	696	76.227	7.52
LuLACS9B	2091	696	76.052	6.85
LuLACS9C	2088	695	75.646	8.59
LuLACS9D	2088	695	75.455	8.50

Table 5.2 Sequence identity and synonymous substitution rates (*K*s values) of the cDNA pairs.

cDNA Pair	Nucleotide (%)	Amino Acid (%)	*K*s (mean±S.E.)	*K*s average
LuLACS8A and *LuLACS8B*	96.2	96.6	0.09951 ± 0.01370	0.083
LuLACS9A and *LuLACS9B*	97.2	98.3	0.09170 ± 0.01373	
LuLACS9C and *LuLACS9D*	97.7	98.1	0.05791 ± 0.01021	

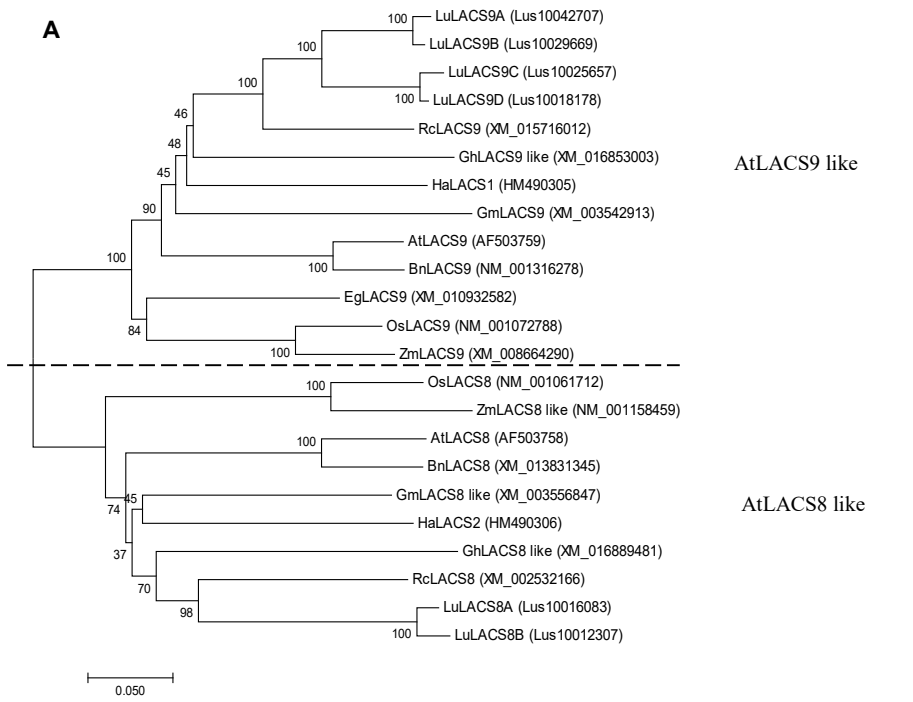

Figure 5.1. Sequence analysis of deduced amino acids of flax LACSs. A, phylogenetic relationship among deduced amino acid sequences of flax LACSs and LACSs from other organisms. *At, Arabidopsis thaliana; Bn, Brassica napus; Eg, Elaeis guineensis; Gh, Gossypium hirsutum; Gm, Glycine max; Ha, Helianthus annuus; Os, Oryza sativa; Rc, Ricinus communis; Zm, Zea mays*. Genbank accession number for each sequence is shown in brackets. Bootstrap values for the neighbour-joining tree are shown at the tree nodes. B, amino acid alignments of the N-terminus, ATP/AMP signature motifs and fatty acyl-CoA synthetase signature motif (FACS signature motif) of each LACS sequence.

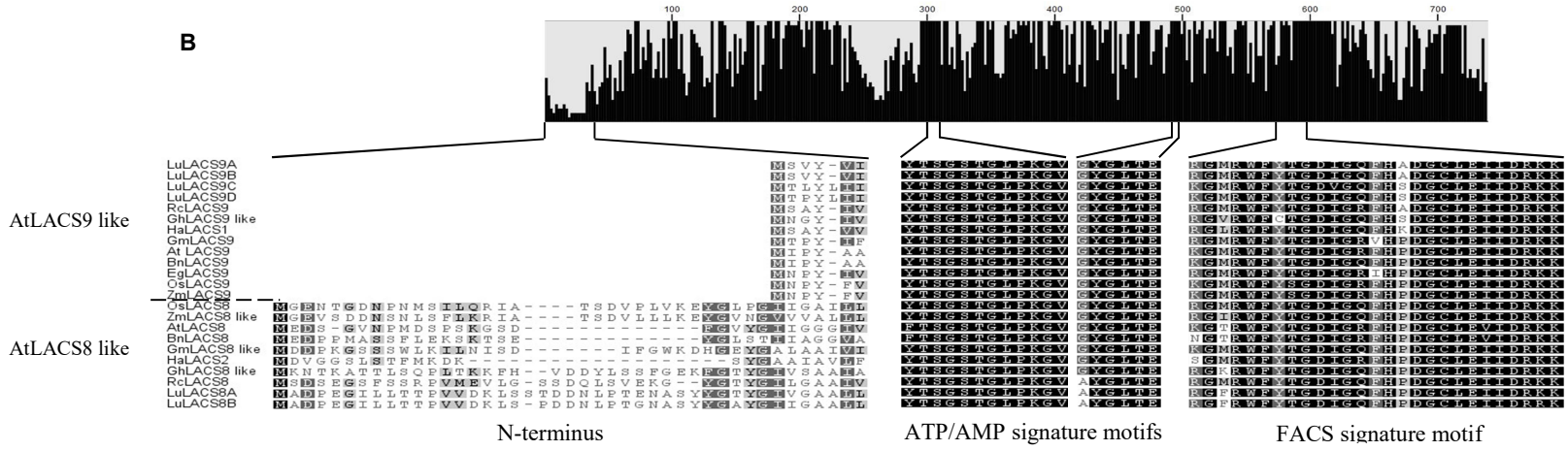

5.2.2. Heterologous expression of *LuLACSs* in *S. cerevisiae BYfaa1,4Δ*

To verify the function of putative *LuLACS* genes, the coding sequences of *LuLACS8A*, *9A* and *9C* were cloned into the pYES2.1 vector and transformed into *S. cerevisiae* mutant *BYfaa1, 4Δ*. *AtLACS9* and empty vector (LacZ) were used as the positive and negative controls, respectively. The yeast mutant *BYfaa1, 4Δ* has both *FAA1* and *FAA4* genes knocked out which together encode LACS enzymes accounting for over 90% of LACS activity in yeast (Guo et al., 2014), and thus cannot grow on media containing fatty acids and cerulenin (an endogenous fatty acid synthesis inhibitor) due to defective formation of acyl-CoAs. The growth of cells can be rescued by transforming with an *LACS* cDNA encoding active LACS. All three putative *LuLACS* cDNAs complemented the yeast mutant phenotype (Figure S5.2), indicating that the *LuLACS*s encoded active LACS enzymes. Yeast cells producing LuLACSs or LacZ were then cultured in liquid medium and subjected to the Nile Red assay after 48 h and 72 h induction. As shown in Figure 5.2A, neutral lipid content in cultures producing LuLACSs accumulated to higher levels than the LacZ control. Previously, plant LACSs have been shown to facilitate fatty acid uptake in yeast (Pulsifer et al., 2012). To investigate whether LuLACSs could contribute to the import of exogenous fatty acids, the yeasts producing LuLACSs were cultured in the presence of oleic acid (OA, 18:1Δ^{9cis}), linoleic acid (LA, 18:2$^{\Delta 9cis,12cis}$) or ALA for 72 h. The yeast total lipid was then extracted and the TAG fractions were analyzed for fatty acid composition by GC-MS. Feeding yeast cultures producing recombinant LuLACSs with OA, LA or ALA led to an increased amount of the corresponding fatty acids in yeast TAG compared to the LacZ control (Figure 5.2B). This result indicated that LuLACSs facilitated the uptake of OA, LA or ALA into yeast cells and catalyzed the activation of the fatty acids to their corresponding acyl-CoAs which could, in turn, then be used for TAG production.

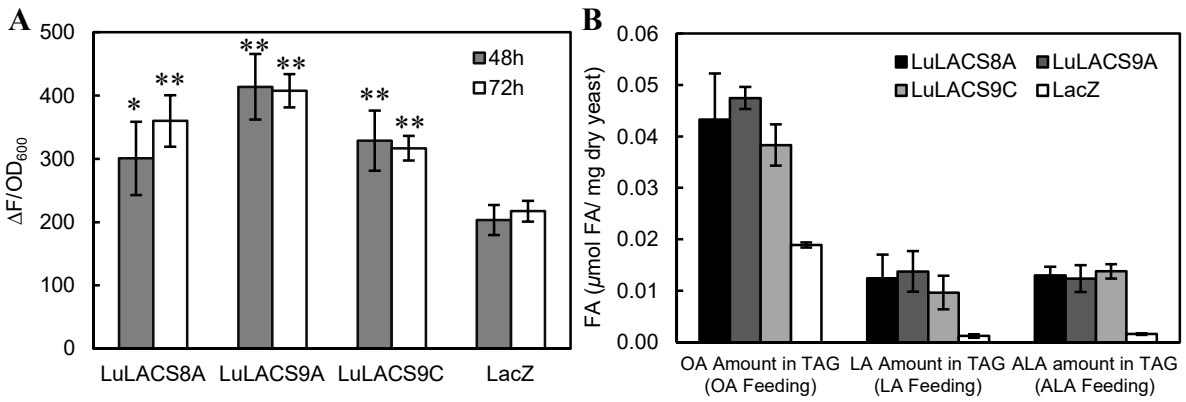

Figure 5.2. Expression of *LuLACSs* in yeast mutant *BYfaa1,4*Δ facilitates fatty acids uptake in cell. A, neutral lipid accumulation of yeast mutant *BYfaa1,4*Δ producing LuLACSs. Data represent means ± S.D, n = 4 biological replicates. B, amount of oleic acid (OA), linoleic acid (LA) or *α*-linolenic acid (ALA) in triacylglycerol of yeast mutant *BYfaa1,4*Δ producing LuLACSs cultured in medium supplemented with OA, LA or ALA, respectively. Yeast cells are harvested after 72 h induction. Data represent means ± S.D, n = 2 biological replicates. The asterisks indicate significant differences in neutral lipid content (A) of yeast producing LuLACSs versus yeast expressing *LacZ* (t-test, *P < 0.05, **P < 0.01).

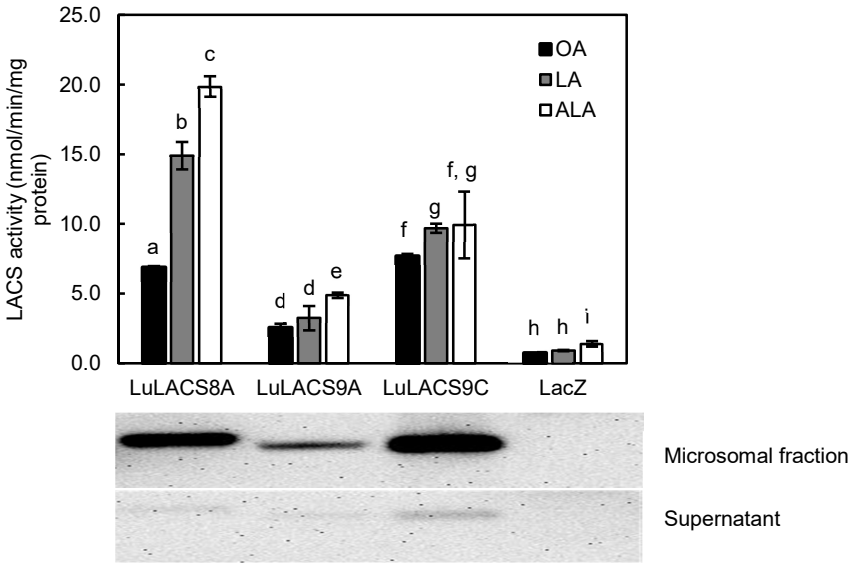

Figure 5.3. Localization of LuLACSs in yeast and their substrate specificities. Microsomal preparations from the yeast mutant *BYfaa1,4*Δ producing LuLACSs were used for analysis of enzyme assay. The same amount of microsomal and cytosolic proteins were used for Western blotting analysis. Data represent means ± S.D, n = 3-5. OA, oleic acid; LA, linoleic acid; ALA, *α*-linolenic acid. The letters indicate significant differences in the substrate specificity for each enzyme (ANOVA with a Tukey test or Welch's robust test with a Games-Howell test) at $P < 0.05$ level.

5.2.3. LuLACS8A has increased substrate specificity towards α-linolenic acid

The fatty acid feeding results revealed that LuLACSs could utilize OA, LA or ALA as substrates. To investigate whether LuLACSs have preference towards certain substrates, the yeast mutant *BYfaa1,4*Δ producing LuLACSs was cultured overnight and the microsomal fractions were isolated for analysis of enzyme polypeptide accumulation by Western blotting and *in vitro* enzyme activity. Based on the blotting results, recombinant LuLACSs were mainly localized in the microsomal fraction rather than the cytosolic fraction (Figure 5.3). The substrate specificity of each LuLACS was then assessed by using the corresponding microsomal fractions and all three LuLACSs showed activity towards OA, LA, or ALA (Figure 5.3). LuLACS8A displayed an enhanced preference towards ALA (Figure 5.3), the dominant fatty acid in flax TAG and PC (Wanasundara et al., 1999). Thus, it is hypothesized that LuLACS8A may be involved in the specific channeling of ALA moieties released from PC of the ER to the acyl-CoA pool, which would then further be utilized by DGAT to form TAG.

5.2.4. LuDGAT2 displays preference for substrate containing α-linolenic acid

Previously, a pair of duplicated *DGAT1* genes and three *DGAT2* genes were identified in the flax genome by our group (Pan et al., 2013). LuDGAT1 has been shown to display enhanced substrate specificity towards linolenoyl-CoA (Pan et al., 2015), whereas the determination of the substrate preference of LuDGAT2 was hindered due to its low activity in yeast microsomes. To increase polypeptide accumulation, *LuDGAT2-3* was codon optimized for expression in yeast. The codon optimized version of *LuDGAT2-3* together with *LuDGAT1-1* or *LuDGAT2-3* were transformed into *S. cerevisiae* strain H1246, which is a quadruple mutant devoid of TAG synthesis capacity (Sandager et al., 2002). Compared to the LacZ control, yeasts producing all

three LuDGATs accumulated higher amount of neutral lipid when grown in the culture with or without ALA (Figure 5.4A and B). The highest neutral lipid content was observed with LuDGAT1-1, whereas LuDGAT2-3 and its codon optimized version only resulted in a slight increase when compared to the control group (LacZ). The fatty acid composition of TAG isolated from yeast cells was differentially affected depending on the *LuDGAT* used for yeast transformation. Yeasts producing LuDGAT2-3, or codon-optimized LuDGAT2-3 generated TAG containing more unsaturated fatty acids than yeast producing LuDGAT1-1 (Figure 5.4C). When ALA was exogenously supplemented in the culture medium, yeast producing LuDGAT2-3 generated TAG containing about 30% more ALA than yeasts producing LuDGAT1-1 and higher ALA content (50% more ALA than that of LuDGAT1-1) was observed with TAG from yeast producing the codon-optimized version of LuDGAT2-3 (Figure 5.4D), suggesting that LuDGAT2-3 displayed enhanced selectivity towards substrate containing ALA.

To further explore the substrate specificity of LuDGAT, the yeasts producing recombinant LuDGATs were cultured overnight and harvested at a similar optical density value at 600 nm (OD_{600}). Microsomal fractions containing the recombinant enzymes were prepared from the cells and used to determine enzyme activity. LuDGAT1-1 displayed the highest DGAT activity whereas the activity of LuDGAT2-3 was very low (Figure 5.5A). LuDGAT2-3, encoded by the codon-optimized cDNA, brought about a 1.6-fold increase in the microsomal DGAT activity compared to that of LuDGAT2-3, which was mainly attributable to increased polypeptide accumulation (Figure 5.5B). The acyl donor substrate specificities of LuDGATs were analyzed using oleoyl-CoA or α-linolenoyl-CoA. Consistent with our previous results (Pan et al., 2015), LuDGAT1-1 showed preference towards α-linolenoyl-CoA over oleoyl-CoA (Figure 5.5C). Even though LuDGAT2-3 and the form of the enzyme encoded by the codon-

optimized cDNA displayed very low activity towards oleoyl-CoA, the DGAT activity of LuDGAT2-3 based on codon-optimization was markedly enhanced when using α-linolenoyl-CoA instead of oleoyl-CoA as substrate (Figure 5.5C). The ratio of substrate specificity for α-linolenoyl-CoA versus oleoyl-CoA was up to 10-fold higher when comparing LuDGAT2-3, based on the codon-optimized cDNA, to LuDGAT1-1 (Figure 5.5D).

5.2.5. Possible substrate channeling between LuLACS8A and LuDGAT-catalyzed reactions

Considering LuLACS8A and LuDGATs displayed preference towards ALA containing substrates, it was hypothesized that α-linolenoyl-CoA produced by LuLACS8A action could be selectively utilized by LuDGAT to form TAG. To test this hypothesis, *LuLACS8A* and *LuDGAT1-1*, or codon-optimized *LuDGAT2-3*, were co-expressed in *S. cerevisiae* strain *BYQMfaa1,4*Δ, which is devoid of TAG synthesis combined with low LACS activity. Yeasts co-expressing *LuLACS8A* and *LuDGAT1-1*, or *LuDGAT1-2* accumulated large amounts of neutral lipid (based on the Nile red assay) whereas expression of empty vector p*NC* or *LuLACS8A* alone failed to complement neutral lipid synthesis in the yeast (Figure 5.6A). Production of LuDGAT1-1 or LuDGAT2-3 in the yeast mutant resulted in the accumulation of neutral lipid at a lower level than that from the co-expression groups (Figure 5.6A), probably due to a limitation in the acyl-CoA pool. When ALA was added to the medium, yeasts co-expressing *LuLACS8A* and either *LuDGAT* accumulated a similar or higher amount of neutral lipid (Figure 5.6B) with significantly increased ALA content when compared to the results from cultures without fatty acid supplementation (Figure 5.6C and D). Co-expressing *LuLACS8A* and *LuDGAT2-3* resulted in TAG containing more ALA in yeast than co-expressing *LuLACS8A* and *LuDGAT1-1*(Figure 5.6D), indicating that LuDGAT2-3 may be more effective in channeling ALA into TAG than LuDGAT1-1.

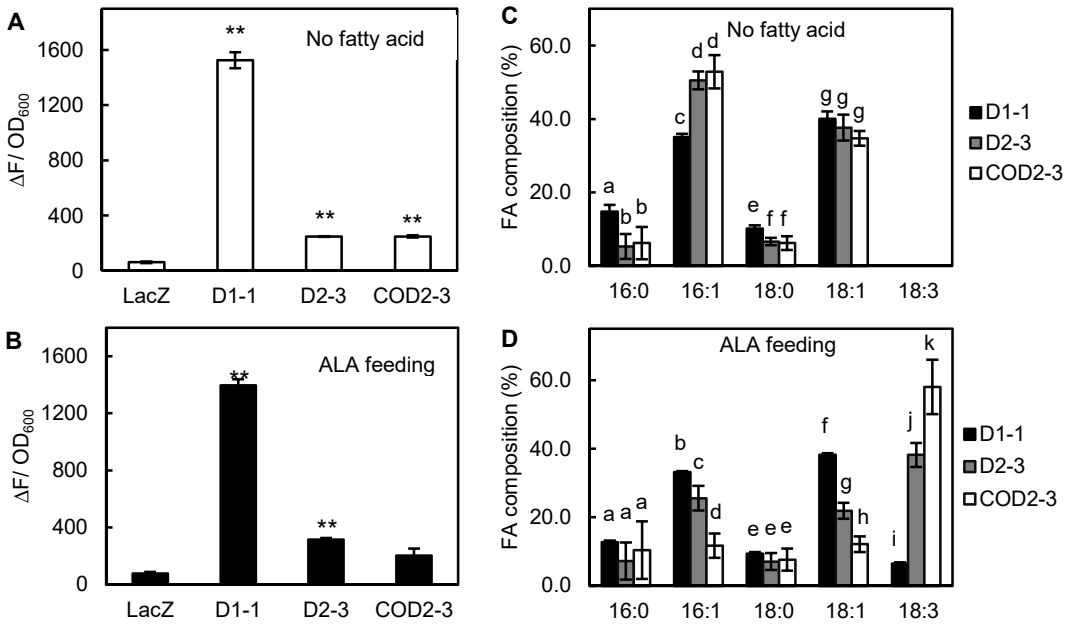

Figure 5.4. Effect of expressing flax *DGATs* in yeast H1246 on neutral lipid content and fatty acid composition of triacylglycerol. A and B, neutral lipid accumulation of yeast producing LuDGATs after 48 h induction. C and D, fatty acid composition of triacylglycerol isolated from yeast producing LuDGATs. Yeast cells were cultured in the absence (A and C) or presence (B and D) of exogenous α-linolenic acid (ALA: 18:3) and harvested after 48 h induction. Data represent means ± S.D. For A, n = 2 biological replicates. For B and C, n=3 biological replicates. D1-1, LuDGAT1; D2-3, LuDGAT2-3; COD2-3, LuDGAT2-3 based on the codon-optimized cDNA. For A and B, the asterisks indicate significant differences in neutral lipid content of yeast producing LuDGATs versus yeast expressing *LacZ* using t-test (**P<0.01). For C and D, the letters indicate significant differences in the composition of each fatty acid from yeast producing different LuDGATs (ANOVA with a Tukey test or Welch's robust test with a Games-Howell test) at $P < 0.05$ level.

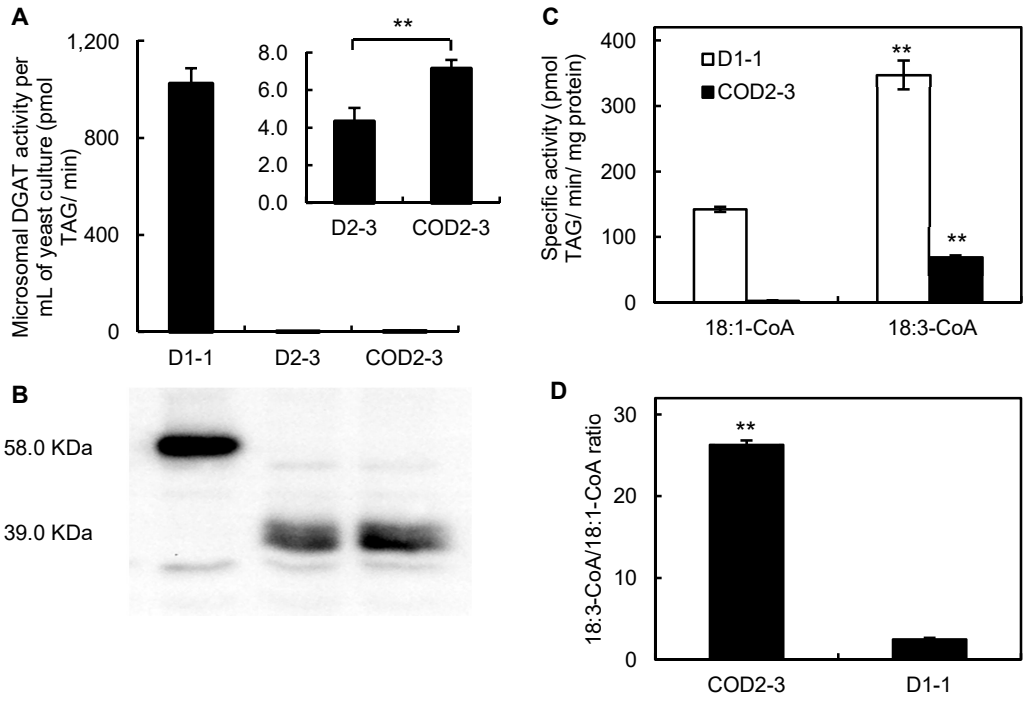

Figure 5.5. Enzyme activities and substrate specificities of LuDGATs. Microsomal preparations from the yeast mutant H1246 expressing *LuDGAT1* (*D1-1*), *LuDGAT2-3* (*D2-3*) or codon-optimized *LuDGAT2-3* (*COD2-3*) were used for analysis of enzyme assay and Western blotting. A, microsomal DGAT activities of recombinant D1-1, D2-3 and COD2-3. B, protein accumulation of LuDGATs. The same batch of microsomes used to assess enzyme activity were used for Western blotting analysis. C, substrate specificity of LuDGAT towards oleoyl-CoA (18:1-CoA) or α-linolenoyl-CoA (18:3-CoA). D, ratio of substrate specificity towards 18:3-CoA versus 18:1-CoA of LuDGATs. Data represent means ± S.D, n = 3. For A, C and D, the asterisks indicate significant differences (t-test) at $P < 0.01$ level.

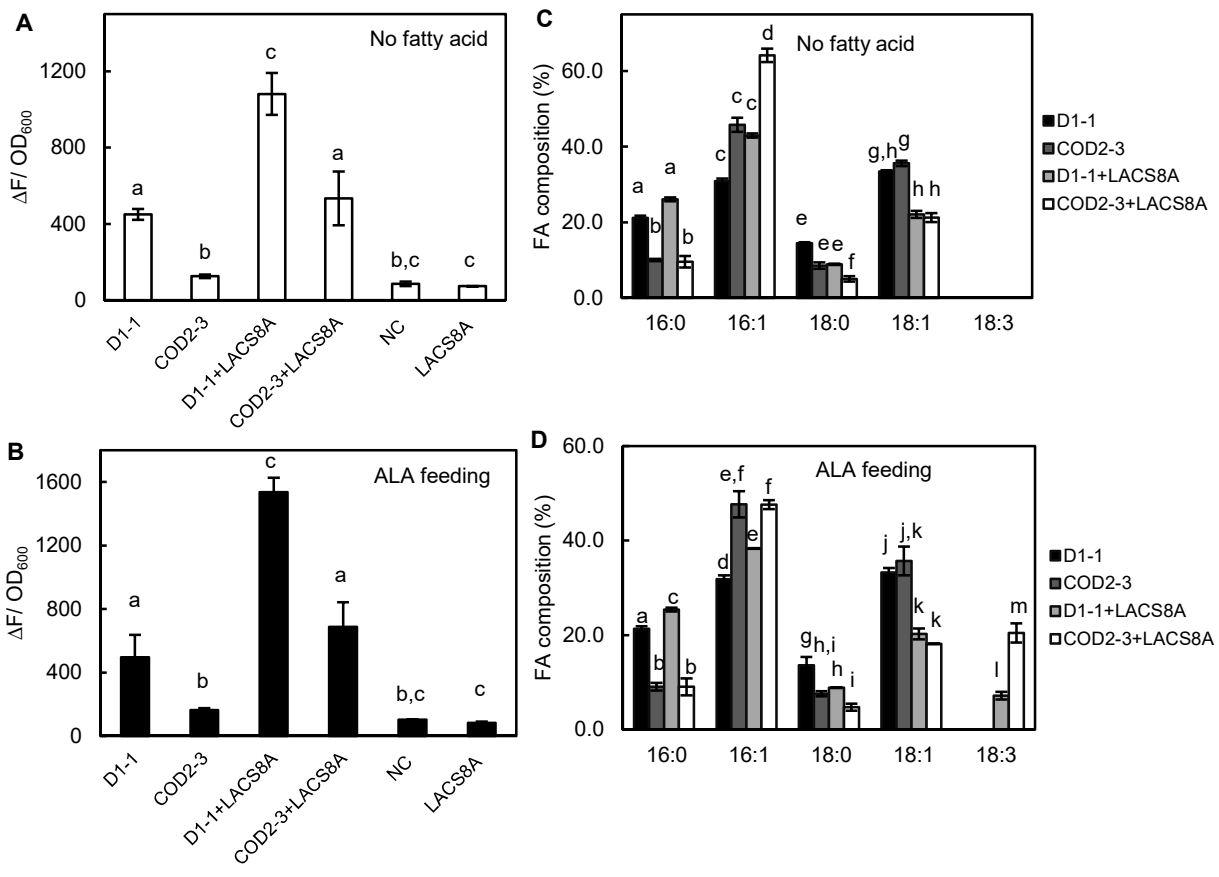

Figure 5.6. Effect of co-expressing *LuLACS8A* and *LuDGATs* in yeast mutant *BYQMfaa1,4*Δ on neutral lipid content and fatty acid composition of triacylglycerol. A and B, neutral lipid accumulation of yeast co-expressing *LuLACS8A* and *LuDGAT*s after 48 h induction. C and D, fatty acid composition of triacylglycerol isolated from yeast co-expressing *LuLACS8A* and *LuDGAT*s. Yeast cells were cultured in the absence (A and C) or presence (B and D) of exogenous *α*-linolenic acid (ALA) and harvest after 48 h induction. Data represent means ± S.D, n = 3 biological replicates. D1-1, LuDGAT1; COD2-3, LuDGAT2-3 encoded by codon-optimized cDNA. The letters indicate significant differences in neutral lipid content (A and B), and the composition of each fatty acid (C and D) from the co-expression yeast (ANOVA with a Tukey test or Welch's robust test with a Games-Howell test) at $P < 0.05$ level.

The microsomal fractions from the recombinant yeasts transformed with different co-expression vectors were isolated and used for *in vitro* enzyme assays. Incubation of ALA with yeast microsomes containing LuLACS8A along with either form of LuDGAT for 15 min resulted in the production of acyl-CoA and TAG (Figure 5.7). LuLACS8A combined with LuDGAT2-3 was more efficient at channeling ALA into TAG than LuLACS8A combined with LuDGAT1-1. The formation of TAG was also detected after 15 min incubation of ALA with microsomes containing LuDGAT1-1 or LuDGAT2-3 alone (Figure 5.7A), even though only very small amounts of radiolabeled acyl-CoA were formed (Figure 5.7B) from the remaining LACS activity of the yeast mutant background. Microsomes from yeast co-expressing *LuLACS8A* with *LuDGAT1-1* or *LuDGAT2-3* resulted in increased TAG formation when compared to the microsomes containing LuDGAT1-1 or LuDGAT2-3 alone after 15 min reaction, but extended incubation to 2 h did not result in a difference in TAG formation for the microsomes containing LuDGAT2-3 or both LuDGAT2-3 and LuLACS8A. Microsomes containing LuLACS8A alone also led to the production of a high amount of acyl-CoA but, no TAG was formed due to the absence of DGAT (Figure 5.7).

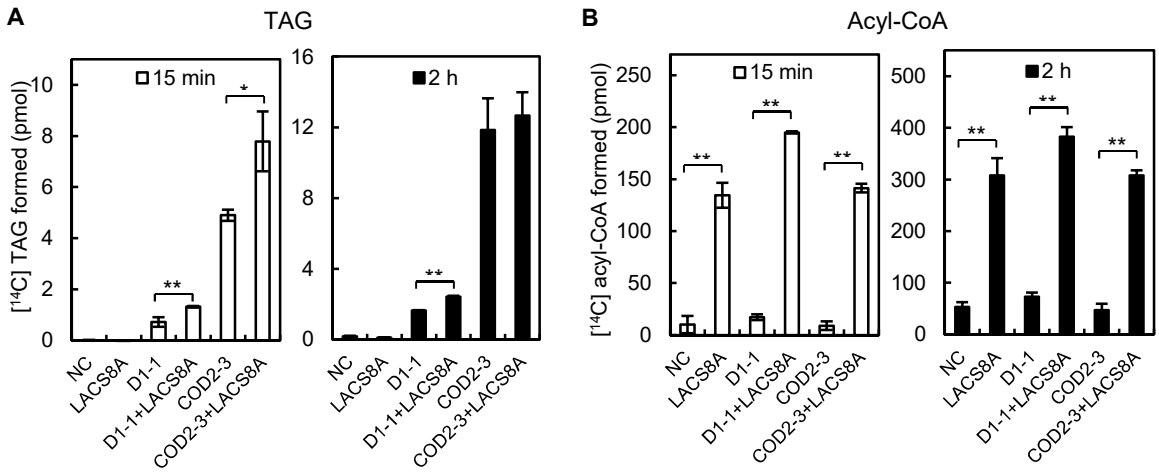

Figure 5.7. Analysis of substrate channeling between reactions catalyzed by LuLACS8A and LuDGAT. Microsomal preparations from the yeast mutant *BYQMfaa1,4*Δ individually transformed with p*LACS8A+CODGAT2-3*, p*CODGAT2-3*, p*LACS8A+DGAT1-1*, p*DGAT1-1*, p*LACS8A* or p*NC* were incubated with [^{14}C] α-linolenic acid, ATP, CoA and *sn*-1,2-diolein. After incubation, the reaction mixture was subjected to thin-layer chromatography plates and the amounts of the formed radiolabeled triacylglycerol (TAG) (A) and acyl-CoA (B) were calculated based on the radioactivity of the corresponding spots, respectively. Data represent means ± S.D, n = 3. D1-1, LuDGAT1; COD2-3, LuDGAT2-3 encoded by codon-optimized cDNA. The asterisks indicate significant differences (t- test, *P < 0.05; **P < 0.01).

5.3. Discussion

Seed oil from flax contains 45 to 65% ALA, and is considered one of the richest sources of this essential fatty acid. It has been suggested that flax contains various lipid biosynthetic enzymes with enhanced preference for substrates containing ALA (Pan et al., 2013, 2015; Wickramarathna et al., 2015). The substrate specificity of flax LACS and DGAT2 may also contribute to the ALA enrichment of seed TAG.

Six *LACS* cDNAs were identified from the developing flax embryo (Table 5.1) and separated into two groups based on amino acid sequence homology with AtLACS8 and AtLACS9 (Figure 5.1). The presence of N-terminal extensions was identified from AtLACS8-like proteins rather than AtLACS9-like protein (Figure 5.1), which might result in the different subcellular localizations and functions of these two groups of proteins. Two AtLACS9-like proteins, including AtLACS9 and *Helianthus annuus* LACS1 (HaLACS1), have been found to reside in the plastid with debatable function of AtLACS9 in lipid trafficking between the ER and plastid, whereas AtLACS8 and HaLACS2 from the AtLACS8-like proteins group have been shown to localize in the ER with unknown functions (Zhao et al., 2010; Aznar-Moreno et al., 2014; Schnurr et al., 2002; Jessen et al., 2015). Even though the function of AtLACS8-like proteins in plant lipid metabolism remains unclear, it has been suggested that AtLACS8 is predominantly expressed in the seed (Zhao et al., 2010) and might be involved in TAG biosynthesis (Kim et al., 2015).

The activities of LuLACS enzymes in yeast were verified by a yeast complementation experiment (Figure S5.2). Expression of *LuLACSs* in the yeast mutant *BYfaa1,4*Δ (Figure 5.1) facilitated the incorporation of exogenously added OA, LA or ALA into yeast lipid, suggesting

that LuLACSs might have broad substrate specificities. The Western blotting results indicated that recombinant LuLACSs were mainly associated with the yeast microsomal fraction (Figure 5.3). This was consistent with a protein topology prediction of LuLACSs containing one transmembrane domain at the N-terminus (SOSUI) (Table S5.3 and Figure S5.1). *In vitro* LACS assays confirmed the ability of recombinant LuLACSs to utilize OA, LA, or ALA. LuLACS8A was found, however, to display increased substrate preference towards ALA, which might contribute to another biochemical route in developing flax seed for channeling ALA into TAG. Similarly, AtLACS8-like protein from sunflower (HaLACS2) was found to display unique substrate preference and postulated to be involved in the acyl turnover of PC from the ER (Aznar-Moreno et al., 2014).

Flax LACS with unique substrate preference might contribute to the channeling of ALA from the PC to the acyl-CoA pool, and the resulting α-linolenoyl-CoA would then be utilized to form TAG by the acyltransferases, including DGAT, from the Kennedy pathway. Interestingly, an earlier study with microsomes from the developing flax seed indicated that DGAT activity exhibited increased specificity for α-linolenoyl-CoA over oleoyl-CoA or linoleoyl-CoA (Sørensen et al., 2005). The observed substrate specificity, however, was probably the net result of LuDGAT1 and LuDGAT2 action. In the current study, the capabilities of recombinant LuDGATs in TAG production in the yeast mutant H1246 were analyzed *in vivo* (Figure 5.4) and *in vitro* (Figure 5.5). Overexpression of *LuDGAT1-1* in yeast H1246 produced a large amount of TAG (Figure 5.4A), which is consistent with its high *in vitro* enzyme activity (Figure 5.5A) and protein accumulation (Figure 5.5B). The contribution of LuDGAT2-3 to yeast TAG accumulation was less (Figure 5.4A) and probably related to lower enzyme activity and protein accumulation, even though a codon-optimized version of the cDNA encoding LuDGAT2-3 was

adopted (Figure 5.5A and B). The activity of LuDGAT2-3, however, increased more than 20-fold when oleoyl-CoA was replaced by α-linolenoyl-CoA (Figure 5.5C and D). This was consistent with the *in vivo* results demonstrating a 30% to 50% increase in ALA content in yeast TAG when using recombinant LuDGAT2-3 as opposed to recombinant LuDGAT1-1 in the presence of ALA, regardless of the large differences in TAG content (Figure 5.4). Based on previous analysis of gene expression, *LuDGAT2-3* exhibited higher expression than *LuDGAT1-1* in developing flax seed and the expression of both *LuDGAT1-1* and *LuDGAT2-3* was closely correlated with ALA biosynthesis and total oil accumulation (Pan et al., 2013). Taking into account the potential role of DGAT2 in unusual fatty acid enrichment (Burgal et al., 2008; Li et al., 2010a), it is possible that LuDGAT2-3 might contribute to the specific channeling of ALA into flax TAG.

The ability of the combined reactions catalyzed by LuLACS8A and LuDGAT to channel ALA into TAG was confirmed by *in vivo* (Figure 5.6) and *in vitro* (Figure 5.7) experiments. LuDGAT2-3 was more effective in ALA-channeling than LuDGAT1-1 in the substrate channeling process (Figure 5.6 and 7), which is probably due to its enhanced substrate specificity for α-linolenoyl-CoA. A large amount of acyl-CoA was produced when incubating ALA with yeast microsomes containing both LuLACS8A and LuDGAT, but only a small amount (approximately 1-6%) of acyl-CoA was further utilized in TAG formation (Figure 5.7), suggesting that the DGAT-catalyzed reaction might be a limiting step. This is also consistent with the *in vitro* enzyme assay results for LuLACS8A (Figure 5.3) and either LuDGAT1-1 or LuDGAT2-3 (Figure 5.5), where the microsomal specific activity of LuLACS8A was approximately 20-200 times higher than that of the LuDGATs. Indeed, the level of DGAT activity in developing seeds of *Brassica napus* may have a substantial effect on the flow of

carbon into TAG (Perry and Harwood, 1993; Weselake et al., 2008). The possibility of limited formation of TAG, because of unbalanced recombinant protein accumulation between LuLACS8A and LuDGAT in yeast microsomes cannot be ruled out, athough both of the encoding cDNAs were expressed under the *GAL1* promoter.

In developing flax seed, the LuLACS8A-LuDGAT2-3 catalyzed substrate channeling process may be coordinated with other ALA-enriching processes which include PDAT action (Pan et al., 2013), PDCT action (Wickramarathna et al., 2015) and coupling of the LPCAT-catalyzed reaction to the DGAT-catalyzed reaction (Pan et al., 2015). The four possible routes for ALA-enrichment of TAG during flax seed development are outlined in Figure 5.8. Besides the proposed substrate channeling between LuLACS8A and LuDGAT2, LuPDAT also has been suggested to display preference towards ALA containing substrate and contribute to the channeling of ALA from PC into TAG (Pan et al., 2013). Evidence from the LuPDCT work indicates that the modified PC can be incorporated into the diacylglycerol (DAG) pool directly via the catalysis of LuPDCT (Wickramarathna et al., 2015). The resulting *sn*-1,2-DAG enriched in ALA could be an effective acyl acceptor for LuDGAT (especially LuDGAT2-3), selectively utilizing α-linolenoyl-CoA or LuPDAT to form TAG. In addition, the previous biochemical coupling of LuDGAT1 and LuLPCAT-catalyzed reactions showed that these two enzymes may incorporate with each other for incorporating ALA into TAG (Pan et al., 2015).

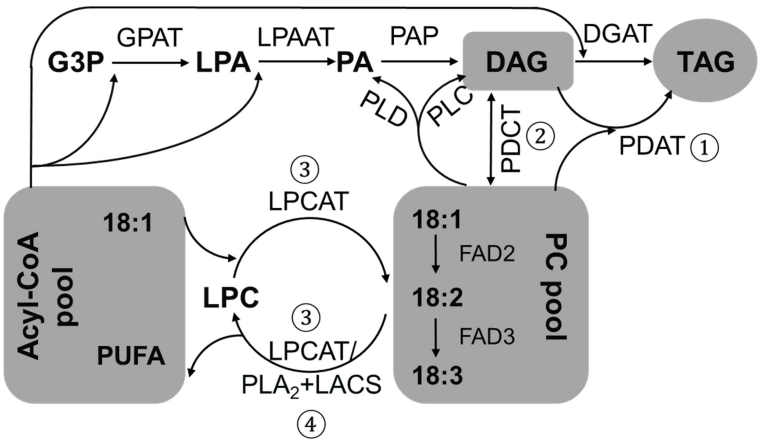

Figure 5.8. Four possible routes for enriching the α-linolenic acid (ALA; 18:3) content of triacylglycerol (TAG) during flax seed development. In route 1, phospholipid:diacyglycerol acyltransferase (PDAT) catalyzes the transfer of 18:3 from the *sn*-2 position of phosphatidylcholine (PC) enriched in 18:3 to *sn*-1,2-diacylglycerol (DAG) enriched in 18:3 to form 18:3-enriched TAG (Pan et al., 2013). In route 2, phosphatidylcholine:diacylglycerol cholinephosphotransferase (PDCT) catalyzes the transfer of the phosphocholine headgroup of PC enriched in 18:3 to *de novo* DAG formed in the Kennedy pathway thus producing 18:3-enriched DAG for synthesis of TAG via either the PDAT or diacylglycerol acyltransferase (DGAT)-catalyzed reaction (Wickramarathna et al., 2015). In route 3, coupling of the lysophosphatidylcholine acyltransferase (LPCAT)-catalyzed reverse reaction to the DGAT-catalyzed forward reaction results in the transfer of 18:3 from the *sn*-2 position of 18:3-enriched PC to the *sn*-3 position of DAG (Pan et al., 2015). Use of 18:3-enriched DAG by route 3 would result in TAG highly enriched in 18:3. For route 4, the current study suggests that 18:3 can be channeled into TAG via the sequential actions of long-chain acyl-CoA synthetase (LACS) and DGAT displaying enhanced specificity for substrate containing 18:3. Route 4 assumes that there is a phospholipase A_2 (PLA_2) which can selectively release free 18:3 from 18:3-enriched PC. Other abbreviations: FAD, fatty acid desaturase; GPAT, *sn*-glycerol-3-phosphate acyltransferase; G3P, *sn*-glycerol-3- phosphate; LPA, lysophosphatidic acid; LPAAT, lysophosphatidic acid acyltransferase; LPC, lysophosphatidylcoline; PA, phosphatidic acid; PAP, phosphatidic acid phosphatase; PLC, phospholipase C; PLD, phospholipase D; PUFA, polyunsaturated fatty acid.

In conclusion, the results of this study provide further insights into the ALA-channeling process in developing flax seed. Recombinant LuLACS8A and LuDGAT2-3 with enhanced preference for ALA and α-linolenoyl-CoA, respectively, were identified. *In vivo* and *in vitro* analysis of substrate channeling between LuLACS8A-catalyzed reaction and LuDGAT2-3-catalyzed reaction indicate this represents a route for ALA accumulation in TAG. This process, however, would be dependent on the identification of a flax phospholipase A_2 which could effectively liberate ALA from PC making this PUFA available for activation by LuLACS8A. It is not unreasonable to assume that such an α-18:3-PC selective phospholipase A_2 exists, given that a candidate small molecular weight phospholipase A_2 has recently been identified by Bayon et al. (2015) in castor for catalyzing the release of ricinoleic acid from modified PC.

5.4. Experimental procedures

5.4.1. *LuLACSs* identification, cloning and plasmid construction

To identify putative *LACS* genes, the AtLACS8 and AtLACS9 protein sequence was used to query the flax genomic database (www.phytozome.net/flax, cited 29 Sept 2017). Six putative *LACS* genes were identified and the primer pairs (Table S5.1) were designed accordingly for cDNA amplification. Specific restriction sites were introduced in forward (Not I) and reverse primers (Sal I). A Kozak translation initiation sequence (italic) was also introduced in the forward primer of *LuLACS8A* to improve the translation of the protein. In order to amplify the target genes, total mRNA was extracted from developing flax embryos (12 days after flowering) using a RNeasy plant mini kit (Qiagen, Toronto, ON, Canada) and then cDNAs were synthesized using SuperScript III reverse transcriptase (Invitrogen, Burlington, ON, Canada). The target genes were amplified by PCR using the resulting cDNA as the template and the generated PCR

products were subcloned between the corresponding restriction sites of the pYES2 vector; the pYES2 vector is a modified pYES2.1 vector (pYES2.1-V5/HIS vector, Invitrogen) which was constructed in our laboratory.

The *LuDGAT1-1* cDNA was cloned into the multiple cloning site 2 (MCS2) of the pESC-URA vector in the previous study (Pan et al., 2013). Codon sequence of *LuDGAT2-3* was optimized for expression in *S. cerevisiae* by Eurofins Genomics (Toronto, ON, Canada) and was then subcloned into the MCS2 of the pESC-URA vector. The coding sequences of *LuDGAT1-1*, *LuDGAT2-3* and codon optimized *LuDGAT2-3* were cloned into the pYES-NT vector (Invitrogen) under the control of the *GAL1* promoter and with the addition of an N-terminal His-tag.

The co-expression constructs were prepared as described previously (Pan et al., 2015). Briefly, the region from *CYC1* terminator to *ADH1* terminator of pESC construct (pESC-URA, *LuDGAT1-1* in pESC, or codon optimized *LuDGAT2-3* in pESC) and the entire plasmid of pYES2 or *LuLACS8A* in pYES2 were amplified by PCR and the resulting DNA fragments were assembled using the method described by Gibson (2011). Six different plasmids from the DNA fragments assembly are referred to as: 1) p*LACS8A+DGAT1-1* contains both *LuLACS8A* and *LuDGAT1-1* genes; 2) p*LACS8A+CODGAT2-3* contains both *LuLACS8A* and codon optimized *LuDGAT2-3* genes; 3) p*LACS8A* contains only *LuLACS8A*; 4) p*DGAT1-1* contains only *LuDGAT1-1;* 5) p*CODGAT2-3* contains only codon optimized *LuDGAT2-3*; 6) pNC is the control plasmid. The expression of all above genes in the co-expression constructs is under the *GAL1* promoter. All the plasmids used in the current study are listed in Table S5.2. The integrity of all constructs was confirmed by DNA sequencing.

5.4.2. Yeast mutant construction and heterologous expression of *LuLACSs*

Wild-type *S. cerevisiae* strain BY4742 (*MATα, his3Δ1, leu2Δ0, lys2Δ0, ura3Δ0*) was obtained from the Euroscarf collection. Quadruple mutant (QM) lacking lipid droplets in BY4742 genetic background (*MATa, his3Δ1*, *leu2Δ0*, *lys2Δ0*, *ura3Δ0*, *are1::KanMX*, *are2::KanMX*, *dga1::KanMX*, *lro1::KanMX*) was kindly provided by K. Athenstaedt (Graz University of Technology, Austria). Construction of *BYQMfaa1,4Δ* (*MATα, his3Δ1, leu2Δ0, lys2Δ0, ura3Δ0, dga1 Δ::kanMX, lro1 Δ::kanMX, are1 Δ::kanMX, are2 Δ ::kanMX, faa1 Δ::HIS3, faa4 Δ::LYS2)*was described by Sec et al. (2015). Construction of *BYfaa1,4Δ* (*MATα, his3Δ1, leu2Δ0, lys2Δ0 ura3Δ0, faa1 Δ::HIS3, faa4 Δ::LYS2*) was done in our laboratory using the same approach as with *BYQMfaa1,4Δ* (Sec et al., 2015).

All yeast transformation was performed using the *S.c.* EasyComp Transformation Kit (Invitrogen). Transformants were selected on minimal medium plates lacking uracil (0.67% (w/v) yeast nitrogen base, 0.2 % (w/v) synthetic complete medium lacking uracil (SC-Ura), 2% (w/v) dextrose, and 2% (w/v) agar). For yeast culture conditions, the recombinant yeast cells were first grown in liquid minimal medium (0.67% (w/v) yeast nitrogen base and 0.2 % (w/v) SC-Ura) with 2% (w/v) raffinose. After overnight culture, the yeast cells were used to inoculate minimal medium containing 2% (w/v) galactose and 1% (w/v) raffinose (referred to as induction medium) at a starting OD_{600} value of 0.4. For the feeding experiment, recombinant yeasts were induced in induction medium with supplementation of 200 μM various fatty acids, including OA, LA or ALA. Fatty acids were dissolved first in 0.5 M ethanol and then mixed with induction medium containing 0.1% (v/v) tyloxapol. Cultures for all experiments were grown at 30^{o}C with shaking at 220 rpm.

For heterologous expression of *LACS* cDNAs, the recombinant *LuLACS* plasmids were transformed into *S.cerevisiae* strain *BYfaa1,4Δ*. For yeast complementation, after being grown in induction medium for 12 h, the recombinant yeast cells were harvested and washed with minimal medium with 2% (w/v) raffinose. The cells were then centrifuged and resuspended with the same medium at an OD_{600} value of 0.4. Aliquots of each culture were diluted serially and 2 μL of each diluted culture was spotted on induction plate containing only 100 mM OA or 45 mM cerulenin or both. To disperse the fatty acids into the medium better, 1% (v/v) tyloxapol also was added into all induction plates. The plates were covered with foil and incubated at dark at 30^{o}C for 3~4 days.

For heterologous expression of *DGAT* cDNAs, the recombinant *LuDGAT* plasmids were transformed into *S. cerevisiae* strain H1246 (*MATα are1-Δ::HIS3, are2-Δ::LEU2, dga1-Δ::KanMX4, lro1-Δ::TRP1 ADE2*), which was kindly provided by Dr. Sten Stymne of the Swedish University of Agricultural Science. For the co-expression study, the co-expression constructs were transformed into *S. cerevisiae* strain *BYQMfaa1,4Δ*.

5.4.3. Nile red fluorescence assay

The Nile red fluorescence assay was performed as described previously (Pan et al., 2013) using a Synergy H4 Hybrid reader (Biotek, Winooskit, VT, USA). In brief, 100 μL of yeast culture was placed in 96-well dark plate and then 5 μL of Nile red solution (0.1 mg/mL in methanol) was added. The fluorescence was measured before and after the addition of Nile red solution with excitation at 485 nm and emission at 538 nm. The Nile red results were calculated based on the change in fluorescence divided by OD_{600} ($\Delta F/OD_{600}$).

5.4.4. Yeast lipid extraction and analysis

Yeast lipid was extracted from approximately 30 mg of lyophilized yeast cells. For quantification, 100 μg of triheptadecanoin (C17:0 TAG) was added to each sample as a TAG internal standard. The total yeast lipids were extracted using the method described previously (Pan et al., 2013). The extracted lipids were separated on thin-layer chromatography (TLC) plates (0.25 mm Silica gel, DC-Fertigplatten, Macherey-Nagel, Germany) using hexane/diethyl ether/acetic acid (80:20:1, v/v/v) as the development solvent. After visualization by primulin staining, corresponding TAG bands were scraped and transmethylated in 1 mL methanolic HCl for 1 h at 80°C. The resulting fatty acid methyl esters (FAMEs) were extracted twice with hexane and then dried under nitrogen gas. Isolated FAMEs were resuspended with iso-octane before being analyzed by gas chromatography (GC)/mass spectrometry (MS). The samples were separated on a capillary column DB 23 (30 m×0.25 mm×0.25 μm, Agilent Technologies, Wilmington, DE, USA) by an Agilent 6890N GC equipped with a 5975 inert XL Mass Selective Detector (Agilent Technologies) as described previously (Pan et al., 2013).

5.4.5. Protein extraction and Western blotting

Microsomal and cytosolic fractions were isolated from yeast cells as described previously (Pan et al., 2013). Briefly, after overnight induction, the recombinant yeast cells were collected, washed and then resuspended in 1 mL of lysis buffer (20 mM Tris-HCl pH 7.9, 10 mM $MgCl_2$, 1 mM EDTA, 5% (v/v) glycerol, 300 mM ammonium sulfate and 2 mM dithiothreitol). The cells were then homogenized in the presence of 0.5 mm glass beads with a bead beater (Biospec, Bartlesville, OK, USA). The crude homogenate was centrifuged for 30 min at 10 000 g. To separate microsomal and cytosolic fractions, the supernatant was further centrifuged at 105 000 g

for 70 min. The microsomal pellet was resuspended in 3 mM imidazole buffer (pH 7.4) containing 125 mM sucrose. All procedures were conducted at 4^{o}C. Microsomal suspensions and supernatant samples (cytosolic fractions) were kept at 80^{o}C before use. The crude protein concentration was determined using the Bradford assay with BSA as a standard (Bradford, 1976).

For the detection of C-terminal V5-tagged recombinant proteins, 6.5 μg of microsomal and cytosolic proteins were separated by 8-16% gradient Mini-Protean TGX Precast Gels (Bio-Rad, Mississauga, ON, Canada) and then transferred to polyvinylidene difluoride membrane (Amersham, GE Healthcare, Mississauga, ON, Canada). After blocking with 2% ECL prime blocking reagent (Amersham), the membrane was incubated with V5-HRP-conjugated antibody (Invitrogen), followed by detection using ECL Advance Western Blotting Detection Kit (Amersham) by a FluorChem SP imager (Alpha Innotech Corp., San Leandro, CA, USA). For N-terminal His-tagged recombinant proteins, equal volumes of microsomal suspensions were loaded on the gel and the target proteins were detected using anti-HisG-HRP antibody (Invitrogen).

5.4.6. *In vitro* enzyme assays

5.4.6.1. LACS assay

LACS assay was conducted according to the procedures described by de Azevedo Souza et al. (2009) and Shockey et al. (2002), with slight modifications. The enzyme assay was conducted at 30^{o}C with shaking for 5 min in a reaction mixture containing 100 mM Bis-Tris-propane (pH 7.6), 10 mM $MgCl_2$, 5 mM ATP, 2.5 mM dithiothreitol, 1 mM CoA, 20 μM [1-^{14}C] fatty acid (OA, 56.3 mCi/mmol; LA, 58.2 mCi/mmol; ALA, 51.7 mCi/mmol; PerkinElmer,

Waltham, MA, USA) and 10 μg of microsomal protein in a total volume of 100 μl. The reaction was initiated by addition of microsomal protein and quenched with 100 μL of 10% (v/v) acetic acid in isopropanol and extracted 4 times with 900 μL of 50% (v/v) isopropanol saturated hexane. Aliquots of the aqueous phase were analyzed for radioactivity by a LS 6500 multi-purpose scintillation counter (Beckman-Coulter, Mississauga, ON, Canada).

5.4.6.2. DGAT assay

DGAT assay was performed as described previously (Pan et al., 2015). Briefly, the enzyme assay was conducted at 30^{o}C with shaking in a 60-μL reaction mixture containing 200 mM HEPES-NaOH (pH 7.4), 3.2 mM $MgCl_2$, 333 μM *sn*-1,2-diolein dispersed in 0.2% (v/v) Tween 20, 15 μM [1-^{14}C] oleoyl-CoA (55 μCi/μmol) (PerkinElmer), and microsomal protein. The amount of microsomal protein and reaction time were as follows: for LuDGAT1-1, 2 μg of microsomal protein and a 4 min reaction were adopted; for LuDGAT2-3 and codon-optimized LuDGAT2-3, 10μg of microsomal protein and a 30 min reaction were adopted. The reaction was then quenched with 10 μL of 10% (w/v) SDS. The entire reaction mixture was spotted onto a TLC plate (0.25 mm Silica gel, DC-Fertigplatten) and then resolved with hexane/diethyl ether/acetic acid (80:20:1, v/v/v). After visualization by phosphorimaging (Typhoon Trio Variable Mode Imager, GE Healthcare), corresponding TAG spots were scraped and radioactivity was quantified by a LS 6500 multi-purpose scintillation counter (Beckman-Coulter). For the substrate specificity assay, radiolabelled oleoyl-CoA or linolenoyl-CoA was synthesized from [1-^{14}C] OA (56.3 mCi/mmol) and ALA (51.7 mCi/mmol), respectively, as described by (Taylor et al., 1990) and 15 μM of radiolabeled acyl-CoA was used in the DGAT assay.

5.4.6.3. LACS-DGAT substrate channeling assay

The channeling assay was performed at 30^{o}C with shaking for 15 min or 2 h. The reaction mixture contained 200 mM HEPES-NaOH (pH 7.4), 3.2 mM $MgCl_2$, 333 μM *sn*-1,2-diolein dispersed in 0.2% (v/v) Tween 20, 5 mM ATP, 2.5 mM dithiothreitol, 1 mM CoA, 10 μM [1-^{14}C] linolenic acid (51.7 mCi/mmol) and 10 μg of microsomal protein in a total volume of 60 μL. The reaction was initiated by adding microsomal protein and quenched with 10 μL of 10% (w/v) SDS. The total reaction mixture was then separated on TLC plates (0.25 mm Silica gel, DC-Fertigplatten) and the radioactivity of the corresponding TAG and acyl-CoA spots was analyzed as described above.

5.4.7. Sequence analysis

Sequence alignments of LACS proteins were conducted using ClustalW in MEGA 7 under the default settings (Kumar et al., 2016). A neighbour-joining tree was built using the same software under the *Poisson* model, pairwise deletion and 1000 bootstrap repetitions. For calculating the *K*s values (synonymous substitution rates) for each gene pair, the aligned protein sequences were used to guide the alignment of their corresponding coding sequences using PAL2NAL server (http://www.bork.embl.de/pal2nal/, cited 29 Sept 2017). *K*s values were calculated by the codon-based likelihood method with the F3X4 codon frequency model in the CodeML program of the PAML version 4 software (Yang, 2007). The approximate divergence time (T) was calculated using the mean *K*s value by following equation T= *K*s/2λ, where λ is the synonymous substitution rate of 6.1×10^{-9} substitutions per synonymous site per year (Lynch and Conery, 2000). The theoretical molecular mass and isoelectric point value of the deduced

LuLACS proteins were calculated by Compute pI/Mw server (http://web.expasy.org/compute_pi/, cited 29 Sept 2017). The topology organization of LACSs was predicted using the following algorithms: TMpred (Hofmann and Stoffel, 1993), TMHMM (Krogh et al., 2001), SOSUI (Hirokawa et al., 1998), and Phobius (Käll et al., 2007). A membrane protein topology prediction of LuLACS8A was visualized by Protter (Omasits et al., 2014).

5.4.8. Statistical analysis

Data are shown as mean ± standard deviation (S.D.) or standard error (S.E.) for the number of independent experiments indicated. Statistical analysis was performed using the SPSS statistical package (SPSS 16.0, Chicago, IL, USA). Significant differences between two groups were assessed using a two-tailed Student's t-test. The Levene's test was used to test equality of variance. When the variances were equal, the unpaired Student's t-test assuming equal variances was performed. When the variances were unequal, the unpaired Student's t-test with Welch corrections assuming unequal variances was used. For multiple comparisons, one-way analysis of variance (ANOVA) with Tukey's post-hoc analysis was used. In cases where the assumption of homogenous variances was not met (tested by Levene's test), Welch's robust test followed by Games-Howell post hoc test was performed.

5.5. Supplementary material

Supplementary Table S5.1. Sequences of the PCR primers employed in the current study.

*Restriction sites are indicated with underline and a Kozak translation initiation sequence is indicated in italic.

Primer name	Sequence*
	Primers used for pYES2.1 cloning of *LuLACS* cDNAs
AtLACS9-F	5'-GCAGAGCGGCCGCATGATTCCTTATGCTGCTGGTG-3'
AtLACS9-R	5'-TATGTCGACGGCATATAACTTGGTGAGATCTTCA-3'
LuLACS8A-F	5'-GCAGAGCGGCCGC*AACA*ATGGCAGATCCGGAGGGG-3'
LuLACS8A-R	5'-TATGTCGACATGATAGAGCTTCTGCAGTTCATCTT-3'
LuLACS9A-F	5'-GCAGAGCGGCCGCATGAGCGTGTACGTGATCG-3'
LuLACS9A-R	5'-TATGTCGACTTCATATAGCTCAGCTAGCTCTTCAG-3'
LuLACS9C-F	5'-GCAGAGCGGCCGCATGACCCTGTACCTGATCAT-3'
LuLACS9C-R	5'-TATGTCGACAGATTCATACATCTTAGATAGATCTTCAG-3'
	Primers used for pYES-NTA or pESC cloning of *LuDGATs*
LuDGAT1-1-F	5'-TATAGGATCC*ACACA*ATGTCCGTGCTAGACACTCCT-3'
LuDGAT1-1-R	5'-TATACTCGAGTTAGATTCCATCTTTCCCATTCC-3'
LuDGAT2-3-F	5'-TATAGGATCC*ACACA*ATGTCGGTACAGAAAGTAGAGGAGG-3'
LuDGAT2-3-R	5'-TATACTCGAGTTAAAGAATTTTGAGTTGAAGATCAGC-3'
Codon optimized-LuDGAT2-3-F	5'-TATAGGATCC*ACACA*ATGTCGGTTCAGAAAGTCGAA-3'
Codon optimized-LuDGAT2-3-R	5'-TATACTCGAGTTACAAGATTTTCAACTGAAGATCCG-3'
	Primers used for cloning co-expression constructs
pESC-F	5'-GAGAGGCGGTTTGCGTATTGGGCGCGCTGAATTGGAGCGACCTCATGC-3'
pESC-R	5'-GTCAGTGAGCGAGGAAGCGGAAGACTGGATCTTCGAGCGTCCCAAAACC-3'
pYES-F	5'-GGTTTTGGGACGCTCGAAGATCCAGTCTTCCGCTTCCTCGCTCACTGAC-3'
pYES-R	5'-GCATGAGGTCGCTCCAATTCAGCGCGCCCAATACGCAAACCGCCTCTC-3'

Supplementary Table S5.2. Plasmids used in the current study.

Plasmid name	Description
pYES-LACS8A	pYES- P_{GAL1}- LACS8A-V5 tag-T_{CYC1}
pYES-LACS9A	pYES- P_{GAL1}- LACS9A-V5 tag-T_{CYC1}
pYES-LACS9C	pYES- P_{GAL1}- LACS9C-V5 tag-T_{CYC1}
pYES-DGAT1-1	pYES- P_{GAL1}- His tag-DGAT1-1-T_{CYC1}
pYES-DGAT2-3	pYES- P_{GAL1}- His tag-DGAT2-3-T_{CYC1}
pYES-CODGAT2-3	pYES- P_{GAL1}- His tag-codon optimized DGAT2-3-T_{CYC1}
pLACS8A+DGAT1-1	pYES-P_{GAL1}-LACS8A-T_{CYC1}/P_{GAL1}- DGAT1-1-T_{CYC1}
pLACS8A+CODGAT 2-3	pYES-P_{GAL1}-LACS8A-T_{CYC1}/P_{GAL1}-codon optimized DGAT2-3-T_{CYC1}
pLACS8A	pYES-P_{GAL1}-LACS8A-T_{CYC1}/P_{GAL1}-T_{CYC1}
pDGAT1-1	pYES-P_{GAL1}-T_{CYC1}/P_{GAL1}- DGAT1-1-T_{CYC1}
pCODGAT2-3	pYES-P_{GAL1}-T_{CYC1}/P_{GAL1}-codon optimized DGAT2-3-T_{CYC1}
pNC	pYES-P_{GAL1}- T_{CYC1}/P_{GAL1}-T_{CYC1}

Supplementary Table S5.3. Predicted transmembrane domains (TMDs) in LuLACSs and AtLACSs by TMpred, TMHMM, SOSUI or Phobius.

	TMpred	TMHMM	SOSUI	Phobius
AtLACS8	18-41 179-197 274-294 335-353	20-42 167-189	19-41	20-41
No. of TMD	4	2	1	1
AtLACS9	1-18 262-285 307-327 584-604		1-20	
No. of TMD	4	0	1	0
LuLACS8A	35-57 303-326 347-365	35-57	34-56	32-55
No. of TMD	3	1	1	1
LuLACS9A	1-18 106-124 243-264 267-286 388-409		1-18	
No. of TMD	5	0	1	0
LuLACS9C	1-21 265-289 310-330 386-407	2-21	2-23	6-23
No. of TMD	4	1	1	1

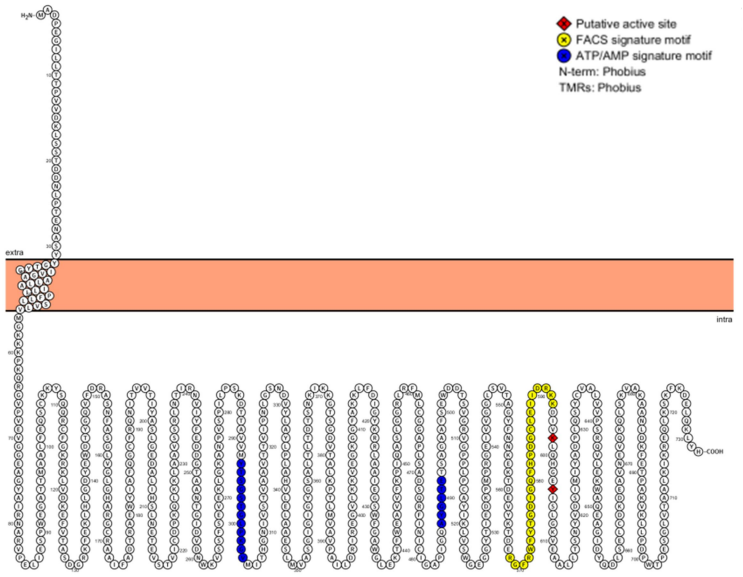

Supplementary Figure S5.1. The predicted topology of LuLACS8A. The membrane topology of LuLAC8A was predicted by Protter. The original AA sequence of LuLACS8A is represented by black circles. The putative active sites are represented by red-filled diamonds. The fatty acyl-CoA synthetase signature motif (FACS signature motif) is represented by yellow-filled circles. The ATP/AMP signature motifs are represented by blue-filled circles.

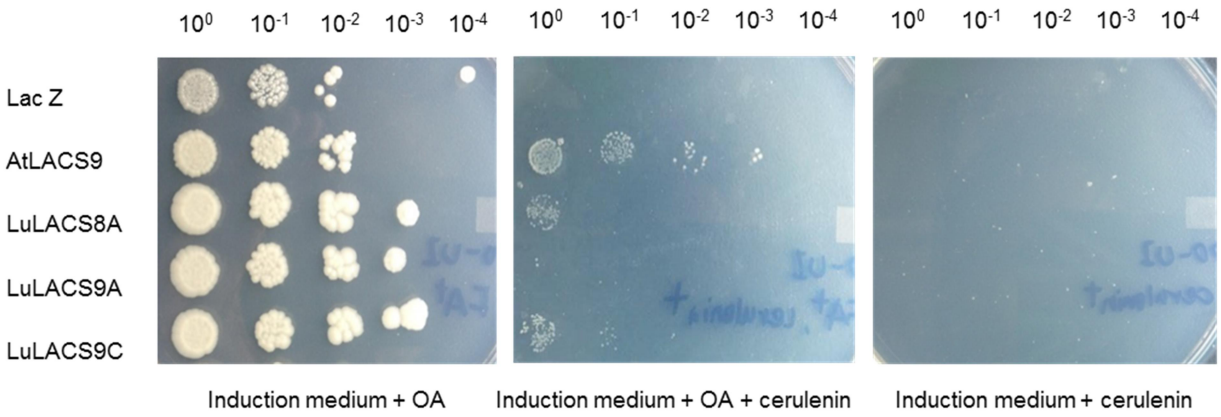

Supplementary Figure S5.2. LuLACSs complement yeast growth defect under oleic acid (OA) auxotrophic conditions. The growth defect of yeast strain *BYfaa1,4*Δ under fatty acid auxotrophic conditions is rescued by LuLACSs. Serial dilutions of *BYfaa1,4*Δ cells transformed with *LuLACS*s were spotted onto induction medium containing OA, or cerulenin, or both. Yeast mutant cells containing *AtLACS9* and empty vector (LacZ) were used as positive and negative controls, respectively.

Chapter 6 – Membrane Yeast Two-Hybrid Assays Reveal Several Interactions between Storage Lipid Biosynthetic Enzymes from Flax

6.1. Introduction

Seed oil from flax (*Linum usitatissimum*) contains around 45% to 65% α-linolenic acid (ALA; 18:3$\Delta^{9cis,12cis,15cis}$), which is of great nutritional and industrial value. As an essential fatty acid, ALA is a precursor for nutritionally essential very long chain omega-3 polyunsaturated fatty acids (PUFA), including eicosapentaenoic acid (EPA; 20:5$\Delta^{5cis,8cis,11cis,14cis,17cis}$) and docosahexaenoic acid (DHA; 22:6$\Delta^{4cis,7cis,10cis,13cis,16cis,19cis}$) (Das, 2006; Lorente-Cebrián et al., 2013). In addition, the enrichment of flax seed oil with ALA enhances the drying quality of the oil, making it suitable for various industrial applications (Jhala and Hall, 2010; Hall et al., 2016).

In developing oilseeds, fatty acid biosynthesis occurs in the plastids and the resulting fatty acids, predominantly as oleic acid (OA; 18:1Δ^{9cis}), palmitic acid (16:0), and stearic acid (18:0), are exported to the cytosol in the form of acyl-CoAs for phosphatidylcholine (PC) and triacylglycerol (TAG) synthesis (Chapman and Ohlrogge, 2012; Chen et al., 2015). PC is the major site for further modification of the *de novo* synthesized fatty acids, where OA at the *sn*-2 position of PC can be further converted to linoleic acid (LA; 18:2$\Delta^{9cis,12cis}$), and then ALA, through the catalytic action of ER-bounded fatty acid desaturase 2 and 3, respectively, before incorporated into TAG (Radovanovic et al., 2014; Vrinten et al., 2005). PUFA on PC can be channeled into TAG via various possible metabolic routes (Bates et al., 2012; Lager et al., 2015). PUFAs at the *sn*-2 position of PC can enter the acyl-CoA pool through the combined catalytic action of phospholipase A_2 and long-chain acyl-CoA synthetase or through the reverse reaction catalyzed by lysophosphatidylcholine acyltransferase (LPCAT). The resulting PUFA-CoAs are then supplied as the acyl donors for the acyl-CoA-dependent acyltransferases from the Kennedy

pathway to form TAG, including *sn*-glycerol-3-phosphate acyltransferase, lysophosphatidic acid acyltransferase and diacylglycerol acyltransferase (DGAT) (Snyder et al., 2009). Alternatively, PUFAs on PC can be incorporated into TAG in the form of *sn*-1,2-diacylglycerol (DAG) by removing the phosphocholine headgroup through the catalytic action of phosphatidylcholine diacylglycerol cholinephosphotransferase (PDCT). In addition, CDP-choline:diacylglycerol cholinephosphotransferase and phospholipase C and/or D also contribute to the PC/DAG conversion. Furthermore, PUFAs can also be directly incorporated into TAG by the catalytic action of phospholipid:diacylglycerol acyltransferase (PDAT), which transfers the PUFA from the *sn*-2 position of PC onto the *sn*-3 position of DAG. The resulting lysophosphatidylcholine (LPC) produced from the reaction catalyzed by PDAT, phospholipase A_2 or the reverse reaction of LPCAT can be recycled into PC via the forward reaction catalyzed by LPCAT.

In flax, different potential metabolic routes for channeling ALA into TAG have been explored and various acyltransferases including PDAT (Pan et al., 2013), PDCT (Wickramarathna et al., 2015), DGAT and LPCAT (Pan et al., 2015) have been shown to display preference towards ALA containing substrates and contribute to the ALA-enriching processes. These acyltransferases either share the same substrate/product or catalyze consecutive reactions in which the product of the reaction catalyzed by the first enzyme is the substrate for the second enzyme. Thus, it is possible that these enzymes might form multicomponent complexes to effectively transfer the α-linolenoyl moieties from PC to the final TAG. Indeed, physical interactions between some TAG-synthesizing enzymes from Arabidopsis (*Arabidopsis thaliana*) and tung tree (*Vernicia fordii*) have been reported (Gidda et al., 2011; Shockey et al., 2016).

In the current study, potential physical interactions between enzymes involved in the flax ALA-enriching process, including LuDGAT1, LuDGAT2, LuPDAT1, LuPDAT2, LuLPCAT2,

and LuPDCT1, were explored using the split-ubiquitin membrane yeast two-hybrid (MYTH) system (Snider et al., 2010). Our results suggest that physical interactions between storage lipid biosynthetic enzymes may assist in the channeling of ALA into TAG.

6.2. Results and discussion

To explore the potential physical interaction between enzymes in flax ALA-enriching processes, LuDGAT1, LuDGAT2, LuPDAT1, LuPDAT2, LuLPCAT2, or LuPDCT1 was used as bait and prey individually and the interaction within each bait and prey combination was tested using the split-ubiquitin MYTH system (Snider et al., 2010). The principle of the split-ubiquitin MYTH system (Snider et al., 2010; Fetchko and Stagljar, 2004) is illustrated in Figure 6.1. In brief, the wild type ubiquitin can be divided into two fragments: the N-terminal fragment ($N_{ub}I$) and the C-terminal fragment (C_{ub}). $N_{ub}I$ and C_{ub} would spontaneously re-associate into a stable 'pseudoubiquitin' molecule, which would be recognized by cytosolic deubiquitinating enzymes (DUBs). This kind of re-association could be prevented by introducing an isoleucine to glycine mutation in $N_{ub}I$ ($N_{ub}G$). In a MYTH system, bait and prey are fused to C_{ub}-LexA (C_{ub} fused to a transcription factor) and $N_{ub}G$, respectively, and then co-produced in *Saccharomyces cerevisiae* strain NMY51. If the bait and prey proteins interact, it would bring C_{ub} and $N_{ub}G$ into close proximity and thus leads to re-association of ubiquitin (pseudoubiquitin). The pseudoubiquitin is then recognized by DUBs, and the transcription factor linked to the C_{ub} is released, which can then enter the nucleus to activate the expression of reporter genes, including *HIS3*, *ADE2* and *LacZ*. As a result, when the bait and prey proteins interact, the yeast cells co-expressing bait and prey would grow on media lacking adenine and histidine and produce blue colonies at the presence of X-Gal (5-bromo-4-chloro-3-indolyl-β-D-galactopyranoside).

As shown in Figure 6.2, interactions were observed between LuDGAT1-1 and itself or LuPDCT1, when LuDGAT1-1 was used as bait. The interaction between LuLPCAT2 and LuDGAT1-1 was also observed by using LuLPCAT2 as bait and LuDGAT1-1 as prey. LuDGAT2-3 was found to interact with LuLPCAT2 and LuPDCT1 by using LuDGAT2-3 as prey, whereas these interactions were not observed when LuDGAT2-3 was changed to bait. It is still unknown why different bait and prey combinations of the same two proteins would lead to different results. It is probably because the membrane-bound feature of these proteins would restrict the orientation of both termini of protein and thus affect the re-association process of ubiquitin. This discrepancy has also been reported when testing the interactions between DGAT and LPCAT or LPAAT from Arabidopsis (Shockey et al., 2016). Furthermore, LuLPCAT2 was found to interact with itself, LuPDAT1, LuPDAT2, and LuPDCT1. The interaction of LuLPCAT2 with LuDGATs, LuPDATs, or LuPDCT1 was also observed when using C-terminus fused LuLPCAT2 as the bait (data not shown). In addition, LuPDCT1 showed self-interaction. The observed self-interaction of LuDGAT1-1, LuLPCAT2, or LuPDCT1 suggests that these enzymes might form multimeric complexes. Indeed, self-association of DGAT1 mediated by the hydrophilic N-terminal domain has been demonstrated for the recombinant enzymes from *Brassica napus* (Weselake et al., 2006), mouse (*Mus musculus*) (McFie et al., 2010) and human (*Homo sapiens*) (Cheng et al., 2001).

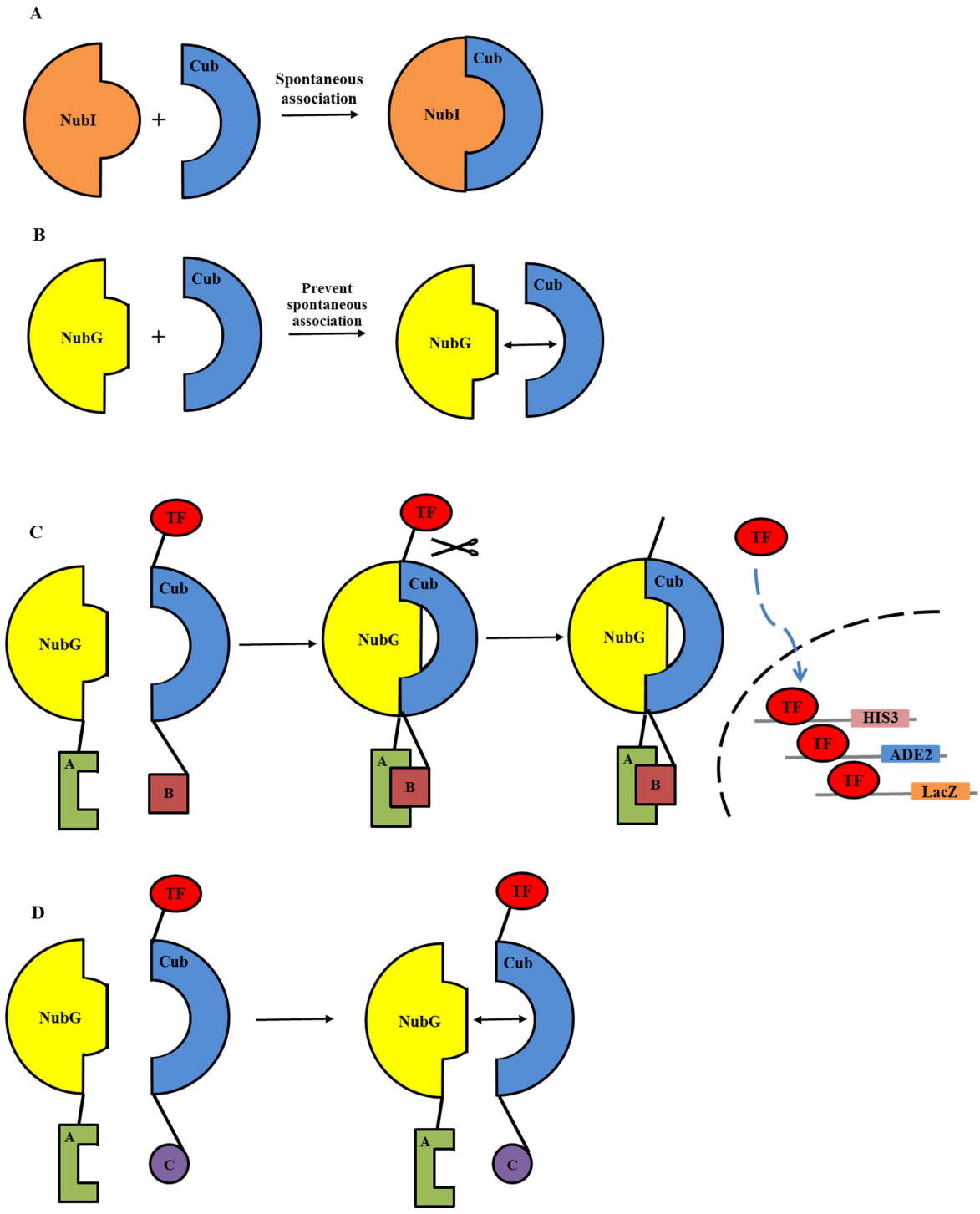
A
NubI
Cub
Spontaneous association
NubI
Cub
B
NubG
Cub
Prevent spontaneous association
NubG
Cub
C
TF
Cub
NubG
A
B
TF
Cub
NubG
A
B
Cub
NubG
A
B
TF
TF
HIS3
TF
ADE2
TF
LacZ
D
TF
Cub
NubG
A
C
NubG
TF
Cub
A
C

Figure 6.1. Split-ubiquitin membrane yeast two-hybrid system. (A) The N-terminal fragment ($N_{ub}I$, shown in orange) and the C-terminal fragment (C_{ub}, shown in blue) of the wild type ubiquitin are able to spontaneously associate into an ubiquitin. (B) Introduction of an isoleucine to glycine mutation in the $N_{ub}I$ ($N_{ub}G$, shown in yellow) would block the spontaneous association. C and D, the bait (protein B or C, shown in dark-red or purple) and prey (protein A, shown in green) proteins are fused to C_{ub} and $N_{ub}G$, respectively. (C) If bait and prey interact with each other, the $N_{ub}G$ and C_{ub} are brought into close proximity leading to re-association of ubiquitin. The transcription factor linked to the C_{ub} (TF, shown in red) would be cleaved by deubiquitinating enzymes (DUBs, scissors) and enter the nucleus to activate the reporter system. (D) If there is no interaction between bait and prey, the reporter system would not be activated. This figure was re-drawn with modification according to Snider et al. (2010) and Fetchko and Stagljar (2004).

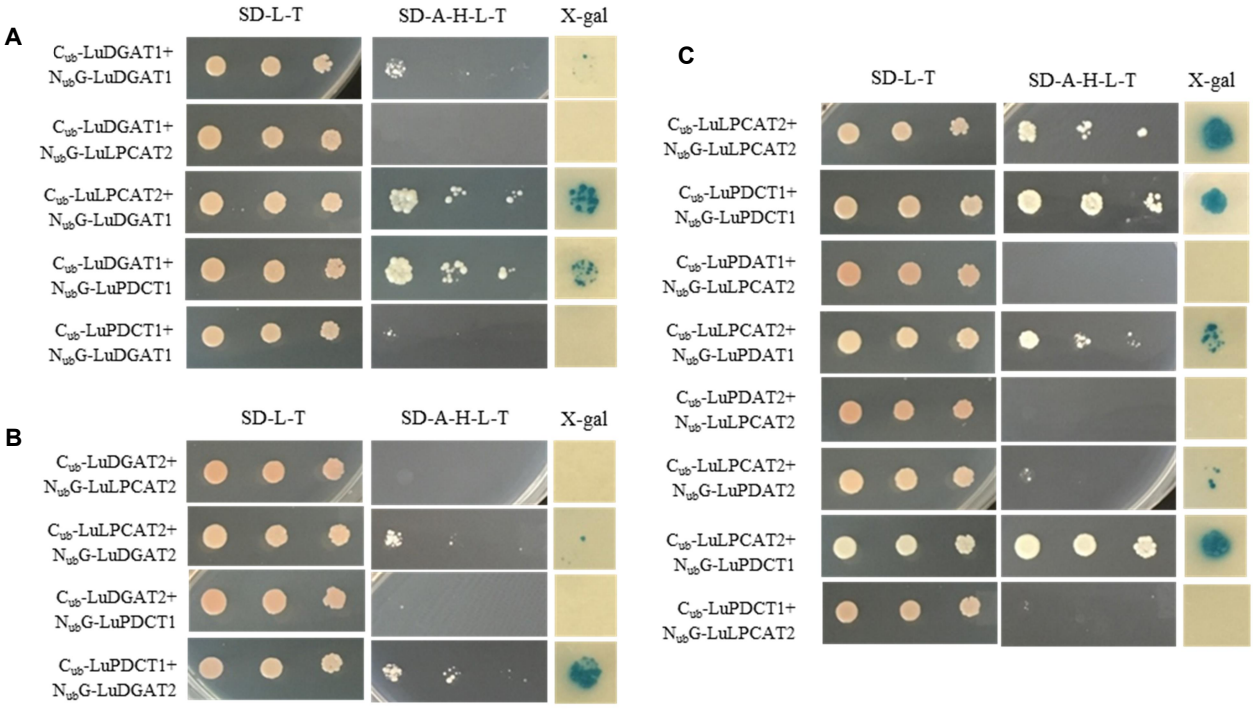

Figure 6.2. LuDGATs physically interact with other enzymes in acyl-editing pathways. Protein-protein interaction between LuDGATs and other lipid metabolic enzymes were tested using split-ubiquitin membrane yeast two-hybrid (MYTH) assays. MYTH was tested for LuDGAT1-1 (A) and LuDGAT2-3 (B) and the interactions between LuPDAT1, LuPDAT2, LuLPCAT2 and LuPDCT1 (C). cDNA encoding each enzyme of interest was ligated to the Lex A- C-terminal fragment of ubiquitin (C_{ub}) and the N-terminal fragment of ubiquitin containing an Ile/Gly point mutation ($N_{ub}G$), yielding C_{ub}-bait and $N_{ub}G$-prey, respectively. Serial dilutions of yeast cells producing each bait/prey combination were spotted on synthetic drop-out (SD) agar plates lacking Leu and Trp (SD-L-T) or SD agar plates lacking Ade, His, Leu and Trp (SD-A-H-L-T). Activation of the *LacZ* reporter gene was visualized by spotting yeast cells onto SD-A-H-L-T plates containing X-Gal (5-bromo-4-chloro-3-indolyl-β-D-galactopyranoside).

The identified protein-protein interactions (Figure 6.2) revealed a possible metabolic network (Figure 6.3), in which the enzymes from the acyl-editing processes and DGAT, which catalyzes the final reaction in the Kennedy pathway (Weiss and Kennedy, 1956; Liu et al., 2012) might form multicomponent complexes to allow for effective channeling of α-linolenoyl moieties from PC into final TAG. The protein-protein interaction between LuPDCT1 and LuDGAT2-3 or LuDGAT1-1 (Figure 6.2) suggests that DAG enriched in ALA through PDCT action (Wickramarathna et al., 2015) could be an effective acyl acceptor for LuDGATs (especially LuDGAT2-3), selectively utilizing α-linolenoyl-CoA. In addition, LuLPCAT2, an acyl-editing enzyme involved in PC and LPC interconversion, may operate at a strategic intersection between the acyl-editing process and the Kennedy pathway for enriching the ALA content of TAG. LuLPCAT2 interacted with LuDGAT1, which is consistent with the recent observation of the interaction between Arabidopsis LPCAT2 and DGAT1 (Shockey et al., 2016). The demonstrated interaction between LuLPCAT2 and LuDGAT1-1 further supports the previous evidence for biochemical coupling of LuDGAT1 and LuLPCAT-catalyzed reactions for incorporating ALA into TAG (Pan et al., 2015). Considering its high ALA selectivity (Chapter 5), the LuDGAT2-3-catalyzed forward reaction may exhibit even more effective coupling with the LuLPCAT-catalyzed reverse reaction. Furthermore, the interaction between LuLPCAT2 and other PC-utilizing enzymes (LuPDAT1, 2 and LuPDCT1) suggests the presence of a specific complex for PC/LPC recycling and editing in developing flax seed, in which PDAT, PDCT and the reverse reaction of LPCAT could efficiently channel the ALA moieties from PC into TAG directly, or in the form of DAG or α-linolenoyl-CoA, and the resulting LPC could be recycled to PC by the forward reaction of LPCAT, and then undergo further modification.

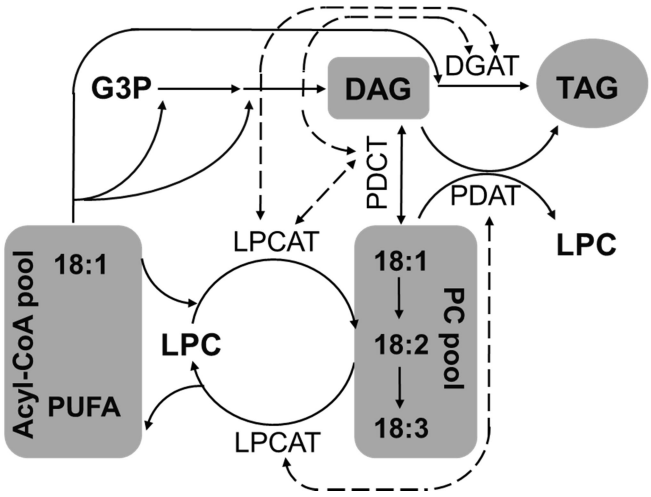

Figure 6.3. Protein-protein interactions between enzymes involved in the biosynthesis of flax triacylglycerol (TAG) enriched in α-linolenic acid (ALA; 18:3). Observed physical interactions, based on the membrane yeast two-hybrid assay, are indicated by the dashed arrows. Other abbreviations: G3P, *sn*-glycerol 3- phosphate; DAG, *sn*-1,2-diacylglycerol; DGAT, diacylglycerol acyltransferase; LPC, lysophosphatidylcoline; LPCAT, lysophosphatidylcholine acyltransferase; PC, phosphatidylcholine; PDAT, phospholipid:diacyglycerol acyltransferase; PDCT, phosphatidylcholine:diacylglycerol cholinephosphotransferase; PUFA, polyunsaturated fatty acid.

Previously, a flax LACS (LuLACS8A) was suggested to display enhanced substrate preference towards ALA, which may provide the acyl-donor for the ALA-selective LuDGAT2 catalyzing TAG synthesis (Chapter 5). Considering that acyl-CoA synthetase has been reported to interact with DGAT2 in a mammalian system (Xu et al., 2012), the physical interaction between LuLACS8A and LuDGAT2 was explored through the MYTH assay. LuLACS8A, however, failed in in the activation of the reporter gene in the N_{ub}GI control test, suggesting that the MYTH system might not be applicable for this enzyme.

Together, these results suggested that storage lipid biosynthetic enzymes from flax physically interact with each other to allow for effective transfer of ALA from PC into TAG.

6.3. Experimental procedures

Protein-protein interactions between LuLACS8A, LuDGAT1, LuDGAT2, and other lipid biosynthetic enzymes contributing to flax ALA enrichment, including LuPDAT1, LuPDAT2, LuLPCAT2 and LuPDCT1 were tested using the MYTH system (kindly provided by Dr. Igor Stagljar, University of Toronto), as described by Snider et al. (2010). Briefly, cDNAs encoding LuLACS8A, LuDGAT1, LuDGAT2, LuPDAT1, LuPDAT2, LuLPCAT2 and LuPDCT1 were amplified by PCR and cloned into the pBT3N or pAMBV bait vector or pPR3N prey vector. The resulting pAMBV:bait or pBT3N:bait and pPR3N:prey or control prey (Ost-N_{ub}I 'positive' control prey or Ost-N_{ub}G 'negative' control prey) were co-transformed into yeast strain NMY51 (*MATa, his3Δ200, trp1-901, leu2- 3,112, ade2, LYS2::(lexAop)4-HIS3,ura3::(lexAop)8-lacZ,ade2::(lexAop)8-ADE2, GAL4*). Yeast cells expressing each bait/prey combination were selected on synthetic drop-out (SD) agar plates lacking Leu and Trp (SD-L-T) to ensure the presence of both bait and prey vector, and the interaction was assayed on SD agar plates lacking

Ade, His, Leu and Trp (SD-A-H-L-T) by 1: 10 serial dilution of cell cultures starting from an OD600 value of 0.4. Activation of the *LacZ* gene in the yeast strain was visualized by spotting yeast cells (with an OD600 value of 0.4) onto SD-A-H-L-T plates containing 80 mg/L 5-bromo-4-chloro-3-indolyl-*β*-D-galactopyranoside (X-Gal).

Various baits constructed by fusing Lex A-C_{ub} to the N-terminus (pBT3N) or fusing C_{ub}-Lex A to the C-terminus (pAMBV) of each enzyme were subsequently validated via the N_{ub}GI control test. With exception for LuLACS8A and LuLPCAT2, only fusing the Lex A-C_{ub} to the N-terminus of the enzymes showed positive reporter gene activation when paired with the N_{ub}I positive control prey, whereas fusion proteins containing the C_{ub}-Lex A linked at the C-terminus of the enzymes failed to activate the reporter gene when paired with N_{ub}I. In terms of LuLPCAT2, both C- and N-termini fusion proteins activated the reporter gene. However, neither the C- or N-terminus fused LuLACS8A passed the test.

Chapter 7 – Summary and Future Directions

Triacylglycerol (TAG) biosynthesis in plants is controlled by a complex network of various enzymes and proteins. As the enzyme catalyzing the last committed step in the acyl-CoA-dependent TAG biosynthesis, diacylglycerol acyltransferase (DGAT) has been regarded as the target of numerous studies attempting to manipulate seed oil content and fatty acid composition. Another enzyme, long-chain acyl-CoA synthetase (LACS), which provides the acyl-substrate to all the acyl-CoA-dependent acyltransferases (including DGAT) in TAG biosynthesis, has also been proposed to impact on TAG content and composition. Thus, the overall goals of this thesis were to manipulate the enzyme performance of DGAT and LACS, and to explore their potential role in modifying oil content and fatty acid composition.

The first part of this thesis was to characterize performance-enhanced variants of *Brassica napus* DGAT1 (BnaDGAT1, specifically isoform BnaC.DGAT1.a) generated by directed evolution. Previously, directed evolution of BnaDGAT1 has generated numerous BnaDGAT1 variants with improved neutral lipid accumulation ability in yeast. In this study, the TAG fractions of yeast cells producing 50 BnaDGAT1 variants were separated and analyzed by GC/MS and the BnaDGAT1 variants were confirmed to result in increased TAG content when produced in yeast. Multiple sequence alignment and positive selection suggested that most of the amino acid residue substitutions identified from the BnaDGAT1 variants were conserved among plant DGAT1s, and for the unconserved amino acid residues from the variants, many of them were predicted as positively selected sites. By mapping the beneficial amino acid residue substitutions of the BnaDGAT1 variants onto a predicted topology model, it was revealed that the ninth and tenth predicted transmembrane domains (TMDs) may have important roles in affecting DGAT1 performance. BnaDGAT1 was predicted to possess 8 to 10 TMDs by different

prediction algorithms, whereas the presence of the last two predicted TMDs (TMD9 corresponding to amino acid residues 441-460 and TMD10 corresponding to amino acid residues 472-491, predicted by Phobius (Käll et al., 2007)) and other five TMDs was preserved. It has been suggested previously that the most conserved C-terminal region of DGAT1 is likely to contain the catalytic pocket of the enzyme (Liu et al., 2012). Removal of the last three amino acid residues in predicted TMD10 through C-terminal truncation in *Ricinus communis* DGAT1 (RcDGAT1) abolished enzyme activity (Siloto et al., 2009b), suggesting that the C-terminal region of RcDGAT1 is critical for maintaining enzyme function. Insertion mutation of F469 in maize DGAT1-2 (within the predicted TMD10) was demonstrated to be associated with enhanced DGAT activity and TAG accumulation (Zheng et al., 2008). Thus, in future work, it would be interesting to explore the roles of the predicted TMD9 and 10 in DGAT activity through site-directed/saturation mutagenesis.

To further investigate how the amino acid residues would affect the enzyme performance, several BnaDGAT1 variants with amino acid residue substitutions residing in PTMD9 were characterized in detail. The BnaDGAT1 variants were found to stimulate yeast TAG content for different reasons, including improved enzyme activity, polypeptide accumulation and/or desensitization to apparent substrate inhibition. The most promising BnaDGAT1 variant, L441P, was found to display possible reduced substrate inhibition and increased catalytic efficiency. The amino acid residue substitutions shown to benefit BnaDGAT1 activity were then transferred to *C. sativa* DGAT1 (CsDGAT1) and resulted in improved enzyme performance of the recombinant CsDGAT1 enzymes variants. It is interesting to note that CsDGAT1 variant L460P, equivalent to BnDGAT1 variant L441P, also had possible reduced substrate inhibition. Even though the exact mechanism of substrate inhibition in BnaDGAT1 is not well understood due to

the lack of a three-dimensional structure of any DGATs, it is likely that replacing the bulky aliphatic Leu 441 in BnaDGAT1, or Leu 460 in CsDGAT1B with Pro might relieve the substrate inhibition by disturbing the further binding of acyl-CoA to ES complex. It is possible that Leu 441 might be related to a third acyl-CoA binding site, besides the other two putative acyl-CoA binding sites in the hydrophobic segment (FYXDWWN) (Lopes et al., 2014) and the hydrophilic N-terminus (probably an allosteric regulation site) (Liu et al., 2012; Siloto et al., 2008; Weselake et al., 2006), respectively. Detailed structural information will be necessary to gain more insight into the catalytic mechanism of this enzyme.

The above directed evolution of BnaDGAT1 relied on the screening of the randomly mutagenized *BnaDGAT1* libraries using oleic acid as a selective agent. In order to identify novel BnaDGAT1 variants with desirable substrate specificity, the mutagenized libraries of *BnaDGAT1* were screened again using linoleic acid or *α*-linolenic acid (ALA). One variant containing seven amino acid residue substitutions was found to display altered preference towards linoleoyl-CoA and *α*-linolenoyl-CoA. Even though it is difficult to conclude which amino acid residue substitution(s) contribute to the altered substrate preference based on the current results, one amino acid substitution (L419I) of that variant should draw more attention. Four DGAT1 isoforms from *B. napus* with high sequence similarity have been identified previously and can be separated into two clades, with clade I enzymes (including BnaC.DGAT1.a) preferring linolenoyl-CoA, while clade II enzymes preferring linoleoyl-CoA (Greer et al., 2015, 2016). Based on the sequence alignment of the four BnaDGAT1 isoforms, one amino acid residue substitution site (L419I) from the identified BnaDGAT1 (BnaC.DGAT1.a) variant was found to be present only in the enzymes from clade I rather than clade II, whereas the enzymes from clade II have an I at that position. Position L419 of

BnaDGAT1 is just after the putative acyl-CoA binding site and putative DAG binding site. Thus, it would be interesting to further explore the substrate preference of single mutant L419I in the future.

The beneficial amino acid residue substitutions identified from BnaDGAT1 variants were successfully used to improve DGAT1 from *C. sativa*, suggesting that it is possible to manipulate DGAT1 performance by taking advantage of the amino acid residue substitution database generated based on the BnaDGAT1 variants. In addition, our results also suggest that it is possible to improve DGAT1 performance via a single amino acid residue substitution. Thus, it would be worthwhile to further explore the application of these performance-enhanced DGAT1 variants in improving oil content *in planta* by using non-transgenic approaches such as Targeting-Induced Local Lesions IN Genomes (TILLING) (Till et al., 2006) or clustered regularly interspaced short palindromic repeats (CRISPR) (Belhaj et al., 2013). Together, our findings suggest that direct evolution is an efficient approach to manipulate DGAT performance and gain insight into structure-function relationships in this enzyme in the absence of a three-dimensional structure.

The second part of this thesis was to generate performance-enhanced variants of *Arabidopsis thaliana* LACS9 (AtLACS9). Random mutagenesis combined with site-directed mutagenesis was used to generate several AtLACS9 variants with improved enzyme performance. The substitutions of C207F and D238E were found to result in increased enzyme activity. C207 was conserved among LACS9s from plant eudicots, whereas the unconserved site D238 might be under positive selection, suggesting that both the moderately conserved sites and the positively selected sites might contain target amino acid residues for substitution to increase activity. Another two variants, E520D and E630D, were identified to possess altered substrate

specificity. Both E520 and E630 are moderately conserved and E520 resides in the vicinity of the fatty acyl-CoA synthetase signature motif (FACS motif), which was proposed to be involved in fatty acid binding (Watkins and Ellis, 2012). The mechanisms behind AtLACS9 substrate specificity are not well elucidated, athough many crystal structures of LACS homologs have been solved, including LACS from *Thermus thermophiles* (Hisanaga et al., 2004), medium-chain fatty acyl-CoA synthetase from *Homo sapiens* (Kochan et al., 2009) and very-long-chain fatty acyl-CoA synthetase from *Mycobacterium tuberculosis* (Watkins and Ellis, 2012). These fatty acyl-CoA synthetases share similar structural features which consist of a large N-terminal and a small C-terminal domain, but the proposed fatty acid binding tunnels were slightly different. In addition, no experimental evidence has shown that changing the size of the proposed tunnels can alter substrate specificity. It would be interesting to explore the crystal structure of AtLACS9 to further elucidate the findings in the research and allow us to understand the molecular mechanism of this enzyme. Furthermore, certain amino acid residue substitutions of AtLACS9 were also found to affect the protein accumulation of the enzyme variants in yeast. Further analysis of the expression level and plasmid burden of the *AtLACS9* variants and stability of the variant proteins in yeast may help us have a better understanding about the differences in protein accumulation.

Although many studies have shown that over-expression of *LACS* genes could increase lipid accumulation in yeast (Guo et al., 2014; Tan et al., 2014; Tonon et al., 2005; Pulsifer et al., 2012), the attempts to increase yeast oil content using activity-improved AtLACS9 variants were not successful in this project. It is possible that the improved acyl-CoA by AtLACS9 variants could not be further channeled into TAG due to the limitations in the DGAT1-catalyzed reaction. Indeed, as suggested in the first part of the thesis, DGAT1 displayed strong substrate inhibition

at high oleoyl-CoA concentration. It would be interesting to co-produce AtLACS9 with BnaDGAT1 variant L441P, which displayed possible reduced substation inhibition. Furthermore, to explore the potential application of AtLACS9 variants in the production of other fatty acid-derived compounds, such as fatty esters, fatty alcohols or waxes would also represent potential strategies for engineering oleaginous microorganisms.

The third part of this thesis was to explore the potential roles of LACS and DGAT2 in channeling ALA into TAG in developing flax (*Linum usitatissimum*) seed. Previously, it has been suggested that in flax ALA-channeling process may involve the action of phospholipid:diacylglycerol acyltransferase (PDAT) (Pan et al., 2013), phosphatidylcholine:diacylglycerol cholinephosphotransferase (PDCT) (Wickramarathna et al., 2015), and/or through coupling of the reverse reaction catalyzed by lysophosphatidylcholine acyltransferase (LPCAT) to the reaction catalyzed by DGAT1 (Pan et al., 2015). In this study, a potential process for channeling ALA into flax seed TAG which involves the catalytic action of flax LACS and flax DGAT was proposed. ALA-selective LACS (LuLACS8A) was identified from flax. The resulting linolenoyl-CoA from LACS action could be potentially utilized by the acyltransferases from the Kennedy pathway to form TAG. Since flax DGAT2 (LuDGAT2-3) was found to display ~20 times increased preference towards α-linolenoyl-CoA over oleoyl-CoA, it was co-produced with LuLACS8A to test whether the cooperation of these two enzymes could contribute to ALA-channelling. Both *in vitro* and *in vivo* results confirmed that substrate channeling between LuLACS8A and LuDGAT2-3-catalyzed reactions could selectively channel ALA into TAG. This ALA-channeling process might even be made more effective by introducing equivalent amino acid substitutions into LuLACS8A which were shown to enhance the performance of AtLACS9A. In addition, directed evolution of LuDGAT2-3 to increase

enzyme performance might also be worth exploring. The involvement of LuLACS8A in ALA channeling, however, is dependent on the identification of a flax phospholipase A_2 to liberate ALA from phosphatidylcholine (PC) and make it available for LuLACS8A. Indeed, substrate selective phospholipase A_2 has been identified from castor for catalyzing the release of ricinoleic acid from modified PC (Bayon et al., 2015).

The proposed LuLACS8A-LuDGAT2-3 substrate channeling process may be coordinated with other ALA-enriching processes. In the fourth part of the thesis, several potential interactions between enzymes involved in TAG biosynthesis and acyl-editing from flax were revealed by membrane yeast two-hybrid assays. The identified protein-protein interactions between LuPDCT1 and LuDGAT2-3 or LuDGAT1-1 suggested that the ALA enriched *sn*-1,2-diacylglycerol (DAG) produced via PDCT action could be an effective acyl acceptor for LuDGATs (especially LuDGAT2-3) selectively utilizing α-linolenoyl-CoA. The DAG specificity and selectivity of LuDGAT2-3, however, is not known. It would be interesting to explore the substrate channeling in yeast through combined production of recombinant LuLACS8A, LuPDCT and LuDGAT2-3. Combined over-expression of *LuLACS8A*, *LuPDCT* and *LuDGAT2-3* during flax seed development could potentially further enhance the ALA content of TAG by making ALA-enriched acyl-CoA and ALA-enriched TAG more readily available for LuDGAT2-3. In addition, membrane yeast two-hybrid data indicated that LuLPCAT2 interacted with LuDGAT1-1, supporting the previous biochemical coupling of LuLPCAT-LuDGAT1-catalyzed reactions for incorporating ALA into TAG (Pan et al., 2015). The process of ALA-enrichment of TAG might even be further enhanced through enhanced production of PDAT exhibiting high selectivity for substrates containing ALA.

The PC-derived DAG pool, rather than the *de novo* DAG pool, has been proposed as the major source of DAG for TAG biosynthesis (Bates et al., 2009; Lu et al., 2009). Recently, an independent acyl-CoA pool in the ER lumen has also been proposed (Kim et al., 2013). Thus, to identify the relative contribution of each TAG assembly and acyl-editing enzyme to the ALA enrichment process in flax, future investigators must take into consideration the different DAG and acyl-CoA substrate pools. This represents a challenging task for elucidating the process of TAG assembly in flax and other oleaginous plants that produce modified fatty acids on PC prior to their incorporation into TAG. In turn, this information could lead to the development of efficient metabolic engineering strategies to produce unusual fatty acids in oil crops that do not typically produce them.

In the foreseeable future, more genes encoding the lipid associated proteins and enzymes/isozymes will be identified, and their regulation, direct and indirect interaction and relative contribution to the whole lipid metabolic network will be explored. All of these will further benefit our understanding in plant lipid metabolism.

In conclusion, directed evolution was used to generate performance-enhanced variants of BnaDGAT1 and AtLACS9. The potential roles of LACS and DGAT in the ALA-channeling process also were explored. The findings of this work provide insight into the amino acid residues underlying plant DGAT1 and LACS9 function and will benefit the development of novel strategies for improving the oil content and producing designer oils in oleaginous plants and microorganisms.

References

Abe T, Fujino T, Fukuyama R, Minoshima S, Shimizu N, Toh H, Suzuki H, and Yamamoto T (1992) Human long-chain acyl-coA synthetase: Structure and chromosomal. J Biochem 111: 123–128

Andersson CS, Lundgren CAK, Magnúsdóttir A, Ge C, Wieslander Å, Molina DM, and Högbom M (2012) The *Mycobacterium tuberculosis* very-long-chain fatty acyl-CoA synthetase: Structural basis for housing lipid substrates longer than the enzyme. Structure 20: 1062–1070

Andersson MX, Goksör M, and Sandelius AS (2007) Optical manipulation reveals strong attracting forces at membrane contact sites between endoplasmic reticulum and chloroplasts. J Biol Chem 282: 1170–1174

Andersson MX, Kjellberg JM, and Sandelius AS (2004) The involvement of cytosolic lipases in converting phosphatidyl choline to substrate for galactolipid synthesis in the chloroplast envelope. Biochim Biophys Acta (BBA)-Mol Cell Biol Lipids 1684: 46–53

Andrews J, and Keegstra K (1983) Acyl-CoA synthetase is located in the outer membrane and acyl-CoA thioesterase in the inner membrane of pea chloroplast envelopes. Plant Physiol 72: 735–740

Aymé L, Baud S, Dubreucq B, Joffre F, and Chardot T (2014) Function and localization of the *Arabidopsis thaliana* diacylglycerol acyltransferase DGAT2 expressed in yeast. PLoS One 9: 1–9

de Azevedo Souza C, Kim SS, Koch S, Kienow L, Schneider K, McKim SM, Haughn GW,

Kombrink E, and Douglas CJ (2009) A novel fatty acyl-CoA synthetase is required for pollen development and sporopollenin biosynthesis in Arabidopsis. Plant Cell 21: 507–525

Aznar-Moreno JA, and Durrett TP (2017) Simultaneous targeting of multiple gene homeologs to alter seed oil production in *Camelina sativa.* Plant Cell Physiol: pcx058

Aznar-Moreno JA, Venegas Calerón M, Martínez-Force E, Garcés R, Mullen R, Gidda SK, and Salas JJ (2014) Sunflower (*Helianthus annuus*) long-chain acyl-coenzyme A synthetases expressed at high levels in developing seeds. Physiol Plant 150: 363–373

Aznar-Moreno J, Denolf P, Van Audenhove K, De Bodt S, Engelen S, Fahy D, Wallis JG, and Browse J (2015) Type 1 diacylglycerol acyltransferases of *Brassica napus* preferentially incorporate oleic acid into triacylglycerol. J Exp Bot 66: 6497-6506

Bafor M, Smith MA, Jonsson L, Stobart K, and Stymne S (1993) Biosynthesis of vernoleate (*cis*-12-epoxyoctadeca-*cis*-9-enoate) in microsomal preparations from developing endosperm of *Euphorbia lagascae*. Arch Biochem Biophys 303: 145–151

Bafor M, Stobart AK, and Stymne S (1990) Properties of the glycerol acylating enzymes in microsomal preparations from the developing seeds of safflower (*Carthamus tinctorius*) and turnip rape (*Brassica campestris*) and their ability to assemble cocoa-butter type fats. J Am Oil Chem Soc 67: 217–225

Bansal S, and Durrett TP (2015) *Camelina sativa*: An ideal platform for the metabolic engineering and field production of industrial lipids. Biochimie 120: 9–16

Bates PD (2016) Understanding the control of acyl flux through the lipid metabolic network of

plant oil biosynthesis. Biochim Biophys Acta (BBA)-Mol Cell Biol Lipids 1861: 1214–1225

Bates PD, Durrett TP, Ohlrogge JB, and Pollard, M (2009) Analysis of acyl fluxes through multiple pathways of triacylglycerol synthesis in developing soybean embryos. Plant Physiol 150: 55–72

Bates PD, Fatihi A, Snapp AR, Carlsson AS, Browse J, and Lu C (2012) Acyl editing and headgroup exchange are the major mechanisms that direct polyunsaturated fatty acid flux into triacylglycerols. Plant Physiol 160: 1530–1539

Bates PD, Ohlrogge JB, and Pollard M (2007) Incorporation of newly synthesized fatty acids into cytosolic glycerolipids in pea leaves occurs via acyl editing. J Biol Chem 282: 31206–31216

Bates PD, Stymne S, and Ohlrogge J (2013) Biochemical pathways in seed oil synthesis. Curr Opin Plant Biol 16: 358–364

Baud S, and Lepiniec L (2010) Physiological and developmental regulation of seed oil production. Prog Lipid Res 49: 235–249

Bayon S, Chen G, Weselake RJ, and Browse J (2015) A small phospholipase A2-α from castor catalyzes the rremoval of hydroxy fatty acids from phosphatidylcholine in transgenic *Arabidopsis seeds.* Plant Physiol 167: 1259–1270

Belhaj K, Chaparro-Garcia A, Kamoun S, and Nekrasov V (2013) Plant genome editing made easy: targeted mutagenesis in model and crop plants using the CRISPR/Cas system. Plant

Methods 9: 39

De Bhowmick G, Koduru L, and Sen R (2015) Metabolic pathway engineering towards enhancing microalgal lipid biosynthesis for biofuel application—A review. Renew Sustain Energy Rev 50: 1239–1253

Biermann U, Bornscheuer U, Meier MAR, Metzger JO, and Schäfer HJ (2011) Oils and fats as renewable raw materials in chemistry. Angew Chemie Int Ed 50: 3854–3871

Biswas S, and Akey JM (2006) Genomic insights into positive selection. Trends Genet 22: 437–446

Black PN, Dirusso CC, Metzger AK, and Heimert TL (1992) Cloning, sequencing, and expression of the *FadD* gene of *Escherichia coli* encoding acyl coenzyme-A synthetase. J Biol Chem 267: 25513–25520

Black PN, Zhang Q, Weimar JD, and DiRusso CC (1997) Mutational analysis of a fatty acyl-coenzyme A synthetase signature motif identifies seven amino acid residues that modulate fatty acid substrate specificity. J Biol Chem 272: 4896–4903

Blazeck J, Hill A, Liu L, Knight R, Miller J, Pan A, Otoupal P, and Alper HS (2014) Harnessing *Yarrowia lipolytica* lipogenesis to create a platform for lipid and biofuel production. Nat Commun: 5

Block MA, Joyard J, and Deuce R (1983) The acyl-CoA synthetase and acyl-CoA thioesterase are located on the outer and inner membrane of the chloroplast envelope, respectively. FEBS Lett 153: 377–381

Blom N, Sicheritz-Pontén T, Gupta R, Gammeltoft S, and Brunak S (2004) Prediction of post-translational glycosylation and phosphorylation of proteins from the amino acid sequence. Proteomics 4: 1633–1649

Bouvier-Navé P, Benveniste P, Oelkers P, Sturley SL, and Schaller H (2000) Expression in yeast and tobacco of plant cDNAs encoding acyl CoA:diacylglycerol acyltransferase. Eur J Biochem 267: 85–96

Bradford MM (1976) A rapid and sensitive method for the quantitation of microgram quantities of protein utilizing the principle of protein-dye binding. Anal Biochem 72: 248–254

Brandt C, McFie PJ, and Stone SJ (2016a) Biochemical characterization of human acyl coenzyme A: 2-monoacylglycerol acyltransferase-3 (MGAT3). Biochem Biophys Res Commun 475: 264–270

Brandt C, McFie PJ, and Stone SJ (2016b) Diacylglycerol acyltransferase-2 and monoacylglycerol acyltransferase-2 are ubiquitinated proteins that are degraded by the 26S proteasome. Biochem J 473: 3621–3637

Browse J, McConn M, James D, and Miquel M (1993) Mutants of Arabidopsis deficient in the synthesis of α-linolenate: Biochemical and genetic characterization of the endoplasmic reticulum linoleoyl desaturase. J Biol Chem 268: 16345–16351

Burgal J, Shockey J, Lu C, Dyer J, Larson T, Graham I, and Browse J (2008) Metabolic engineering of hydroxy fatty acid production in plants: RcDGAT2 drives dramatic increases in ricinoleate levels in seed oil. Plant Biotechnol J 6: 819–831

Cahoon EB, Carlson TJ, Ripp KG, Schweiger BJ, Cook GA, Hall SE, and Kinney AJ (1999) Biosynthetic origin of conjugated double bonds: production of fatty acid components of high-value drying oils in transgenic soybean embryos. Proc Natl Acad Sci USA 96: 12935–12940

Cahoon EB, and Kinney AJ (2005) The production of vegetable oils with novel properties: Using genomic tools to probe and manipulate plant fatty acid metabolism. Eur J Lipid Sci Technol 107: 239–243

Caldo KMP, Greer MS, Chen G, Lemieux MJ, and Weselake RJ (2015) Purification and properties of recombinant *Brassica napus* diacylglycerol acyltransferase 1. FEBS Lett 589: 773–778

Caldo KMP, Acedo JZ, Panigrahi R, Vederas JC, Weselake RJ, and Lemieux MJ (2017) Diacylglycerol acyltransferase 1 is regulated by its N-terminal domain in response to allosteric effectors. Plant Physiol doi: 10.1104/pp.17.00934

Canola Council of Canada (2017). http://www.canolacouncil.org/, cited 29 Sept 2017.

Cao J, Lockwood J, Burn P, and Shi Y (2003) Cloning and functional characterization of a mouse intestinal acyl-CoA:monoacylglycerol acyltransferase, MGAT2. J Biol Chem 278: 13860–13866

Cases S, Smith SJ, Zheng YW, Myers HM, Lear SR, Sande E, Novak S, Collins C, Welch CB, Lusis AJ, Erickson SK, and Farese RV (1998) Identification of a gene encoding an acyl CoA:diacylglycerol acyltransferase, a key enzyme in triacylglycerol synthesis. Proc Natl Acad Sci USA 95: 13018–13023

Cases S, Stone SJ, Zhou P, Yen E, Tow B, Lardizabal KD, Voelker T, and Farese RV (2001) Cloning of DGAT2, a second mammalian diacylglycerol acyltransferase, and related family members. J Biol Chem 276: 38870–38876

Chang CCY, Sun J, Chang TY (2011) Membrane-bound O-acyltransferases (MBOATs). Front Biol 6: 177–182

Chapman KD, and Ohlrogge JB (2012) Compartmentation of triacylglycerol accumulation in plants. J Biol Chem 287: 2288–2294

Chen G, Snyder CL, Greer MS, and Weselake RJ (2011a) Biology and biochemistry of plant phospholipases. Crit Rev Plant Sci 30: 239–258

Chen G, Woodfield HK, Pan X, Harwood JL, and Weselake RJ (2015) Acyl-trafficking during plant oil accumulation. Lipids 50: 1057–1068

Chen G, Xu Y, Siloto RMP, Caldo KMP, Vanhercke T, Tahchy A El, Niesner N, Chen Y, Mietkiewska E, and Weselake RJ (2017) High performance variants of plant diacylglycerol acyltransferase 1 generated by directed evolution provide insights into structure-function. Plant J doi: 10.1111/tpj.13652

Chen X, Truksa M, Snyder CL, El-Mezawy A, Shah S, and Weselake RJ (2011b) Three homologous genes encoding *sn*-glycerol-3-phosphate acyltransferase 4 exhibit different expression patterns and functional divergence in *Brassica napus*. Plant Physiol 155: 851–865

Cheng D, Meegalla RL, He B, Cromley DA, Billheimer JT, and Young PR (2001) Human acyl-

CoA:diacylglycerol acyltransferase is a tetrameric protein. Biochem J 359: 707–714

Cheng F, Zhu L, and Schwaneberg U (2015) Directed evolution 20: improving and deciphering enzyme properties. Chem Commun 51: 9760–9772

Chi X, Hu R, Zhang X, Chen M, Chen N, Pan L, Wang T, Wang M, Yang Z, Wang Q, and Yu S (2014) Cloning and functional analysis of three diacylglycerol acyltransferase genes from peanut (*Arachis hypogaea L*). PLoS One 9: e105834

Choi K, Kim H, Kang H, Lee SY, Lee SJ, Back SH, Lee SH, Kim MS, Lee JE, Park JY, Kim J, Kim S, Song JH, Choi Y, Lee S, Lee HJ, Kim JH, and Cho S (2014) Regulation of diacylglycerol acyltransferase 2 protein stability by gp78-associated endoplasmic-reticulum-associated degradation. FEBS J 281: 3048–3060

Chung MY, Rho MC, Lee SW, Park HR, Kim K, Lee IA, Kim DH, Jeune KH, Lee HS, and Kim YK (2006) Inhibition of diacylglycerol acyltransferase by betulinic acid from *Alnus hirsuta.* Planta Med 72: 267–269

Cohen GN (2014) Allosteric enzymes. In Microbial Biochemistry. Springer, Netherlands pp 59–71

Dahlqvist A, Stahl U, Lenman M, Banas A, Lee M, Sandager L, Ronne H, and Stymne S (2000) Phospholipid:diacylglycerol acyltransferase: an enzyme that catalyzes the acyl-CoA-independent formation of triacylglycerol in yeast and plants. Proc Natl Acad Sci USA 97: 6487–6492

Daniel J, Deb C, Dubey VS, Sirakova TD, Abomoelak B, Morbidoni HR, and Kolattukudy PE

(2004) Induction of a novel class of diacylglycerol acyltransferases and triacylglycerol accumulation in *Mycobacterium tuberculosis* as it goes into a dormancy-like state in culture. J Bacteriol 186: 5017–5030

Das UN (2006) Essential fatty acids - A review. Curr Pharm Biotechnol 7: 467–482

Dovala D, Rath CM, Hu Q, Sawyer WS, Shia S, Elling RA, Knapp MS, and Metzger LE (2016) Structure-guided enzymology of the lipid A acyltransferase LpxM reveals a dual activity mechanism. Proc Natl Acad Sci USA 113: E6064–E6071

Duronio RJ, Knoll LJ, and Gordon JI (1992) Isolation of a *Saccharomyces cerevisiae* long chain fatty acyl:CoA synthetase gene (FAA1) and assessment of its role in protein N-myristoylation. J Cell Biol 117: 515–529

Durrett TP, McClosky DD, Tumaney AW, Elzinga DA, Ohlrogge J, and Pollard M (2010) A distinct DGAT ith *sn*-3 acetyltransferase activity that synthesizes unusual, reduced-viscosity oils in *Euonymus* and transgenic seeds. Proc Natl Acad Sci USA 107: 9464–9469

Dyer JM, Stymne S, Green AG, and Carlsson AS (2008) High-value oils from plants. Plant J 54: 640–655

Efimov I, Basran J, Sun X, Chauhan N, Chapman SK, Mowat CG, and Raven EL (2012) The mechanism of substrate inhibition in human indoleamine 2,3-dioxygenase. J Am Chem Soc 134: 3034–3041

Elamin AA, Stehr M, Spallek R, Rohde M, and Singh M (2011) The *Mycobacterium tuberculosis* Ag85A is a novel diacylglycerol acyltransferase involved in lipid body

formation. Mol Microbiol 81: 1577–1592

van Erp H, Bates PD, Burgal J, Shockey J, and Browse J (2011) Castor phospholipid:diacylglycerol acyltransferase facilitates efficient metabolism of hydroxy fatty acids in transgenic Arabidopsis. Plant Physiol 155: 683–693

Faergeman NJ, and Knudsen J (1997) Role of long-chain fatty acyl-CoA esters in the regulation of metabolism and in cell signalling. Biochem J 323: 1–12

Fetchko M, and Stagljar I (2004) Application of the split-ubiquitin membrane yeast two-hybrid system to investigate membrane protein interactions. Methods 32: 349-362

Feussner I (2015) Camelina-a promissing oilseed crop to contribute to the growing demand for vegetable oils. Eur J Lipid Sci Technol 117: 271–273

Food and Agriculture Organization of the United Nations (2016) Food outlook. http://www.fao.org/giews/reports/food-outlook/en/, cited 29 Sept 2017.

Ford TJ, and Way JC (2015) Enhancement of *E coli* acyl-CoA synthetase FadD activity on medium chain fatty acids. PeerJ 3: e1040

Fujino T, and Yamamoto T (1992) Cloning and functional expression of a novel long-chain acyl-CoA synthetase expressed in brain. J Biochem 111: 197–203

Fulda M, Schnurr J, Abbadi A, and Heinz E (2004) Peroxisomal acyl-CoA synthetase activity is essential for seedling development in *Arabidopsis thaliana*. Plant Cell 16: 394–405

Fulda M, Shockey J, Werber M, Wolter FP, and Heinz E (2002) Two long-chain acyl-CoA synthetases from *Arabidopsis thaliana* involved in peroxisomal fatty acid beta-oxidation.

Plant J 32: 93–103

Ganji SH, Tavintharan S, Zhu D, Xing Y, Kamanna VS, and Kashyap ML (2004) Niacin noncompetitively inhibits DGAT2 but not DGAT1 activity in HepG2 cells. J Lipid Res 45: 1835–1845

Ghanevati M, and Jaworski JG (2001) Active-site residues of a plant membrane-bound fatty acid elongase *β*-ketoacyl-CoA synthase, FAE1 KCS. Biochim Biophys Acta (BBA)-Mol Cell Biol Lipids 1530: 77–85

Ghosh AK, Chauhan N, Rajakumari S, Daum G, and Rajasekharan R (2009) At4g24160, a soluble acyl-coenzyme A-dependent lysophosphatidic acid acyltransferase. Plant Physiol 151: 869–881

Giannoulia K, Haralampidis K, Poghosyan Z, Murphy DJ, and Hatzopoulos P (2000) Differential expression of diacylglycerol acyltransferase (DGAT) genes in olive tissues. Biochem Soc Trans 28: 695–697

Gibson DG (2011) Enzymatic assembly of overlapping DNA fragments. Methods Enzymol 498: 349–361

Gidda SK, Shockey JM, Falcone M, Kim PK, Rothstein SJ, Andrews DW, Dyer JM, and Mullen RT (2011) Hydrophobic-domain-dependent protein-protein interactions mediate the localization of GPAT enzymes to ER subdomains. Traffic 12: 452–472

Greer MS, Pan X, and Weselake RJ (2016) Two clades of type-1 *Brassica napus* diacylglycerol acyltransferase exhibit differences in acyl-CoA preference. Lipids 51: 781–786

Greer MS, Truksa M, Deng W, Lung S, Chen G, and Weselake RJ (2015) Engineering increased triacylglycerol accumulation in *Saccharomyces cerevisiae* using a modified type 1 plant diacylglycerol acyltransferase. Appl Microbiol Biotechnol 99: 2243–2253

Greer MS, Zhou T, and Weselake RJ (2014) A novel assay of DGAT activity based on high temperature GC/MS of triacylglycerol. Lipids 49: 831–838

Guindon S, Dufayard JF, Lefort V, Anisimova M, Hordijk W, and Gascuel O (2010) New algorithms and methods to estimate maximum-likelihood phylogenies: Asessing the performance of PhyML 20. Syst Biol 59: 307–321

Guindon S, Lethiec F, Duroux P, and Gascuel O (2005) PHYML Online - A web server for fast maximum likelihood-based phylogenetic inference. Nucleic Acids Res 33: 557–559

Gulick AM (2009) Conformational dynamics in the acyl-CoA synthetases, adenylation domains of non-ribosomal peptide synthetases, and firefly luciferase. ACS Chem Biol 4: 811–827

Gunstone FD (2008) Disappearance. Lipid Technol 20: 48–48

Gunstone FD (2009) Nonfood uses of vegetable oils. Lipid Technol 21: 164–164

Guo X, Jiang M, Wan X, Hu C, and Gong Y (2014) Identification and biochemical characterization of five long-chain acyl-coenzyme A synthetases from the diatom *Phaeodactylum tricornutum.* Plant Physiol Biochem 74: 33–41

Hall LM, Booker H, Siloto RMP, Jhala AJ, and Weselake RJ (2016) Flax (*Linum usitatissimum L.*). In Industrial Oil Crops (eds McKeon TA, Hildebrand DF, Hayes DG, and Weselake RJ). Elsevier/AOCS Press, Urbana pp 157-194

Han GS, Wu WI, and Carman GM (2006) The *Saccharomyces cerevisiae* lipin homolog is a Mg^{2+}-dependent phosphatidate phosphatase enzyme. J Biol Chem 281: 9210–9218

Hanson MR, and Sattarzadeh A (2011) Stromules: recent insights into a long neglected feature of plastid morphology and function. Plant Physiol 155: 1486–1492

Harwood JL (2005) Fatty acid biosynthesis. In Plant Lipids: Biology, Utilisation and Manipulation. Blackwell Publishing, Oxford pp 27–66

Harwood JL, Ramli US, Tang M, Quant PA, Weselake RJ, Fawcett T, and Guschina IA (2013) Regulation and enhancement of lipid accumulation in oil crops: The use of metabolic control analysis for informed genetic manipulation. Eur J Lipid Sci Technol 115: 1239–1246

He X, Chen GQ, Kang ST, and McKeon TA (2007) *Ricinus communis* contains an acyl-CoA synthetase that preferentially activates ricinoleate to its CoA thioester. Lipids 42: 931–938

He X, Chen GQ, Lin JT, and McKeon TA (2004a) Regulation of diacylglycerol acyltransferase in developing seeds of castor. Lipids 39: 865–871

He X, Turner C, Chen GQ, Lin JT, and McKeon TA (2004b) Cloning and characterization of a cDNA encoding diacylglycerol acyltransferase from castor bean. Lipids 39: 311–318

Heath RJ, and Rock CO (1998) A conserved histidine is essential for glycerolipid acyltransferase catalysis. J Bacteriol 180: 1425–1430

Hernández ML, Whitehead L, He Z, Gazda V, Gilday A, Kozhevnikova E, Vaistij FE, Larson TR, and Graham IA (2012) A cytosolic acyltransferase contributes to triacylglycerol

synthesis in sucrose-rescued Arabidopsis seed oil catabolism mutants. Plant Physiol 160: 215–225

Hirokawa T, Boon-Chieng S, and Mitaku S (1998) SOSUI: classification and secondary structure prediction system for membrane proteins. Bioinformatics 14: 378–379

Hisanaga Y, Ago H, Nakagawa N, Hamada K, Ida K, Yamamoto M, Hori T, Arii Y, Sugahara M, Kuramitsu S, Yokoyama S, and Miyano M (2004) Structural basis of the substrate-specific two-step catalysis of long chain fatty acyl-CoA synthetase dimer. J Biol Chem 279: 31717–31726

Hobbs DH, Lu C, and Hills MJ (1999) Cloning of a cDNA encoding diacylglycerol acyltransferase from *Arabidopsis thaliana* and its functional expression. FEBS Lett 452: 145–149

Hofmann K, and Stoffel W (1993) TMbase-A database of membrane spanning protein segments. Biol Chem Hoppe Seyler 374: 166

Hongo S, Matsumoto T, and Sato T (1978) Purification and properties of asparagine synthetase from rat liver. Biochim Biophys Acta (BBA)-Enzymol 522: 258–266

Ichihara K, Kobayashi N, and Saito K (2003) Lipid synthesis and acyl-CoA synthetase in developing rice seeds. Lipids 38: 881–884

Ichihara K, Murota N, and Fujii S (1990) Intracellular translocation of phosphatidate phosphatase in maturing safflower seeds: A possible mechanism of feedforward control of triacylglycerol synthesis by fatty acids. Biochim Biophys Acta (BBA)-Lipids Lipid Metab

1043: 227–234

Iskandarov U, Silva JE, Kim HJ, Andersson M, Cahoon RE, Mockaitis K, and Cahoon EB (2017) Specialized diacylglycerol acyltransferase contributes to extreme fatty acid content of *Cuphea* seed oil. Plant Physiol 174: pp01894

IUPAC-IUB Commission on Biochemical Nomenclature (1967) The nomenclature of lipids. Biochemical J 105: 897-902

Jako C, Kumar A, Wei Y, Zou J, Barton DL, Giblin EM, Covello PS, and Taylor DC (2001) Seed-specific over-expression of an Arabidopsis cDNA encoding a diacylglycerol acyltransferase enhances seed oil content and seed weight. Plant Physiol 126: 861–874

Jessen D, Olbrich A, Knüfer J, Krüger A, Hoppert M, Polle A, and Fulda M (2011) Combined activity of LACS1 and LACS4 is required for proper pollen coat formation in Arabidopsis. Plant J 68: 715–726

Jessen D, Roth C, Wiermer M, and Fulda M (2015) Two activities of long-chain acyl-CoA synthetase are involved in lipid trafficking between the endoplasmic reticulum and the plastid in Arabidopsis. Plant Physiol 167: 351–366

Jhala AJ and Hall LM (2010) Flax (*Linum usitatissimum L*): Current uses and future applications. Aust J Basic Appl Sci 4: 4304–4312

Jia B, Song Y, Wu M, Lin B, Xiao K, Hu Z, and Huang Y (2016) Characterization of long-chain acyl-CoA synthetases which stimulate secretion of fatty acids in green algae *Chlamydomonas reinhardtii.* Biotechnol Biofuels 9: 184

Jin Y, McFie PJ, Banman SL, Brandt CJ, and Stone SJ (2014) Diacylglycerol acyltransferase-2 (DGAT2) and monoacylglycerol acyltransferase-2 (MGAT2) interact to promote triacylglycerol synthesis. J Biol Chem 289: 28237–28248

Johnson DR, Knoll LJ, Levin DE, and Gordon JI (1994a) *Saccharomyces cerevisiae* contains four fatty acid activation (FAA) genes: An assessment of their role in regulating protein N-myristoylation and cellular lipid metabolism. J Cell Biol 127: 751–762

Johnson DR, Knoll LJ, Rowley N, and Gordon JI (1994b) Genetic analysis of the role of *Saccharomyces cerevisiae* acyl-CoA synthetase genes in regulating protein N-myristoylation. J Biol Chem 269: 18037–18046

Käll L, Krogh A, and Sonnhammer ELL (2007) Advantages of combined transmembrane topology and signal peptide prediction-the Phobius web server. Nucleic Acids Res 35: 429–432

Kalscheuer R, and Steinbüchel A (2003) A novel bifunctional wax ester synthase/acyl-CoA:diacylglycerol acyltransferase mediates wax ester and triacylglycerol biosynthesis in *Acinetobacter calcoaceticus*. ADP1 J Biol Chem 278: 8075–8082

Karim AS, Curran KA, and Alper HS (2013) Characterization of plasmid burden and copy number in *Saccharomyces cerevisiae* for optimization of metabolic engineering applications. FEMS Yeast Res 13: 107–116

Katavic V, Reed DW, Taylor DC, Ciblin EM, Zou J, Mackenzie S, Covello PS, and Kunst L (1995) Alteration of seed fatty acid composition by an ethyl methanesulfonate-induced mutation in *Arabidopsis thaliana* affecting diacylglycerol acyltransferase activity. Plant

Physiol 108: 399–409

Khare G, Gupta V, Gupta RK, Gupta R, Bhat R, and Tyagi AK (2009) Dissecting the role of critical residues and substrate preference of a fatty acyl-CoA synthetase (FadD13) of *Mycobacterium tuberculosis*. PLoS One 4: e8387

Kim H, Park JH, Kim DJ, Kim AY, and Suh MC (2016) Functional analysis of *diacylglycerol acyltransferase1* genes from *Camelina sativa* and effects of *CsDGAT1B* overexpression on seed mass and storage oil content in *C. sativa.* Plant Biotechnol Rep 10: 141–153

Kim HU, Lee KR, Go YS, Jung JH, Suh MC, and Kim JB (2011) Endoplasmic reticulum-located PDAT1-2 from castor bean enhances hydroxy fatty acid accumulation in transgenic plants. Plant Cell Physiol 52: 983–993

Kim HU, Lee KR, Jung SJ, Shin HA, Go YS, Suh MC, and Kim JB (2015) Senescence-inducible LEC2 enhances triacylglycerol accumulation in leaves without negatively affecting plant growth. Plant Biotechnol J 13: 1346–1359

Kim S, Yamaoka Y, Ono H, Kim H, Shim D, Maeshima M, Martinoia,E, Cahoon EB, Nishida I, and Lee Y (2013) AtABCA9 transporter supplies fatty acids for lipid synthesis to the endoplasmic reticulum. Proc Natl Acad Sci USA 110: 773–778

King AJ, He W, Cuevas JA, Freudenberger M, Ramiaramanana D, and Graham IA (2009) Potential of *Jatropha curcas* as a source of renewable oil and animal feed. J Exp Bot 60: 2897–905

Kochan G, Pilka ES, von Delft F, Oppermann U, and Yue WW (2009) Structural snapshots for

the conformation-dependent catalysis by human medium-chain acyl-coenzyme A synthetase ACSM2A. J Mol Biol 388: 997–1008

Kornberg A, and Pricer WE (1953) Enzymatic synthesis of the coenzyme A derivatives of long chain fatty acids. J Biol Chem 204: 329–343

Krogh A, Larsson B, von Heijne G, and Sonnhammer E (2001) Predicting transmembrane protein topology with a hidden Markov model: application to complete genomes. J Mol Biol 305: 567–580

Kroon JTM, Wei W, Simon WJ, and Slabas AR (2006) Identification and functional expression of a type 2 acyl-CoA:diacylglycerol acyltransferase (DGAT2) in developing castor bean seeds which has high homology to the major triglyceride biosynthetic enzyme of fungi and animals. Phytochemistry 67: 2541–2549

Kumar S, Stecher G, and Tamura K (2016) MEGA7: Molecular evolutionary genetics analysis version 7.0 for bigger datasets. Mol Biol Evol 33: msw054

Lager I, Glab B, Eriksson L, Chen G, Banas A, and Stymne S (2015) Novel reactions in acyl editing of phosphatidylcholine by lysophosphatidylcholine transacylase (LPCT) and acyl-CoA:glycerophosphocholine acyltransferase (GPCAT) activities in microsomal preparations of plant tissues. Planta 241: 347–358

Lager I, Yilmaz JL, Zhou XR, Jasieniecka K, Kazachkov M, Wang P, Zou J, Weselake R, Smith MA, Bayon S, Dyer JM, Shockey JM, Heinz E, Green A, Banas A, and Stymne S (2013) Plant acyl-CoA:lysophosphatidylcholine acyltransferases (LPCATs) have different specificities in their forward and reverse reactions. J Biol Chem 288: 36902–36914

Lands W (1960) Metabolism of glycerolipids: II The enzymatic acylation of lysolecithin. J Biol Chem 235: 2233–2237

Lardizabal K, Effertz R, Levering C, Mai J, Pedroso MC, Jury T, Aasen E, Gruys K, and Bennett K (2008) Expression of *Umbelopsis ramanniana* DGAT2A in seed increases oil in soybean. Plant Physiol 148: 89–96

Lardizabal KD, Mai JT, Wagner NW, Wyrick A, Voelker T, and Hawkins DJ (2001) DGAT2 is a new diacylglycerol acyltransferase gene family: purification, cloning, and expression in insect cells of two polypeptides from *Mortierella ramanniana* with diacylglycerol acyltransferase activity. J Biol Chem 276: 38862–38869

Leber C, Polson B, Fernandez-Moya R, and Da Silva NA (2015) Overproduction and secretion of free fatty acids through disrupted neutral lipid recycle in *Saccharomyces cerevisiae.* Metab Eng 28: 54–62

Lee AH, Scapa EF, Cohen DE, and Glimcher LH (2014) Regulation of hepatic lipogenesis by the transcription factor XBP1. Science 1492: 1492–1497

Lewis SE, Listenberger LL, Ory DS, and Schaffer JE (2001) Membrane topology of the murine fatty acid transport protein 1. J Biol Chem 276: 37042–37050

Li F, Wu X, Lam P, Bird D, Zheng H, Samuels L, Jetter R, and Kunst L (2008) Identification of the wax ester synthase/acyl-coenzyme A: diacylglycerol acyltransferase WSD1 required for stem wax ester biosynthesis in Arabidopsis. Plant Physiol 148: 97–107

Li N, Gügel IL, Giavalisco P, Zeisler V, Schreiber L, Soll J, and Philippar K (2015) FAX1, a

novel membrane protein mediating plastid fatty acid export. PLOS Biol 13: e1002053

Li R, Yu K, Hatanaka T, and Hildebrand DF (2010a) *Vernonia* DGATs increase accumulation of epoxy fatty acids in oil. Plant Biotechnol J 8: 184–195

Li R, Yu K, and Hildebrand DF (2010b) DGAT1, DGAT2 and PDAT expression in seeds and other tissues of epoxy and hydroxy fatty acid accumulating plants. Lipids 45: 145–157

Li R, Yua K, Wub Y, Tateno M, Hatanaka T, and Hildebrand DF (2012a) *Vernonia* DGATs can complement the disrupted oil and protein metabolism in epoxygenase-expressing soybean seeds. Metab Eng 14: 29–38

Li X, Guo D, Cheng Y, Zhu F, Deng Z, and Liu T (2014) Overproduction of fatty acids in engineered *Saccharomyces cerevisiae.* Biotechnol Bioeng 111: 1841–1852

Li X, van Loo EN, Gruber J, Fan J, Guan R, Frentzen M, Stymne S, and Zhu L (2012b) Development of ultra-high erucic acid oil in the industrial oil crop *Crambe abyssinica.* Plant Biotechnol J 1: 862–870

Liao J, Okuyama M, Ishihara K, Yamori Y, Iki S, Tagami T, Mori H, Chiba S, and Kimura A (2016) Kinetic properties and substrate inhibition of *α*-galactosidase from *Aspergillus niger.* Biosci Biotechnol Biochem 80: 1747–1752

Lippold F, vom Dorp K, Abraham M, Hölzl G, Wewer V, Yilmaz JL, Lager I, Montandon C, Besagni C, Kessler F, Stymne S, and Dörmann P (2012) Fatty acid phytyl ester synthesis in chloroplasts of Arabidopsis. Plant Cell 24: 2001–2014

List G (2015) Nonfood uses of vegetable oils. Lipid Technol 27: 72–72

Little D, Weselake R, Pomeroy K, Furukawa-Stoffer T, and Bagu J (1994) Solubilization and characterization of diacylglycerol acyltransferase from microspore-derived cultures of oilseed rape. Biochem J 304: 951–958

Liu L, Hammond EG, and Nikolau BJ (1998) In vivo studies of the biosynthesis of vernolic acid in the seed of *Vernonia galamensis.* Lipids 33: 1217–1221

Liu Q, Siloto RMP, Lehner R, Stone SJ, and Weselake RJ (2012) Acyl-CoA:diacylglycerol acyltransferase: molecular biology, biochemistry and biotechnology. Prog Lipid Res 51: 350–377

Liu Q, Siloto RMP, Snyder CL, and Weselake RJ (2011) Functional and topological analysis of yeast acyl-CoA:diacylglycerol acyltransferase 2, an endoplasmic reticulum enzyme essential for triacylglycerol biosynthesis. J Biol Chem 286: 13115–13126

Liu T, Vora H, and Khosla C (2010) Quantitative analysis and engineering of fatty acid biosynthesis in *E coli.* Metab Eng 12: 378–386

Livak KJ, and Schmittgen TD (2001) Analysis of relative gene expression data using real-time quantitative PCR and the 2(−ΔΔC(T)) method. Methods 25: 402–408

Lock YY, Snyder CL, Zhu W, Siloto RMP, Weselake RJ, and Shah S (2009) Antisense suppression of type 1 diacylglycerol acyltransferase adversely affects plant development in *Brassica napus.* Physiol Plant 137: 61–71

van de Loo FJ, Broun P, Turner S, and Somerville C (1995) An oleate 12-hydroxylase from *Ricinus communis L* is a fatty acyl desaturase homolog. Proc Natl Acad Sci USA 92: 6743–

6747

Lõoke M, Kristjuhan K, and Kristjuhan A (2011) Extraction of genomic DNA from yeasts for PCR-based applications. Biotechniques 50: 325–328

Lopes JLS, Beltramini LM, Wallace BA, and Araujo APU (2015) Deconstructing the DGAT1 enzyme: membrane interactions at substrate binding sites. PLoS One 10: e0118407

Lopes JLS, Nobre TM, Cilli EM, Beltramini LM, Araújo APU, and Wallace BA (2014) Deconstructing the DGAT1 enzyme: Binding sites and substrate interactions. Biochim Biophys Acta (BBA)-Biomemb 1838: 3145–3152

Lorente-Cebrián S, Costa AGV, Navas-Carretero S, Zabala M, Martínez JA, and Moreno-Aliaga MJ (2013) Role of omega-3 fatty acids in obesity, metabolic syndrome, and cardiovascular diseases: A review of the evidence. J Physiol Biochem 69: 633–651

Lu C, Napier JA, Clemente TE, and Cahoon EB (2011) New frontiers in oilseed biotechnology: Meeting the global demand for vegetable oils for food, feed, biofuel, and industrial applications. Curr Opin Biotechnol 22: 252–259

Lu C, De Noyer SB, Hobbs DH, Kang J, Wen Y, Krachtus D, and Hills MJ (2003) Expression pattern of diacylglycerol acyltransferase-1, an enzyme involved in triacylglycerol biosynthesis, in *Arabidopsis thaliana*. Plant Mol Biol 52: 31–41

Lu C, Xin Z, Ren Z, Miquel M, and Browse J (2009) An enzyme regulating triacylglycerol composition is encoded by the ROD1 gene of Arabidopsis. Proc Natl Acad Sci USA 106: 18837–18842

Lü S, Song T, Kosma DK, Parsons EP, Rowland O, and Jenks MA (2009) Arabidopsis *CER8* encodes LONG-CHAIN ACYL-COA SYNTHETASE 1 (LACS1) that has overlapping functions with LACS2 in plant wax and cutin synthesis. Plant J 59: 553–564

Lu X, Vora H, and Khosla C (2008) Overproduction of free fatty acids in *E coli*: Implications for biodiesel production. Metab Eng 10: 333–339

Lung SC, and Weselake RJ (2006) Diacylglycerol acyltransferase: a key mediator of plant triacylglycerol synthesis. Lipids 41: 1073–1088

Lynch M, and Conery JS (2000) The evolutionary fate and consequences of duplicate genes. Science 290: 1151–1155

Man WC, Miyazaki M, Chu K, and Ntambi J (2006) Colocalization of SCD1 and DGAT2: implying preference for endogenous monounsaturated fatty acids in triglyceride synthesis. J Lipid Res 47: 1928–1939

Mañas-Fernández A, Vilches-Ferrón M, Garrido-Cárdenas JA, Belarbi EH, Alonso DL, and García-Maroto F (2009) Cloning and molecular characterization of the acyl-CoA:Diacylglycerol Acyltransferase 1 (DGAT1) gene from *Echium.* Lipids 44: 555–568

Matevossian A, and Resh MD (2015) Membrane topology of hedgehog acyltransferase. J Biol Chem 290(4):2235-2243

Mavraganis I, Meesapyodsuk D, Vrinten P, Smith M, and Qiu X (2010) Type II diacylglycerol acyltransferase from *Claviceps purpurea* with ricinoleic acid, a hydroxyl fatty acid of industrial importance, as preferred substrate. Appl Environ Microbiol 76: 1135–1142

McFie PJ, Banman SL, Kary S, and Stone SJ (2011) Murine diacylglycerol acyltransferase-2 (DGAT2) can catalyze triacylglycerol synthesis and promote lipid droplet formation independent of its localization to the endoplasmic reticulum. J Biol Chem 286: 28235–28246

McFie PJ, Stone SL, Banman SL, and Stone SJ (2010) Topological orientation of acyl-CoA:diacylglycerol acyltransferase-1 (DGAT1) and identification of a putative active site histidine and the role of the N-terminus in dimer/tetramer formation. J Biol Chem 285: 37377–37387

Milcamps A, Tumaney AW, Paddock T, Pan DA, Ohlrogge J, and Pollard M (2005) Isolation of a gene encoding a 1,2-diacylglycerol-sn-acetyl-CoA acetyltransferase from developing seeds of *Euonymus alatus.* J Biol Chem 280: 5370–5377

Misra A, Khan K, Niranjan A, Nath P, and Sane VA (2013) Over-expression of *JcDGAT1* from *Jatropha curcas* increases seed oil levels and alters oil quality in transgenic *Arabidopsis thaliana.* Phytochemistry 96: 37–45

Mongrand S, Cassagne C, and Bessoule JJ (2000) Import of lyso-phosphatidylcholine into chloroplasts likely at the origin of eukaryotic plastidial lipids. Plant Physiol 122: 845–852

Nielsen R, Hellmann I, Hubisz M, Bustamante C, and Clark AG (2007) Recent and ongoing selection in the human genome. Nat Rev Genet 8: 857–868

Nykiforuk CL, Furukawa-Stoffer TL, Huff PW, Sarna M, Laroche A, Moloney MM, and Weselake RJ (2002) Characterization of cDNAs encoding diacylglycerol acyltransferase from cultures of *Brassica napus* and sucrose-mediated induction of enzyme biosynthesis.

Biochim Biophys Acta (BBA)-Mol Cell Biol Lipids 1580: 95–109

Oakes J, Brackenridge D, Colletti R, Daley M, Hawkins DJ, Xiong H, Mai J, Screen SE, Val D, Lardizabal K, Gruys K, and Deikman J (2011) Expression of fungal diacylglycerol acyltransferase2 genes to increase kernel oil in maize. Plant Physiol 155: 1146–1157

Obermeyer T, Fraisl P, DiRusso CC, and Black PN (2007) Topology of the yeast fatty acid transport protein Fat1p: mechanistic implications for functional domains on the cytosolic surface of the plasma membrane. J Lipid Res 48: 2354–2364

Ohlrogge JB, and Jaworski JG (2003) Regulation of fatty acid synthesis. Annu Rev Plant Physiol Plant Mol Biol 48: 109–138

Omasits U, Ahrens CH, Müller S, and Wollscheid B (2014) Protter: Interactive protein feature visualization and integration with experimental proteomic data. Bioinformatics 30: 884–886

Packer MS and Liu DR (2015) Methods for the directed evolution of proteins. Nat Rev Genet 16: 379–394

Pan X, Chen G, Kazachkov M, Greer MS, Caldo KMP, Zou J, and Weselake RJ (2015) *In vivo* and *in vitro* evidence for biochemical coupling of reactions catalyzed by lysophosphatidylcholine acyltransferase and diacylglycerol acyltransferase. J Biol Chem 290: 18068–18078

Pan X, Siloto RMP, Wickramarathna AD, Mietkiewska E, and Weselake RJ (2013) Identification of a pair of phospholipid:diacylglycerol acyltransferases from developing flax (*Linum usitatissimum L*) seed catalyzing the selective production of trilinolenin. J Biol

Chem 288: 24173–24188

Payne VA, Au WS, Gray SL, Nora ED, Rahman SM, Sanders R, Hadaschik D, Friedman JE, O'Rahilly S, and Rochford JJ (2007) Sequential regulation of diacylglycerol acyltransferase 2 expression by CAAT/enhancer-binding protein β(C/EBPβ) and C/EBPα during adipogenesis. J Biol Chem 282: 21005–21014

Peng FY, and Weselake RJ (2011) Gene coexpression clusters and putative regulatory elements underlying seed storage reserve accumulation in Arabidopsis. BMC Genomics 12: 286

Perry HJ, and Harwood JL (1993) Changes in the lipid content of developing seeds of *Brassica napus*. Phytochemistry 32: 1411–1415

Pulsifer IP, Kluge S, and Rowland O (2012) Arabidopsis long-chain acyl-CoA synthetase 1 (LACS1), LACS2, and LACS3 facilitate fatty acid uptake in yeast. Plant Physiol Biochem 51: 31–39

Radivojac P, Vacic V, Haynes C, Cocklin RR, Mohan A, Heyen JW, Goebl MG, and Iakoucheva LM (2010) Identification, analysis, and prediction of protein ubiquitination sites. Proteins Struct Funct Bioinforma 78: 365–380

Radovanovic N, Thambugala D, Duguid S, Loewen E, and Cloutier S (2014) Functional characterization of flax fatty acid desaturase FAD2 and FAD3 isoforms expressed in yeast reveals a broad diversity in activity. Mol Biotechnol 56: 609–620

Rani SH, Krishna THA, Saha S, Negi AS, and Rajasekharan R (2010) Defective in cuticular ridges (*DCR*) of *Arabidopsis thaliana*, a gene associated with surface cutin formation,

encodes a soluble diacylglycerol acyltransferase. J Biol Chem 285: 38337–38247

Roesler K, Shen B, Bermudez E, Li C, Hunt J, Damude HG, Ripp KG, Everard JD, Booth JR, Castaneda L, Feng L, and Meyer K (2016) An improved variant of soybean type 1 diacylglycerol acyltransferase increases the oil content and decreases the soluble carbohydrate content of soybeans. Plant Physiol 171: 878–893

Rossak M, Smith M, and Kunst L (2001) Expression of the FAE1 gene and FAE1 promoter activity in developing seeds of *Arabidopsis thaliana.* Plant Mol Biol 46: 717–725

Roughan PG, and Slack CR (1977) Long-chain acyl-coenzyme A synthetase activity of spinach chloroplasts is concentrated in the envelope. Biochem J 162: 457–459

Routaboul JM, Benning C, Bechtold N, Caboche M, and Lepiniec L (1999) The *TAG1* locus of Arabidopsis encodes for a diacylglycerol acyltransferase. Plant Physiol Biochem 37: 831–840

Ruiz-López N, Garcés R, Harwood JL, and Martínez-Force E (2010) Characterization and partial purification of acyl-CoA:glycerol 3-phosphate acyltransferase from sunflower (*Helianthus annuus L*) developing seeds. Plant Physiol Biochem 48: 73–80

Saha S, Enugutti B, Rajakumari S, and Rajasekharan R (2006) Cytosolic triacylglycerol biosynthetic pathway in oilseeds. Molecular cloning and expression of peanut cytosolic diacylglycerol acyltransferase. Plant Physiol 141: 1533–1543

Salas JJ, Martínez-Force E, Harwood JL, Venegas-Calerón M, Aznar-Moreno JA, Moreno-Pérez AJ, Ruíz-López N, Serrano-Vega MJ, Graham IA, Mullen RT, and Garcés R (2014)

Biochemistry of high stearic sunflower, a new source of saturated fats. Prog Lipid Res 55: 30–42

Sandager L, Gustavsson MH, Stahl U, Dahlqvist A, Wiberg E, Banas A, Lenman M, Ronne H, and Stymne S (2002) Storage lipid synthesis is non-essential in yeast. J Biol Chem 277: 6478–6482

Santorum JM, Darriba D, Taboada GL, and Posada D (2014) Jmodeltestorg: Selection of nucleotide substitution models on the cloud. Bioinformatics 30: 1310–1311

Sasaki Y, and Nagano Y (2004) Plant acetyl-CoA carboxylase: structure, biosynthesis, regulation, and gene manipulation for plant breeding. Biosci Biotechnol Biochem 68: 1175–1184

Scharnewski M, Pongdontri P, Mora G, Hoppert M, and Fulda M (2008) Mutants of *Saccharomyces cerevisiae* deficient in acyl-CoA synthetases secrete fatty acids due to interrupted fatty acid recycling. FEBS J 275: 2765–2778

Schneider CA, Rasband WS, and Eliceiri KW (2012) NIH Image to ImageJ: 25 years of image analysis. Nat Methods 9: 671–675

Schnurr JA, Shockey JM, Boer GJ De, and Browse JA (2002) Fatty acid export from the chloroplast molecular characterization of a major plastidial acyl-coenzyme A synthetase from Arabidopsis. Plant Physiol 129: 1700–1709

Schnurr J, and Shockey J (2004) The acyl-CoA synthetase encoded by LACS2 is essential for normal cuticle development in Arabidopsis. Plant Cell 16: 629–642

Schwender J, Goffman F, Ohlrogge JB, and Shachar-Hill Y (2004) Rubisco without the Calvin

cycle improves the carbon efficiency of developing green seeds. Nature 432: 779–783

Sec P, Garaiova M, Gajdos P, Certik M, Griac P, Hapala I, and Holic R (2015) Baker's yeast deficient in storage lipid synthesis uses cis-vaccenic acid to reduce unsaturated fatty acid toxicity. Lipids 50: 621–630

Shearer HL, Turpin DH, and Dennis DT (2004) Characterization of NADP-dependent malic enzyme from developing castor oil seed endosperm. Arch Biochem Biophys 429: 134–144

Shockey J, Regmi A, Cotton K, Neil A, Browse J, and Bates PD (2016) Identification of Arabidopsis *GPAT9* (*At5g60620*) as an essential gene involved in triacyglycerol biosynthesis. Plant Physiol 170: 163–179

Shockey JM, Fulda MS, and Browse JA (2002) Arabidopsis contains nine long-chain acyl-coenzyme a synthetase genes that participate in fatty acid and glycerolipid metabolism. Plant Physiol 129: 1710–1722

Shockey JM, Gidda SK, Chapital DC, Kuan JC, Dhanoa PK, Bland JM, Rothstein SJ, Mullen RT, and Dyer JM (2006) Tung tree DGAT1 and DGAT2 have nonredundant functions in triacylglycerol biosynthesis and are localized to different subdomains of the endoplasmic reticulum. Plant Cell 18: 2294–2313

Siloto RMP, Madhavji M, Wiehler WB, Burton TL, Boora PS, Laroche A, and Weselake RJ (2008) An N-terminal fragment of mouse DGAT1 binds different acyl-CoAs with varying affinity. Biochem Biophys Res Commun 373: 350–354

Siloto RMP, Truksa M, Brownfield D, Good AG, and Weselake RJ (2009a) Directed evolution

of acyl-CoA:diacylglycerol acyltransferase: development and characterization of *Brassica napus* DGAT1 mutagenized libraries. Plant Physiol Biochem 47: 456–461

Siloto RMP, Truksa M, He X, McKeon T, and Weselake RJ (2009b) Simple methods to detect triacylglycerol biosynthesis in a yeast-based recombinant system. Lipids 44: 963–973

Singer SD, Chen G, Mietkiewska E, Tomasi P, Jayawardhane K, Dyer JM, and Weselake RJ (2016) Arabidopsis GPAT9 contributes to synthesis of intracellular glycerolipids but not surface lipids. J Exp Bot 67: 4627–4638

Slack CR, Campbell LC, Browse JA, and Roughan PG (1983) Some evidence for the reversibility of the cholinephosphotransferasecatalysed reaction in developing linseed cotyledons *in vivo.* Biochim Biophys Acta (BBA)-Lipids and Lipid Metab 754: 10–20

Slack CR, Roughan PG, Browse JA, and Gardiner SE (1985) Some properties of cholinephosphotransferase from developing safflower cotyledons. Biochim Biophys Acta(BBA)-Lipids and Lipid Metab 833: 438–448

Smith SJ, Cases S, Jensen DR, Chen HC, Sande E, Tow B, Sanan DA, Raber J, Eckel RH, and Farese RV (2000) Obesity resistance and multiple mechanisms of triglyceride synthesis in mice lacking *Dgat*. Nat Genet 25: 87–90

Snider J, Kittanakom S, Damjanovic D, Curak J, Wong V, and Stagljar I (2010) Detecting interactions with membrane proteins using a membrane two-hybrid assay in yeast. Nat Protoc 5: 1281–1293

Snyder CL, Yurchenko OP, Siloto RMP, Chen X, Liu Q, Mietkiewska E, and Weselake RJ

(2009) Acyltransferase action in the modification of seed oil biosynthesis. N Biotechnol 26: 11–16

Sørensen BM, Furukawa-Stoffer TL, Marshall KS, Page EK, Mir Z, Forster RJ, and Weselake RJ (2005) Storage lipid accumulation and acyltransferase action in developing flaxseed. Lipids 40: 1043–1049

Soupene E, Fyrst H, and Kuypers FA (2008) Mammalian acyl-CoA:lysophosphatidylcholine acyltransferase enzymes. Proc Natl Acad Sci USA 105: 88–93

Soupene E, Wang D, and Kuypers FA (2015) Remodeling of host phosphatidylcholine by *Chlamydia* acyltransferase is regulated by acyl-CoA binding protein ACBD6 associated with lipid droplets. Microbiologyopen 4: 235–251

Srivastava A, and Prasad R (2000) Triglycerides-based diesel fuels. Renew Sustainable energy Rev 4: 111–133

Stahl U, Carlsson A, Lenman M, Dahlqvist A, Huang B, Banás W, Banás A, and Stymne S (2004) Cloning and functional characterization of a phospholipid:diacylglycerol acyltransferase from Arabidopsis. Am Soc Plant Biol 135: 1324–1335

Steen EJ, Kang Y, Bokinsky G, Hu Z, Schirmer A, McClure A, del Cardayre SB, and Keasling JD (2010) Microbial production of fatty-acid-derived fuels and chemicals from plant biomass. Nature 463: 559–562

Stone SJ, Levin MC, and Farese RV (2006) Membrane topology and identification of key functional amino acid residues of murine acyl-CoA:diacylglycerol acyltransferase-2. J Biol

Chem 281: 40273–40282

Stone SJ, Levin MC, Zhou P, Han J, Walther TC, and Farese R V (2009) The endoplasmic reticulum enzyme DGAT2 is found in mitochondria-associated membranes and has a mitochondrial targeting signal that promotes its association with mitochondria. J Biol Chem 284: 5352–5361

Stone SJ, Myers HM, Watkins SM, Brown BE, Feingold KR, Elias PM, and Farese R V (2004) Lipopenia and skin barrier abnormalities in DGAT2-deficient mice. J Biol Chem 279: 11767–11776

Stöveken T, Kalscheuer R, Malkus U, Reichelt R, and Steinbüchel A (2005) The wax ester synthase/acyl coenzyme A:diacylglycerol acyltransferase from *Acinetobacter* sp strain ADP1: characterization of a novel type of acyltransferase. J Bacteriol 187: 1369–1376

Stymne S, and Stobart AK (1984) Evidence for the reversibility of the acyl-CoA:lysophosphatidylcholine acyltransferase in microsomal preparations from developing safflower (*Carthamus tinctorius L*) cotyledons and rat liver. Biochem J 223: 305–314

Suplatov DA, Besenmatter W, Švedas VK, and Svendsen A (2012) Bioinformatic analysis of alpha /beta-hydrolase fold enzymes reveals subfamily-specific positions responsible for discrimination of amidase and lipase. Protein Eng Des Sel 25: 689–697

Suzuki H, Kawarabayasi Y, Kondo J, Abe T, Nishikawa K, Kimura S, Hashimoto T, and Yamamoto T (1990) Structure and regulation of rat long-chain acyl-CoA synthetase. J Biol Chem 265: 8681–8685

Szegletes T, Mallender WD, Thomas PJ, and Rosenberry TL (1999) Substrate binding to the peripheral site of acetylcholinesterase initiates enzymatic catalysis. Substrate inhibition arises as a secondary effect. Biochemistry 38: 122–133

Tan X, Zheng X, Zhang Z, Wang Z, Xia H, Lu C, and Gu S (2014) Long chain acyl-coenzyme A synthetase 4 (BnLACS4) gene from *Brassica napus* enhances the yeast lipid contents. J Integr Agric 13: 54–62

Tang D, Simonich MT, and Innes RW (2007) Mutations in LACS2, a long-chain acyl-coenzyme A synthetase, enhance susceptibility to avirulent *Pseudomonas syringae* but confer resistance to *Botrytis cinerea* in Arabidopsis. Plant Physiol 144: 1093–1103

Taylor D, and Smith,M (2011) Metabolic engineering of higher plants to produce bio-industrial oils. Compr Biotechnol 1: 67–85

Taylor DC, Weber N, Hogge LR, and Underhill EW (1990) A simple enzymatic method for the preparation of radiolabeled erucoyl-CoA and other long-chain fatty acyl-CoAs and their characterization by mass spectrometry. Anal Biochem 316: 311–316

Taylor DC, Zhang Y, Kumar A, Francis T, Giblin EM, Barton DL, Ferrie JR, Laroche A, Shah S, Zhu W, Snyder CL, Hall L, Rakow G, Harwood JL, and Weselake RJ (2009) Molecular modification of triacylglycerol accumulation by over-expression of DGAT1 to produce canola with increased seed oil content under field conditions. Botany 87: 533–543

Till BJ, Zerr T, Comai L, and Henikoff S (2006) A protocol for TILLING and Ecotilling in plants and animals. Nat Protoc 1: 2465–2477

Tonon T, Qing R, Harvey D, Li Y, Larson TR, and Graham IA (2005) Identification of a long-chain polyunsaturated fatty acid acyl-coenzyme A synthetase from the diatom *Thalassiosira pseudonana.* Plant Physiol 138: 402–408

Tumaney AW, Shekar S, and Rajasekharan R (2001) Identification, purification, and characterization of monoacylglycerol acyltransferase from developing peanut cotyledons. J Biol Chem 276: 10847–10852

Turchetto-Zolet AC, Maraschin FS, de Morais GL, Cagliari A, Andrade CM, Margis-Pinheiro M, and Margis R (2011) Evolutionary view of acyl-CoA diacylglycerol acyltransferase (DGAT), a key enzyme in neutral lipid biosynthesis. BMC Evol Biol 11: 263

Turnbull AP, Rafferty JB, Sedelnikova SE, Slabas AR, Schierer TP, Kroon JTM, Simon JW, Fawcett T, Nishida I, Murata N, and Rice DW (2001) Analysis of the structure, substrate specificity, and mechanism of squash glycerol-3-phosphate (1)-acyltransferase. Structure 9: 347–353

Tzen J, Cao Y, Laurent P, Ratnayake C, and Huang A (1993) Lipids, proteins, and structure of seed oil bodies from diverse species. Plant Physiol 101: 267–276

United States Department of Agriculture (2016) Oilseeds: World markets and trade. https://www.fas.usda.gov/data/oilseeds-world-markets-and-trade, cited 29 Sept 2017.

Vogel C, and Browse J (1996) Cholinephosphotransferase and diacylglycerol acyltransferase (substrate specificities at a key branch point in seed lipid metabolism). Plant Physiol: 923–931

Vrinten P, Zhiyuan H, Munchinsky MA, Rowland G, and Qiu X (2005) Two FAD3 desaturase genes control the level of linolenic acid in flax seed. Plant Physiol 139: 79–87

Wanasundara PKJPD, Wanasundara UN, and Shahidi F (1999) Changes in flax (*Linum usitatissimum L*) seed lipids during germination. J Am Oil Chem Soc 76: 41–48

Wang HW, Zhang JS, Gai JY, and Chen SY (2006) Cloning and comparative analysis of the gene encoding diacylglycerol acyltransferase from wild type and cultivated soybean. Theor Appl Genet 112: 1086–1097

Wang L, Shen W, Kazachkov M, Chen G, Chen Q, Carlsson AS, Stymne S, Weselake RJ, and Zou J (2012a) Metabolic interactions between the Lands cycle and the Kennedy pathway of glycerolipid synthesis in Arabidopsis developing seeds. Plant Cell 24: 4652–4669

Wang Z, Hobson N, Galindo L, Zhu S, Shi D, McDill J, Yang L, Hawkins S, Neutelings G, Datla R, Lambert G, Galbraith DW, Grassa CJ, Geraldes A, Cronk QC, Cullis C, Dash PK, Kumar PA, Cloutier S, Sharpe AG, Wong GK-SS, Wang J, and Deyholos MK (2012b) The genome of flax (*Linum usitatissimum*) assembled *de novo* from short shotgun sequence reads. Plant J 72: 461–473

Wang Z, Huang W, Chang J, Sebastian A, Li Y, Li H, Wu X, Zhang B, Meng F, and Li W (2014) Overexpression of SiDGAT1, a gene encoding acyl-CoA:diacylglycerol acyltransferase from *Sesamum indicum L* increases oil content in transgenic Arabidopsis and soybean. Plant Cell, Tissue Organ Cult 119: 399–410

Waterhouse AM, Procter JB, Martin DMA, Clamp M, and Barton GJ (2009) Jalview Version 2-A multiple sequence alignment editor and analysis workbench. Bioinformatics 25: 1189–

1191

Watkins PA (1997) Fatty acid activation. Prog Lipid Res 36: 55–83

Watkins PA, and Ellis JM (2012) Peroxisomal acyl-CoA synthetases. Biochim Biophys Acta (BBA)-Mol Basis Dis 1822: 1411–1420

Weimar JD, DiRusso CC, Delio R, and Black PN (2002) Functional role of fatty acyl-coenzyme A synthetase in the transmembrane movement and activation of exogenous long-chain fatty acids. J Biol Chem 277: 29369–29376

Weiss SB, and Kennedy EP (1956) The enzymatic synthesis of triglycerides. J Am Chem Soc 78: 3550–3550

Weiss SB, Kennedy EP, and Kiyasu JY (1960) The enzymatic synthesis of triglycerides. J Biol Chem 235: 40–44

Weng H, Molina I, Shockey J, and Browse J (2010) Organ fusion and defective cuticle function in a *lacs1 lacs2* double mutant of Arabidopsis. Planta 231: 1089–1100

Weselake R (2005) Storage lipids. In Plant Lipids: Biology, Utilization and Manipulation (ed Murphy D). Blackwell Publishing, Oxford pp 162–221

Weselake R, Taylor D, and Pomeroy M (1991) Properties of diacylglycerol acyltransferase from microspore-derived embryos of *Brassica napus*. Phytochemistry 30: 3533–3538

Weselake RJ, Madhavji M, Szarka SJ, Patterson NA, Wiehler WB, Nykiforuk CL, Burton TL, Boora PS, Mosimann SC, Foroud NA, Thibault BJ, Moloney MM, Laroche A, and Furukawa-Stoffer TL (2006) Acyl-CoA-binding and self-associating properties of a

recombinant 133 kDa N-terminal fragment of diacylglycerol acyltransferase-1 from oilseed rape. BMC Biochem 7: 24

Weselake RJ, Pomeroy MK, Furukawa TL, Golden JL, Little DB, and Laroche A (1993) Developmental profile of diacylglycerol acyltransferase in maturing seeds of oilseed rape and safflower and microspore-derived cultures of oilseed rape. Plant Physiol 102: 565–571

Weselake RJ, Shah S, Tang M, Quant PA, Snyder CL, Furukawa-Stoffer TL, Zhu W, Taylor DC, Zou J, Kumar A, Hall L, Laroche A, Rakow G, Raney P, Moloney MM, and Harwood JL (2008) Metabolic control analysis is helpful for informed genetic manipulation of oilseed rape (*Brassica napus*) to increase seed oil content. J Exp Bot 59: 3543–3549

White SW, Robertson RM, Yao J, Gajewski S, Kumar G, and Rock CO (2017) Crystal structure of lysophosphatidic acid acyltransferase reveals a paired reentrant helix membrane anchor that positions the active site inside the phospholipid bilayer. FASEB J 31: 13

Wickramarathna AD, Siloto RMP, Mietkiewska E, Singer SD, Pan X, and Weselake RJ (2015) Heterologous expression of flax PHOSPHOLIPID:DIACYLGLYCEROL CHOLINEPHOSPHOTRANSFERASE (PDCT) increases polyunsaturated fatty acid content in yeast and Arabidopsis seeds. BMC Biotechnol 15: 1–15

Xiao S, and Chye ML (2011) New roles for acyl-CoA-binding proteins (ACBPs) in plant development, stress responses and lipid metabolism. Prog Lipid Res 50: 141–151

Xu J, Francis T, Mietkiewska E, Giblin EM, Barton DL, Zhang Y, Zhang M, and Taylor DC (2008a) Cloning and characterization of an acyl-CoA-dependent diacylglycerol acyltransferase 1 (DGAT1) gene from *Tropaeolum majus*, and a study of the functional

motifs of the DGAT protein using site-directed mutagenesis to modify enzyme activity and oil content. Plant Biotechnol J 6: 799–818

Xu N, Zhang SO, Cole RA, McKinney SA, Guo F, Haas JT, Bobba S, Farese R V, and Mak HY (2012) The FATP1-DGAT2 complex facilitates lipid droplet expansion at the ER-lipid droplet interface. J Cell Biol 198: 895–911

Yang W, Wang G, Li J, Bates PD, Wang X, and Allen DK (2017) Phospholipase Dζ enhances diacylglycerol flux into triacylglycerol. Plant Physiol 174: 110–123

Yang Y, Yu X, Song L, and An C (2011) ABI4 activates DGAT1 expression in Arabidopsis seedlings during nitrogen deficiency. Plant Physiol 156: 873–883

Yang Z (2007) PAML 4: Phylogenetic analysis by maximum likelihood. Mol Biol Evol 24: 1586–1591

Yang Z, Wong WSW, and Nielsen R (2005) Bayes empirical bayes inference of amino acid sites under positive selection. Mol Biol Evol 22: 1107–1118

Yen CLE, Stone SJ, Koliwad S, Harris C, and Farese R V (2008) Thematic review series: Glycerolipids. DGAT enzymes and triacylglycerol biosynthesis. J Lipid Res 49: 2283–2301

Yu J, Li Y, Zou F, Xu S, and Liu P (2015) Phosphorylation and function of DGAT1 in skeletal muscle cells. Biophys Reports 1: 41–50

Yu YH, Zhang Y, Oelkers P, Sturley SL, Rader DJ, and Ginsberg HN (2002) Posttranscriptional control of the expression and function of diacylglycerol acyltransferase-1 in mouse adipocytes. J Biol Chem 277: 50876–50884

Yuan H, Wu J, Wang X, Chen J, Zhong Y, Huang Q, and Nan P (2017) Computational identification of amino-acid mutations that further improve the activity of a chalcone–flavonone isomerase from *Glycine max.* Front Plant Sci 8: 1–8

Yurchenko O, Singer SD, Nykiforuk CL, Gidda S, Mullen RT, Moloney MM, and Weselake RJ (2014) Production of a *Brassica napus* low-molecular mass acyl-coenzyme A-binding protein in Arabidopsis alters the acyl-coenzyme A pool and acyl composition of oil in seeds. Plant Physiol 165: 550–560

Yurchenko OP, Nykiforuk CL, Moloney MM, Ståhl U, Banaś A, Stymne S, and Weselake RJ (2009) A 10-kDa acyl-CoA-binding protein (ACBP) from *Brassica napus* enhances acyl exchange between acyl-CoA and phosphatidylcholine. Plant Biotechnol J 7: 602–610

Zanetti F, Vamerali T, and Mosca G (2009) Yield and oil variability in modern varieties of high-erucic winter oilseed rape (*Brassica napus L var oleifera*) and Ethiopian mustard (*Brassica carinata A Braun*) under reduced agricultural inputs. Ind Crops Prod 30: 265–270

Zhang H, Damude HG, and Yadav NS (2012) Three diacylglycerol acyltransferases contribute to oil biosynthesis and normal growth in *Yarrowia lipolytica.* Yeast 29: 25–38

Zhang M, Fan J, Taylor DC, and Ohlrogge JB (2009) DGAT1 and PDAT1 acyltransferases have overlapping functions in Arabidopsis triacylglycerol biosynthesis and are essential for normal pollen and seed development. Plant Cell 21: 3885–3901

Zhao L, Katavic V, Li F, Haughn GW, and Kunst L (2010) Insertional mutant analysis reveals that long-chain acyl-CoA synthetase 1 (LACS1), but not LACS8, functionally overlaps with LACS9 in Arabidopsis seed oil biosynthesis. Plant J 64: 1048–1058

Zheng P, Allen WB, Roesler K, Williams ME, Zhang S, Li J, Glassman K, Ranch J, Nubel D, Solawetz W, Bhattramakki D, Llaca V, Deschamps S, Zhong GY, Tarczynski MC, and Shen B (2008) A phenylalanine in DGAT is a key determinant of oil content and composition in maize. Nat Genet 40: 367–372

Zhou XR, Shrestha P, Yin F, Petrie JR, and Singh SP (2013) AtDGAT2 is a functional acyl-CoA:Diacylglycerol acyltransferase and displays different acyl-CoA substrate preferences than AtDGAT1. FEBS Lett 587: 2371–2376

Ziegler J, Brandt W, Geißler R, and Facchini PJ (2009) Removal of substrate inhibition and increase in maximal velocity in the short chain dehydrogenase/reductase salutaridine reductase involved in morphine biosynthesis. J Biol Chem 284: 26758–26767

Zou J, Wei Y, Jako C, Kumar A, Selvaraj G, and Taylor DC (1999) The *Arabidopsis thaliana TAG1* mutant has a mutation in a diacylglycerol acyltransferase gene. Plant J 19: 645–653

Appendix

The following list describes my other contributions as a co-author or co-inventor.

1. Chen G, **Xu Y**, Siloto RMP, Caldo KMP, Vanhercke T, Tahchy AE, Niesner N, Chen Y, Mietkiewska E and Weselake RJ (2017) High Performance Variants of Plant Diacylglycerol Acyltransferase 1 Generated by Directed Evolution Provide Insights into Structure-Function. Plant J doi: 10.1111/tpj.13652

● For this work, I performed experiments including lipid analysis, microsomes isolation, enzyme assay and sequences analysis including multiple sequence alignment and positive selection and contributed to the results interpretation and discussion. I also critically reviewed and revised the manuscript.

2. Caldo KMP, Shen W, **Xu Y**, Hanley-Bowdoin L, Weselake RJ, Lemieux MJ (2017) *Brassica napus* diacylglycerol acyltransferase 1 is feed-forward activated by phosphatidic acid and inhibited by SnRK1 phosphorylation. Manuscript in preparation

● For this work, I assisted with lipid analysis and critically reviewed the manuscript.

3. Weselake RJ, Chen G, Siloto RMP, Truksa M, **Xu Y**, Caldo K (2017) Plant DGAT-1 Variants. United States Provisional Patent Application Serial No. 62/443,102

● For this work, I performed experiments including lipid analysis, microsomes isolation and enzyme assay and also analyzed the corresponding data. I also critically reviewed the draft of the patent.